Monitoring Poly(ADP-ribosyl)glycohydrolase Activity with a Continuous Fluorescent Substrate

Bryon S. Drown,[1] Tomohiro Shirai,[1] Johannes Gregor Matthias Rack,[2] Ivan Ahel,[2] and Paul J. Hergenrother[1,3,*]

SUMMARY

The post-translational modification (PTM) and signaling molecule poly(ADP-ribose) (PAR) has an impact on diverse biological processes. This PTM is regulated by a series of ADP-ribosyl glycohydrolases (PARG enzymes) that cleave polymers and/or liberate monomers from their protein targets. Existing methods for monitoring these hydrolases rely on detection of the natural substrate, PAR, commonly achieved via radioisotopic labelling. Here we disclose a general substrate for monitoring PARG activity, **TFMU-ADPr**, which directly reports on total PAR hydrolase activity via release of a fluorophore; this substrate has excellent reactivity, generality (processed by the major PARG enzymes), stability, and usability. A second substrate, **TFMU-IDPr**, selectively reports on PARG activity only from the enzyme ARH3. Use of these probes in whole-cell lysate experiments has revealed a mechanism by which ARH3 is inhibited by cholera toxin. **TFMU-ADPr** and **TFMU-IDPr** are versatile tools for assessing small-molecule inhibitors in vitro and probing the regulation of ADP-ribosyl catabolic enzymes.

INTRODUCTION

Many biological processes are regulated by post-translational modifications (PTMs), with ADP-ribosylation being one of the most thoroughly studied nucleotide-containing modifications. This modification includes a collection of “writers”, “readers”, and “erasers”. The writers, poly(ADP-ribosyl) polymerases (PARPs), modify protein substrates with adenine diphosphate ribose (ADPr). Nearly all nucleophilic amino acids have been shown to be modified: glutamate, aspartate, cysteine, lysine, and serine (Altmeyer et al., 2009; Barkauskaite et al., 2015; Leidecker et al., 2016; Vyas et al., 2014; Zhen et al., 2017). While the majority of PARPs can only transfer a single ADPr unit from NAD^+ (Feijs et al., 2013), the founding member of the family, PARP1 (but also PARP2 and tankyrases), can synthesize large polymers termed poly(ADP-ribose) (PAR) (Vyas et al., 2014). A wealth of literature over several decades has established PARylation as central for proper DNA damage response (Andrabi et al., 2006;

[1] Department of Chemistry and Institute for Genomic Biology, University of Illinois at Urbana-Champaign, 261 Roger Adams Lab Box 36-5, 600 S. Mathews Avenue, Urbana, IL 61801, USA
[2] Sir William Dunn School of Pathology, University of Oxford, South Parks Road, OX1 3RE, United Kingdom
[3] Lead Contact
* Correspondence: hergenro@illinois.edu

Schreiber et al., 2000; Wang et al., 2016), chromatin maintenance (Becker et al., 2016), cell division (Chang et al., 2005), and DNA replication (Illuzzi et al., 2014).

In contrast, much is still unknown about the regulation of ADPr erasure. Several families of enzymes are responsible for removal and degradation of PARylation. Poly(ADP-ribose) glycohydrolase (PARG) hydrolyzes the 2',1'' glycosidic linkage (red in Fig. 1A) of polymers mainly in an *exo* manner (Barkauskaite et al., 2013). PARG modifies PARylated proteins by removing polymers down to the last unit, which it is incapable of removing (Slade et al., 2011). ADP-ribosyl hydrolase 3 (ARH3 or ADPRHL2) is also capable of degrading PAR polymers, albeit at a reduced rate (Mashimo et al., 2014; 2013; Niere et al., 2012; Oka et al., 2006; Ono et al., 2006). Until recently, neither of these proteins were believed capable of removing the last ADPr unit directly bonded to the protein side chain. This hydrolysis is carried out by ARH1 or an enzymatic member of the macrodomain family (terminal ADP-ribosyl protein glycohydrolase (TARG1), MACROD1, and MACROD2 in mammals) (Barkauskaite et al., 2015; Feijs et al., 2013; Jankevicius et al., 2013; Mashimo et al., 2013; Moss et al., 1992; Rosenthal et al., 2013; Sharifi et al., 2013). Recently ARH3 was shown to be the sole enzyme capable of hydrolyzing mono-ADP-ribosyl serine (Abplanalp et al., 2017; Fontana et al., 2017). Beyond substrate recognition, little is known about how these ADPr erasers are regulated or the relative importance of different erasers in various biological contexts. In particular, study of PAR cleavage has been limited by the challenge of separating contributions to PAR degradation by PARG and by ARH3. Several reports suggest that the specific activity of PARG is significantly greater than ARH3, however, the cellular distribution of these two enzymes differ as do their regulatory domains (Mashimo et al., 2014). Genetic knockout of ARH3 does not affect the lifetime of long polymers but does result in longer lived short polymers (Fontana et al., 2017), thus much more detailed information on the relative contribution of PAR-degrading enzymes is needed.

The most widely employed enzyme assays for measuring PARG/ARH3 activity rely on radioisotopically labelled and enzymatically produced PAR (Cortes et al., 2004; Finch et al., 2012; Ménard and Poirier, 2011; Sharifi et al., 2013). The production and isolation of labelled PAR is limited to 0.3-2 mg scale (Ménard and Poirier, 2011). After treatment with PARG, reaction mixtures are separated by TLC or HPLC and quantified by autoradiography or liquid scintillation counting. This technique, while sensitive, is laborious and not scalable. Recent efforts to develop more scalable PARG activity assays have been modestly successful, for example, a four-component FRET system to detect the interaction between a PARylated protein and XRCC1 (Kim et al., 2015; Stowell et al., 2016). While this approach has been implemented in microtiter format and utilized to discover a first-in-class PARG inhibitor, it suffers from an inability to accurately measure enzyme kinetics and cannot operate in cell lysate (James et al., 2016). There clearly is still an unmet need for a facile and continuous activity assay for PAR-degrading enzymatic activity. Herein is described the design, synthesis, and evaluation of fluorescent probes for

PAR hydrolyzing enzymes, including a compound that is processed by both ARH3 and PARG, and another that is a selective substrate for ARH3. This latter probe has enabled the first direct measurements of ARH3 activity in cells and was then used to discover the first specific means for cellular ARH3 inhibition.

RESULTS AND DISCUSSION

Design and synthesis of PARG substrates

Reporter substrates for PARG and ARH3, **pNP-ADPr** and **TFMU-ADPr**, were designed, inspired by the natural substrate, PAR. The 2',1''-glycosidic bond that is cleaved in PAR (highlighted red in Figure 1A) was replaced with a phenolic glycoside. Initial efforts focused on utilizing 4-nitrophenol (**pNP**) as a chromaphore reporter but also extended to the fluorophore 4-(trifluoromethyl)umbelliferone (**TFMU**) for applications requiring greater sensitivity and specificity. Retrosynthetic analysis of **pNP-ADPr** identified two major synthetic hurdles (Figure 1B): a late-stage pyrophosphate coupling and a 1,2-*cis* selective glycosylation of a furanoside. Recent work on the synthesis of dimeric PAR (Lambrecht et al., 2015) overcame similar challenges, and it was envisioned that an analogous strategy could be applied to the synthesis of this simplified PARG substrate.

Glycosylation of electron-deficient phenols such as **pNP** and **TFMU** is often challenging. Most methods rely of anchimeric assistance leading to the undesired 1,2-*trans* product (Bordoni et al., 2010). We found that acceptable α-selectivity could be achieved by directly activating a hemi-acetal with bulky protecting groups under Mitsunobu conditions. As outlined in Figure 2, this strategy was employed using orthogonally protected ribose **3**, prepared in three steps from D-ribonic γ-lactone (Figure S1A) (Lambrecht et al., 2015); subsequent removal of the trityl group proceeded smoothly under strictly anhydrous conditions to prevent hydrolysis of the glycoside, producing **4** and **5**. Although direct phosphorylation with $POCl_3$ was possible, we found phosphoramidite coupling followed by fluorenylmethyl removal more amenable on scale to give phosphates **6** and **7** (Figure 2, Figure S1B, C). Pyrophosphate formation was accomplished via in situ oxidative chlorination of H-phosphonate **8** (Figure 2, Figure S1D), to produce **9** and **10**, followed by global desilylation to provide **pNP-ADPr** and **TFMU-ADPr**.

The late-stage pyrophosphate coupling featured in the synthesis of these compounds also facilitates the construction of other non-natural substrates for PARG. The recently co-crystalized structure of *L. chalumnae* ARH3 with ADPr (not shown, co-submitted) indicates that the binding modes of hPARG and LchARH3 are dramatically different. In particular, the adenine binding site of LchARH3 is much less organized and more solvent exposed. Molecular docking sugar nucleotides with varied purine bases suggests that PARG is highly discriminatory while ARH3 would accommodate other bases (Table S1).

Key interactions between ADPr and hPARG Glu727 and Ile726 cannot be recapitulated with IDPr, and the hPARG binding site is too restrictive to allow for additional favorable interactions (Figure 3A). Conversely, the LchARH3 binding site is predicted to allow IDPr to shift and make additional interactions with Lys132 (Figure 3B). We thus hypothesized that replacing the nucleobase of phenolic substrates, specifically substitution of adenine for hypoxanthine, would provide a substrate selective for ARH3. Therefore the compounds **TFMU-IDPr** and **pNP-IDPr** were designed and synthesized from inosine (Figure 3C, and Figure S2).

In vitro processing of substrates

Using **pNP-ADPr** and **TFMU-ADPr**, the first continuous PARG and ARH3 activity assays were developed. Enzymatic hydrolysis of phenolic glycosides was easily monitored by an increased absorbance or fluorescence (Figure S3A, B). Kinetic parameters for human PARG and ARH3 were determined by non-linear fitting of initial reaction rates (Table 1 and Figure 4A, B). A commonly used ortholog of PARG from *T. thermophila* (ttPARG) (Barkauskaite et al., 2013; Dunstan et al., 2012; Lambrecht et al., 2015) was also characterized and found to effectively hydrolyze **pNP-ADPr** and **TFMU-ADPr** (Table 1 and Figure S3A). The measured K_M of ARH3 was similar to the enzyme's reported activity against *O*-acetyl-ADP-ribose (Kasamatsu et al., 2011). The kinetic parameters of **pNP-ADPr** and **TFMU-ADPr** were quite similar likely due to the leaving groups having similar pK_as (7.15 and 7.26). Gratifyingly, the predicted selectivity of **TFMU-IDPr** for ARH3 over PARG was confirmed (Figure 4C). Further, both PARG and ARH3 selectively hydrolyzed the α anomer of **pNP-ADPr** over the β anomer as is consistent with their natural substrates (Figure S3C, D). Hydrolysis of substrates depends on catalytically active protein; inactivating mutations in hPARG (the E756N mutant, Lambrecht et al., 2015) and hARH3 (the D77N/D78N mutant, Fontana et al., 2017) abolish substrate processing (Figure S3F, G).

Use of substrates to monitor ARH3 activity assay in cell culture

The ability of **TFMU-IDPr** to selectively report on ARH3 activity within the cellular milieu would be an important application of these probes. While the experiments in Figure 4 demonstrate the selectivity of this substrate for ARH3 over PARG in a purified enzymatic system, in cells other hydrolases that recognize ADP-ribose could potentially process this substrate, thus two experiments were conducted to assess the activity of ARH3 and PARG with these substrates in cell lysate. First, the hydrolysis of **TFMU-IDPr** was evaluated in cell lysate from a ARH3 knockout isogenic cell line pair derived from U2OS cells (Fontana et al., 2017). Knockout of ARH3 resulted in near complete loss of **TFMU-IDPr** activity (Figure 5A) while **TFMU-ADPr** hydrolysis was only partially decreased (Figure 5B). Second, substrate processing was evaluated in the presence of the selective PARG inhibitor PDD00017273 (James et al., 2016). Hydrolysis of **TFMU-ADPr** was completely abolished by PDD00017273 in $ARH3^{-/-}$ cell lysate, but

TFMU-IDPr was unaffected by PARG inhibitor. Taken together, these experiments indicate that **TFMU-IDPr** is selectively cleaved by ARH3 in cell lysate, and **TFMU-ADPr** is cleaved only by ARH3 and PARG.

Survey of cancer cell lines

As the activity of ARH3 in various cell types is unknown, experiments were conducted to assess ARH3 activity in a variety of cancer cell lines. Twenty cell lines were analyzed for ARH3 activity, measured using **TFMU-IDPr**, and compared to ARH3 abundance (measured by Western blot, Figure 5D); in general ARH3 activity and abundance are well correlated (Figure 5E, Table S2). Strikingly, no ARH3 activity is observed with MCF10A cells despite the obvious presence of ARH3 by Western blot. Thus, it was hypothesized that in this cell line ARH3 is mutated or being affected by an endogenous inhibitor.

A unique feature of MCF10A cells are the particular additives in the growth media, and most notable is the inclusion of cholera toxin (CTX), a known ADP-ribosyltransferase (Gill and Meren, 1978; Wang and Schultz, 2014). Suspecting that the presence of CTX may impact ARH3 activity, MCF10A cells were passaged five times in the absence of CTX, and ARH3 activity was restored (Figure S5A). This recovery of activity was reversed (in a dose and time-dependent manner) with subsequent addition CTX, and this phenotype was reproduced in other cell lines (MCF7 and MIA PaCa-2) (Figure S5A, B). In all these cell lines, CTX-mediated ARH3 inhibition occurred rapidly ($t_{1/2}$ < 60 min, Figure S5B). The treatment of cells with CTX appears to be the first example of selective inhibition ARH3 in cells.

Mechanism of ARH3 inhibition by ADP-ribosyl-arginine

Having identified cholera toxin as causing ARH3 inhibition in cell culture, several experiments were performed to elucidate the toxin's mechanism of action. CTX was first found to have no direct effect on ARH3 *in vitro* (Figure S5C). The canonical mechanism of CTX involves mono-ADP-ribosylation of an active-site arginine on $G_{s\alpha}$ (G-protein alpha subunit); this post-translational modification results in the constitutive activation of adenylyl cyclase (AC), which synthesizes cAMP (Figure S6) (Inageda et al., 1991; Kato et al., 2007). Thus the role of AC and cAMP in CTX-dependent ARH3 inactivation were investigated. cAMP was found to only weakly inhibit ARH3 (IC_{50} = 2.96±0.05 mM, Figure S5D). Furthermore, treatment with forskolin, a known activator of AC (Florio et al., 1999; Takeda et al., 1983), did not result in ARH3 inhibition (Figure S5E). Finally, other ADP-ribosyltransferase bacterial ecto-toxins that target other amino acid residues do not inhibit ARH3 activity (Figure S5F). With these experiments pointing upstream of AC, direct interaction with ADP-ribosyl arginine (ADPr-Arg) was considered. To make assessments, ADPr-Arg was synthesized as described previously (Oppenheimer, 1978) and assessed in the in vitro assay. This compound was found to potently inhibit ARH3 *in vitro*, with a K_i value of 18±2 nM (Figure 6A, B). Interestingly, ADPr-Arg demonstrates markedly reduced activity against PARG (Figure 6C). This differential inhibition is in contrast to the results for the substrate

analogue inhibitor of PARG, the compound ADP-HPD (Koh et al., 2003; Slama et al., 1995a; 1995b); analysis of ADP-HPD shows that this compound inhibits both PARG and ARH3 (Figure 6C). Importantly, ADPr-Arg substantially accumulated in MCF7 cells following CTX treatment, from concentrations below the limit of detection in untreated cells to 2.62±0.05 μM in the treated cells (Figure S5G). Changes in related metabolites were also observed: cAMP concentration increased as expected for the canonical activity of CTX, NAD^+ concentration decreased (it is a substrate for ADPr-Arg synthesis), but arginine remained unchanged, perhaps due to the presence of exogenous arginine in media. The same trend for these metabolic changes was also observed in U2OS cells (Figure S5H).

DISCUSSION

This manuscript describes the first continuous substrates for the glycohydrolases that catabolize PAR. The syntheses of these substrates are robust and scalable (hundreds of milligrams of each were prepared), and as such these compounds should find routine use for the measurement of kinetics, the assessment of inhibitors, and for high-throughput screening applications. In addition, their ability to report on this enzymatic activity in cell lysate will enable a variety of experiments where PARG or ARH3 activity is the needed readout, and in such experiments the ARH3-selective substrate **TFMU-lDPr** can be used to differentiate cellular ARH3 enzymatic activity from PARG activity.

Selective enzyme assays are powerful for assessment of the differential contribution of enzyme family members to total enzymatic activity. The potential impact such experiments can have is apparent in the widespread use of a variety of compounds as caspase substrates. For caspases, specificity can be imbued through use of peptide sequences known to be specifically recognized by different caspases isozymes, and such tool compounds have been widely employed to understand conditions under which specific caspases are activated, and have been critical to mapping the apoptotic cell death pathway (Berger et al., 2006; Poręba et al., 2013). The lack of analogous reagents for monitoring of PAR processing has necessitated reliance on non-ideal methods such as isozyme-general processing of radiolabeled substrates. In the case of PAR-processing enzymes, the development of specific substrates is considerably more complicated than for a protease (where specificity can be built in though understanding of the endogenous protein substrates). The recently solved X-ray structures of ARH3 and PARG, and subsequent docking studies, has now allowed for the design of reporter substrates, one that is general for ARH3 and PARG, and one that is specific for ARH3.

As a first application, these substrates have been used to discover that CTX suppresses cellular ARH3 activity through the production of ADPr-arginine, an ARH3-selective inhibitor. While the effect of bacterial exotoxins on cAMP synthesis and downstream processes has been extensively described (Figure S6), their effects off-pathway are less understood. CTX, *Clostridium difficile* binary toxin (CDT), and pertussis toxin (PT) catalyze the mono-ADP-ribosylation of arginine (CTX and CDT) and cysteine

(PT) residues. While the background ADP-ribosylation of arginine by CTX has been observed with isolated protein (Oppenheimer, 1978), the activity of CTX has largely been regarded to be highly selective for proteinaceous arginine. We observe and quantify ADP-ribosylation of free arginine for the first time in cell culture at concentrations that rationalize ARH3 inhibition. The absence of ARH3 inhibition following CDT treatment, despite creating the same PTM, may result from differential propensities to produce free and proteinaceous ADPr-arginine. However, the possibility remains that the observed ADPr-arginine results from proteolytic breakdown of ADP-ribosylated G proteins rather than direct ADP-ribosylation. In this case, the differential activities of bacterial toxins can be attributed to stabilities of their respective protein targets. Some of the phenotypes described upon treatment by bacterial toxins (i.e. lose of tight junctions) has also been described for PAR overproduction (Cuzzocrea and Genovese, 2000; Guichard et al., 2013; Mazzon et al., 2002; Nusrat et al., 2001). While the exact mechanism by which these processes operate is yet unknown, inhibition of ARH3 may assist in toxins' ability to elevate PAR concentrations. The ready availability of these ARH3 and PARG substrates will now facilitate additional discoveries about the regulation of cellular PAR processing.

SIGNIFICANCE

ADP-ribosylation has long captured interest due to its prevalence in normal biological processes and in disease states, but study of this PTM has traditionally relied on imprecise and laborious methods for measuring the activity of ADPr erasers. As such, the conditions and mechanisms by which PAR is regulated are poorly understood. Here we introduce a rapid and precise technology for measuring poly(ADP-ribose) glycohydrolase activity. Recent advances in pyrophosphate couplings have also improved our capability to construct sugar nucleotides in a modular and scalable fashion, leading to robust and scalable syntheses of the target substrates. These substrates are useful for the detection and quantitation of endogenous cellular PARG and ARH3 activity, and the utility of this tool is increased with the discovery that replacement of the nucleobase provides selectivity for ARH3 over PARG. Together this toolset is expected to greatly enhance the ability to interrogate PAR-cleaving enzymes.

ACKNOWLEDGMENTS

We express our thanks to Prof. Hening Lin (Cornell U.) for ARH3 plasmid. We thank David Boothman (Indiana University School of Medicine) for the MIA-PaCa cell line, Timothy Fan (University of Illinois, Urbana) for the CA46 cell line, Navdeep Chandel (Northwestern U.) for the MEF cell line, Gregory Riggins (Johns Hopkins) for the D54 cell line, and Richard Hotchkiss (Washington University, St. Louis) for the Jurkat cell line. We are grateful for the University of Illinois and the NIH (R21 CA212732) for funding this work. The work in I.A. laboratory is funded by the Wellcome Trust (grant number 101794) and Cancer Research United Kingdom (grant number C35050/A22284).

AUTHOR CONTRIBUTIONS

B.S.D. performed chemical synthesis of PARG/ARH3 substrates, molecular docking, cell culture and enzyme assays. T.S. performed chemical synthesis of ADP-HPM. J.G.M.R. obtained structure of LchARH3. B.S.D. and P.J.H. wrote the manuscript, designed experiments, and analyzed data.

DECLARATIONS OF INTERESTS

The University of Illinois has filed a patent on materials related to this work.

REFERENCES

Abplanalp, J., Leutert, M., Frugier, E., Nowak, K., Feurer, R., Kato, J., Kistemaker, H.V.A., Filippov, D.V., Moss, J., Caflisch, A., et al. (2017). Proteomic analyses identify ARH3 as a serine mono-ADP-ribosylhydrolase. Nat. Commun. *8*, 2055.

Altmeyer, M., Messner, S., Hassa, P.O., Fey, M., and Hottiger, M.O. (2009). Molecular mechanism of poly(ADP-ribosyl)ation by PARP1 and identification of lysine residues as ADP-ribose acceptor sites. Nucleic Acids Res. *37*, 3723–3738.

Andrabi, S.A., Kim, N.S., Yu, S.-W., Wang, H., Koh, D.W., Sasaki, M., Klaus, J.A., Otsuka, T., Zhang, Z., Koehler, R.C., et al. (2006). Poly(ADP-ribose) (PAR) polymer is a death signal. Proc. Natl. Acad. Sci. USA *103*, 18308–18313.

Barkauskaite, E., Brassington, A., Tan, E.S., Warwicker, J., Dunstan, M.S., Banos, B., Lafite, P., Ahel, M., Mitchison, T.J., Ahel, I., et al. (2013). Visualization of poly(ADP-ribose) bound to PARG reveals inherent balance between exo- and endo-glycohydrolase activities. Nat. Commun. *4*, 2164.

Barkauskaite, E., Jankevicius, G., and Ahel, I. (2015). Structures and Mechanisms of Enzymes Employed in the Synthesis and Degradation of PARP-Dependent Protein ADP-Ribosylation. Mol. Cell *58*, 935–946.

Becker, A., Zhang, P., Allmann, L., Meilinger, D., Bertulat, B., Eck, D., Hofstaetter, M., Bartolomei, G., Hottiger, M.O., Schreiber, V., et al. (2016). Poly(ADP-ribosyl)ation of Methyl CpG Binding Domain Protein 2 Regulates Chromatin Structure. J. Biol. Chem. *291*, 4873–4881.

Berger, A.B., Witte, M.D., Denault, J.-B., Sadaghiani, A.M., Sexton, K.M.B., Salvesen, G.S., and Bogyo, M. (2006). Identification of Early Intermediates of Caspase Activation Using Selective Inhibitors and Activity-Based Probes. Mol. Cell *23*, 509–521.

Chang, P., Coughlin, M., and Mitchison, T.J. (2005). Tankyrase-1 polymerization of poly(ADP-ribose) is required for spindle structure and function. Nat. Cell Biol. *7*, 1133–1139.

Cortes, U., Tong, W.-M., Coyle, D.L., Meyer-Ficca, M.L., Meyer, R.G., Petrilli, V., Herceg, Z., Jacobson, E.L., Jacobson, M.K., and Wang, Z.-Q. (2004). Depletion of the 110-kilodalton isoform of poly(ADP-ribose) glycohydrolase increases sensitivity to genotoxic and endotoxic stress in mice. Mol. Cell. Biol. *24*, 7163–7178.

Cuzzocrea, S., and Genovese, T. (2000). Role of Free Radicals and Poly(ADP-ribose) Synthetase in Intestinal Tight Junction Permeability. Mol. Med. *6*, 766–778.

Dunstan, M.S., Barkauskaite, E., Lafite, P., Knezevic, C.E., Brassington, A., Ahel, M., Hergenrother, P.J., Leys, D., and Ahel, I. (2012). Structure and mechanism of a canonical poly(ADP-ribose) glycohydrolase. Nat. Commun. *3*, 878.

Feijs, K.L.H., Forst, A.H., Verheugd, P., and Lüscher, B. (2013). Macrodomain-containing proteins: regulating new intracellular functions of mono(ADP-ribosyl)ation. Nat. Rev. Mol. Cell Biol. *14*, 443–453.

Finch, K.E., Knezevic, C.E., Nottbohm, A.C., Partlow, K.C., and Hergenrother, P.J. (2012). Selective small molecule inhibition of poly(ADP-ribose) glycohydrolase (PARG). ACS Chem. Biol. *7*, 563–570.

Florio, C., Frausin, F., Vertua, R., and Gaion, R.M. (1999). Amplification of the cyclic AMP response to forskolin in pheochromocytoma PC12 cells through adenosine A(2A) purinoceptors. J. Pharmacol. Exp. Ther. *290*, 817–824.

Fontana, P., Bonfiglio, J.J., Palazzo, L., Bartlett, E., Matic, I., and Ahel, I. (2017). Serine ADP-ribosylation reversal by the hydrolase ARH3. eLife *6*, 861.

Gill, D.M., and Meren, R. (1978). ADP-ribosylation of membrane proteins catalyzed by cholera toxin: basis of the activation of adenylate cyclase. Proc. Natl. Acad. Sci. USA *75*, 3050–3054.

Guichard, A., Cruz-Moreno, B., Cruz-Moreno, B.C., Aguilar, B., van Sorge, N.M., Kuang, J., Kurkciyan, A.A., Wang, Z., Hang, S., Pineton de Chambrun, G.P., et al. (2013). Cholera toxin disrupts barrier function by inhibiting exocyst-mediated trafficking of host proteins to intestinal cell junctions. Cell Host Microbe *14*, 294–305.

Höbartner, C., and Silverman, S.K. (2005). Modulation of RNA tertiary folding by incorporation of caged nucleotides. Angew. Chem. Int. Ed. Engl. *44*, 7305–7309.

Illuzzi, G., Fouquerel, E., Amé, J.-C., Noll, A., Rehmet, K., Nasheuer, H.-P., Dantzer, F., and Schreiber, V. (2014). PARG is dispensable for recovery from transient replicative stress but required to prevent detrimental accumulation of poly(ADP-ribose) upon prolonged replicative stress. Nucleic Acids Res. *42*, 7776–7792.

Inageda, K., Nishina, H., and Tanuma, S.-I. (1991). Mono-ADP-ribosylation of Gs by an eukaryotic arginine-specific ADP-ribosyltransferase stimulates the adenylate cyclase system. Biochem. Biophys. Res. Commun. *176*, 1014–1019.

James, D.I., Smith, K.M., Jordan, A.M., Fairweather, E.E., Griffiths, L.A., Hamilton, N.S., Hitchin, J.R., Hutton, C.P., Jones, S., Kelly, P., et al. (2016). First-in-Class Chemical Probes against Poly(ADP-ribose) Glycohydrolase (PARG) Inhibit DNA Repair with Differential Pharmacology to Olaparib. ACS Chem. Biol. *11*, 3179–3190.

Jankevicius, G., Hassler, M., Golia, B., Rybin, V., Zacharias, M., Timinszky, G., and Ladurner, A.G. (2013). A family of macrodomain proteins reverses cellular mono-ADP-ribosylation. Nat. Struct. Mol. Biol. *20*, 508–514.

Kasamatsu, A., Nakao, M., Smith, B.C., Comstock, L.R., Ono, T., Kato, J., Denu, J.M., and Moss, J. (2011). Hydrolysis of O-Acetyl-ADP-ribose Isomers by ADP-ribosylhydrolase 3. J. Biol. Chem. *286*, 21110–21117.

Kato, J., Zhu, J., Liu, C., and Moss, J. (2007). Enhanced sensitivity to cholera toxin in ADP-ribosylarginine hydrolase-deficient mice. Mol. Cell. Biol. *27*, 5534–5543.

Kim, I.-K., Stegeman, R.A., Brosey, C.A., and Ellenberger, T. (2015). A quantitative assay reveals ligand specificity of the DNA scaffold repair protein XRCC1 and efficient disassembly of complexes of XRCC1 and the poly(ADP-ribose) polymerase 1 by poly(ADP-ribose) glycohydrolase. J. Biol. Chem. *290*, 3775–3783.

Koh, D.W., Coyle, D.L., Mehta, N., Ramsinghani, S., Kim, H., Slama, J.T., and Jacobson, M.K. (2003). SAR Analysis of Adenosine Diphosphate (Hydroxymethyl)pyrrolidinediol Inhibition of Poly(ADP-ribose) Glycohydrolase. J. Med. Chem. *46*, 4322–4332.

Lambrecht, M.J., Brichacek, M., Barkauskaite, E., Ariza, A., Ahel, I., and Hergenrother, P.J. (2015). Synthesis of Dimeric ADP-Ribose and Its Structure with Human Poly(ADP-ribose) Glycohydrolase. J. Am. Chem. Soc. *137*, 3558–3564.

Leidecker, O., Bonfiglio, J.J., Colby, T., Zhang, Q., Atanassov, I., Žaja, R., Palazzo, L., Stockum, A., Ahel, I., and Matic, I. (2016). Serine is a new target residue for endogenous ADP-ribosylation on histones. Nat. Chem. Biol. *12*, 998–1000.

Mashimo, M., Kato, J., and Moss, J. (2013). ADP-ribosyl-acceptor hydrolase 3 regulates poly (ADP-ribose) degradation and cell death during oxidative stress. Proc. Natl. Acad. Sci. USA *110*, 18964–18969.

Mashimo, M., Kato, J., and Moss, J. (2014). Structure and function of the ARH family of ADP-ribosyl-acceptor hydrolases. DNA Repair *23*, 88–94.

Mazzon, E., De Sarro, A., Caputi, A.P., and Cuzzocrea, S. (2002). Role of tight junction derangement in the endothelial dysfunction elicited by exogenous and endogenous peroxynitrite and poly(ADP-ribose) synthetase. Shock *18*, 434–439.

Ménard, L., and Poirier, G.G. (2011). Rapid assay of poly(ADP-ribose) glycohydrolase. Biochem. Cell Biol. *65*, 668–673.

Moss, J., Stanley, S.J., Nightingale, M.S., Murtagh, J.J., Monaco, L., Mishima, K., Chen, H.C., Williamson, K.C., and Tsai, S.C. (1992). Molecular and immunological characterization of ADP-ribosylarginine hydrolases. J. Biol. Chem. *267*, 10481–10488.

Nusrat, A., Eichel-Streiber, von, C., Turner, J.R., Verkade, P., Madara, J.L., and Parkos, C.A. (2001). Clostridium difficile toxins disrupt epithelial barrier function by altering membrane microdomain localization of tight junction proteins. Infect. Immun. *69*, 1329–1336.

Oppenheimer, N.J. (1978). Structural determination and stereospecificity of the choleragen-catalyzed reaction of NAD^+ with guanidines. J. Biol. Chem. *253*, 4907–4910.

Poręba, M., Stróżyk, A., Salvesen, G.S., and Drąg, M. (2013). Caspase substrates and inhibitors. Cold Spring Harb. Perspect Biol. *5*, a008680–a008680.

Rosenthal, F., Feijs, K.L.H., Frugier, E., Bonalli, M., Forst, A.H., Imhof, R., Winkler, H.C., Fischer, D., Caflisch, A., Hassa, P.O., et al. (2013). Macrodomain-containing proteins are new mono-ADP-ribosylhydrolases. Nat. Struct. Mol. Biol. *20*, 502–507.

Schreiber, V., Dantzer, F., Murcia, J.M.-D., La Rubia, de, G., Ménissier-De Murcia, J., Hostomsky, Z., and de Murcia, G. (2000). Base excision repair is impaired in mammalian cells lacking Poly(ADP-ribose) polymerase-1. Biochemistry *39*, 7559–7569.

Sharifi, R., Morra, R., Appel, C.D., Tallis, M., Chioza, B., Jankevicius, G., Simpson, M.A., Matic, I., Ozkan, E., Golia, B., et al. (2013). Deficiency of terminal ADP-ribose protein glycohydrolase TARG1/C6orf130 in neurodegenerative disease. Embo J. *32*, 1225–1237.

Slade, D., Dunstan, M.S., Barkauskaite, E., Weston, R., Lafite, P., Dixon, N., Ahel, M., Leys, D., and Ahel, I. (2011). The structure and catalytic mechanism of a poly(ADP-ribose) glycohydrolase. Nature *477*, 616–620.

Slama, J.T., Aboul-Ela, N., and Jacobson, M.K. (1995a). Mechanism of Inhibition of Poly(ADP-ribose) Glycohydrolase by Adenosine Diphosphate (Hydroxymethyl)pyrrolidinediol. J. Med. Chem. *38*, 4332–4336.

Slama, J.T., Aboul-Ela, N., Goli, D.M., Cheesman, B.V., Simmons, A.M., and Jacobson, M.K. (1995b). Specific Inhibition of Poly(ADP-ribose) Glycohydrolase by Adenosine Diphosphate (Hydroxymethyl)pyrrolidinediol. J. Med. Chem. *38*, 389–393.

Stowell, A.I.J., James, D.I., Waddell, I.D., Bennett, N., Truman, C., Hardern, I.M., and Ogilvie, D.J. (2016). A high-throughput screening-compatible homogeneous time-resolved fluorescence assay measuring the glycohydrolase activity of human poly(ADP-ribose) glycohydrolase. Analytical Biochemistry *503*, 58–64.

Takeda, J., Adachi, K., Halprin, K.M., Itami, S., Levine, V., and Woodyard, C. (1983). Forskolin Activates Adenylate Cyclase Activity and Inhibits Mitosis in In Vitro in Pig Epidermis. J. Investig. Dermatol. *81*, 236–240.

Taylor, C.M., Barker, W.D., Weir, C.A., and Park, J.H. (2002). Toward a General Strategy for the Synthesis of 3,4-Dihydroxyprolines from Pentose Sugars. J. Org. Chem. *67*, 4466–4474.

Tucker, J.A., Bennett, N., Brassington, C., Durant, S.T., Hassall, G., Holdgate, G., McAlister, M., Nissink, J.W.M., Truman, C., and Watson, M. (2012). Structures of the human poly (ADP-ribose) glycohydrolase catalytic domain confirm catalytic mechanism and explain inhibition by ADP-HPD derivatives. PLoS ONE *7*, e50889.

Vyas, S., Matic, I., Uchima, L., Rood, J., Žaja, R., Hay, R.T., Ahel, I., and Chang, P. (2014). Family-wide analysis of poly(ADP-ribose) polymerase activity. Nat. Commun. *5*, 7–13.

Wang, Q., and Schultz, B.D. (2014). Cholera toxin enhances Na+ absorption across MCF10A human mammary epithelia. Am. J. Physiol. Cell Physiol. *306*, C471–C484.

Wang, Y., An, R., Umanah, G.K., Park, H., Nambiar, K., Eacker, S.M., Kim, B., Bao, L., Harraz, M.M., Chang, C., et al. (2016). A nuclease that mediates cell death induced by DNA damage and poly(ADP-ribose) polymerase-1. Science *354*, aad6872–aad6872.

Zhen, Y., Zhang, Y., and Yu, Y. (2017). A Cell-Line-Specific Atlas of PARP-Mediated Protein Asp/Glu-ADP-Ribosylation in Breast Cancer. Cell Rep. *21*, 2326–2337.

Main Figure Titles

Figure 1. Design of PARG/ARH3 substrate. A. PAR is cleaved by PARG and ARH3 via hydrolysis of the glycosyl bond (red). B. Synthetic PARG/ARH3 substrates mimic ADP-ribose and release a chromophore or fluorophore upon hydrolysis. Synthesis of these compounds requires a late-stage pyrophosphate formation and 1,2-*cis* selective glycosylation.

Figure 2. Synthesis of **pNP-ADPr** and **TFMU-ADPr**. Abbreviations: ADDP = 1,1'-(azodicarbonyl)dipiperidine, DIAD = diisopropyl azodicarboxylate, Fm = 9H-fluorenylmethyl, DCI = 4,5-dicyanoimidazole, NCS = N-chlorosuccinimide, DBU = 1,8-diazabicycloundec-7-ene, TBS = tert-butyldimethylsilyl.

Figure 3. Molecular docking sugar nucleotides with hPARG and LchARH3 using Glide XP. A. ADPr (blue) and IDPr (yellow) are docking into hPARG (PDB: 5A7R). B. ADPr (blue) and IDPr (yellow) are docking into LchARH3 (PDB: 6G1Q). C. Synthesis of **TFMU-IDPr**; for **pNP-IDPr** synthesis please see Figure S2.

Figure 4. Michaelis-Menton kinetics of recombinantly expressed human PARG and ARH3. A. Kinetics of human PARG processing **TFMU-ADPr**. B. Kinetics of human ARH3 processing **TFMU-ADPr**. C. Selectivity of **TFMU-IDPr** for processing by human ARH3 over human PARG. Error bars indicate SEM, n = 3.

Figure 5. Measurement of PARG activity in cell lysate and validation of TFMU-IDPr selectivity. A. Selectivity for ARH3 by **TFMU-IDPr** validated by CRISPR-Cas9 knockout of ARH3 in U2OS cells. PARG activity was measured in the presence and absence of PARG inhibitor PDD00017273 using **TFMU-IDPr** at 200 µM. Error bars indicated SEM, n=3. Significance levels are given by asterisks: $p<0.05$ (*), $p<0.01$ (**), $p<0.001$ (***), $p>0.05$ (n.s.). B. Same as A but with 200 µM **TFMU-ADPr**. C. Validation of ARH3 knockout in U2OS as measured by Western blotting. D. Western blotting to determine ARH3 expression levels in various indicated cell lines; representative blot of two independent replicates shown, see Figure S4 for all replicates. E. Correlation of ARH3 expression (measured by Western blotting) with ARH3 activity (measured by **TFMU-IDPr** hydrolysis). Data points reflect average values from different mammalian cell lines. Red indicates MCF10A. ARH3 activity was measured with 200 µM **TFMU-IDPr**.

Figure 6. Selective inhibition of ARH3 by ADP-ribosylated arginine. A. Kinetics of inhibition of ARH3 by ADPr-Arg. B. Lineweaver-Burke plot of ADPr-Arg inhibition of ARH3. C. Selectivity of ADPr-Arg for ARH3 over hPARG is indicated by a shift in dose-response curve. D. Structure of ADPr-Arg.

Table 1. Kinetic parameters derived for ADP-ribosylhydrolase substrates.

Substate	Enzyme	K_M (µM)	V_{max} (µmol/min/mg)
TFMU-ADPr	hPARG[a]	66.2±15	0.84±0.05
	ttPARG[b]	210±13	28.6±0.6
	hARH3[c]	6.3±0.2	1.61±0.02
TFMU-IDPr	hPARG	>1500	n.d.
	ttPARG	>1500	n.d.
	hARH3	312±30	1.79±0.06
pNP-ADPr	ttPARG	210±10	16.9±0.5
	hARH3	3.2±0.6	1.7±0.1
pNP-IDPr	ttPARG	>1500	n.d.
	hARH3	410±20	5.2±0.2

[a]*H. sapiens* full length PARG
[b]*T. thermophila* PARG
[c]*H. sapiens* full length ARH3

STAR Methods

- **Key Resources Table**
- **Contact for Reagent and Resource Sharing**
- **Experimental Model and Subject Details**
    - **Cell Lines**
- **Methods Details**
    - **Buffer composition**
    - **In vitro Enzyme Kinetics**
    - **Cell Lysate ARH3 Activity Assay**
    - **ADP-ribosylated arginine enzymatic synthesis**
    - **Metabolic profiling**
    - **Recombinant protein expression and purification**
    - **Western blotting analysis**
    - **Molecular docking**
    - **General chemical synthesis**
    - **Synthesis of PARG substrates**
- **Quantification and Statistical Analysis**

KEY RESOURCES TABLE

REAGENT or RESOURCE	SOURCE	IDENTIFIER
Antibodies		
Mouse anti-ARH3	Santa Cruz Biotech	Cat# sc-374162
Rabbit anti-beta-actin	Cell Signaling	Cat# 4970
Rabbit anti-PARP1	Cell Signaling	Cat# 9542
HRP-conjugated goat anti-rabbit	Cell Signaling	Cat# 7074
HRP-conjugated horse anti-mouse	Cell Signaling	Cat# 7076
Chemicals, Peptides, and Recombinant Proteins		
TFMU-ADPr	This paper	
TFMU-IDPr	This paper	
pNP-ADPr	This paper	
pNP-IDPr	This paper	
ADPr-Arg	This paper	
ADP-HPD	Calbiochem	Cat# 118415
ADP-ribose	Sigma-Aldrich	Cat# A0752
PDD 00017273	Tocris	Cat# 5952
4-(trifluoromethyl)umbelliferone	Enamine Building Blocks	Cat# EN300-05279
4-nitrophenol	Sigma-Aldrich	Cat# 241326
2,3-di-(tert-butyldimethylsilyl)-5-(triphenylmethyl)-D-ribofuranose	(Lambrecht et al., 2015)	n/a
1,1'-(azodicarbonyl)dipiperidine	Accela ChemBio Inc.	Cat# SY001006
Diisopropyl azodicarboxylate	Sigma-Aldrich	Cat# 225541
Triphenylphosphine	Sigma-Aldrich	Cat# T84409

Tributylphosphine	Sigma-Aldrich	Cat# 90827
1,2-dimethoxyethane	GFS Chemicals	Cat# 2510
N,*N*-diisopropyl bis(9-methylfluorenyl)phosphoramidite	(Lambrecht et al., 2015)	n/a
4,5-Dicyanoimidazole	Sigma-Aldrich	Cat# 554030
N-chlorosuccinimide	Sigma-Aldrich	Cat# 109681
Triethylamine trihydrofluoride	Oakwood Chemical	Cat# 003029
L-Arginine	Sigma-Aldrich	Cat# A3784
NAD+	Sigma-Aldrich	Cat# N0632
Silicagel 60M	Macherey-Nagel	Cat# 815381.25P
Dowex 50Wx8	Sigma-Aldrich	Cat# 217514
Acetic Acid	Fisher Scientific	Cat# A38-212
Sodium Chloride	Fisher Scientific	Cat# S271-500
DTT	Sigma Aldrich	Cat# DTT-RO ROCHE
EDTA	Fisher Scientific	Cat# S311-100
Triton-X-100	Fisher Scientific	Cat# BP151-100
Sodium phosphate dibasic	EMD	Cat# SX0715-1
Potassium phosphate dibasic	VWR Analytical	Cat# BDH9266.500
Magnesium chloride	Fisher Scientific	Cat# M33
Glycine	Bio-Rad	Cat# 161-0718
2-mercaptoethanol	Sigma-Aldrich	Cat# M6250
Glycerol	Fisher Scientific	Cat# G33
Tween 20	Fisher Scientific	Cat# BP337
0.05% Trypsin	Corning	Cat# 25-052-CI
Protease Inhibitor Cocktail Set III, EDTA-free	Calbiochem	Cat# 539134
Fetal Bovine Serum	Gemini	Cat# 100-106
BSA	Research Products International Corp.	Cat# A30075-100.0
INTERFERin Transfection Agent	Polyplus	Cat# 409-10
Opti-MEM Media	ThermoFisher	Cat# 11058-021
Cholera Toxin from *Vibrio cholerae*	List Biological Labs	Cat# 100B
Binary Toxin from *Clostridium difficile*, Subunit A	List Biological Labs	Cat# 157A
Binary Toxin from *Clostridium difficile*, Subunit B	List Biological Labs	Cat# 157B
Pertussis Toxin from *B. pertussis*	List Biological Labs	Cat# 180
Ni-NTA	Qiagen	Cat# 30230
IPTG	Gold Biotechnology	Cat# 12481C100
Kanamycin	Research Products International	Cat# K22000
Ampicillin	Fisher Scientific	Cat# BP1760
Chloramphenicol	Sigma-Aldrich	Cat# C0378
Tris base	Fisher Scientific	Cat# BP152
Imidazole	Sigma-Aldrich	Cat# I202
Leupeptin	Sigma-Aldrich	Cat# L2884
Pepstatin A	Sigma-Aldrich	Cat# P4265
Aprotinin	Sigma-Aldrich	Cat# A1153
PMSF	Sigma-Aldrich	Cat# 78830
Human full-length PARG	(Barkauskaite et al., 2013; Tucker et al., 2012)	
T. thermophila PARG protein	(Dunstan et al., 2012)	

Human ARH3 protein	(Barkauskaite et al., 2013; Finch et al., 2012)	
Human ARH3 D77N/D78N protein	(Fontana et al., 2017)	
Human PARG catalytic domain wild type protein	(Tucker et al., 2012)	PARG26
Human PARG catalytic domain E756N protein	(Tucker et al., 2012)	
Critical Commercial Assays		
Pierce BCA Protein Assay Kit	ThermoFisher	Cat# 23227
SuperSignal West Pico	ThermoFisher	Cat# 34577
Penicillin/Streptomycin	Lonza	Cat# 17-602E
Mini-PROTEAN TGX 4-20% Precast Gel	Bio-Rad	Cat# 456-1093
SDS (Tris/Glycine) Buffer (10x)	Bio-Rad	Cat# 161-0732
Laemmili Sample Buffer	Bio-Rad	Cat# 161-0737
Restore Western Blot Stripping Buffer	ThermoFisher	Cat# 21059
Immobilon-P PVDF Transfer Membrane	EMD Millipore	Cat# IPV00010
Deposited Data		
Structure of Human PARG	(Lambrecht et al., 2015)	PDB:5A7R
Structure of *Latimeria chalumnae* ARH3	Unpublished	PDB:6G1Q
Experimental Models: Cell Lines		
Human: A549	ATCC	Cat# CCL-185, RRID:CVCL_0023
Human: CA46	From Tim Fan (University of Illinois, Urbana)	RRID:CVCL_1101
Human: HCT-116	ATCC	Cat# CCL-247, RRID:CVCL_0291
Human: HEK293TN	System Biosciences	Cat# LV900A-1
Human: HeLa	ATCC	Cat# CCL-2, RRID:CVCL_0030
Human: HepG2	ATCC	Cat# HB-8065, RRID:CVCL_0027
Mouse: MEF	From Navdeep Chandel (Northwestern University)	
Human: MIA PaCa-2	From David Boothman (Indiana University School of Medicine)	RRID:CVCL_0428
Human: U2OS	ATCC	Cat# HTB-96, RRID:CVCL_0042
Human: U2OS ARH3 KO	(Fontana et al., 2017)	
Human: U87	ATCC	Cat# HTB-14, RRID:CVCL_0022
Human: U937	ATCC	Cat# CRL-1593, RRID:CVCL_0007
Human: D54	From Gregory Riggins (Johns Hopkins)	RRID:CVCL_7185
Human: Daudi	ATCC	ATCC Cat# CCL-213, RRID:CVCL_0008
Human: HCC1937	ATCC	Cat# CRL-2336, RRID:CVCL_0290
Human: HCC38	ATCC	Cat# CRL-2314, RRID:CVCL_1267

Human: HFF-1	ATCC	Cat# SCRC-1041, RRID:CVCL_3285
Human: Hs578t	ATCC	Cat# HTB-126, RRID:CVCL_0332
Human: Jurkat	From Richard Hotchkiss (Washington University, St. Louis)	
Human: MCF7	ATCC	Cat# HTB-22, RRID:CVCL_0031
Human: MCF10A	ATCC	Cat# CRL-10317, RRID:CVCL_0598
Human: SK-MEL-5	ATCC	Cat# HTB-70, RRID:CVCL_0527
Human: T98G	ATCC	Cat# CRL-1690, RRID:CVCL_0556
Experimental Models: Organisms/Strains		
E. coli: Rosetta 2 (DE3)	Novagen	Cat# 71400
Recombinant DNA		
Plasmid: hARH3-pDEST	Hening Lin (Cornell University)	
Plasmid: hPARG-pColdTF	Ivan Ahel (Oxford University)	
Plasmid: ttPARG-pET28a	Ivan Ahel (Oxford University)	
Software and Algorithms		
Prism 6	GraphPad	
SoftMax Pro 6.4	Molecular Devices	Build 204720
ImageJ (FIJI)	NIH	http://imagej.net/Fiji/Downloads
Image Lab 4.1	Bio-Rad	
PyMOL	PyMOL Molecular Graphics System (built from source)	https://www.pymol.org/
Small Molecule Drug Discovery Suite	Schrödinger	Version 2018-1
Other		
CombiFlash Rf+	Teledyne Isco	Cat# 68-5230-022
SpectraMax Multi-mode Microplate Reader	Molecular Devices	Model# M3
ChemiDoc MP Imaging System	Bio-Rad	Cat# 170-8280
RediSep Rf C18 Gold 5.5g	Teledyne Isco	Cat# 69-2203-328
RediSep Rf C18 Gold 150g	Teledyne Isco	Cat# 69-2203-338
Zorbax Eclipse Plus C18 1.8µm 2.1x50mm	Agilent	Cat# 959741-902
Luna C18 5 µm 21.2x150mm	Phenomenex	Cat# 00F-4252-P0-AX
Digital Sonifier	Branson Ultrasonics	Model# S-450

Contact for Reagent and Resource Sharing

All requests for reagents and resources should be directed to the lead contact, Paul Hergenrother (hergenro@illinois.edu).

EXPERIMENTAL MODEL AND SUBJECT DETAILS

Cell Lines

A549, D54, HCC1937, HCC38, HCT-116, Jurkat, and U937 cells were grown in RPMI 1640 supplemented with 10% fetal bovine serum (Gemini) and 1% pen/strep. U2OS, Daudi, HEK293TN, HeLa, Hs578t, MEF, MIA PaCa-2, and SK-MEL-5 cells were grown in Dulbecco's modified Eagle's medium supplemented with 10% fetal bovine serum and 1% pen/strep. HFF-1 cells were grown in Dulbecco's modified Eagle's medium supplemented with 15% fetal bovine serum and 1% pen/strep. HepG2, MCF7, T98G, and U87 cells were grown in Eagle's Minimum Essential Medium supplemented with 10% fetal bovin serum and 1% pen/strep. MCF10A cells were grown in Dulbecco's modified Eagle's medium supplemented with 2% horse serum, 20 ng/mL EGF, 0.5 µg/mL hydrocortisone, 10 µg/mL insulin, 100 ng/mL cholera toxin, and 1% pen/strep. Phenol red was added to all media except for MCF10A as a pH indicator. All cells were cultured at 37°C in a 5% CO_2 environment. Media were prepared by the University of Illinois School of Chemical Sciences Cell Media Facility. Sex of cell lines: A549 (Male, 58 years old), CA46 (Male, age unknown), D54 (Female, age unknown), Daudi (Male, 16 years old), HCC1937 (Female, 23 years old), HCC38 (Female, 50 years old), HCT-116 (Male, age unknown), HEK293TN (Female, fetus), HeLa (Female, 31 years old), HepG2 (Male, 15 years old), HFF-1 (Male, newborn), Hs578t (Female, 74 years old), MCF7 (Female, 69 years old), MCF10A (Female, 36 years old), MEF (sex and age unknown), MIA PaCa-2 (Male, 65 years old), Jurkat (Male, 14 years old), SK-MEL-5 (Female, 24 years old), T98G (Male, 61 years old), U2OS (Female, 15 years old), U87 (Male, age unknown), U937 (Male, 37 years old).

METHOD DETAILS

Buffer Composition:

PARG Activity Lysis Buffer: 30 mM Tris (pH 7.5), 500 mM NaCl, 20% glycerol, 1% Triton X-100, 1:500 protease inhibitor cocktail

Lysate Activity Buffer: 50 mM K_2HPO_4 (pH 7.4), 50 mM KCl, 5 mM $MgCl_2$, 5 mM DTT

T. thermophila PARG reaction buffer: 50 mM K_2HPO_4, 50 mM KCl, 10 mM β-mercaptoethanol, pH 7.40

Human PARG reaction buffer: 50 mM K_2HPO_4, 50 mM KCl, 10 mM β-mercaptoethanol, pH 7.40

Human ARH3 reaction buffer: 50 mM Na_2HPO_4, 10 mM $MgCl_2$, 5 mM DTT, pH 7.40

PARG Purification Lysis buffer: 50 mM NaH_2PO_4, 300 mM NaCl, 10 mM imidazole, 0.5 mg/mL lysozyme, 1 ug/mL leupeptin, 1 ug/mL pepstatin A, 2 ug/mL aprotinin, 1 mM PMSF, pH 8.0

PARG Purification Wash buffer: 50 mM NaH_2PO_4, 300 mM NaCl, 10 mM imidazole, pH 8.0

PARG Purification Elution buffer: 50 mM NaH_2PO_4, 300 mM NaCl, 300 mM imidazole, pH 8.0

PARG Purification Dialysis buffer: 25 mM Tris, 50 mM NaCl, 1 mM DTT, 10% glycerol, pH 7.5

Towbin Transfer Buffer: 20% CH_3OH, 192 mM glycine, 50 mM Tris, pH 8.3

In vitro Enzyme Kinetics

10X dilutions of substrate were prepared from 10 mM stock solutions in MilliQ H_2O into reaction buffer. 5 µL 10X substrate was added to a 384-well plate. 45 µL 2.2 nM enzyme

solution in reaction buffer was added to a single column of the 384-well plate via 16-channel Matrix pipet. Plate was placed into plate reader. After shaking for 5 s, absorbance or fluorescence was recorded at 2 s intervals for 5 min. Initial reaction rates were determined by fitting the linear portions of reaction progress curves using SoftMax Pro 6.4. Initial rates were plotted against substrate concentration and fit to the Michaelis-Menton equation using a non-linear curve-fitting algorithm with GraphPad Prism 6. For pNP detection, plate reader was configured: absorbance at 405 nm. For TFMU detection, plate reader was configured: Excitation 385 nm, Cutoff 495 nm, Emission 502 nm, 6 reads/well, Low Gain.

Cell Lysate ARH3 Activity Assay

Cells were cultured in T75 flasks in appropriate medium. Cells were trypsinized, and scrapped (if necessary), and counted. $1x10^6$ cells were harvested and washed with cold PBS 2x. Cell pellet was lysed by addition of activity lysis buffer (150 μL) and incubated on ice for 30 min. Lysate was clarified by centrifugation at 14,300xg at 4°C for 10 min. Supernatant was transferred to chilled, empty 500 μL tube. Total protein content of lysate was evaluated by BCA assay. ARH3 expression level was determined by western blotting analysis. 5 μL lysate was added to well of 384-well black plate. 45 μL TFMU-IDPr (200 μM final) in reaction buffer was added to well. Reaction progress was monitored by fluorescent plate reader (ex 385 nm, cutoff 495, em 502 nm, 6 reads/well, high gain).

ADP-ribosylated arginine enzymatic synthesis

CTX (100 μL, 500μg/mL, 10μg/mL final) was added to 5 mL buffer (400 mM K_2HPO_4, 20 mM DTT, pH 7.2) containing 200 mM arginine and 10 mM NAD. Mixture was incubated at 37°C for 16 h. Protein was removed from reaction mixture by filtration through 3k MWCO spin filter. Filtrate was direction subjected to ion-pairing preparative HPLC using Luna C18 21.5x150mm column. Solvent A: 20 mM Et_3N•HOAc (pH 7.2), solvent B: acetonitrile. Gradient (A:B, 20 mL/min): 98:2, 0 min; 98:2, 2 min; 75:25, 16 min; 75:25, 23 min; 40:60, 27 min, 40:60, 30 min. ADP-ribosylated arginine eluted at ~5 min as two separate anomers. Individual anomers gradually interconverted in ~1 h, so characterization and inhibition experiments were performed with mixture of anomers. Product-containing fractions were determined by LCMS and lyophilized to yield flocculent white solid (7.8 mg, 21%). ^{1}H NMR was consistent with previous reports (Oppenheimer, 1978).

Metabolic profiling

Six-well plates were seeded with cells at 3x105 cells/well. When cells were ~80% confluent, cells were treated with 100 ng/mL CTX for 6 h. Cells were washed with PBS once and detached with trypsin, quenching trypsin with media with 10% FBS. Cell viability was verified by Trypan Blue exclusion. Cells were centrifuged at 400xg at 4°C for 4 min and washed with PBS twice. Cell pellets were resuspended with cold 70:30 methanol:water and placed on ice. Cell suspension was sonicated on ice (20%, 10 s on, 10 s off, 30 s total) and continued to be incubated on ice for 30 min. Lysate was clarified by centrifugation at 14,300xg at 4°C for 30 min. Supernatent was transferred to an empty 0.5 mL tube and stored at -80°C until analysis. Samples were analyzed with the 5500 QTRAP LC/MS/MS system (Sciex, Framingham, MA) in Metabolomics Lab of Roy J. Carver Biotechnology Center, University of Illinois at Urbana-Champaign. Software Analyst 1.6.2 was used for data acquisition and analysis. The 1200 series HPLC system (Agilent Technologies, Santa Clara, CA) includes a degasser, an autosampler, and a binary pump. The LC separation was performed on an Agilent SB-Aq (4.6

x 50mm, 5µm) with mobile phase A (0.1% formic acid in water) and mobile phase B (0.1% formic acid in acetontrile). The flow rate was 0.3 mL/min. The linear gradient was as follows: 0-3min, 100%A; 5-10min, 2%A; 11-15min, 100%A. The autosampler was set at 10°C. The injection volume was 5 µL. Mass spectra were acquired under positive electrospray ionization (ESI) with the ion spray voltage of +5500 V. The source temperature was 450 °C. The curtain gas, ion source gas 1, and ion source gas 2 were 36, 65, and 60, respectively. Multiple reaction monitoring (MRM) was used for quantitation: Arg m/z 175.1 --> m/z 70.1; ADP-Arg m/z 716.2 --> m/z 428.1; cAMP m/z 330.2 --> 232.0; ADP-ribose m/z 560.1 --> m/z 348.1; NAD m/z 664.2 --> m/z 136. Limit of quantitation (LOQ) for the compounds were: 10 ng/mL ADPr-Arg, 10 ng/mL ADP-ribose, 10 ng/mL arginine, 20 ng/mL cAMP, and 100 ng/mL NAD^+.

Recombinant Protein Expression and Purification

Human ARH3 was expressed as previously described (Barkauskaite et al., 2013; Finch et al., 2012). Briefly, human ARH3 cloned into a pDEST vector with an N-terminal His_6-tag was obtained from Hening Lin (Cornell University, Cornell, NY) was transformed into Rosetta2 (DE3) *E. coli* cells. 500 mL culture of LB (100 µg/mL ampicillin and 20 µg/mL chloramphenicol) was inoculated with 10 mL of overnight culture. The culture was grown at 37°C to mid-log phase (OD_{600} = 0.5) and cooled to 18°C. Protein expression was induced with 0.1 mM IPTG for 18 h and harvested. Pellet was resuspended in 13 mL lysis buffer and lysed by sonication. Lysate was clarified by centrifugation (35,000xg, 30 min, 4°C). Supernatent was purified on Ni-NTA beads by batch protocol. Fractions containing pure protein were combined, dialyzed, and stored at -80°C. Protein concentration was determined by BCA assay.

T. thermophila PARG enzyme was expressed using a modified protocol a previously reported (Dunstan et al., 2012). Briefly, *T. thermophila* PARG2 cloned into a pET28a vector was obtained from Ivan Ahel (University of Oxford, Oxford, UK) and transformed into Rosetta2 (DE3) *E. coli*. 500 mL culture of LB (100 µg/mL kanamycin and 20 µg/mL chloramphenicol) was inoculated with 10 mL of overnight culture. The culture was grown to mid-log phase (OD_{600} = 0.7). Culture was induced with 0.3 mM IPTG at 30°C for 3 h and harvested. Pellet was resuspended in 13 mL lysis buffer and lysed by sonication. Lysate was clarified by centrifugation. Protein was purified on Ni-NTA beads by batch protocol. Fractions containing pure protein were combined, dialyzed, and stored at -80°C. Protein concentration was determined by BCA assay.

Human PARG cloned into a pColdTF vector was obtained from Ivan Ahel (University of Oxford, Oxford, UK) and transformed into Rosetta2 (DE3) *E. coli*. Culture of Terrific Broth supplemented with appropriate antibiotics was grown to an OD_{600} = 0.6-0.8 at 37°C. Culture was induced with 0.1 mM IPTG at 18°C for 16 h and harvested. Pellet was resuspended in lysis buffer (40 mM HEPES, 300 mM NaCl, 20 mM imidazole, 10% glycerol, 1 mM TCEP, pH 8.0) supplemented with benzonase, lysozyme and protease inhibitor (Roche Complete EDTA-free protease inhibitor tablet) and lysed by freeze/thaw. Lysate was clarified by centrifugation. Protein was purified on Ni-NTA beads by batch and eluted with lysis buffer supplemented with 500 mM imidazole.

Western blot analysis

Samples loading was normalized based on total protein content as assessed by BCA assay and subjected to SDS-PAGE. Protein was transferred to PVDF membranes (Merck Millipore). Membranes were cut along molecular weight markers and then blocked with TBS-T buffer (25

mM Tris-HCl, 150 mM NaCl, 0.05% Tween 20, pH 7.5) supplemented with either 5% BSA (PARP1) or 5% non-fat dried milk (ARH3) for 1 h. Membrane strips were incubated overnight with primary antibodies in blocking buffer at 4°C with gentle rocking. Membranes were washed 3x with TBS-T and incubated with HRP-conjugated secondary antibody in TBS-T for 1 h. Membranes were washed 3x with TBS-T, developed using SuperSignal West Pico and imaged using a ChemiDoc MP system. Membrane strip containing ARH3 bands was stripped and reimaged with anti-actin antibody. Dilutions for antibodies were: anti-PARP1 (1:3000), anti-ARH3 (1:1000), anti-actin (1:3000), anti-rabbit (1:3000), and anti-mouse (1:3000). Band quantification was performed using FIJI.

Molecular docking

Protein and ligand preparation, docking, and scoring was performed using the Schrodinger Suite 2018-1. Proteins were prepared using the Protein Prep Wizard using standard settings with pH set to 7.4. Receptor grids were generated based on bound ADP-ribose. Additional positional constraints were applied so that the nucleobase occupies the adenine binding site and the ribose ring occupies the active site. Sugar nucleotide protonation state and tautomer form was determined using LigPrep. Docking was performed with Glide using both standard precision (SP) and extra precision (XP). Docking poses were exported and rendered using PyMOL.

General chemical synthesis

All reactions were run in flame or oven dried glassware under and atmosphere of dry nitrogen unless otherwise noted. Acetonitrile, tetrahydrofuran, methanol, dimethylformamide, toluene, and methylene chloride using in reactions were obtained from a solvent dispensing system. 4 Å molecular sieves were dried at 150°C on high vacuum overnight. Pyridine, diazabicyclo[5.4.0]undec-7-ene, diisopropylethylamine, and trimethylamine were distilled from CaH_2 and stored on 4 Å sieves. All other reagents were of standard commercial purity and were used as received. Analytical thin-layer chromatography was performed on EMD Merck silica gel plates with F254 indicator. Plates were visualized with UV light (254 nm) or staining with p-anisaldehyde. Silica gel for column chromatography was purchased from Macherey-Nagel (40-63 μm particle size).

Unless otherwise indicated, ^{1}H, ^{13}C, ^{19}F, and ^{31}P NMR spectra were recorded at 500, 126, 470, and 202 MHz, respectively. ^{1}H and ^{13}C NMR spectra were referenced to the residual solvent peak. ^{19}F NMR spectra were referenced using absolute referencing based on 1H spectra. ^{31}P NMR spectra were externally referenced to 85% H_2PO_4 (0.00 ppm) in water. Chemical shits are reported in ppm and multiplicities are reported as s (singlet), d (doublet), t (triplet), q (quartet), p (pentet), h (hextet), m (multiplet), and br (broad). For annotated NMR spectra see Data File S1. Mass spectrometry analysis was performed by the University of Illinois Mass Spectrometry Center.

Preparative C18 chromatography was performed using a Teledyne Isco Combiflash Rf system with RediSep Gold columns. Silyl ether protected intermediates were separated using a gradient of H_2O/CH_3CN beginning with 95% H_2O:5% CH_3CN, ramping to 65% H_2O:35% CH_3CN over 6 min, ramping to 100% CH_3CN over 6 min, and holding 100% CH_3CN for 5 min. Unprotected substrates were separated using a gradient of 10 mM Et_3N•HOAc (pH 7.2)/CH_3CN

beginning with 100% buffer, ramping to 15% buffer:85% CH_3CN over 10 min, ramping to 50% buffer:50% CH_3CN over 6 min, and holding 50% buffer:50% CH_3CN for 4 min.

Synthesis of PARG substrates

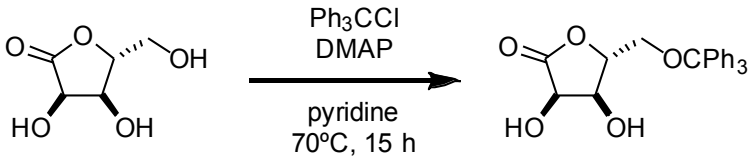

D-ribonic acid γ-lactone **S1**

5-*O*-trityl-D-ribono-1,4-lactone (S1): Synthesized with modification of previous report (Taylor et al., 2002). Specifically, to a 250 mL round bottom flask was added D-ribonic acid γ-lactone (2.15 g, 14.5 mmol, 1 eq), 4-dimethylaminopyridine (360 mg, 2.9 mmol, 0.2 eq), and pyridine (42 mL). Once fully dissolved, triphenylmethyl chloride (4.86 g, 17.4 mmol, 1.2 eq) was added as a solid in one portion to the stirring reaction mixture at room temperature. The solution was stirred at 70°C for 16 h. The cooled reaction mixture was diluted with dichloromethane and washed with 1 M HCl twice and satd aq $NaHCO_3$ once. The organic layer was dried over $MgSO_4$, filtered through a pad of celite, and concentrated *in vacuo*. The residue was purified by silica gel chromatography, eluting with 1:1 hexanes-EtOAc, yielding compound **S1** as a white solid (5.0 g, 88%).

^{1}H NMR (500 MHz, DMSO-d_6) δ 7.41 – 7.24 (m, 15H), 5.93 (d, J = 7.6 Hz, 1H), 5.45 (d, J = 4.0 Hz, 1H), 4.54 (dd, J = 7.6, 5.5 Hz, 1H), 4.39 – 4.34 (m, 1H), 4.02 (ddd, J = 5.3, 4.0, 1.2 Hz, 1H), 3.41 – 3.33 (m, 1H), 3.14 (dd, J = 11.0, 3.8 Hz, 1H).

^{13}C NMR (126 MHz, DMSO-d_6) δ 176.2, 143.2, 128.2, 128.1, 127.3, 86.7, 83.4, 69.4, 68.6, 63.0.

HRMS (ESI-TOF) m/z: $[M+Na]^+$ Calcd for $C_{24}H_{22}O_5Na$ 413.1365; Found 413.1362

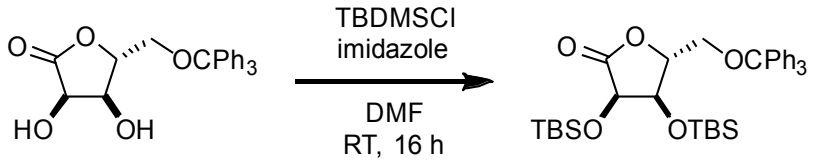

S1 **S2**

2,3-bis-*O*-tert-butyldimethylsilyl-5-*O*-trityl-D-ribono-1,4-lactone (S2): Synthesized with modification of previous reports (Taylor et al., 2002). Specifically, to a 100 mL round bottom flask was added **S1** (2.0 g, 5.1 mmol, 1 eq), imidazole (1.9 g, 27 mmol, 5 eq), and dimethylformamide (20 mL). The solution was cooled to 0°C. Tert-butyldimethylsilyl chloride (2.9 g, 19 mmol, 4 eq) was added as a solid in one portion. Solution was allowed to warm to room temperature and was stirred for 16 h. Reaction mixture was diluted with diethyl ether and quenched with the addition of satd aq NH_4Cl. Organic layer was washed with satd aq $NaHCO_3$ thrice and brine once. Organic layer was dried over Na_2SO_4, filtered, and concentrated. Residue was purified by silica gel chromatography, eluting with 5% Et_2O-hexane, to yield compound **S2** as a white foam (3.1 g, 97%).

^{1}H NMR (500 MHz, $CDCl_3$) δ 7.40 (d, *J* = 8.4 Hz, 6H), 7.31 (t, *J* = 7.6 Hz, 6H), 7.25 (t, *J* = 7.1 Hz, 3H), 4.68 (d, *J* = 5.2 Hz, 1H), 4.29 (t, *J* = 3.0 Hz, 1H), 3.95 (dd, *J* = 5.2, 1.1 Hz, 1H), 3.62 (dd, *J* = 11.0, 3.7 Hz, 1H), 3.21 (dd, *J* = 11.0, 2.8 Hz, 1H), 0.93 (s, 9H), 0.80 (s, 9H), 0.18 (s, 3H), 0.11 (s, 3H), 0.01 (s, 3H), -0.06 (s, 3H).

^{13}C NMR (126 MHz, $CDCl_3$) δ 175.27, 143.19, 128.63, 128.18, 127.49, 84.70, 77.16, 72.16, 70.44, 62.39, 25.96, 25.75, 18.51, 18.20, -3.45, -4.47, -4.70, -5.04.

HRMS (ESI-TOF) m/z: $[M+Na]^+$ Calcd for $C_{36}H_{50}O_5Si_2Na$ 641.3094; Found 641.3093

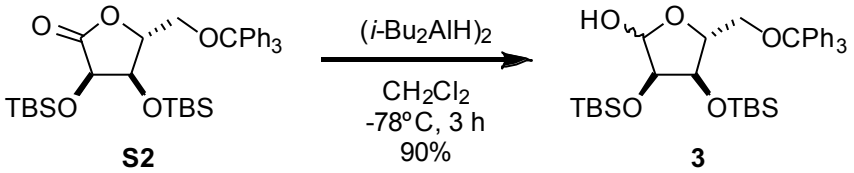

S2 **3**

2,3-bis-*O*-tert-butyldimethylsilyl-5-*O*-trityl-D-ribose (3): A 1 M solution of (i-$Bu_2AlH)_2$ in hexane (17.5 mL, 17.5 mmol, 1.5 eq) was added dropwise via addition funnel over 5 min to a stirring solution of **S2** (7.25 g, 11.7 mmol, 1 eq) in CH_2Cl_2 (120 mL) at -78 °C. The resulting solution was stirred at -78 °C for 3 h. Reaction was quenched with the addition of CH_3OH (4 mL) added dropwise via addition funnel and allowed to warm to 0 °C. After stirring for 30 min, 200 mL 0.5 M potassium sodium tartrate was added and mixture was stirred until aluminum salts were fully dissolved. Extracted mixture with CH_2Cl_2 three times. The combined organic layers were dried over $MgSO_4$, filtered through a pad of celite, and concentrated. The residue was purified by silica gel chromatography, eluting with 10% Et_2O-hexanes, to yield an interconverting mixture of diastereomers of compound **3** as a white foam (6.5 g, 90%).

β anomer (major)
^{1}H NMR (500 MHz $CDCl_3$) δ 7.50 – 7.43 (m, 6H), 7.35 – 7.30 (m, 6H), 7.29 – 7.24 (m, 3H), 5.13 (dd, *J* = 11.4, 4.3 Hz, 1H), 4.24 (d, *J* = 11.4 Hz, 1H), 4.16 (t, *J* = 4.5 Hz, 1H), 3.92 (d, *J* = 4.6 Hz, 1H), 3.26 (dd, *J* = 10.4, 4.9 Hz, 1H), 3.11 (dd, *J* = 10.4, 3.3 Hz, 1H), 0.93 (s, 9H), 0.85 (s, 9H), 0.13 (s, 3H), 0.10 (s, 3H), 0.04 (s, 3H), -0.02 (s, 3H)

α anomer (minor)
^{1}H NMR (500 MHz $CDCl_3$) δ 7.50 – 7.43 (m, 6H), 7.35 – 7.30 (m, 6H), 7.29 – 7.24 (m, 3H), 5.19 (d, *J* = 4.6 Hz, 1H), 4.40 (dd, *J* = 7.3, 4.0 Hz, 1H), 4.20 (t, *J* = 4.0 Hz, 1H), 4.11 (ddd, *J* = 7.0, 3.8, 2.6 Hz, 1H), 3.97 (d, *J* = 4.1 Hz, 1H), 3.49 (dd, *J* = 10.3, 2.7 Hz, 1H), 3.10 (dd, *J* = 10.2, 3.9 Hz, 1H), 2.71 (d, *J* = 4.6 Hz, 1H), 0.91 (s, 9H), 0.75 (s, 9H), 0.11 (s, 3H), 0.09 (s, 3H), -0.03 (s, 3H), -0.19 (s, 3H)

Both anomers
^{13}C NMR (126 MHz, $CDCl_3$) δ 143.80, 129.01, 128.77, 128.01, 127.95, 127.26, 127.23, 102.19, 97.90, 87.05, 87.01, 84.43, 81.78, 77.06, 74.56, 72.58, 71.74, 63.77, 63.31, 26.06, 25.96, 25.92, 25.86, 18.42, 18.26, 18.11, 18.09, -4.08, -4.29, -4.46, -4.49, -4.55, -4.67, -4.90, -4.94.

HRMS (ESI-TOF) m/z: $[M+Na]^+$ Calcd for $C_{36}H_{52}O_5NaSi_2$ 643.3251; Found 643.3251

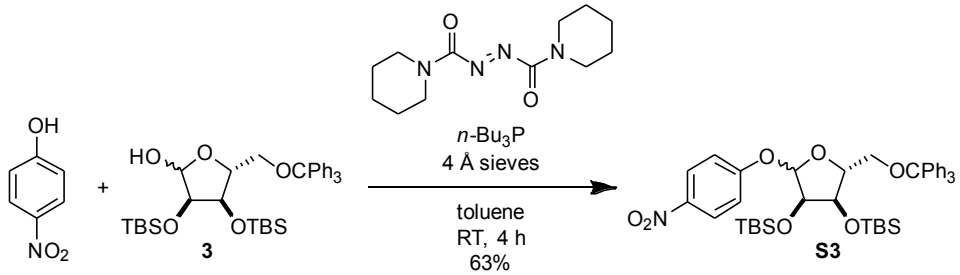

4-nitrophenyl 2,3-bis-*O*-tert-butyldimethylsilyl-5-*O*-trityl-D-ribofuranoside (S3): To a 250 mL round bottom flask, were added **3** (3.80 g, 6.11 mmol, 1 eq), 4-nitrophenol (2.51 g, 18.1 mmol, 3 eq), 4 Å molecular sieves (200 mg), and toluene (100 mL). Cooled mixture to 0 °C. Added n-Bu_3P (3.80 mL, 0.81 g/mL, 3.1 g, 15 mmol, 2.5 eq) dropwise via syringe. Added 1,1'-(azodicarbonyl)dipiperidine as a solid in one portion. Mixture was stirred at 0 °C for 30 min and then allowed to warm to room temperature and stirred for an additional 4 h. The reaction mixture was cooled to 0 °C, and 30% H_2O_2 (5 mL) was added to fully quench phosphine. After stirring for 30 min, the reaction mixture was diluted with hexane (100 mL). The resulting yellow precipitate was removed by filtration through a pad of celite. The filtrate was washed with satd aq $NaHCO_3$ five times, dried over Na_2SO_4, filtered, and concentrated. The residue was

purified by silica gel chromatography, eluting with 5% Et_2O-hexanes, to yield compounds **S3** (a mixture of anomers, α:β 69:31) as a pale yellow foam (2.87 g, 63%).

α-anomer
^{1}H NMR (500 MHz, $CDCl_3$) δ 8.21 (d, *J* = 9.0 Hz, 2H), 7.48 – 7.43 (m, 6H), 7.32 (t, *J* = 7.7 Hz, 6H), 7.29 – 7.24 (m, 3H), 7.13 (d, *J* = 9.3 Hz, 2H), 5.65 (d, *J* = 4.1 Hz, 1H), 4.38 (t, *J* = 4.7 Hz, 1H), 4.18 (q, *J* = 3.0 Hz, 1H), 4.05 (dd, *J* = 5.2, 2.2 Hz, 1H), 3.42 (dd, *J* = 10.5, 3.5 Hz, 1H), 3.12 (dd, *J* = 10.6, 3.1 Hz, 1H), 0.92 (s, 9H), 0.84 (s, 9H), 0.09 (s, 3H), 0.08 (s, 3H), 0.04 (s, 3H), -0.12 (s, 3H).

^{13}C NMR (126 MHz, $CDCl_3$) δ 162.98, 143.82, 142.01, 128.79, 128.04, 127.33, 125.94, 116.35, 100.21, 86.98, 86.66, 73.83, 72.23, 63.43, 26.00, 25.86, 18.44, 18.17, -4.37, -4.39, -4.40, -4.73.

HRMS (ESI-TOF) m/z: $[M+Na]^+$ Calcd for $C_{42}H_{55}NO_7Si_2Na$ 764.3415; Found 764.3413

β-anomer
^{1}H NMR (500 MHz, $CDCl_3$) δ 8.20 (d, *J* = 9.2 Hz, 2H), 7.38 – 7.33 (m, 6H), 7.20 – 7.13 (m, 11H), 5.59 (d, *J* = 1.4 Hz, 1H), 4.41 (dd, *J* = 6.9, 4.1 Hz, 1H), 4.30 (dd, *J* = 4.1, 1.4 Hz, 1H), 4.23 (ddd, *J* = 6.9, 4.1, 2.6 Hz, 1H), 3.38 (dd, *J* = 10.6, 2.7 Hz, 1H), 3.00 (dd, *J* = 10.6, 4.2 Hz, 1H), 0.92 (s, 9H), 0.76 (s, 9H), 0.13 (s, 3H), 0.13 (s, 3H), 0.02 (s, 3H), -0.16 (s, 3H).

^{13}C NMR (126 MHz, $CDCl_3$) δ 162.09, 143.74, 142.27, 128.82, 127.75, 127.09, 125.87, 116.26, 105.06, 86.55, 83.33, 76.60, 71.64, 62.95, 25.92, 25.89, 18.26, 18.11, -3.99, -4.28, -4.38, -4.86.

HRMS (ESI-TOF) m/z: $[M+Na]^+$ Calcd for $C_{42}H_{55}NO_7Si_2Na$ 764.3415; Found 764.3414

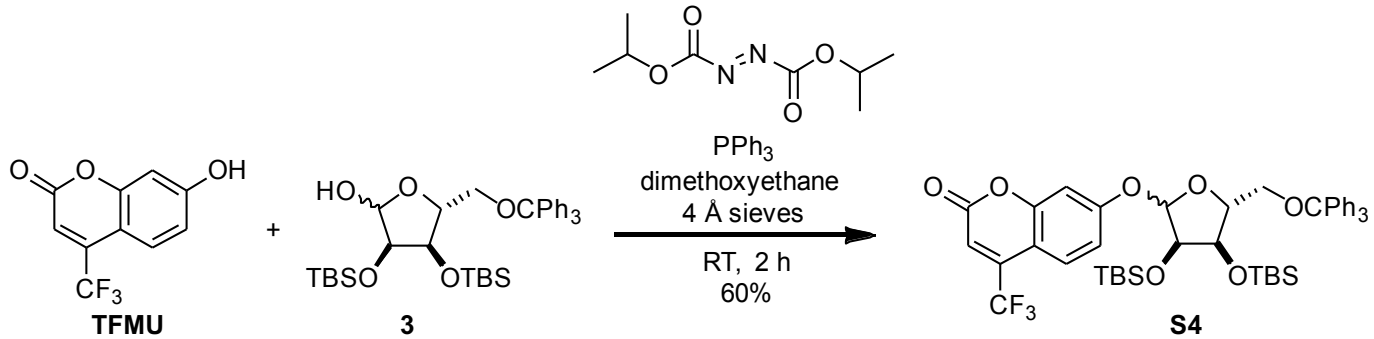

TFMU **3** **S4**

4-(trifluoromethyl)umbellifer-7-yl 2,3-bis-*O*-tert-butyldimethylsilyl-5-*O*-trityl-D-ribofuranoside (S4)
A 100 mL round bottom flask was charged with 4-(trifluoromethyl)umbelliferone (1.69 g, 7.36 mmol, 1.5 eq), 2,3-di-(tert-butyldimethylsilyl)-5-(triphenylmethyl)-D-ribofuranose (**3**) (3.05 g, 4.91 mmol, 1 eq), triphenylphosphine (1.93 g, 7.37 mmol, 1.5 eq), and 4 Å molecular sieves (600 mg). Material was dissolved in dimethoxyethane (35 mL) and stirred for 15 min at room temperature. DIAD (1.45 mL, 7.36 mmol, 1.5 eq) was added dropwise. Reaction mixture was stirred at room temperature for 2 hours and then poured into hexane (400 mL). Resulting precipitate was removed by filtration. Filtrate was washed with satd aq $NaHCO_3$ 4x. Organic phase was dried over Na_2SO_4 and evaporated. Residue was purified by silica gel (5% Et_2O:hexane) to give **S4** (2.47 g, 60%) as a mixture of anomers. While anomers were could be separated by silica gel chromatography, the mixture of diastereomers was routinely carried into the next step as they were more easily separable with the trityl group removed.

α-anomer
^{1}H NMR (500 MHz, $CDCl_3$) δ 7.55 (dt, *J* = 9.1, 1.9 Hz, 1H), 7.39 – 7.34 (m, 6H), 7.27 – 7.21 (m, 6H), 7.20 – 7.15 (m, 3H), 7.03 (d, *J* = 2.3 Hz, 1H), 6.95 (dd, *J* = 9.0, 2.4 Hz, 1H), 6.54 (s, 1H), 5.55 (d, *J* = 4.2 Hz, 1H), 4.31 (dd, *J* = 5.3, 4.3 Hz, 1H), 4.08 (q, *J* = 3.1 Hz, 1H), 3.96 (dd, *J* = 5.2, 1.9 Hz, 1H), 3.32

(dd, *J* = 10.6, 3.4 Hz, 1H), 3.03 (dd, *J* = 10.6, 3.1 Hz, 1H), 0.83 (s, 9H), 0.75 (s, 9H), -0.00 (s, 6H), -0.05 (s, 3H), -0.21 (s, 3H).

^{13}C NMR (126 MHz, $CDCl_3$) δ 161.79, 159.62, 156.25, 143.83, 141.75 (q, $^2J_{CF}$ = 32.8 Hz), 128.79, 128.07, 127.34, 126.43 (d, $^3J_{CF}$ = 2.3 Hz), 121.79 (q, $^1J_{CF}$ = 275.5 Hz), 114.85, 112.50 (q, $^3J_{CF}$ = 5.7 Hz), 107.61, 104.46, 100.23, 87.03, 86.87, 73.87, 72.25, 63.49, 26.01, 25.85, 18.44, 18.16, -4.37, -4.41, -4.43, -4.72.

^{19}F NMR (471 MHz, $CDCl_3$) δ -64.68.

β-anomer

^{1}H NMR (500 MHz, $CDCl_3$) δ 7.50 (dq, *J* = 8.9, 1.8 Hz, 1H), 7.25 – 7.20 (m, 6H), 7.06 – 7.01 (m, 10H), 6.99 (dd, *J* = 9.0, 2.5 Hz, 1H), 6.48 (s, 1H), 5.45 (d, *J* = 1.3 Hz, 1H), 4.32 (dd, *J* = 6.9, 4.0 Hz, 1H), 4.17 (dd, *J* = 4.1, 1.4 Hz, 1H), 4.09 (dt, *J* = 6.8, 3.3 Hz, 1H), 3.30 (dd, *J* = 10.6, 2.8 Hz, 1H), 2.86 (dd, *J* = 10.7, 3.8 Hz, 1H), 0.80 (s, 9H), 0.63 (s, 9H), 0.00 (s, 3H), 0.00 (s, 3H), -0.11 (s, 3H), -0.28 (s, 3H).

^{13}C NMR (126 MHz, $CDCl_3$) δ 160.98, 159.37, 156.10, 143.77, 141.55 (q, $^2J_{CF}$ = 32.7 Hz), 128.85, 127.75, 127.07, 126.43 (q, $^3J_{CF}$ = 2.4 Hz), 121.70 (q, $^1J_{CF}$ = 275.6 Hz), 114.14, 112.96 (q, $^3J_{CF}$ = 5.7 Hz), 107.92, 105.19, 104.79, 86.55, 83.32, 76.62, 71.46, 62.51, 25.93, 25.90, 18.27, 18.11, -3.98, -4.28, -4.37, -4.84.

^{19}F NMR (471 MHz, $CDCl_3$) δ -64.75.

HRMS (ESI-TOF) m/z: $[M+Na]^+$ Calcd for $C_{46}H_{55}O_7F_3NaSi_2$ 855.3336; Found 855.3342.

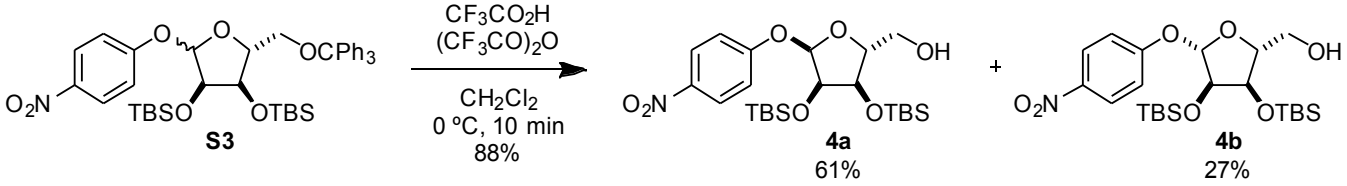

4-nitrophenyl 2,3-bis-*O*-tert-butyldimethylsilyl-D-ribofuranoside (4): To a stirring solution of compound **S3** (5.26 g, 7.09 mmol, 1 eq) in dichloromethane (60 mL) at 0 °C was added trifluoroacetic anhydride (4.00 mL, 1.487 g/mL, 5.95 g, 28.3 mmol, 4 eq) as a 2 M solution in CH_2Cl_2 dropwise via addition funnel. Trifluoroacetic acid (1.6 mL, 1.489 g/mL, 2.38 g, 20.9 mmol, 3 eq) was added as a 2 M solution in CH_2Cl_2 dropwise via addition funnel. Reaction was stirred at room temperature for another 10 min. Reaction mixture was quenched with the addition of Et_3N (4 mL, 0.7255 g/mL, 2.9 g, 29 mmol, 4.1 eq) followed by CH_3OH (30 mL). Mixture was stirred for an additional 15 min at room temperature before being diluted with H_2O. Extracted three times with CH_2Cl_2. Combined organic layers were dried over Na_2SO_4 and concentrated *in vacuo*. Resulting residue was purified by silica gel chromatography (5:1 Hexane:EtOAc) to yield compound **4a** (2.15 g, 61%) and compound **4b** (0.96 g, 27%) .

α-anomer (4a)

^{1}H NMR (500 MHz, $CDCl_3$) δ 8.17 (d, *J* = 9.2 Hz, 2H), 7.10 (d, *J* = 9.3 Hz, 2H), 5.60 (d, *J* = 3.6 Hz, 1H), 4.20 – 4.15 (m, 3H), 3.81 (ddd, *J* = 12.2, 4.5, 2.5 Hz, 1H), 3.67 (ddd, *J* = 12.3, 7.0, 3.1 Hz, 1H), 1.94 (dd, *J* = 7.4, 4.5 Hz, 1H), 0.91 (s, 18H), 0.12 (s, 3H), 0.09 (s, 3H), 0.07 (s, 6H).

^{13}C NMR (126 MHz, $CDCl_3$) δ 162.65, 142.13, 125.91, 116.34, 100.21, 86.99, 77.16, 73.96, 71.45, 62.32, 25.96, 25.90, 18.42, 18.20, -4.30, -4.39, -4.40, -4.71.

HRMS (ESI-TOF) m/z: $[M+Na]^+$ Calcd for $C_{23}H_{41}NNaO_7Si_2$ 522.2314; Found 522.2297

β-anomer (4b)

^{1}H NMR (500 MHz, $CDCl_3$) δ 8.15 (d, *J* = 9.2 Hz, 2H), 7.07 (d, *J* = 9.2 Hz, 2H), 5.46 (d, *J* = 1.3 Hz, 1H), 4.36 (dd, *J* = 7.0, 4.1 Hz, 1H), 4.21 (dd, *J* = 4.2, 1.3 Hz, 1H), 4.15 (dt, *J* = 6.7, 3.1 Hz, 1H), 3.80 (ddd, *J* = 12.5, 4.4, 2.7 Hz, 1H), 3.54 (ddd, *J* = 12.4, 8.8, 3.5 Hz, 1H), 1.68 (dd, *J* = 8.8, 4.3 Hz, 1H), 0.91 (s, 9H), 0.91 (s, 9H), 0.13 (s, 6H), 0.10 (s, 3H).

^{13}C NMR (126 MHz, $CDCl_3$) δ 161.52, 142.47, 125.92, 116.23, 105.00, 84.24, 77.16, 76.85, 70.72, 61.21, 25.94, 25.85, 18.20, 18.17, -4.15, -4.45, -4.46, -4.90.

HRMS (ESI-TOF) m/z: $[M-H]^-$ Calcd for $C_{23}H_{40}NO_7Si_2$ 498.2343; Found 498.2336

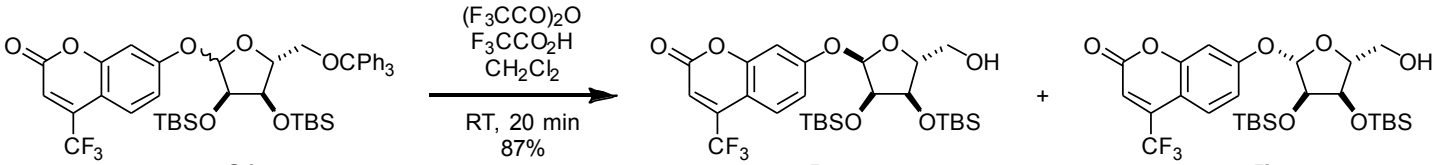

S4 | **5a** 40% | **5b** 47%

4-(trifluoromethyl)umbellifer-7-yl 2,3-bis-*O*-tert-butyldimethylsilyl-D-ribofuranoside (5)

To a 100 mL-RBF equipped with addition funnel was added **S4** (2.31 g, 2.77 mmol) and dichloromethane (24 mL). Trifluoroacetic anhydride (1.56 mL, 11.0 mmol, 4 eq) diluted with 5 mL of dichloromethane was added to stirring solution via addition funnel at room temperature. Trifluoroacetic acid (0.64 mL, 8.4 mmol, 3 eq) diluted with 5 mL of dichloromethane was added to stirring solution dropwise. Reaction mixture was stirred at room temperature for 20 min. Reaction mixture was neutralized by addition of neat triethylamine (5.0 mL, 36 mmol, 13 eq) via addition funnel followed by methanol (10 mL). Fuming mixture was stirred for 30 min and poured into satd aq NH_4Cl. Layers were separated and aqueous layer extracted 3x with dichloromethane. Combined organic layers were dried over Na_2SO_4, filtered, and evaporated. Residue was purified by silica gel chromatography (6:1 hexane:EtOAc) to give separable anomers **5a** (658 mg, 40%) and **5b** (767 mg, 47%) as white solids.

α-anomer (**5a**)

^{1}H NMR (600 MHz, $CDCl_3$) δ 7.63 (dd, *J* = 9.0, 1.8 Hz, 1H), 7.09 (d, *J* = 2.4 Hz, 1H), 7.03 (dd, *J* = 9.0, 2.4 Hz, 1H), 6.62 (s, 1H), 5.60 (d, *J* = 3.7 Hz, 1H), 4.22 – 4.14 (m, 3H), 3.81 (dd, *J* = 12.3, 2.7 Hz, 1H), 3.67 (dd, *J* = 12.2, 3.1 Hz, 1Hf), 1.82 (bs, 1H), 0.920 (s, 9H), 0.918 (s, 9H), 0.12 (s, 3H), 0.09 (s, 3H), 0.08 (s, 3H), 0.08 (s, 3H).

^{13}C NMR (151 MHz, $CDCl_3$) δ 161.44, 159.55, 156.17, 141.73 (q, $^2J_{CF}$ = 32.72 Hz), 126.49 (q, $^3J_{CF}$ = 2.40 Hz), 121.74 (q, $^1J_{CF}$ = 275.62 Hz), 114.80, 112.68 (q, $^3J_{CF}$ = 5.68 Hz), 107.80, 104.46, 100.25, 87.04, 74.01, 71.45, 62.34, 25.98, 25.91, 18.44, 18.21, -4.29, -4.36, -4.37, -4.69.

^{19}F NMR (564 MHz, $CDCl_3$) δ -64.74.

HRMS (ESI-TOF) m/z: $[M+H]^+$ Calcd for $C_{27}H_{42}O_7F_3Si_2$ 591.2421; Found 591.2437.

β-anomer (**5b**)

^{1}H NMR (500 MHz, $CDCl_3$) δ 7.64 (dd, *J* = 8.9, 1.9 Hz, 1H), 7.06 (d, *J* = 2.4 Hz, 1H), 7.01 (dd, *J* = 9.0, 2.4 Hz, 1H), 6.65 (s, 1H), 5.47 (d, *J* = 1.2 Hz, 1H), 4.38 (dd, *J* = 7.2, 4.1 Hz, 1H), 4.21 (dd, *J* = 4.1, 1.2 Hz, 1H), 4.17 (dt, *J* = 7.2, 3.0 Hz, 1H), 3.86 – 3.79 (m, 1H), 3.56 (ddd, *J* = 12.4, 9.1, 3.3 Hz, 1H), 1.46 (dd, *J* = 9.1, 4.2 Hz, 1H), 0.93 – 0.92 (s, 18H), 0.14 (s, 9H), 0.12 (s, 3H).

^{13}C NMR (151 MHz, $CDCl_3$) δ 160.36, 159.23, 156.13, 141.54 (q, $^2J_{CF}$ = 32.82 Hz), 126.71 (q, $^3J_{CF}$ = 2.40 Hz), 121.69 (q, $^1J_{CF}$ = 275.34 Hz), 114.34, 113.23 (q, $^3J_{CF}$ = 5.66 Hz), 108.27, 105.14, 104.57, 84.23, 76.90, 70.68, 61.22, 25.99, 25.91, 18.28, 18.23, -4.08, -4.38, -4.41, -4.83.

^{19}F NMR (564 MHz, $CDCl_3$) δ -64.77.

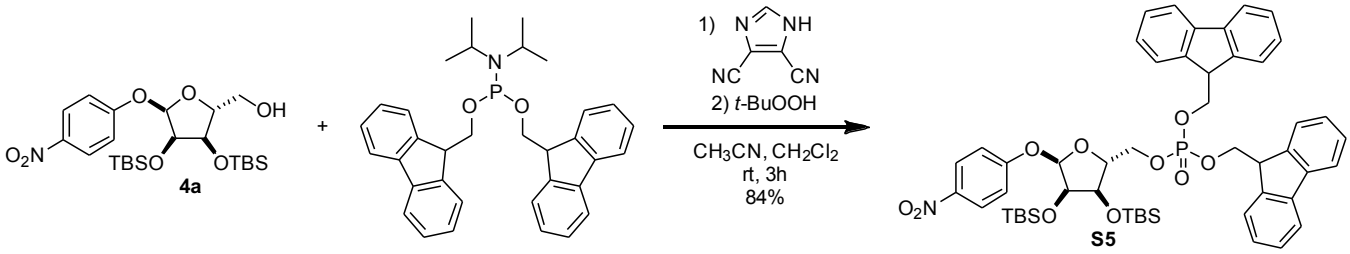

4-nitrophenyl 2,3-bis-*O*-tert-butyldimethylsilyl-α-D-ribose-5-(difluorenylmethyl phosphate) (S5): To a 20 mL reaction vial, **4a** (71.1 mg, 0.142 mmol, 1 eq) and bis-(9H-fluoren-9-ylmethyl)-N,N-diisopropylamidophosphite (Lambrecht et al., 2015) (95.5 mg, 0.183 mmol, 1.3 eq) were added. Dissolved material by addition of CH_2Cl_2 (1.25 mL). Cooled solution to 0 ºC. 4,5-dicyanoimidazole (24.0 mg, 0.203 mmol, 1.4 eq) was added as a solution in acetonitrile (0.25 mL). After stirring at 0 ºC for 15 min, mixture was allowed to warm to room temperature and was stirred for an additional 2 h. Once starting material was consumed as indicated by TLC (75:25 hexane:EtOAc), mixture was cooled to 0 ºC and subjected to dropwise addition of *tert*-butyl hydroperoxide (0.14 mL, 0.70 mmol, 5 eq) as a 5 M solution in decane. Mixture was stirred for an additional 1 h and quenched with H_2O. Mixture was extracted with CH_2Cl_2 three times. Combined organic layers were dried over Na_2SO_4, concentrated, and purified by silica gel chromatography eluting with 60:40 hexane:EtOAc to yield compound **S5** as a white foam (111.5 mg, 84%).

^{1}H NMR (500 MHz, $CDCl_3$) δ 8.00 (d, *J* = 9.2 Hz, 2H), 7.77 – 7.70 (m, 4H), 7.57 (dd, *J* = 18.2, 7.5 Hz, 2H), 7.52 (dd, *J* = 7.3, 6.3 Hz, 2H), 7.44 – 7.34 (m, 4H), 7.32 – 7.24 (m, 4H), 6.91 (d, *J* = 9.2 Hz, 2H), 5.26 (m, 1H), 4.38 – 4.26 (m, 4H), 4.22 – 4.12 (m, 3H), 4.06 (ddd, *J* = 11.4, 5.8, 3.1 Hz, 1H), 4.04 – 4.00 (m, 2H), 3.91 (ddd, *J* = 11.1, 7.0, 3.8 Hz, 1H), 0.91 (s, 9H), 0.90 (s, 9H), 0.11 (s, 3H), 0.05 (s, 3H), 0.03 (s, 6H).

^{13}C NMR (126 MHz, $CDCl_3$) δ 162.23, 143.16, 143.10, 142.98, 142.94, 142.10, 141.47, 141.44, 128.10, 128.08, 128.06, 127.27, 127.22, 125.78, 125.21, 125.17, 125.13, 125.07, 120.19, 120.18, 120.15, 116.09, 99.76, 83.93, 83.87, 77.16, 73.46, 71.13, 69.56, 69.51, 69.48, 69.43, 66.55, 66.51, 48.03, 48.00, 47.97, 47.93, 25.90, 25.86, 18.38, 18.12, -4.25, -4.37, -4.47, -4.80.

^{31}P NMR (202 MHz, $CDCl_3$) δ -0.41.

HRMS (ESI-TOF) m/z: $[M+Na]^+$ Calcd for $C_{51}H_{62}NO_{10}NaSi_2P$ 958.3548; Found 958.3554.

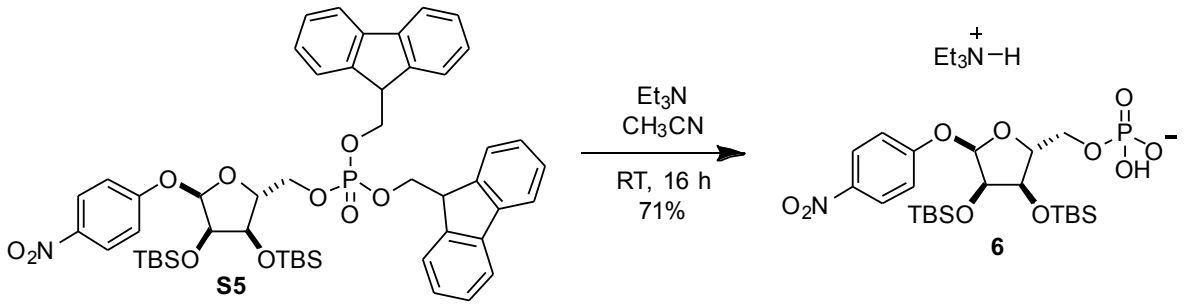

Triethylammonium 4-nitrophenyl 2,3-bis-*O*-tert-butyldimethylsilyl-α-D-ribose-5-phosphate (6): 20 mL reaction vial was charged with compound **S5** (464 mg, 0.50 mmol, 1 eq). Added acetonitrile (5 mL) and triethylamine (freshly distilled from CaH_2, 1 mL) successively. Stirred at room temperature for

16 h. Added 1 mL toluene to stirring solution and concentrated *in vacuo*. Residue was redissolved in methanol (0.5 mL) and purified by C-18 chromatography to yield the triethylammonium salt of compound **6** as a tan foam (241 mg, 71%).

^{1}H NMR (500 MHz, CD_3OD) δ 8.20 (d, *J* = 9.3 Hz, 2H), 7.17 (d, *J* = 9.3 Hz, 2H), 5.71 (d, *J* = 4.2 Hz, 1H), 4.39 (dd, *J* = 5.4, 4.2 Hz, 1H), 4.31 (dd, *J* = 5.4, 2.3 Hz, 1H), 4.20 (dq, *J* = 3.9, 1.9 Hz, 1H), 3.99 (ddd, *J* = 10.1, 4.4, 3.1 Hz, 1H), 3.95 (ddd, *J* = 9.1, 4.6, 3.4 Hz, 1H), 3.17 (q, *J* = 7.3 Hz, 6H), 1.31 (t, *J* = 7.3 Hz, 9H), 0.94 (s, 9H), 0.93 (s, 9H), 0.16 (s, 3H), 0.13 (s, 3H), 0.13 (s, 3H), 0.10 (s, 3H).

^{13}C NMR (126 MHz, CD_3OD) δ 164.14, 143.13, 126.62, 117.36, 101.35, 87.69 (d, *J* = 8.9 Hz), 74.75, 73.14, 65.98 (d, *J* = 5.2 Hz), 47.40, 26.49, 26.46, 19.15, 18.96, 9.11, -4.10, -4.31 (2C), -4.43.

^{31}P NMR (202 MHz, CD_3OD) δ 0.77

HRMS (ESI-TOF) m/z: $[M-H]^-$ Calcd for $C_{23}H_{41}NO_{10}PSi_2$ 578.2012; Found 578.2017.

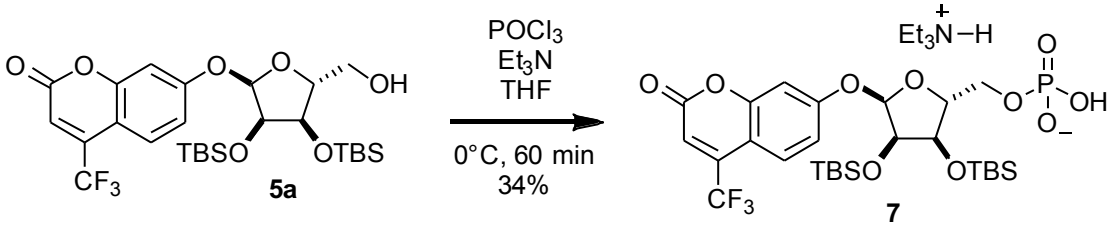

Triethylammonium 4-(trifluoromethyl)umbellifer-7-yl 2,3-bis-*O*-tert-butyldimethylsilyl-α-D-ribose-5-phosphate (7) (method A): To a stirring solution of **5a** (507 mg, 0.858 mmol) in THF (8 mL) at 0 °C was added triethylamine (1.4 mL, 10 mmol, 12 eq) followed by phosphorus oxychloride (0.16 mL, 1.7 mmol, 2 eq). Reaction mixture was stirred at 0 °C for 40 min then warmed to room temperature and stirred for an additional 20 min. After cooling to 0 °C once again, reaction was quenched with addition of water (1 mL). Mixture was stirred for an additional 30 min at room temperature then solvent was removed by rotary evaporator. Residue was purified by C18 chromatography to give **7** (225 mg, 34%) as a white solid.

^{1}H NMR (500 MHz, CD_3OD) δ 7.68 (dd, *J* = 8.8, 2.0 Hz, 1H), 7.12 – 7.06 (m, 2H), 6.71 (s, 1H), 5.72 (d, *J* = 4.3 Hz, 1H), 4.41 (dd, *J* = 5.4, 4.2 Hz, 1H), 4.32 (dd, *J* = 5.4, 2.2 Hz, 1H), 4.21 (dq, *J* = 3.9, 1.9 Hz, 1H), 4.01 – 3.91 (m, 2H), 3.19 (q, *J* = 7.3 Hz, 6H), 1.31 (t, *J* = 7.3 Hz, 9H), 0.95 (s, 9H), 0.93 (s, 9H), 0.16 (s, 3H), 0.14 (s, 6H), 0.11 (s, 3H).

^{13}C NMR (126 MHz, CD_3OD) δ 163.04, 160.83, 157.41, 142.36 (q, $^{2}J_{CF}$ = 32.30 Hz) 127.32 (q, $^{3}J_{CF}$ = 1.72 Hz), 123.22 (q, $^{1}J_{CF}$ = 274.75 Hz), 115.81, 113.88 (q, $^{3}J_{CF}$ = 5.81 Hz), 108.56, 105.05, 101.51, 87.94 (d, $^{3}J_{CP}$ = 9.1 Hz), 74.81, 73.20, 65.99 (d, $^{2}J_{CP}$ = 5.2 Hz), 47.56, 26.48f, 26.46, 19.16, 18.99, 9.15, -4.12, -4.34 (2C), -4.43.

^{19}F NMR (470 MHz, CD_3OD) δ -66.10.

^{31}P NMR (202 MHz, CD_3OD) δ 0.83.

HRMS (ESI-TOF) m/z: $[M-H]^-$ Cald for $C_{27}H_{41}F_3O_{10}PSi_2$ 669.1933; Found 669.1918.

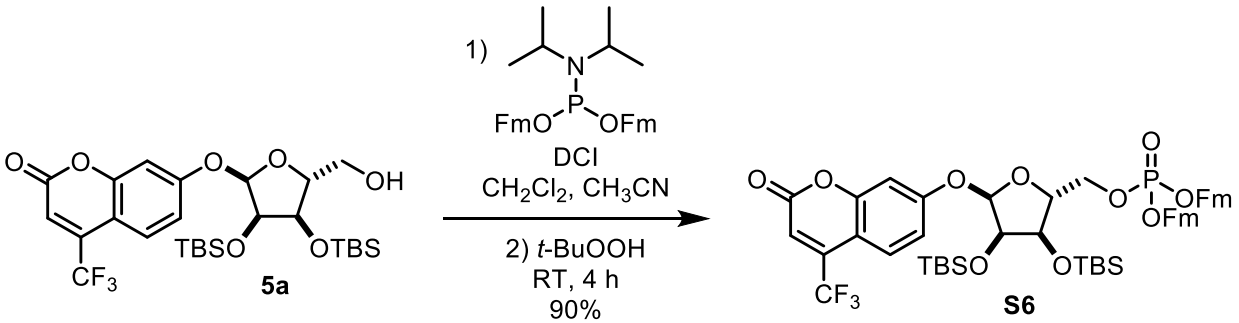

4-(trifluoromethyl)umbellifer-7-yl 2,3-bis-*O*-tert-butyldimethylsilyl-α-D-ribose-5-(difluorenylmethyl phosphate) (S6): To a stirring solution of compound **5a** (373.9 mg, 0.633 mmol) and *N*,*N*-diisopropyl bis(9-methylfluorenyl)phosphoramidite (403.8 mg, 0.774 mmol) in CH_2Cl_2 (12 mL). Dicyanoimidazole (151 mg, 1.3 mmol) was added as a solution in acetonitrile (4.8 mL). Stirred at room temperature for 3 h. Reaction mixture was cooled to 0 °C added t-butylperoxide as a 5 M solution in decane (0.6 mL). Stirred at 0 °C for 1 h. Reaction mixture was quenched with water and extracted with CH_2Cl_2. Combined organic layers were dried over Na_2SO_4 and evaporated. Residue was purified by silica gel chromatography (1:1 hexane:EtOAc) to give compound **S6** as a yellow foam (579.5 mg, 90%).

^{1}H NMR (500 MHz, $CDCl_3$) δ 7.76 – 7.68 (m, 4H), 7.58 – 7.46 (m, 5H), 7.43 – 7.32 (m, 4H), 7.31 – 7.22 (m, 5H), 6.95 (d, *J* = 2.4 Hz, 1H), 6.86 (dd, *J* = 9.0, 2.4 Hz, 1H), 6.61 (s, 1H), 5.34 – 5.30 (m, 1H), 4.34 (td, *J* = 6.3, 1.4 Hz), 4.29 (ddt, *J* = 9.9, 6.8, 3.7 Hz), 4.20 – 4.12 (m, 3H), 4.05 – 4.00 (m, 3H), 3.90 (ddd, *J* = 11.1, 7.1, 3.8 Hz, 1H), 0.90 (s, 9H), 0.89 (s, 9H), 0.10 (s, 3H), 0.04 (s, 3H), 0.02 (s, 3H), 0.02 (s, 3H).

^{13}C NMR (126 MHz, $CDCl_3$) δ 161.13, 159.34, 156.03, 143.16 (d, *J* = 11.6 Hz), 143.04 (d, *J* = 9.6 Hz), 141.53 (q, $^2J_{CF}$ = 32.8 Hz), 141.52, 141.47, 128.07 (d, *J* = 1.7 Hz), 127.28 (d, *J* = 1.2 Hz), 127.26, 126.45 (q, $^3J_{CF}$ = 2.2 Hz), 125.22 (d, *J* = 6.8 Hz), 125.16 (d, *J* = 4.2 Hz), 121.72 (q, $^1J_{CF}$ = 275.5 Hz), 120.19 (d, *J* = 1.9 Hz), 120.16, 114.20, 112.80 (q, $^3J_{CF}$ = 5.7 Hz), 107.81, 104.59, 99.82, 84.30 (d, *J* = 7.4 Hz), 73.54, 71.26, 69.54 (t, *J* = 5.7 Hz), 66.66 (d, *J* = 5.8 Hz), 48.04 (dd, *J* = 7.9, 5.7 Hz), 25.94, 25.88, 18.42, 18.15, -4.25, -4.36, -4.42, -4.74.

^{19}F NMR (471 MHz, $CDCl_3$) δ -64.71.

^{31}P NMR (203 MHz, $CDCl_3$) δ -1.55.

HRMS (ESI-TOF) m/z: $[M+Na]^+$ Calcd for $C_{55}H_{62}O_{10}F_3NaSi_2P$ 1049.3469; Found 1049.3500.

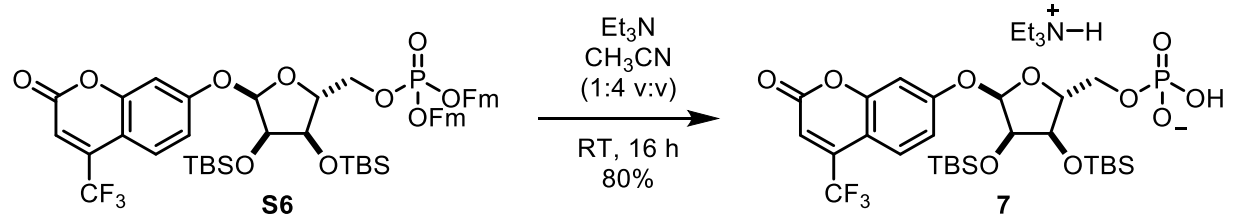

Triethylammonium 4-(trifluoromethyl)umbellifer-7-yl 2,3-bis-*O*-tert-butyldimethylsilyl-α-D-ribose-5-phosphate (7) (method B): To a stirring solution of compound **S6** (1.18 g, 1.00 mmol) in acetonitrile (10 mL) was added Et_3N (freshly distilled from CaH_2, 2.5 mL). Mixture was stirred at room temperature for 16 h. Reaction mixture was co-evaporated with toluene to dryness. Residue was purified by C18 reverse phase chromatography to give compound **7** as a white solid (80%).

^{1}H NMR (500 MHz, $CDCl_3$) δ 7.57 (dt, *J* = 9.0, 1.8 Hz, 1H), 7.04 (d, *J* = 2.4 Hz, 1H), 7.00 (dd, *J* = 9.0, 2.4 Hz, 1H), 6.56 (s, 1H), 5.54 (d, *J* = 4.1 Hz, 1H), 4.25 (dd, *J* = 5.4, 4.1 Hz, 1H), 4.22 (dd, *J* = 5.4, 1.9

Hz, 1H), 4.16 (dt, *J* = 4.0, 2.2 Hz, 1H), 3.98 (ddd, *J* = 11.3, 5.4, 3.8 Hz, 1H), 3.93 (ddd, *J* = 11.2, 5.6, 4.1 Hz, 1H), 3.06 (q, *J* = 7.3 Hz, 6H), 1.30 (t, *J* = 7.3 Hz, 9H), 0.86 (s, 9H), 0.86 (s, 9H), 0.07 (s, 3H), 0.04 (s, 3H), 0.03 (s, 3H), 0.02 (s, 3H).

^{13}C NMR (126 MHz, $CDCl_3$) δ 161.76, 159.58, 156.06, 141.72 (q, $^2J_{CF}$ = 32.6 Hz), 126.33 (q, $^3J_{CF}$ = 1.70 Hz), 121.66 (q, $^1J_{CF}$ = 275.6 Hz), 114.93, 112.20 (q, $^3J_{CF}$ = 5.7 Hz), 107.32, 104.07, 100.00, 86.72 (d, $^3J_{CP}$ = 8.6 Hz), 73.52, 71.66, 64.78 (d, $^2J_{CP}$ = 4.8 Hz), 45.47, 25.90, 25.84, 18.29, 18.08, 8.62, -4.46, -4.47, -4.49, -4.66.

^{19}F NMR (471 MHz, $CDCl_3$) δ -64.74.

^{31}P NMR (203 MHz, $CDCl_3$) δ 1.69.

HRMS (ESI-TOF) m/z: $[M+Na]^+$ Calcd for $C_{27}H_{42}O_{10}NaPF_3Si_2$ 693.1904; Found 693.1901.

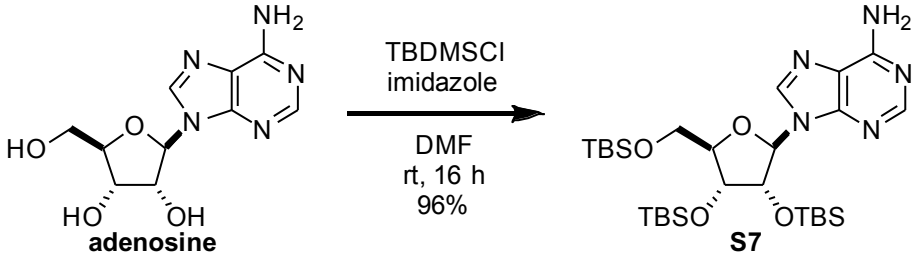

adenosine **S7**

2',3',5'-tris-*O*-(tert-butyldimethylsilyl)-adenosine (S7): To a 100 mL round-bottom flask, adenosine (5.0 g, 19 mmol, 1 eq), imidazole (6.9 g, 102 mmol, 5.4 eq), and dimethylformamide (40 mL) were added. Once fully dissolved, solution was cooled to 0 °C. Tert-butyldimethylsilyl chloride (12.2 g, 81 mmol, 4.2 eq) was added to the stirring solution. Once fully dissolved, reaction vessel was allowed to warm to room temperature. Stirred at room temperature for 16 h. Reaction was quenched by the addition of satd aq NH_4Cl. Extracted three times with CH_2Cl_2. Combined organic layers were dried over $MgSO_4$, filtered through a pad of celite, and evaporated. Residue was purified by silica gel chromatography eluting with 50:50 hexane:EtOAc to yield **S7** as a white foam (12.5 g, 96%).

^{1}H NMR (500 MHz, $CDCl_3$) δ 8.32 (s, 1H), 8.15 (s, 1H), 6.11 (bs, 2H), 6.02 (d, *J* = 5.2 Hz, 1H), 4.68 (t, *J* = 4.8 Hz, 1H), 4.31 (t, *J* = 3.9 Hz, 1H), 4.12 (q, *J* = 3.5 Hz, 1H), 4.02 (dd, *J* = 11.4, 4.2 Hz, 1H), 3.77 (dd, *J* = 11.3, 2.9 Hz, 1H), 0.94 (s, 9H), 0.92 (s, 9H), 0.78 (s, 9H), 0.13 (s, 3H), 0.12 (s, 3H), 0.09 (s, 3H), 0.09 (s, 3H), -0.06 (s, 3H), -0.24 (s, 3H).

^{13}C NMR (126 MHz, $CDCl_3$) δ 155.70, 153.03, 150.05, 139.69, 120.19, 88.41, 85.58, 75.89, 72.11, 62.66, 26.20, 25.98, 25.81, 18.65, 18.22, 17.99, -4.28, -4.57, -4.59, -4.95, -5.24 (2C).

HRMS (ESI-TOF) m/z: $[M+H]^+$ Calcd for $C_{28}H_{56}N_5O_4Si_3$ 610.3640; Found 610.3647

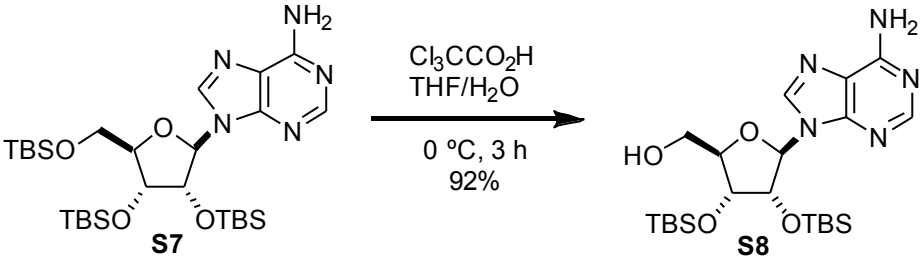

S7 **S8**

2',3'-bis-*O*-(tert-butyldimethylsilyl)-adenosine (S8): A 500 mL round-bottom flask was charged with **S7** (4.4 g, 7.2 mmol, 1 eq). Compound was dissolved in wet tetrahydrofuran (120 mL). Solution was cooled to 0 ºC. To vigorously stirring solution, trichloroacetic acid (56 g, 340 mmol, 47 eq) was added

as an ice-cold solution in H_2O (25 mL). Stirred reaction mixture at 0 ºC for 3 h. Quenched reaction by slowly cannulating reaction mixture into ice cold satd aq $NaHCO_3$. Once evolution of gas ceased, extracted three times with EtOAc. Dried organic layer over Na_2SO_4, filtered, and evaporated. Residue was purified by silica gel chromatography eluting with 95:5 CH_2Cl_2:CH_3OH to yield compound **S8** as a white solid (3.3 g, 92%).

^{1}H NMR (500 MHz, 1:1 $CDCl_3$:DMSO (v:v)) δ 8.24 (s, 1H), 8.11 (s, 1H), 7.29 (s, 2H), 6.08 (dd, *J* = 9.3, 3.3 Hz, 1H), 5.86 (d, *J* = 7.1 Hz, 1H), 4.87 (dd, *J* = 7.2, 4.5 Hz, 1H), 4.26 (dd, *J* = 4.4, 1.4 Hz, 1H), 4.01 (q, *J* = 2.1 Hz, 1H), 3.75 (dt, *J* = 12.6, 3.2 Hz, 1H), 3.58 (ddd, *J* = 12.1, 9.4, 2.6 Hz, 1H), 0.90 (s, 9H), 0.69 (s, 9H), 0.09 (s, 3H), 0.08 (s, 3H), -0.18 (s, 3H), -0.52 (s, 3H).

^{13}C NMR (126 MHz, 1:1 $CDCl_3$:DMSO (v:v)) δ 156.22, 151.89, 148.40, 140.12, 119.86, 88.45, 87.40, 73.99, 73.06, 61.60, 25.52, 25.33, 17.65, 17.36, -4.88, -4.97, -5.07, -6.02.

HRMS (ESI-TOF) m/z: $[M+H]^+$ Calcd for $C_{22}H_{42}N_5O_4Si_2$ 496.2775; Found 496.2774

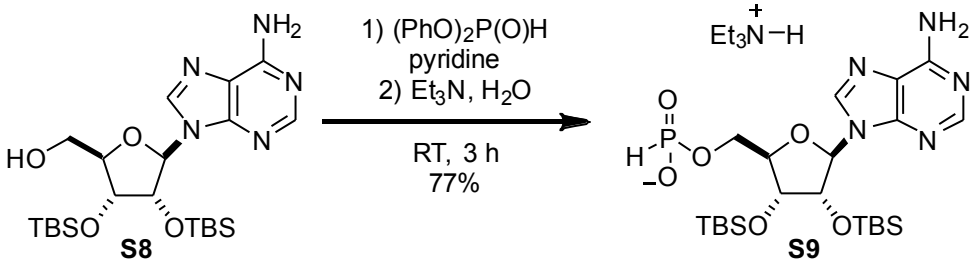

Triethylammonium 2',3'-bis-*O*-(tert-butyldimethylsilyl)-adenosin-5'-yl H-phosphonate (S9): To a 20 mL reaction vial was added compound **S8** (324 mg, 0.654 mmol, 1 eq). Added dry pyridine (6.5 mL). Once fully dissolved, diphenyl phosphite (0.65 mL, 1.22 g/mL, 795 mg, 3.4 mmol, 5 eq) was added, and reaction mixture was stirred at room temperature for 1.5 h. Then, water (0.5 mL) was added followed by triethylamine (0.5 mL). After stirring for an additional 30 min, the reaction mixture was concentrated and purified by C-18 chromatography to yield the triethylammonium salt of compound **S9** as a white foam (331 mg, 77%).

^{1}H NMR (500 MHz, CD_3OD) δ 8.51 (s, 1H), 8.22 (s, 1H), 6.83 (d, $^1J_{HP}$ = 618.5 Hz, 1H), 6.10 (d, *J* = 6.7 Hz, 1H), 4.87 (dd, *J* = 6.7, 4.4 Hz, 1H), 4.41 (dd, *J* = 4.4, 1.9 Hz, 1H), 4.21 (td, *J* = 3.9, 2.1 Hz, 1H), 4.14 (ddd, *J* = 11.0, 6.7, 4.2 Hz, 1H), 4.08 (ddd, *J* = 11.4, 6.7, 3.8 Hz, 1H), 3.15 (q, *J* = 7.3 Hz, 6H), 1.27 (t, *J* = 7.3 Hz, 9H), 0.97 (s, 9H), 0.74 (s, 9H), 0.18 (s, 3H), 0.16 (s, 3H), -0.02 (s, 3H), -0.31 (s, 3H).

^{13}C NMR (126 MHz, CD_3OD) δ 157.20, 153.66, 151.00, 141.41, 120.32, 88.64, 86.71 (d, $^3J_{CP}$ = 8.1 Hz), 77.07, 74.49, 64.22 (d, $^2J_{CP}$ = 4.5 Hz), 47.61, 26.44, 26.24, 18.90, 18.68, 9.16, -4.17, -4.28 (2C), -5.08.

^{31}P NMR (202 MHz, CD_3OD) δ 4.14

HRMS (ESI-TOF) m/z: $[M-H]^-$ Calcd for $C_{22}H_{41}N_5O_6PSi_2$ 558.2338; Found 558.2323

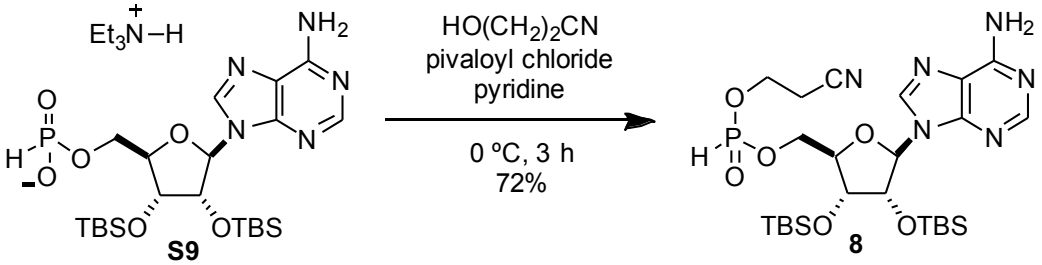

2',3'-bis-*O*-(tert-butyldimethylsilyl)-adenosin-5'-yl 2-cyanoethyl phosphonate (8): To a 25 mL round-bottom flask was added compound **S9** (238 mg, 0.360 mmol, 1 eq). Dried material by co-azeotroping with dry acetonitrile three times. Pyridine was added (4 mL) and solution was cooled to 0 °C. 3-hydroxypropionitrile (0.070 mL, 1.04 g/mL, 73 mg, 1.0 mmol, 3 eq) was added to stirring solution. Pivaloyl chloride (0.09 mL, 0.98 g/mL, 88 mg, 0.73 mmol, 2 eq) was added dropwise. After stirring at 0 °C for 2.5 h, reaction mixture was concentrated, azeotroping with toluene. Resulting residue was redissolved in acetonitrile and purified by C-18 chromatography to yield compound **8** as a white solid as a mixture of diastereomers (159 mg, 72%).

^{1}H NMR (500 MHz, $CDCl_3$) δ 8.30 (s, 1H), 8.30 (s, 1H), 8.00 (s, 1H), 7.98 (s, 1H), 6.91 (d, *J* = 720.9 Hz, 1H), 6.83 (d, *J* = 723.5 Hz, 1H) 6.50 (d, *J* = 7.8 Hz, 2H), 5.87 (dd, *J* = 5.8, 4.2 Hz, 2H), 4.89 (q, *J* = 4.1 Hz, 2H), 4.52 - 4.14 (m, 10H), 2.72 (t, *J* = 6.3 Hz, 2H), 2.69 (t, *J* = 6.2 Hz, 2H), 0.90 (s, 9H), 0.90 (s, 9H), 0.80 (s, 18H), 0.10 (s, 3H), 0.09 (s, 3H), 0.09 (s, 3H), 0.08 (s, 3H), -0.03 (s, 6H), -0.19 (s, 3H), -0.19 (s, 3H)**.**

^{13}C NMR (126 MHz, $CDCl_3$) δ 156.00, 155.96, 153.01, 149.52, 149.49, 140.14, 139.98, 120.54, 116.33, 89.94, 89.83, 82.60, 82.57, 82.55, 82.52, 77.16, 74.42, 74.33, 71.68, 71.60, 64.90, 64.85, 64.77, 64.73, 60.20, 60.16, 60.12, 60.08, 25.87, 25.76, 19.98, 19.93, 18.09, 17.94, -4.30, -4.31, -4.61, -4.63, -4.75, -4.76, -4.83, -4.85.

^{31}P NMR (202 MHz, $CDCl_3$) δ 8.70, 8.23.

HRMS (ESI-TOF) m/z: $[M-H]^-$ Calcd for $C_{25}H_{44}N_6O_6PSi_2$ 611.2604; Found 611.2594

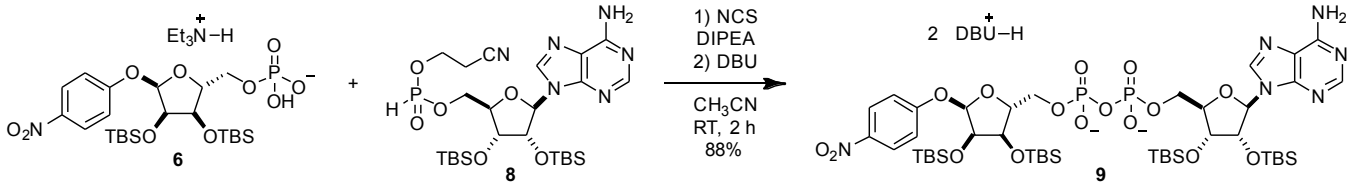

α-1''-*O*-(4-nitrophenyl)-2',2'',3',3''-*O*-tetrakis-(tert-butyldimethylsilyl)-ADP-ribose (9): To a 20 mL reaction vial was added **6** (158.6 mg, 0.233 mmol, 1.0 eq) and **8** (138.3 mg, 0.226 mmol, 1.0 eq). Mixture was dried by co-azeotroping with dry acetonitrile three times and placing under vacuum over P_2O_5 for 12 h. The mixture was dissolved in acetonitrile (3.0 mL). Then, $(i\text{-}Pr_2)_2NEt$ (129 mg, 1.00 mmol, 4.4 eq) and *N*-chlorosuccinimide (90.8 mg, 0.68 mmol, 3 eq) were sequentially added as 1 M solutions in acetonitrile and stirred at room temperature for 1 h. 1,8-diazabicycloundec-7-ene (350 mg, 2.3 mmol, 10 eq) was added as a 1 M solution in acetonitrile. After stirring for 30 min, reaction mixture was evaporated *in vacuo* and purified by C18 chromatography to yield compound **9** as a white foam (287 mg, 88%).

^{1}H NMR (500 MHz, CD_3OD) δ 8.67 (s, 1H), 8.18 (s, 1H), 8.14 (d, *J* = 9.2 Hz, 2H), 7.11 (d, *J* = 9.2 Hz, 2H), 6.15 (d, *J* = 7.5 Hz, 1H), 5.64 (d, *J* = 4.3 Hz, 1H), 4.85 (dd, *J* = 7.5, 4.5 Hz, 1H), 4.46 (d, *J* = 4.4 Hz, 1H), 4.37 (dd, *J* = 5.4, 4.2 Hz, 1H), 4.35 - 4.27 (m, 3H), 4.21 (ddt, *J* = 16.3, 4.3, 2.3 Hz, 2H), 4.11 (hept, *J* = 5.7, 5.0 Hz, 2H), 3.58 - 3.53 (m, 4H), 3.50 (t, *J* = 6.5, 1.7 Hz, 4H), 3.36 (t, *J* = 5.6 Hz, 4H), 2.73 - 2.67 (m, 4H), 1.99 (pd, *J* = 5.4, 1.3 Hz, 4H), 1.79 - 1.62 (m, 12H), 1.34 (d, *J* = 6.5 Hz, 2H), 0.98 (s, 9H), 0.93 (s, 9H), 0.91 (s, 9H), 0.70 (s, 9H), 0.20 (s, 3H), 0.17 (s, 3H), 0.15 (s, 3H), 0.13 (s, 3H), 0.11 (s, 3H), 0.08 (s, 3H), -0.01 (s, 3H), -0.38 (s, 3H).

^{13}C NMR (126 MHz, CD_3OD) δ 167.42, 164.19, 157.30, 153.85, 151.17, 143.00, 141.66, 126.58, 120.04, 117.32, 101.23, 87.89, 87.86, 87.82, 87.64, 87.56, 77.60, 74.87, 74.76, 73.28, 66.76, 66.71, 66.66, 55.23, 49.53, 49.00, 39.34, 33.60, 30.01, 27.54, 26.49, 26.44, 26.21, 24.99, 20.43, 19.59, 19.14, 18.97, 18.93, 18.65, -4.07, -4.09, -4.19, -4.26, -4.29, -5.26.

^{31}P NMR (202 MHz, CD_3OD) δ -11.30 (d, *J* = 21.8 Hz), -11.67 (d, *J* = 21.6 Hz).

HRMS (ESI-TOF) m/z: $[M-H]^-$ Calcd for $C_{45}H_{81}N_6O_{16}P_2Si_4$ 1135.4267; Found 1135.4273

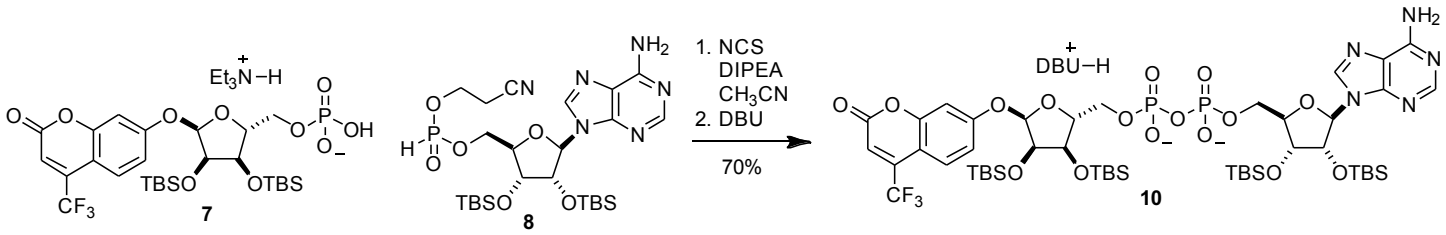

α-1''-*O*-(4-(trifluoromethyl)umbellifer-7-yl)-2',2'',3',3''-*O*-tetrakis-(tert-butyldimethylsilyl)-ADP-ribose (10): To a stirring solution of **7** (95.8 mg, 0.124 mmol) and **8** (76.3 mg, 0.124 mmol) in dichloromethane (5 mL) was added DIPEA as a 1 M solution in CH_3CN (0.74 mL, 0.74 mmol, 6 eq) and N-chlorosuccinimide as a 1 M solution in CH_3CN (0.62 mL, 0.62 mmol, 5 eq). Mixture was stirred for 30 min at room temperature and then 1,8-diazabicycloundec-7-ene as a 1 M solution in THF (1 mL, 1 mmol, 8 eq) was added. After stirring for an additional 30 min, solvent was removed by rotavap. Residue was purified by C18 chromatography to give **10** (124 mg, 70%) as a white solid.

^{1}H NMR (500 MHz, CD_3OD) δ 8.29 (s, 1H), 7.81 (s, 1H), 7.24 (dd, *J* = 8.9, 2.0 Hz, 1H), 6.65 (m, 2H), 6.29 (s, 1H), 5.73 (d, *J* = 7.2 Hz, 1H), 5.27 (d, *J* = 4.3 Hz, 1H), 4.42 (dd, *J* = 7.2, 4.4 Hz, 1H), 4.05 (dd, *J* = 4.4, 1.3 Hz, 1H), 3.99 (dd, *J* = 5.4, 4.3 Hz, 1H), 3.95 – 3.87 (m, 3H), 3.85 – 3.80 (m, 2H), 3.75 – 3.70 (m, 2H), 3.18 – 3.14 (m, 1H), 3.11 (t, *J* = 6.0 Hz, 2H), 2.96 (dd, *J* = 10.1, 4.4 Hz, 2H), 2.91 (p, *J* = 1.6 Hz, 1H), 2.80 (q, *J* = 7.4 Hz, 3H), 2.33 – 2.27 (m, 2H), 1.60 (pd, *J* = 5.5, 1.1 Hz, 2H), 1.38 – 1.24 (m, 4H), 0.97 (ddt, *J* = 14.4, 9.2, 5.2 Hz, 22H), 0.57 (s, 9H), 0.54 (s, 9H), 0.51 (s, 9H), 0.31 (s, 9H), -0.21 (s, 3H), -0.24 (s, 3H), -0.25 (s, 3H), -0.28 (s, 3H), -0.29 (s, 3H), -0.31 (s, 3H), -0.41 (s, 3H), -0.77 (s, 3H).

^{13}C NMR (126 MHz, CD_3OD) δ 163.03, 160.75, 157.36, 153.02, 151.00, 142.21, 141.85, 127.28, 120.00, 115.77, 113.82, 108.45, 105.03, 101.34, 88.03, 87.46, 87.39, 77.72, 74.77, 73.27, 66.76, 66.63, 55.43, 55.25, 43.49, 39.35, 33.62, 30.00, 27.54, 26.49, 26.48, 26.22, 24.99, 20.43, 19.57, 19.14, 18.98, 18.92, 18.86, 18.65, 17.44, 13.05, 9.12, -4.09, -4.18, -4.20, -4.24, -4.28, -4.31, -5.21.

^{19}F NMR (470 MHz, CD_3OD) δ -66.37.

^{31}P NMR (202 MHz, CD_3OD) δ -10.38 (d, *J* = 21.2 Hz), -10.80 (d, *J* = 21.2 Hz).

HRMS (ESI-TOF) m/z: $[M-H]^-$ Cald for $C_{49}H_{81}F_3N_5O_{16}P_2Si_4$ 1226.4188. Found 1226.4139.

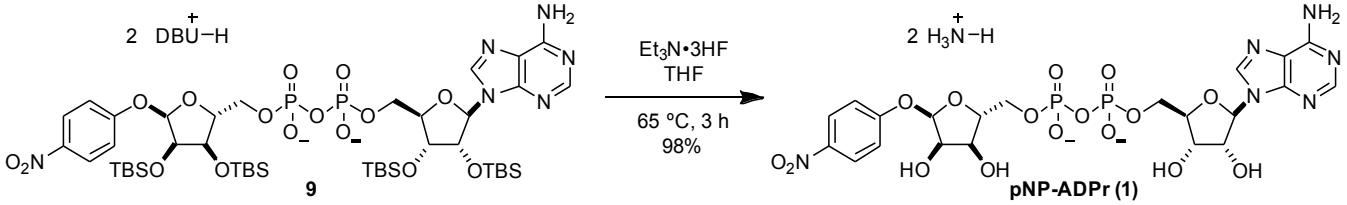

pNP-ADPr (1): To a 25 mL round-bottom flask was added **9** (109.7 mg, 0.0761 mmol, 1 eq) and THF (3.0 mL). Once starting material was fully dissolve, triethylamine trihydrofluoride (0.5 mL) was added neat dropwise. Reaction vessel was sealed and heated to 65 ºC. Reaction was closely monitored by TLC (80:20 2-propanol:0.2% $NH_4OH_{(aq)}$) Once reaction had gone to completion, reaction mixture was cooled to room temperature and concentrated *in vacuo*. Remaining acid was quenched by dropwise addition of satd aq $NaHCO_3$. Aqueous solution of crude product was purified by C18 chromatography utilizing ion-pairing reagent in the mobile phase (10 mM Et_3N-HOAc, pH 7.0) to yield compound **1** as a triethylammonium salt. The triethylammonium salt was eluted through Dowex 50W-8X (ammonium-form) to give the ammonium salt of compound **1** as a white powder (53.8 mg, 98%).

^{1}H NMR (500 MHz, D_2O) δ 8.36 (s, 1H, Ade-2), 8.03 (s, 1H, Ade-8), 7.92 (d, *J* = 9.2 Hz, 2H, pNP-3,5), 6.92 (d, *J* = 9.2 Hz, 2H, pNP-2,6), 6.04 (d, *J* = 5.7 Hz, 1H, Ade-1'), 5.67 (d, *J* = 4.4 Hz, 1H, Rib-1''), 4.62 (t, *J* = 5.7 Hz, 1H, Ade-2'), 4.46 (dd, *J* = 5.1, 3.6 Hz, 1H, Ade-3'), 4.41 (dd, *J* = 6.0, 4.6 Hz, 1H, Rib-2''), 4.36 (m, 2H, Ade-4', Rib-4"), 4.27 (dd, *J* = 6.2, 2.6 Hz, 1H, Rib-3''), 4.23 (m, 2H, Ade-5'), 4.08 (m, 2H, Rib-5'').

^{13}C NMR (126 MHz, D_2O) δ 161.8, 155.2, 152.5, 148.7, 141.5, 139.6, 125.6, 118.3, 116.3, 100.4, 86.8, 84.7, 83.8, 74.5, 71.3, 70.4, 69.7, 65.7, 65.3.

^{31}P NMR (202 MHz, D_2O) δ -11.2

HRMS (ESI-TOF) m/z: $[M-H]^-$ Calcd for 679.0808; Found 679.0805

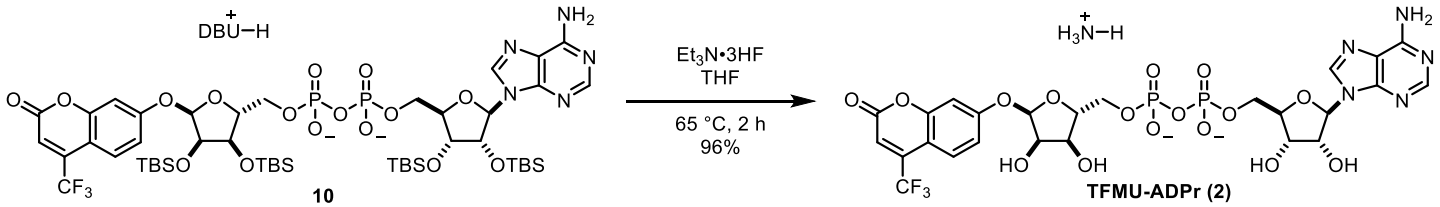

TFMU-ADPr (2)
To a stirring solution of **10** (67.2 mg, 0.044 mmol) in THF (1 mL) was added triethylamine trihydrofluoride (0.3 mL). Mixture was heated to 65 °C and stirred for 2 h. Once cooled to room temperature, reaction was quenched with addition of satd aq $NaHCO_3$. Aqueous mixture was purified by ion-pairing chromatography (10 mM Et_3N-HOAc, C18) followed by ion exchange (Dowex 50W-8, ammonium form) to provide **TFMU-ADPr (2)** as a white solid (33.8 mg, 96%).

^{1}H NMR (500 MHz, D_2O) δ 8.11 (s, 1H), 7.71 (s, 1H), 7.25 (dd, *J* = 9.1, 1.8 Hz, 1H), 6.70 (dd, *J* = 9.0, 2.5 Hz, 1H), 6.58 (d, *J* = 2.5 Hz, 1H), 6.50 (s, 1H), 5.76 (d, *J* = 5.6 Hz, 1H), 5.56 (d, *J* = 4.5 Hz, 1H), 4.41 (t, *J* = 5.3 Hz, 1H), 4.33 – 4.28 (m, 2H), 4.28 – 4.25 (m, 1H), 4.22 (q, *J* = 4.1 Hz, 1H), 4.15 (dd, *J* = 6.2, 2.8 Hz, 1H), 4.15 – 4.05 (m, 2H), 4.01 (ddd, *J* = 11.5, 5.0, 3.0 Hz, 1H), 3.94 (dt, *J* = 11.4, 4.4 Hz, 1H).

^{13}C NMR (126 MHz, D_2O) δ 161.71, 159.94, 154.33, 154.18, 151.56, 147.93, 141.37 (q, $^2J_{CF}$ = 32.8 Hz), 139.31, 125.98, 121.09 (q, $^1J_{CF}$ = 275.1 Hz), 117.67, 114.65, 112.35 (q, $^3J_{CF}$ = 4.3 Hz), 107.33, 103.50, 100.16, 86.90, 84.51 (d, $^3J_{CP}$ = 8.2 Hz), 83.42 (d, $^3J_{CP}$ = 8.3 Hz), 74.46, 71.13, 70.10, 69.57, 65.66 (d, $^2J_{CP}$ = 4.0 Hz), 65.11 (d, $^2J_{CP}$ = 4.2 Hz).

^{19}F NMR (471 MHz, D_2O) δ -64.43.

^{31}P NMR (203 MHz, D_2O) δ -11.08 (d, *J* = 21.9 Hz), -11.28 (d, *J* = 21.5 Hz).

HRMS (ESI-TOF) m/z: $[M-H]^-$ Cald for $C_{25}H_{25}F_3N_5O_{16}P_2$ 770.0729; found 770.0723.

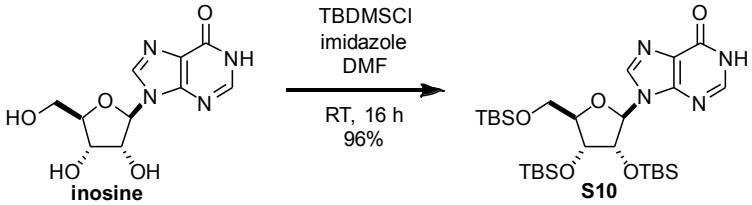

2',3',5'-tris-*O*-(tert-butyldimethylsilyl)-inosine (S10): Intermediate was prepared according to a modified version of a previous report (Höbartner and Silverman, 2005). Briefly, a 100 mL round-bottom flask was charged with inosine (1.0 g, 3.7 mmol, 1 eq) and imidazole (1.7 g, 25 mmol, 6.7 eq). Material was dissolved in dimethylformamide (4 mL). Tert-butyldimethylsilyl chloride (2.8 g, 18.7 mmol, 5 eq)

was added in one portion. The solution was stirred at room temperature for 16 h. Reaction mixture was diluted with CH_2Cl_2 and quenched with the addition of satd aq $NaHCO_3$. Organic layer was washed two times with satd aq $NaHCO_3$, dried over Na_2SO_4, filtered through a pad of celite, and evaporated to give **S10** as a white solid (2.2 g, 96%) which was used in subsequent reactions without further purification. ^{1}H NMR spectrum was consistent with literature.

^{1}H NMR (500 MHz, $CDCl_3$) δ 12.94 (bs, 1H), 8.24 (s, 1H), 8.10 (s, 1H), 6.02 (d, *J* = 4.9 Hz, 1H), 4.50 (t, *J* = 4.6 Hz, 1H), 4.30 (t, *J* = 4.0 Hz, 1H), 4.13 (q, *J* = 3.4 Hz, 1H), 4.00 (dd, *J* = 11.4, 3.7 Hz, 1H), 3.79 (dd, *J* = 11.4, 2.5 Hz, 1H), 0.96 (d, *J* = 0.7 Hz, 9H), 0.93 (d, *J* = 0.7 Hz, 9H), 0.81 (d, *J* = 0.7 Hz, 9H), 0.15 (s, 3H), 0.14 (s, 3H), 0.10 (s, 3H), 0.09 (s, 3H), -0.02 (s, 3H), -0.18 (s, 3H).

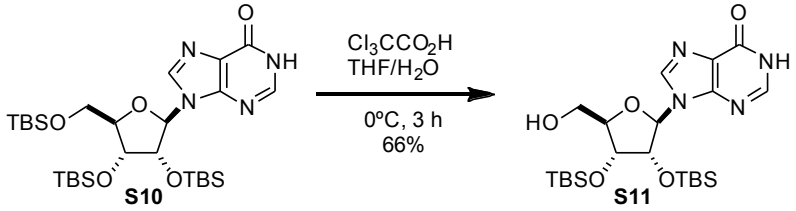

2',3'-bis-*O*-(tert-butyldimethylsilyl)-inosine (S11): A 100 mL round-bottom flask was charged with **S10** (1.2 g, 2.0 mmol, 1 eq). Compound was dissolved in tetrahydrofuran (31 mL). Solution was cooled to 0 ºC. To vigorously stirring solution, trichloroacetic acid (15 g, 92 mmol, 47 eq) was added as an ice-cold solution in H_2O (6.8 mL). Stirred reaction mixture at 0 ºC for 3 h. Quenched reaction by slowly cannulating reaction mixture into satd aq $NaHCO_3$. Once evolution of gas ceased, extracted three times with EtOAc. Dried organic layer over Na_2SO_4, filtered, and evaporated. Residue was purified by silica gel chromatography eluting with 93:7 CH_2Cl_2:CH_3OH to yield compound **S11** as a white solid (641 mg, 66%).

^{1}H NMR (500 MHz, $CDCl_3$) δ 13.34 (bs, 1H), 8.46 (s, 1H), 7.95 (s, 1H), 5.80 (d, *J* = 7.7 Hz, 1H), 5.68 (bs, 1H), 4.87 (dd, *J* = 7.8, 4.6 Hz, 1H), 4.31 (d, *J* = 4.5 Hz, 1H), 4.16 (s, 1H), 3.93 (dd, *J* = 12.9, 2.1 Hz, 1H), 3.72 (d, *J* = 13.0 Hz, 1H), 0.94 (d, *J* = 0.9 Hz, 9H), 0.75 (d, *J* = 0.9 Hz, 9H), 0.12 (s, 3H), 0.11 (s, 3H), -0.12 (s, 3H), -0.52 (s, 3H).

^{13}C NMR (126 MHz, $CDCl_3$) δ 158.90, 147.87, 145.79, 141.04, 126.72, 91.05, 89.33, 74.79, 73.84, 62.91, 25.93, 25.80, 18.20, 17.92, -4.42, -4.46, -4.49, -5.70.

HRMS (ESI-TOF) m/z: $[M+H]^+$ Calc for $C_{22}H_{40}N_4O_5Si_2$ 497.2610; Found 497.2614

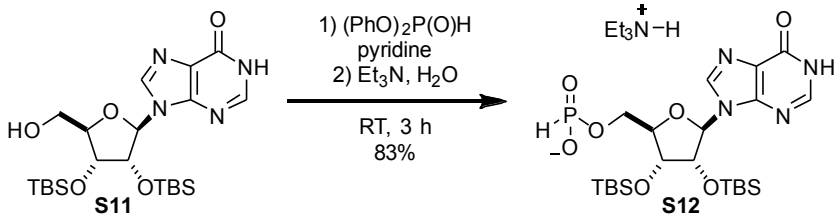

Triethylammonium 2',3'-bis-*O*-(tert-butyldimethylsilyl)-inosin-5'-yl H-phosphonate (S12): A 100 mL round-bottom flask was charged with **S11** (420 mg, 0.85 mmol, 1 eq) and pyridine (8.5 mL). Diphenylphosphite (0.81 mL, 1.223 g/mL, 990 mg, 4.2 mmol, 5 eq) was added dropwise. After stirring reaction mixture at room temperature for 1.5 h, H_2O (0.5 mL) and triethylamine (0.5 mL) were added sequentially. Reaction was stirred for 30 min, then concentrated *in vacuo*. Remaining pyridine was removed by repeated azeotropic evaporation with toluene. Residue was purified by C18 chromatography to provide compound **S12** as a white foam (464 mg, 83%).

^{1}H NMR (500 MHz, CD_3OD) δ 8.48 (s, 1H), 8.16 (s, 1H), 6.84 (d, J_{HP} = 620.8 Hz, 1H), 6.07 (d, *J* = 6.6 Hz, 1H), 4.83 (dd, *J* = 6.5, 4.4 Hz, 1H), 4.41 (dd, *J* = 4.4, 2.1 Hz, 1H), 4.24 - 4.20 (m, 1H), 4.20 - 4.14

(m, 1H), 4.12 - 4.05 (m, 1H), 3.23 (q, *J* = 7.3 Hz, 6H), 1.30 (t, *J* = 7.3 Hz, 9H), 0.96 (s, 9H), 0.77 (s, 9H), 0.17 (s, 3H), 0.15 (s, 3H), 0.00 (s, 3H), -0.27 (s, 3H).

^{13}C NMR (126 MHz, CD_3OD) δ 158.78, 150.22, 146.99, 140.81, 125.52, 89.00, 86.60(d, J_{CP} = 8.0 Hz), 77.09, 74.17, 64.05 (d, *J* = 4.4 Hz), 47.49, 26.44, 26.26, 18.88, 18.67, 9.19, -4.18, -4.29, -4.31, -5.10.

^{31}P NMR (202 MHz, CD_3OD) δ 4.11.

HRMS (ESI-TOF) m/z: $[M-H]^-$ Calc for $C_{22}H_{41}N_4O_7PSi_2$ 559.2179; Found 559.2164.

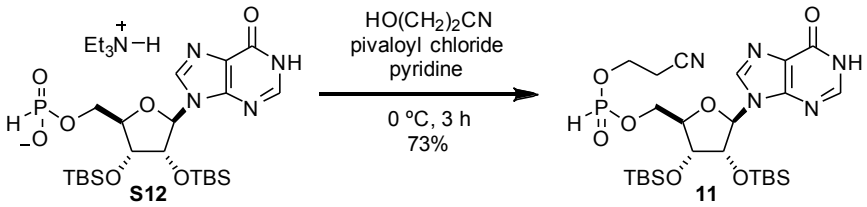

2',3'-bis-*O*-(tert-butyldimethylsilyl)-inosin-5'-yl 2-cyanoethyl phosphonate (11): To a 20 mL reaction vial was added compound **S12** (246 mg, 0.372 mmol, 1 eq) and dry pyridine (4 mL). Solution was cooled to 0 ºC. 3-hydroxypropionitrile (0.070 mL, 1.04 g/mL, 73 mg, 1.0 mmol, 2.8 eq) was added to stirring solution. Pivaloyl chloride (0.09 mL, 0.98 g/mL, 88 mg, 0.73 mmol, 2 eq) was added dropwise. After stirring at 0 °C for 2.5 h, reaction mixture was concentrated, azeotroping with toluene. Resulting residue was redissolved in acetonitrile and purified by C-18 chromatography to yield compound **11** as a white solid as a mixture of diastereomers (166 mg, 73%).

^{1}H NMR (500 MHz, $CDCl_3$) δ 8.40 (s, 0.5H), 8.36 (s, 0.5H), 8.03 (s, 0.5H), 8.01 (s, 0.5H), 6.98 (d, *J* = 722.4 Hz, 0.5H), 6.94 (d, *J* = 722.1 Hz, 0.5H), 5.90 (dd, *J* = 4.7, 3.2 Hz, 1H), 4.79 (t, *J* = 4.5 Hz, 1H), 4.76 (t, *J* = 4.0 Hz, 1H), 4.52 – 4.23 (m, 7H), 2.87 – 2.75 (m, 2H), 0.92 (s, 9H), 0.91 (s, 9H), 0.805 (s, 9H), 0.799 (s, 9H), 0.12 (s, 3H), 0.10 (s, 3H), 0.09 (s, 3H), -0.017 (s, 3 H), -0.022 (s, 3H), -0.19 (s, 3H), -0.21 (s, 3H)

^{13}C NMR (126 MHz, $CDCl_3$) δ 159.03, 148.66, 148.64, 145.75, 145.68, 139.73, 139.53, 125.75, 125.69, 116.73, 116.60, 89.71, 89.64, 83.15, 83.10, 83.03, 82.97, 77.36, 74.94, 74.74, 71.73, 71.66, 64.55, 60.60, 60.56, 60.53, 25.87, 25.75, 20.17, 20.12, 20.08, 18.10, 17.94, -4.30, -4.56, -4.58, -4.69, -4.70, -4.90, -4.93.

^{31}P NMR (202 MHz, $CDCl_3$) δ 8.66, 8.41.

HRMS (ESI-TOF) m/z: $[M-H]^-$ Calc for $C_{25}H_{44}N_5O_7PSi_2$ 612.2444; Found 612.2448.

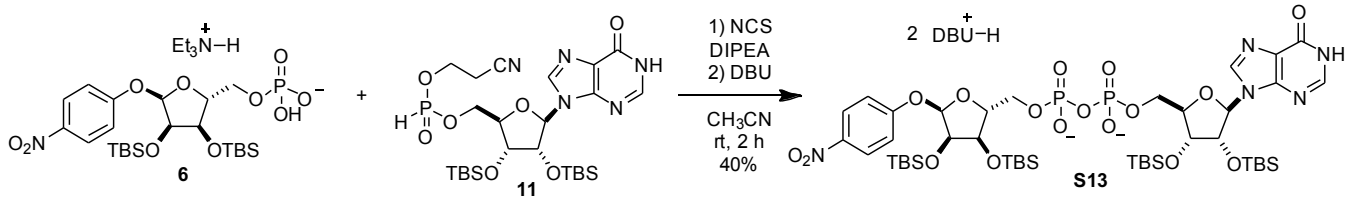

α-1''-*O*-(4-nitrophenyl)-2',2'',3',3''-*O*-tetrakis-(tert-butyldimethylsilyl)-IDP-ribose (S13): To a 20 mL reaction vial was added **6** (41.1 mg, 0.0604 mmol, 1.0 eq) and **11** (38.7 mg, 0.0630 mmol, 1.04 eq). Mixture was dried by co-azeotroping with dry acetonitrile three times and placing under vacuum over P_2O_5 for 12 h. The mixture was dissolved in acetonitrile (1.0 mL). Then, $(i\text{-}Pr_2)_2NEt$ (31 mg, 0.24 mmol, 4.0 eq) and *N*-chlorosuccinimide (24 mg, 0.18 mmol, 3 eq) were sequentially added as 1 M solutions in acetonitrile and stirred at room temperature for 1 h. 1,8-diazabicycloundec-7-ene (92 mg, 0.6 mmol, 10 eq) was added as a 1 M solution in acetonitrile. After stirring for 30 min, reaction mixture was evaporated *in vacuo* and purified by C18 chromatography to yield compound **S13** as a white foam (34.6 mg, 40%).

^{1}H NMR (500 MHz, CD_3OD) δ 8.55 (s, 1H), 8.14 (d, *J* = 9.2 Hz, 2H), 8.08 (s, 1H), 7.12 (d, *J* = 9.3 Hz, 2H), 6.08 (d, *J* = 7.5 Hz, 1H), 5.66 (d, *J* = 4.3 Hz, 1H), 4.46 (d, *J* = 4.3 Hz, 1H), 4.39 (dd, *J* = 5.4, 4.3 Hz, 1H), 4.35 – 4.28 (m, 3H), 4.23 (t, *J* = 4.8 Hz, 1H), 4.19 (dt, *J* = 4.3, 2.6 Hz, 1H), 4.15 – 4.07 (m, 2H), 3.64 – 3.56 (m, 4H), 3.53 (t, *J* = 6.1 Hz, 4H), 3.36 (t, *J* = 5.6 Hz, 4H), 2.74 – 2.65 (m, 4H), 2.02 (tdd, *J* = 6.9, 5.2, 4.2 Hz, 4H), 1.82 – 1.66 (m, 14H), 0.97 (s, 9H), 0.93 (s, 9H), 0.91 (s, 9H), 0.73 (s, 9H), 0.20 (s, 3H), 0.17 (s, 3H), 0.15 (s, 3H), 0.13 (s, 3H), 0.11 (s, 3H), 0.08 (s, 3H), -0.00 (s, 3H), -0.36 (s, 3H).

^{31}P NMR (202 MHz, CD_3OD) δ -11.3 (d, *J* = 21.9 Hz), -11.6 (d, *J* = 21.8 Hz).

^{13}C NMR (126 MHz CD_3OD) δ 167.50, 164.28, 159.27, 150.61, 147.02, 143.00, 141.44, 126.59, 125.58, 117.36, 101.30, 88.57, 88.02 (d, *J* = 9.2 Hz), 87.70 (d, *J* = 9.3 Hz), 77.11, 74.81, 73.33, 66.71 (d, *J* = 5.5 Hz), 66.52 (d, *J* = 5.4 Hz), 55.33, 49.57, 39.37, 33.70, 30.01, 27.53, 26.50 (3C), 26.48, 26.22, 24.97, 20.44, 19.15, 18.99, 18.93, 18.68, -4.04, -4.11, -4.20, -4.23, -4.26, -4.30, -4.32, -5.32.

HRMS (ESI-TOF) m/z: $[M-H]^-$ Calc for $C_{45}H_{80}N_5O_{17}P_2Si_4$ 1136.4107; Found 1136.4115.

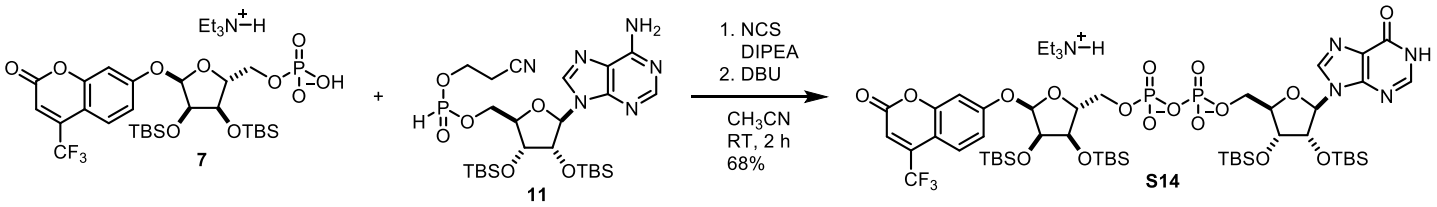

α-1''-*O*-(4-(trifluoromethyl)umbellifer-7-yl)-2',2'',3',3''-*O*-tetrakis-(tert-butyldimethylsilyl)-IDP-ribose (S14): To a stirring solution of **7** (93.6 mg, 0.121 mmol) and **11** (75.5 mg, 0.123 mmol) in dichloromethane (1 mL) was added DIPEA as a 1 M solution in CH_3CN (0.73 mL, 0.73 mmol, 6 eq) and N-chlorosuccinimide as a 1 M solution in CH_3CN (0.61 mL, 0.61 mmol, 5 eq). Mixture was stirred for 30 min at room temperature and then DBU as a 1 M solution in THF (1 mL, 1 mmol, 8 eq) was added. After stirring for an additional 30 min, solvent was removed by rotary evaporator. Residue was purified by C18 chromatography to give **S14** (126 mg, 68%)

^{1}H NMR (500 MHz, CD_3OD) δ 8.56 (s, 1H), 8.09 (s, 1H), 7.65 (dd, *J* = 9.6, 2.0 Hz, 1H), 7.05 (dd, *J* = 6.8, 2.4 Hz, 3H), 6.70 (s, 1H), 6.07 (d, *J* = 7.4 Hz, 1H), 5.70 (d, *J* = 4.3 Hz, 1H), 4.89 (dd, *J* = 7.4, 4.4 Hz, 1H), 4.44 (d, *J* = 4.5 Hz, 1H), 4.40 (dd, *J* = 5.4, 4.3 Hz, 1H), 4.35 – 4.25 (m, 6H), 4.22 (q, *J* = 3.9 Hz, 4H), 4.12 (t, *J* = 4.7 Hz, 3H), 3.72 (hept, *J* = 6.7 Hz, 2H), 3.58 (m, 2H), 3.52 (t, *J* = 5.9 Hz, 2H), 3.37 (t, *J* = 5.7 Hz, 2H), 3.20 (q, *J* = 7.4 Hz, 2H), 2.76 – 2.68 (m, 2H), 2.01 (pd, *J* = 5.6, 1.3 Hz, 2H), 1.80 – 1.64 (m, 6H), 1.38 (t, *J* = 7.2 Hz, 14H), 0.96 (s, 9H), 0.94 (s, 9H), 0.91 (s, 9H), 0.73 (s, 9H), 0.19 (s, 3H), 0.16 (s, 3H), 0.15 (s, 3H), 0.13 (s, 3H), 0.12 (s, 3H), 0.09 (s, 3H), -0.00 (s, 3H), -0.36 (s, 3H).

^{13}C NMR (126 MHz, CD_3OD) δ 167.45, 163.08, 160.79, 158.93, 157.38, 150.54, 146.83, 142.33 (q, $^2J_{CF}$ = 32.6 Hz), 141.41, 129.48, 127.29, 125.52, 123.23 (q, $^1J_{CF}$ = 274.9 Hz), 115.77, 113.81 (q, $^3J_{CF}$ = 6.4 Hz), 108.44, 105.04, 101.36, 88.59, 88.12 (d, $^3J_{CP}$ = 9.2 Hz), 87.55 (d, $^3J_{CP}$ = 9.4 Hz), 77.15, 74.79, 74.74, 73.31, 66.79 (d, $^2J_{CP}$ = 5.5 Hz), 66.54 (d, $^2J_{CP}$ = 5.4 Hz), 55.40, 55.27, 43.49, 39.36, 33.64, 30.04, 27.56, 26.49, 26.49, 26.47, 26.22, 25.00, 20.44, 19.57 (d, *J* = 1.7 Hz), 19.15, 19.00, 18.92, 18.67, 13.11, -4.06, -4.10, -4.20, -4.22, -4.24, -4.30, -4.32, -5.29.

^{31}P NMR (203 MHz, CD_3OD) δ -11.41 (d, *J* = 21.3 Hz), -11.81 (d, *J* = 21.9 Hz).

HRMS (ESI-TOF) m/z: $[M-H]^-$ Cald for $C_{49}H_{80}F_3N_4O_{17}P_2Si_4$ 1227.4028; Found 1227.4056.

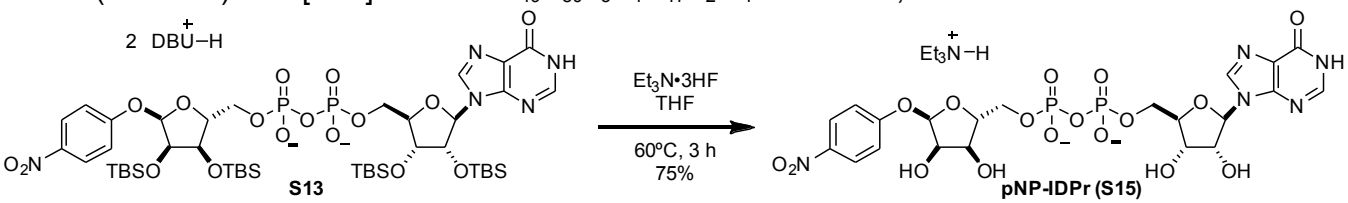

pNP-IDPr (S15): To a 7 mL reaction vial was added **S13** (17.4 mg, 0.0121 mmol, 1 eq) and THF (1.0 mL). Once starting material was fully dissolve, triethylamine trihydrofluoride (0.2 mL) was added neat dropwise. Reaction vessel was sealed and heated to 60 ºC. Reaction was closely monitored by TLC (80:20 2-propanol:0.2% $NH_4OH_{(aq)}$). Once reaction had gone to completion, reaction mixture was cooled to room temperature and concentrated *in vacuo*. Remaining acid was quenched by dropwise addition of satd aq $NaHCO_3$. Aqueous solution of crude product was purified by C-18 chromatography utilizing ion-pairing reagent in the mobile phase (10 mM Et_3N-HOAc) to yield compound **pNP-IDPr (S15)** as a triethylammonium salt. The triethylammonium salt was eluted through Dowex 50W-8X (ammonium-form) to give the ammonium salt of compound **pNP-IDPr (S15)** as a white powder (6.2 mg, 75%).

^{1}H NMR (500 MHz, D_2O) δ 8.37 (s, 1H), 8.09 (s, 1H), 8.06 (d, *J* = 9.1 Hz, 2H), 7.06 (d, *J* = 9.0 Hz, 2H), 6.06 (d, *J* = 5.9 Hz, 1H), 5.79 (d, *J* = 4.5 Hz, 1H), 4.70 (t, *J* = 5.5 Hz, 1H), 4.50 (dd, *J* = 5.2, 3.5 Hz, 1H), 4.45 (dd, *J* = 6.2, 4.5 Hz, 1H), 4.42 - 4.37 (m, 2H), 4.31 (dd, *J* = 6.0, 2.5 Hz, 1H), 4.29 – 4.22 (m, 2H), 4.16 - 4.05 (m, 2H)

^{31}P NMR (202 MHz, D_2O) δ -11.14 (d, *J* = 21.8 Hz, 1P), -11.36 (d, *J* = 21.6 Hz, 1P)

^{13}C NMR (from ^{1}H,^{13}C-HMBC, 500 MHz, D_2O) 162.04, 158.43, 148.37, 146.14, 141.63,139.60, 125.85, 123.59, 116.73, 100.32, 87.36, 84.78, 83.97, 74.53, 71.21, 70.38, 69.64, 65.57, 64.86

HRMS (ESI-TOF) m/z: $[M-H]^-$ Calc for $C_{21}H_{24}N_5O_{17}P_2$ 680.0648; Found 680.0650.

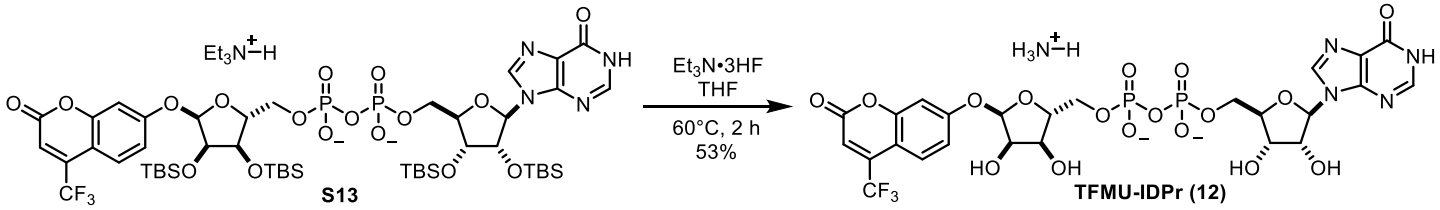

TFMU-IDPr (12)

To a stirring solution of **S13** (119.9 mg, 0.78 mmol) in THF (1.0 mL) was added triethylamine trihydrofluoride (0.5 mL, 3.1 mmol, 40 eq). Reaction mixture was sealed with Teflon cap and heated to 60 °C. After stirring at 60 °C for 2 h, solvent was removed by rotavap. Residue was neutralized with satd aq $NaHCO_3$ and aqueous mixture was purified by ion-pairing chromatography (10 mM Et_3N-HOAc, C18) followed by ion exchange (Dowex 50W-8, ammonium form) to provide **TFMU-IDPr (12)** (33.6 mg, 53%) as a white solid.

^{1}H NMR (500 MHz, D_2O) δ 8.27 (s, 1H), 7.96 (s, 1H), 7.48 (dd, *J* = 9.1, 1.9 Hz, 1H), 6.93 (dd, *J* = 9.0, 2.4 Hz, 1H), 6.85 (d, *J* = 2.4 Hz, 1H), 6.70 (s, 1H), 5.95 (d, *J* = 5.6 Hz, 1H), 5.77 (d, *J* = 4.4 Hz, 1H), 4.61 (t, *J* = 5.4 Hz, 1H), 4.49 – 4.42 (m, 2H), 4.44 – 4.39 (m, 1H), 4.37 (q, *J* = 3.8 Hz, 1H), 4.30 (dd, *J* = 6.3, 2.8 Hz, 1H), 4.28 – 4.21 (m, 2H), 4.16 (ddd, *J* = 11.5, 5.1, 3.2 Hz, 1H), 4.09 (dt, *J* = 11.3, 4.6 Hz, 1H).

^{13}C NMR (126 MHz, D_2O) δ 161.91, 160.21, 157.82, 154.77, 148.22, 145.93, 141.55 (q, $^2J_{CF}$ = 32.9 Hz), 139.48, 126.22, 123.33, 121.31 (q, $^1J_{CF}$ = 276.4, 275.8 Hz), 115.03, 112.72 (q, $^3J_{CF}$ = 8.2 Hz), 107.67, 103.87, 100.30, 87.54, 84.77 (d, $^3J_{CP}$ = 8.2 Hz), 83.86 (d, $^3J_{CP}$ = 8.5 Hz), 74.62, 71.32, 70.36, 69.71, 65.81 (d, $^2J_{CP}$ = 5.1 Hz), 65.29 (d, $^2J_{CP}$ = 5.3 Hz).

^{31}P NMR (202 MHz, D_2O) δ -11.09 (d, *J* = 21.5 Hz), -11.31 (d, *J* = 21.3 Hz).

^{19}F NMR (470 MHz, D_2O) δ -64.55.

HRMS (ESI-TOF) m/z: $[M-H]^-$ Cald for $C_{25}H_{24}F_3N_4O_{17}P_2$ 771.0569; Found 771.0566.

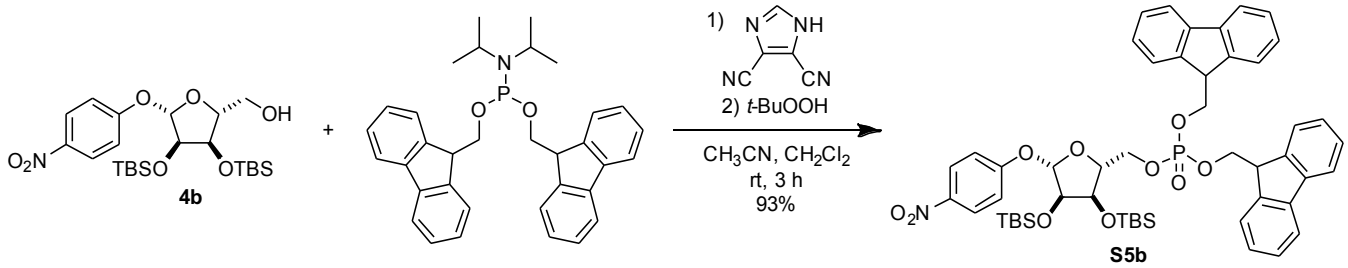

4-nitrophenyl 2,3-bis-*O*-tert-butyldimethylsilyl-β-D-ribose-5-(difluorenylmethyl phosphate) (S5b): To a 20 mL reaction vial, **4b** (360.4 mg, 0.721 mmol, 1 eq) and bis-(9H-fluoren-9-ylmethyl)-N,N-diisopropylamidophosphite (Lambrecht et al., 2015) (488 mg, 0.936 mmol, 1.3 eq) were added. Dissolved material by addition of CH_2Cl_2 (11 mL). Cooled solution to 0 ºC. 4,5-dicyanoimidazole (129 mg, 1.1 mmol, 1.5 eq) was added as a solution in acetonitrile (2 mL). After stirring at 0 ºC for 15 min, mixture was allowed to warm to room temperature and was stirred for an additional 2 h. Once starting material was consumed as indicated by TLC (75:25 hexane:EtOAc), mixture was cooled to 0 ºC and subjected to dropwise addition of *tert*-butyl hydroperoxide (0.5 mL, 2.5 mmol, 3.5 eq) as a 5 M solution in decane. Mixture was stirred for an additional 1 h and quenched with H_2O. Mixture was extracted with CH_2Cl_2 three times. Combined organic layers were dried over Na_2SO_4, concentrated, and purified by silica gel chromatography eluting with 80:20 hexane:EtOAc to yield compound **S5b** as a white foam (628 mg, 93%).

^{1}H NMR (500 MHz, $CDCl_3$) δ 7.80 (d, *J* = 9.2 Hz, 2H), 7.72 (dd, *J* = 11.9, 7.5 Hz, 3H), 7.50 – 7.33 (m, 9H), 7.30 – 7.20 (m, 4H), 6.76 (d, *J* = 9.2 Hz, 2H), 5.31 (m, 1H), 4.28 (dd, *J* = 7.0, 4.0 Hz, 1H), 4.21 – 3.98 (m, 9H), 3.92 (dt, *J* = 11.3, 4.0 Hz, 1H), 0.91 (s, 9H), 0.90 (s, 9H), 0.11 (s, 3H), 0.10 (s, 3H), 0.08 (s, 3H), 0.06 (s, 3H).

^{13}C NMR (126 MHz, $CDCl_3$) δ 161.50, 143.09, 143.07, 143.04, 142.22, 141.43, 141.40, 141.37, 128.07, 128.04, 127.22, 127.20, 127.18, 125.64, 125.20, 125.14, 125.12, 120.19, 120.16, 120.12, 116.01, 105.07, 81.77, 81.70, 76.53, 70.84, 69.47, 69.45, 69.42, 69.41, 65.74, 65.70, 48.02, 47.98, 47.96, 47.92, 25.95, 25.86, 18.21, 18.14, -4.10, -4.43, -4.44, -4.86.

^{31}P NMR (202 MHz, $CDCl_3$) δ -1.68

HRMS (ESI-TOF) m/z: $[M+Na]^+$ Calcd for $C_{51}H_{62}NO_{10}NaSi_2P$ 958.3548; Found 958.3540.

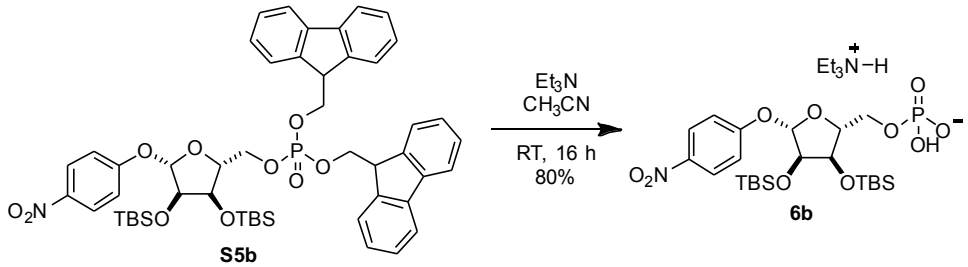

Triethylammonium 4-nitrophenyl 2,3-bis-*O*-tert-butyldimethylsilyl-β-D-ribose-5-phosphate (6b): 20 mL reaction vial was charged with compound **S5b** (551 mg, 0.59 mmol, 1 eq). Added acetonitrile (6 mL) and triethylamine (1.5 mL) successively. Stirred at room temperature for 16 h. Added 1 mL toluene to stirring solution and concentrated *in vacuo*. Residue was redissolved in methanol (0.5 mL) and purified by C-18 chromatography to yield the triethylammonium salt of compound **6b** as a tan foam (322 mg, 80%).

^{1}H NMR (500 MHz, CD_3OD) δ 8.22 (d, *J* = 9.2 Hz, 2H), 7.19 (d, *J* = 9.3 Hz, 2H), 5.55 (d, *J* = 3.0 Hz, 1H), 4.40 (dd, *J* = 4.3, 3.0 Hz, 1H), 4.36 (t, *J* = 4.3 Hz, 1H), 4.23 (dt, *J* = 5.7, 4.4 Hz, 1H), 4.00 (dt, *J* = 10.0,

4.7 Hz, 1H), 3.87 – 3.80 (m, 1H), 3.15 (q, *J* = 7.3 Hz, 6H), 1.28 (t, *J* = 7.3 Hz, 9H), 0.95 (s, 9H), 0.93 (s, 9H), 0.19 (s, 3H), 0.17 (s, 3H), 0.16 (s, 3H), 0.16 (s, 3H).

^{13}C NMR (126 MHz, CD_3OD) δ 163.55, 143.73, 126.70, 117.67, 106.77, 85.92 (d, *J* = 9.2 Hz), 78.04, 73.84, 66.50 (d, *J* = 4.8 Hz), 47.53, 26.46, 26.38, 19.05, 18.97, 9.11, -4.09, -4.17, -4.33, -4.52.

^{31}P NMR (202 MHz, CD_3OD) δ 0.66.

HRMS (ESI-TOF) m/z: $[M-H]^-$ Calcd for $C_{23}H_{41}NO_{10}Si_2P$ 578.2007; Found 578.2009.

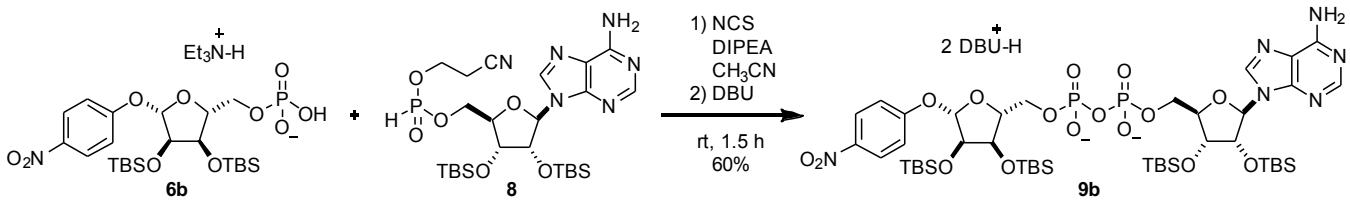

β-1''-*O*-(4-nitrophenyl)-2',2'',3',3''-*O*-tetrakis-(tert-butyldimethylsilyl)-ADP-ribose (9b): To a 20 mL reaction vial was added **6b** (113.7 mg, 0.167 mmol, 1.0 eq) and **8** (110.0 mg, 0.179 mmol, 1.1 eq). Mixture was dried by co-azeotroping with dry acetonitrile three times and placing under vacuum over P_2O_5 for 12 h. The mixture was dissolved in acetonitrile (2.0 mL). Then, $(i\text{-}Pr_2)_2NEt$ (64.6 mg, 0.5 mmol, 3 eq) and *N*-chlorosuccinimide (53.4 mg, 0.4 mmol, 2.4 eq) were sequentially added as 1 M solutions in acetonitrile and stirred at room temperature for 1 h. 1,8-diazabicycloundec-7-ene (350 mg, 2.3 mmol, 10 eq) was added as a 1 M solution in THF. After stirring for 30 min, reaction mixture was evaporated *in vacuo* and purified by C18 chromatography to yield compound **9b** as a white foam (149.6 mg, 60%).

^{1}H NMR (500 MHz, CD_3OD) δ 8.64 (s, 1H), 8.173 (s, 1H), 8.172 (d, *J* = 9.2 Hz, 2H), 7.15 (d, *J* = 9.2 Hz, 2H), 6.10 (d, *J* = 7.5 Hz, 1H), 5.51 (d, *J* = 4.1 Hz, 1H), 4.80 (dd, *J* = 7.5, 4.4 Hz, 1H), 4.45 (t, *J* = 4.2 Hz, 1H), 4.42 (d, *J* = 4.5, 1H), 4.38 (dd, *J* = 4.4, 2.7 Hz, 1H), 4.26 (td, *J* = 5.9, 2.8 Hz, 1H), 4.23 (m, 2H), 4.16 (m, 1H), 4.08 (qt, *J* = 10.9, 5.5 Hz, 2H), 3.55 (m, 4H), 3.49 (t, *J* = 5.9 Hz, 4H), 3.35 (m, 9H), 2.68 (m, 4H), 1.99 (m, 4H), 1.70 (m, 12H), 0.97 (s, 9H), 0.94 (s, 9H), 0.90 (s, 9H), 0.69 (s, 9H), 0.18 (s, 3H), 0.17 (s, 3H), 0.16 (s, 3H), 0.15 (s, 6H), 0.14 (s, 3H), -0.03 (s, 3H), -0.40 (s, 3H)

^{13}C NMR (126 MHz, CD_3OD) δ 167.45, 163.85, 157.31, 153.80, 151.17, 143.64, 141.65, 126.69, 120.02, 117.69, 107.14, 87.75, 87.63 (d, *J* = 8.6 Hz), 86.75 (d, *J* = 9.0 Hz), 78.21, 77.67, 74.85, 74.26, 66.86 (d, *J* = 5.2 Hz), 66.68 (d, *J* = 5.1 Hz), 55.25, 49.85, 49.54, 39.34, 33.62, 30.02, 27.55, 26.51, 26.48, 26.44, 26.21, 24.98, 20.43, 19.08, 18.99, 18.92, 18.64, -4.08, -4.13, -4.19, -4.21, -4.26, -4.29, -5.29.

^{31}P NMR (202 MHz, CD_3OD) δ -11.44 (d, *J* = 21.5 Hz), -11.65 (d, *J* = 21.5 Hz).

HRMS (ESI-TOF) m/z: $[M-H]^-$ Calcd for $C_{45}H_{82}N_6O_{16}P_2Si_4$ 1135.4267; Found 1135.4272.

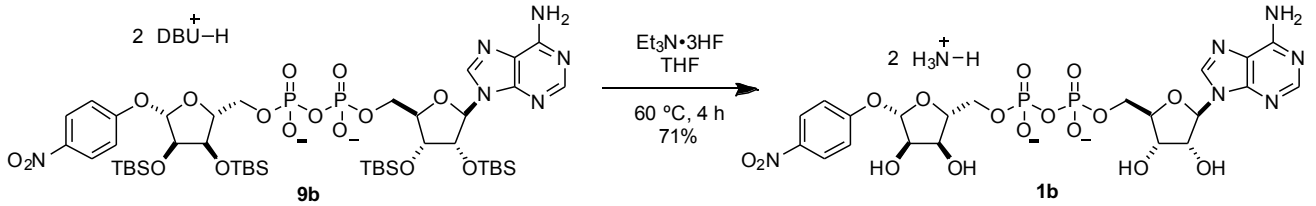

β-pNP-ADPr (1b): To a 20 mL reaction vial was added **9b** (24.1 mg, 0.0167 mmol, 1 eq) and THF (1 mL). Triethylamine trihydrofluoride (0.1 mL, 0.989 g/mL) was added dropwise to stirring solution. Reaction vessel was sealed and heated to 60 C for 4 h. Reaction was closely monitored by TLC (80:20 2-propanol:0.2% $NH_4OH_{(aq)}$) Once reaction had gone to completion, reaction mixture was cooled to room temperature and concentrated *in vacuo*. Remaining acid was quenched by dropwise addition of satd aq $NaHCO_3$. Aqueous solution of crude product was purified by C18 chromatography utilizing ion-pairing

reagent in the mobile phase (10 mM Et_3N-HOAc, pH 7.0) to yield compound **1b** as a triethylammonium salt. The triethylammonium salt was eluted through Dowex 50W-8X (ammonium-form) to give the ammonium salt of compound **1b** as a white powder (8.5 mg, 71%).

^{1}H NMR (500 MHz, D_2O) δ 8.33 (s, 1H), 8.11 (s,1H), 7.94 (d, *J* = 9.3 Hz, 2H), 6.93 (d, *J* = 9.4 Hz, 2H), 5.99 (d, *J* = 5.4, 1H), 5.64 (d, *J* = 1.0 Hz, 1H), 4.62 (t, *J* = 5.2 Hz, 1H), 4.46 (m, 2H), 4.34 (m, 2H), 4.29 (td, *J* = 5.9, 4.1 Hz, 1H), 4.19 (m, 2H), 4.16 (q, *J* = 3.9 Hz, 1H), 4.08 (m, 1H)

^{13}C NMR (126 MHz, D_2O) δ 181.63, 161.38, 155.43, 152.74, 148.68, 141.68, 139.53, 125.67, 118.51, 116.45, 105.24, 87.17, 83.80, 82.78, 74.68, 70.70, 70.32, 66.69, 65.14.

^{31}P NMR (202 MHz, D_2O) δ -10.19.

HRMS (ESI-TOF) m/z: $[M-H]^-$ Calcd for $C_{21}H_{26}N_6O_{16}P_2$ 679.0808; Found 679.0809.

QUANTIFICATION AND STATISTICAL ANALYSIS

All the data were presented as mean ± standard error of mean from at least three independent trials. All data fitting and statistical analysis was performed using GraphPad Prism (version 6).

SUPPLEMENTAL DATAFILES

Data S1: Related to Figure 2. NMR spectra of PARG substrates, inhibitors, and synthetic intermediates.

Figure 1

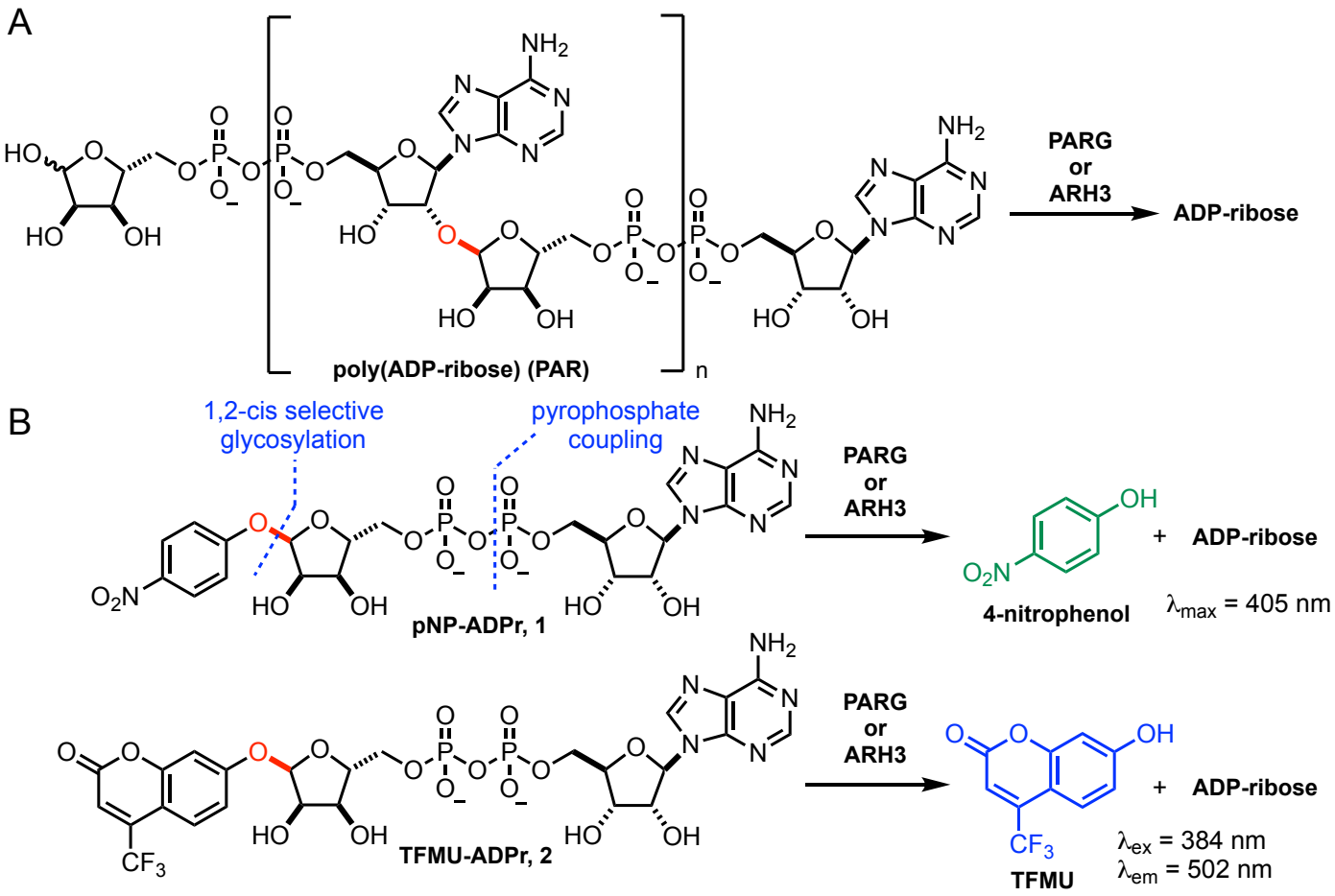
A
poly(ADP-ribose) (PAR)
n
PARG
or
ARH3
ADP-ribose
B
1,2-cis selective
glycosylation
pyrophosphate
coupling
pNP-ADPr, 1
PARG
or
ARH3
4-nitrophenol
+ ADP-ribose
λmax = 405 nm
TFMU-ADPr, 2
PARG
or
ARH3
TFMU
+ ADP-ribose
λex = 384 nm
λem = 502 nm

Figure 2

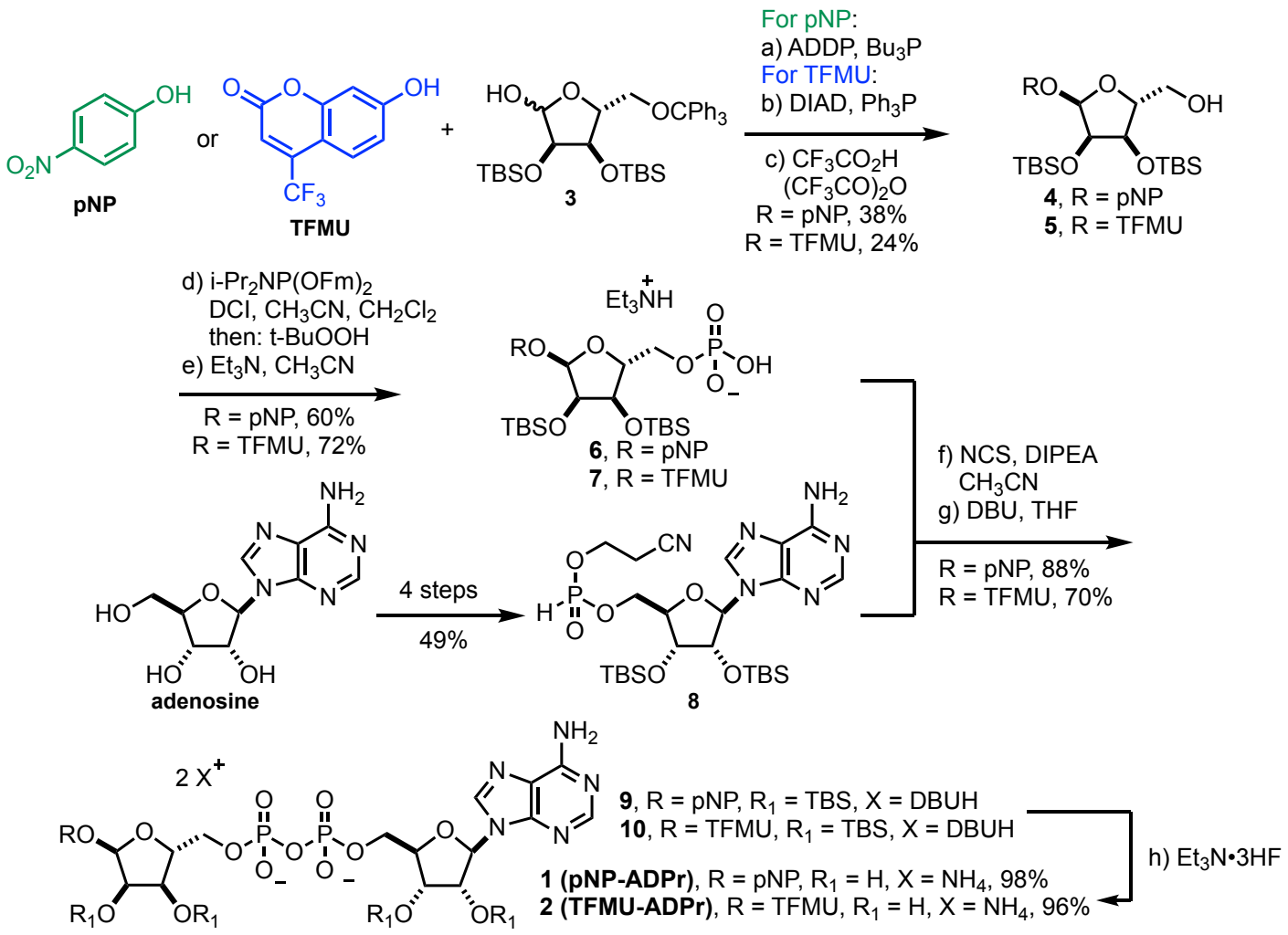
pNP
or
TFMU
+
3
For pNP:
a) ADDP, Bu3P
For TFMU:
b) DIAD, Ph3P
c) CF3CO2H
(CF3CO)2O
R = pNP, 38%
R = TFMU, 24%
4, R = pNP
5, R = TFMU
d) i-Pr2NP(OFm)2
DCI, CH3CN, CH2Cl2
then: t-BuOOH
e) Et3N, CH3CN
R = pNP, 60%
R = TFMU, 72%
6, R = pNP
7, R = TFMU
adenosine
4 steps
49%
8
f) NCS, DIPEA
CH3CN
g) DBU, THF
R = pNP, 88%
R = TFMU, 70%
9, R = pNP, R1 = TBS, X = DBUH
10, R = TFMU, R1 = TBS, X = DBUH
1 (pNP-ADPr), R = pNP, R1 = H, X = NH4, 98%
2 (TFMU-ADPr), R = TFMU, R1 = H, X = NH4, 96%
h) Et3N•3HF

A. Figure 3

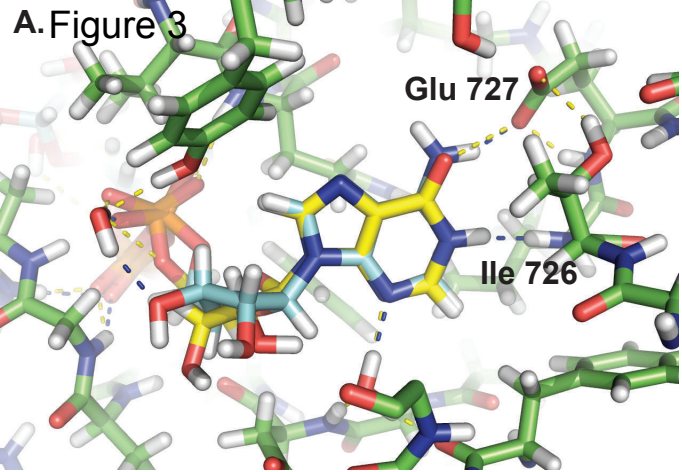
Glu 727
Ile 726

B.

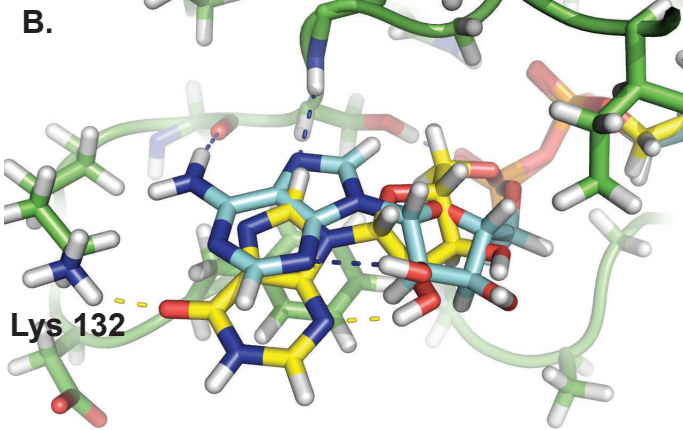
Lys 132

C.

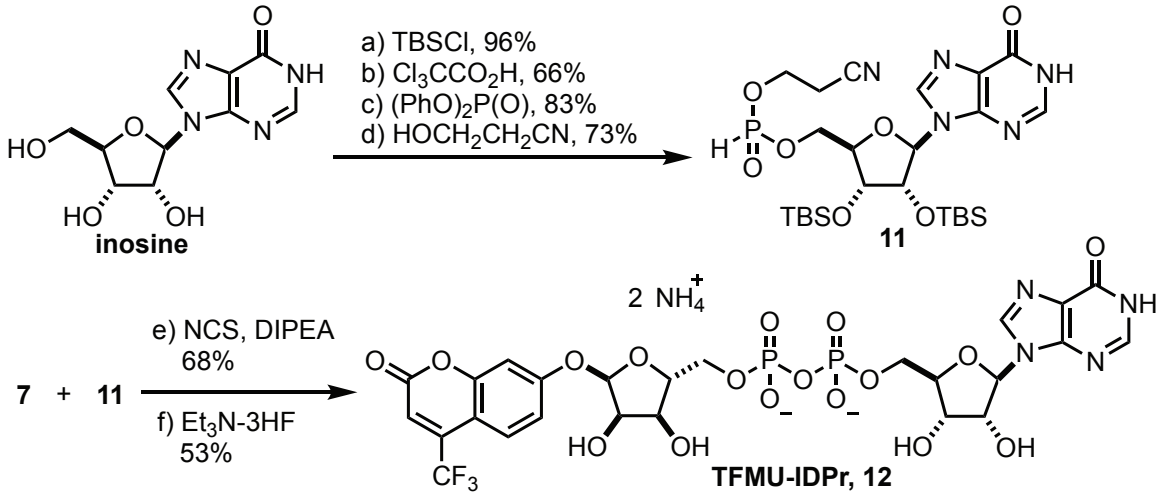
HO
HO
OH
O
N
NH
inosine
a) TBSCl, 96%
b) Cl3CCO2H, 66%
c) (PhO)2P(O), 83%
d) HOCH2CH2CN, 73%
CN
H
TBSO
OTBS
11
7 + 11
e) NCS, DIPEA
68%
f) Et3N-3HF
53%
2 NH4+
CF3
TFMU-IDPr, 12

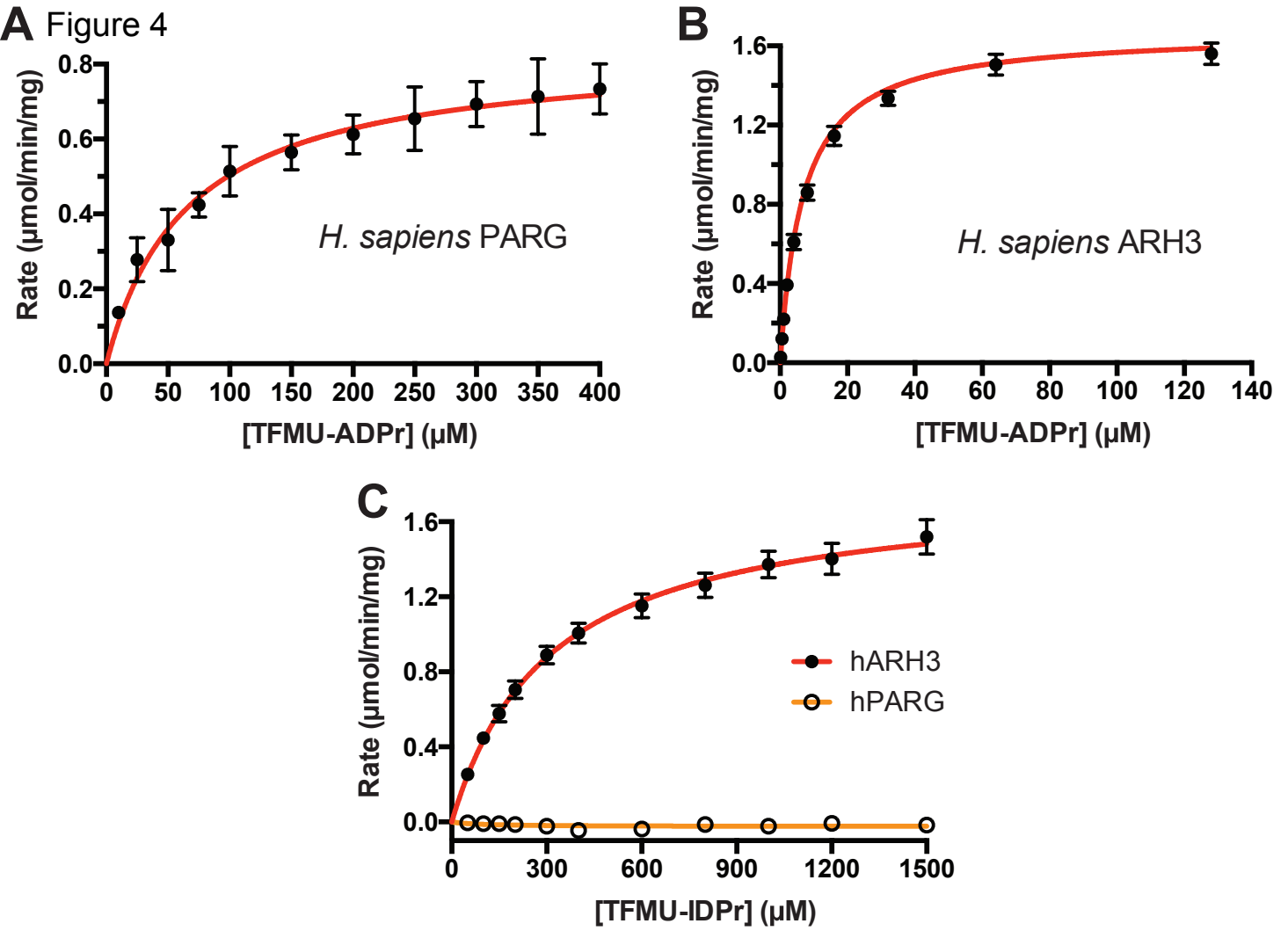
A
Figure 4
Rate (µmol/min/mg)
0.0
0.2
0.4
0.6
0.8
0
50
100
150
200
250
300
350
400
[TFMU-ADPr] (µM)
H. sapiens PARG
B
Rate (µmol/min/mg)
0.0
0.4
0.8
1.2
1.6
0
20
40
60
80
100
120
140
[TFMU-ADPr] (µM)
H. sapiens ARH3
C
Rate (µmol/min/mg)
0.0
0.4
0.8
1.2
1.6
0
300
600
900
1200
1500
[TFMU-IDPr] (µM)
hARH3
hPARG

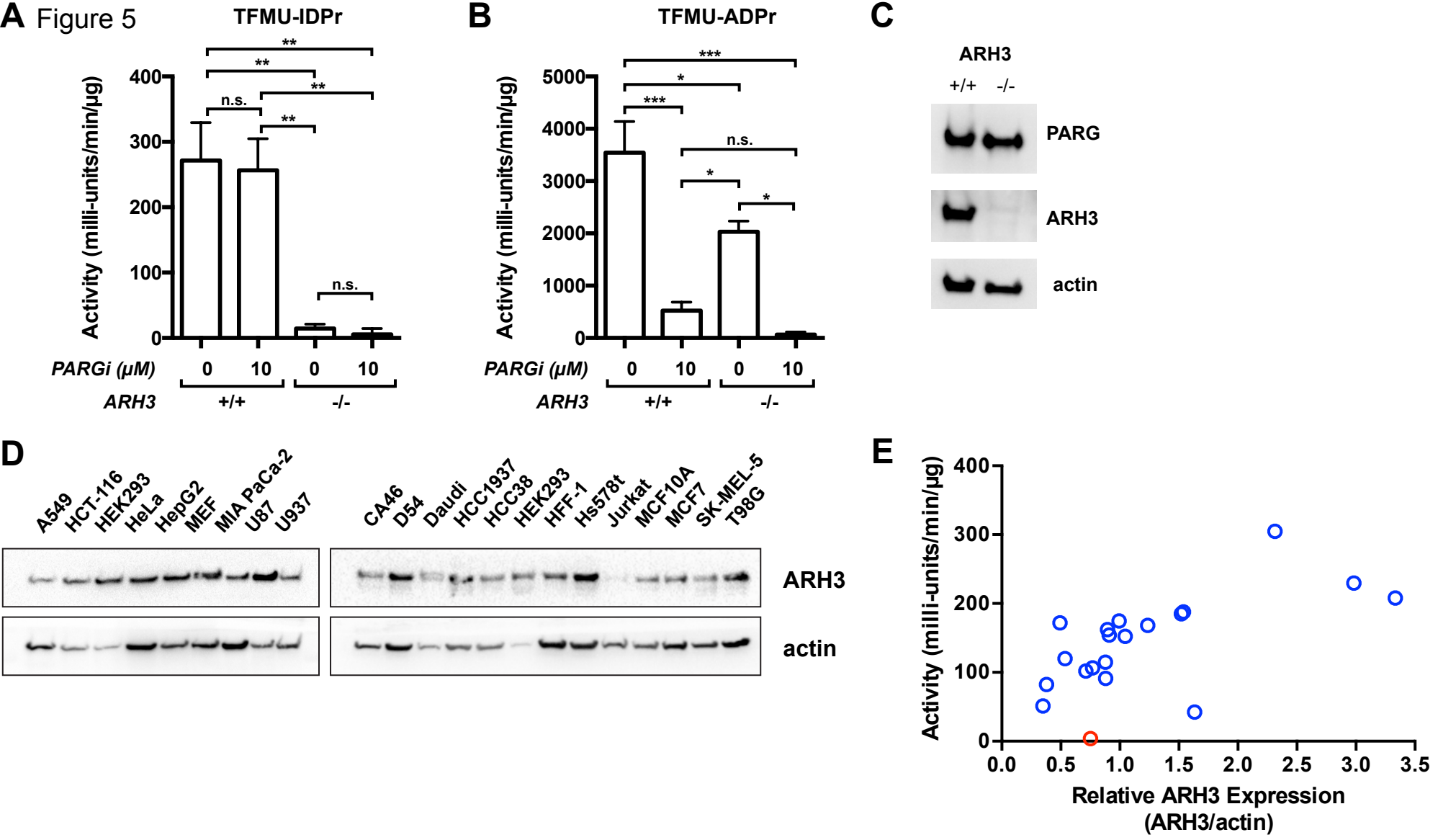
A Figure 5
TFMU-IDPr
Activity (milli-units/min/µg)
400
300
200
100
0
**
**
**
**
n.s.
n.s.
PARGi (µM)
0
10
0
10
ARH3
+/+
-/-
B
TFMU-ADPr
Activity (milli-units/min/µg)
5000
4000
3000
2000
1000
0
***
*
***
n.s.
*
*
PARGi (µM)
0
10
0
10
ARH3
+/+
-/-
C
ARH3
+/+
-/-
PARG
ARH3
actin
D
A549
HCT-116
HEK293
HeLa
HepG2
MEF
MIA PaCa-2
U87
U937
CA46
D54
Daudi
HCC1937
HCC38
HEK293
HFF-1
Hs578t
Jurkat
MCF10A
MCF7
SK-MEL-5
T98G
ARH3
actin
E
Activity (milli-units/min/µg)
400
300
200
100
0
0.0
0.5
1.0
1.5
2.0
2.5
3.0
3.5
Relative ARH3 Expression
(ARH3/actin)

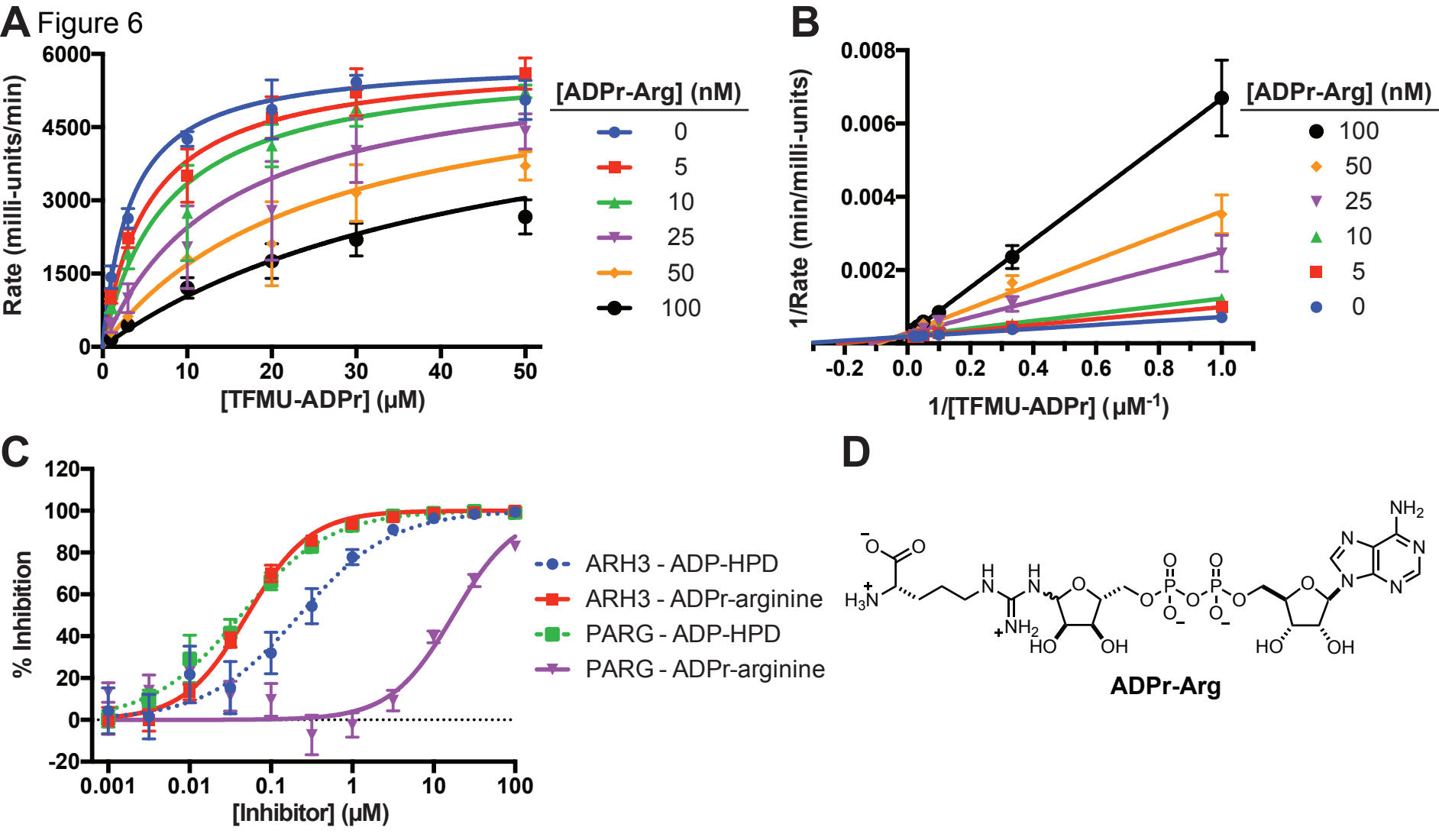
A Figure 6
Rate (milli-units/min)
6000
4500
3000
1500
0
0
10
20
30
40
50
[TFMU-ADPr] (μM)
[ADPr-Arg] (nM)
0
5
10
25
50
100
B
1/Rate (min/milli-units)
0.008
0.006
0.004
0.002
-0.2
0.0
0.2
0.4
0.6
0.8
1.0
1/[TFMU-ADPr] (μM-1)
[ADPr-Arg] (nM)
100
50
25
10
5
0
C
% Inhibition
120
100
80
60
40
20
0
-20
0.001
0.01
0.1
1
10
100
[Inhibitor] (μM)
ARH3 - ADP-HPD
ARH3 - ADPr-arginine
PARG - ADP-HPD
PARG - ADPr-arginine
D
ADPr-Arg

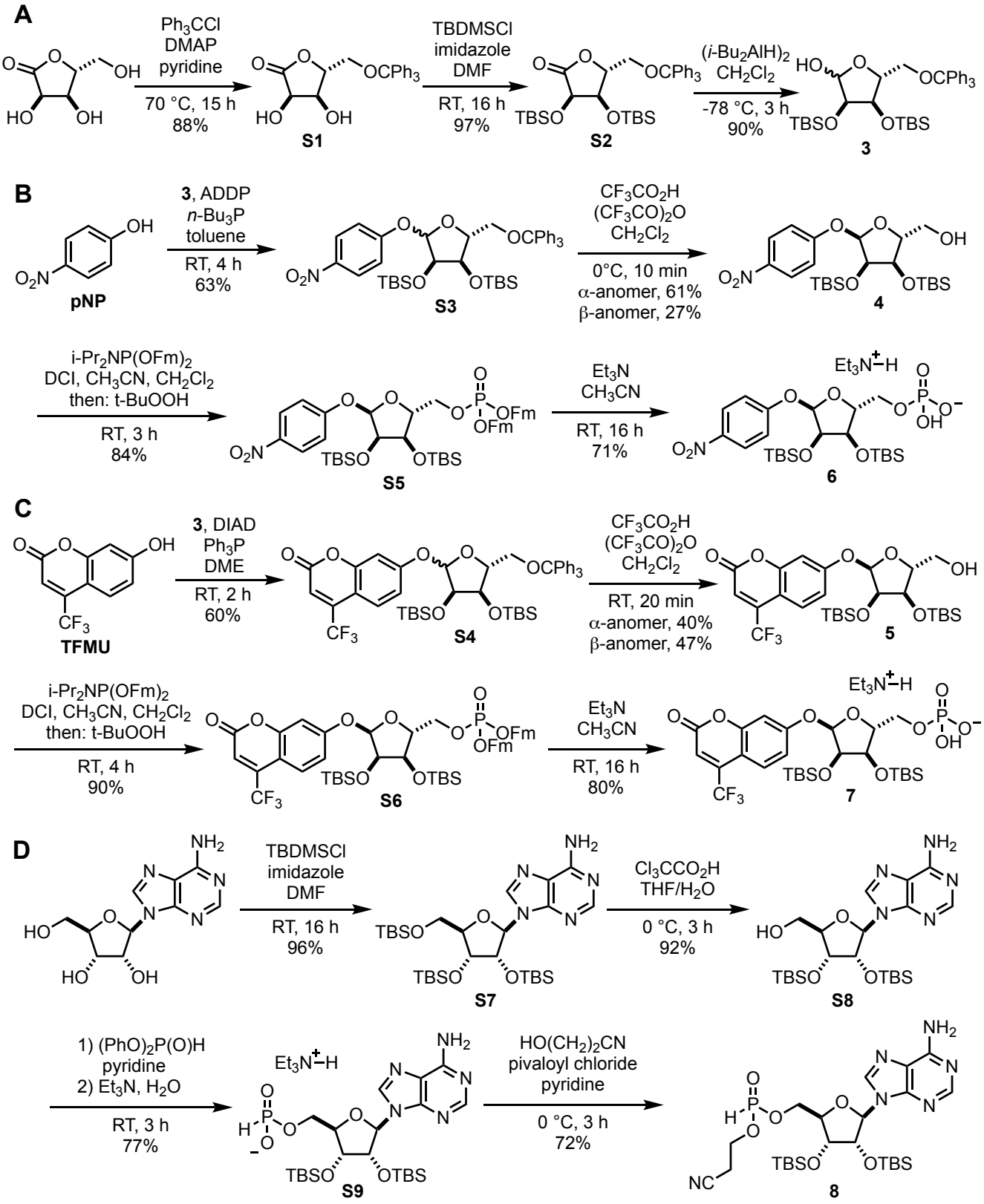

Figure S1: Related to Figure 2. Expanded synthetic scheme of glycosyl donor (A), pNP-ribose (B), TFMU-ribose (C), and adenosine phosphonate (D).

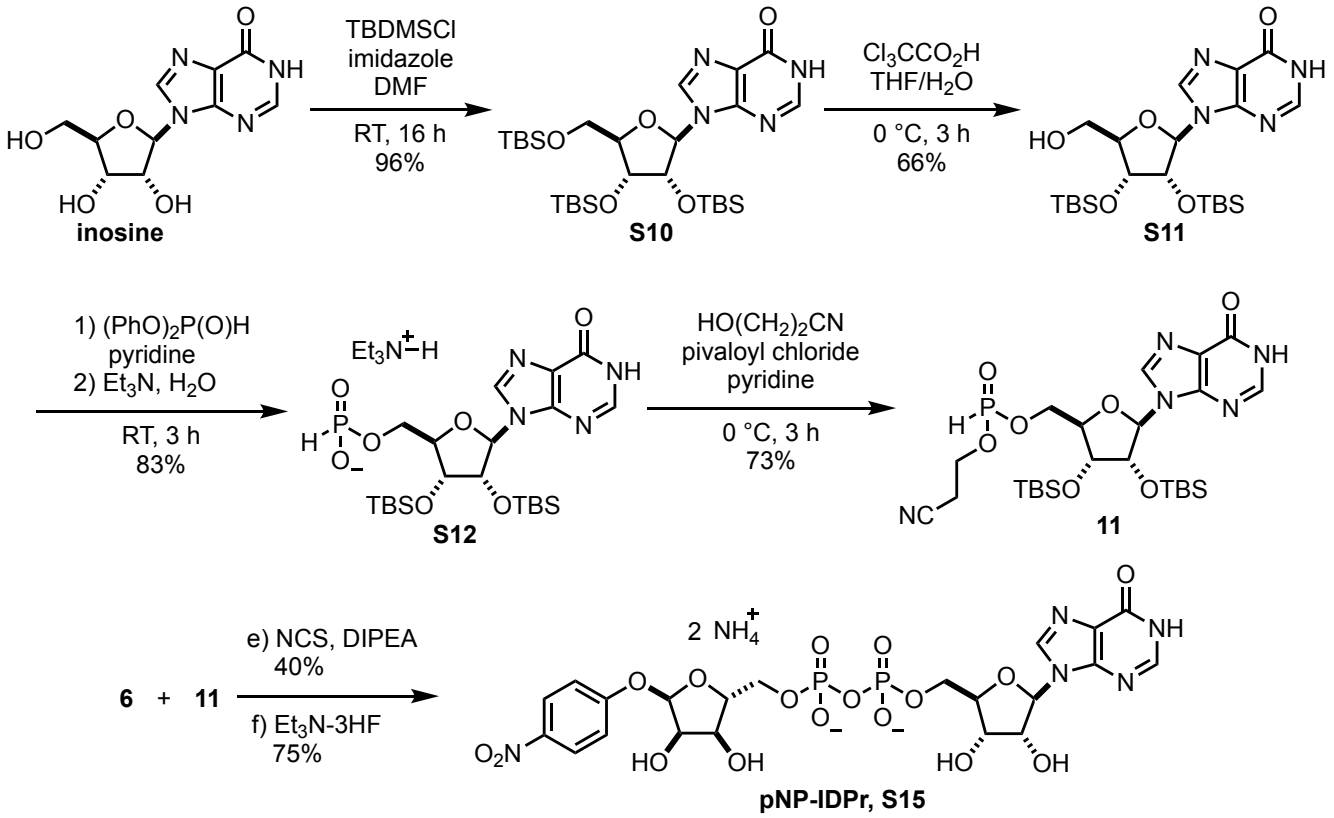

Figure S2: Related to Figure 3. Synthesis of pNP-IDPr.

Table S1: Related to Figure 3. Docking scores for sugar nucleotides in PARG and ARH3.

Enzyme	Ligand	SP score (kcal/mol)	SP Difference (kcal/mol)	XP score (kcal/mol)	XP difference (kcal/mol)
L. chalumnae ARH3	ADPr	-7.539	-	-6.254	-
	IDPr	-6.729	0.810	-7.000	-0.746
	GDPr	-6.692	0.847	-6.131	0.123
	XDPr	-7.100	0.439	-6.732	-0.478
H. sapiens PARG	ADPr	-12.229	-	-8.262	-
	IDPr	-10.332	1.897	-6.613	1.649
	GDPr	-10.906	1.323	-6.323	1.939
	XDPr	-11.292	0.937	-6.090	2.172

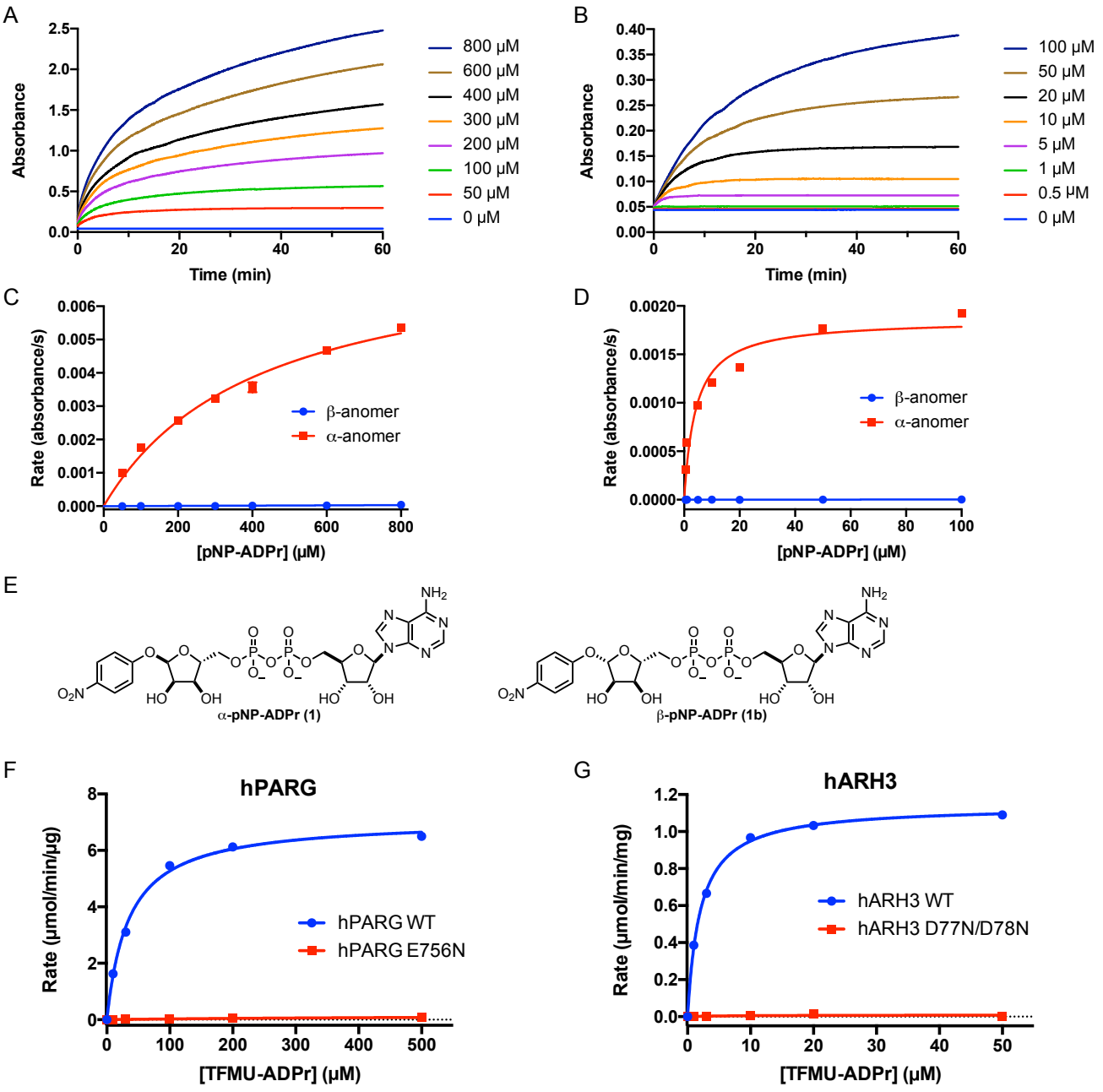

Figure S3: Related to Figure 4. A. Reaction progress curves of ttPARG-catalyzed hydrolysis of **pNP-ADPr**. Enzyme (50 nM) was incubated with varying concentration of **pNP-ADPr** in 50 µL of appropriate reaction buffer in a 384-well plate. Reaction was monitored every 2 s for 60 min. B. Same as B but with hARH3. C. Stereoselectivity of PARG and ARH3 for α glycosidic bonds. ttPARG (50 nM) was incubated with varying concentrations of α and β **pNP-ADPr** in 50 µL of appropriate reaction buffer in a 384-well plate. Initial reaction rates were obtained by monitoring reaction progress using an absorbance plate reader (405 nm). D. Same as C but with hARH3. E. Structures of α and β **pNP-ADPr**. F. Processing of TFMU-ADPr by catalytically active (WT) and inactive (E756N) hPARG. G. Processing of TFMU-ADPr by catalytically active (WT) and inactive (D77N/D78N) hARH3. Error bars represent SEM, n = 3.

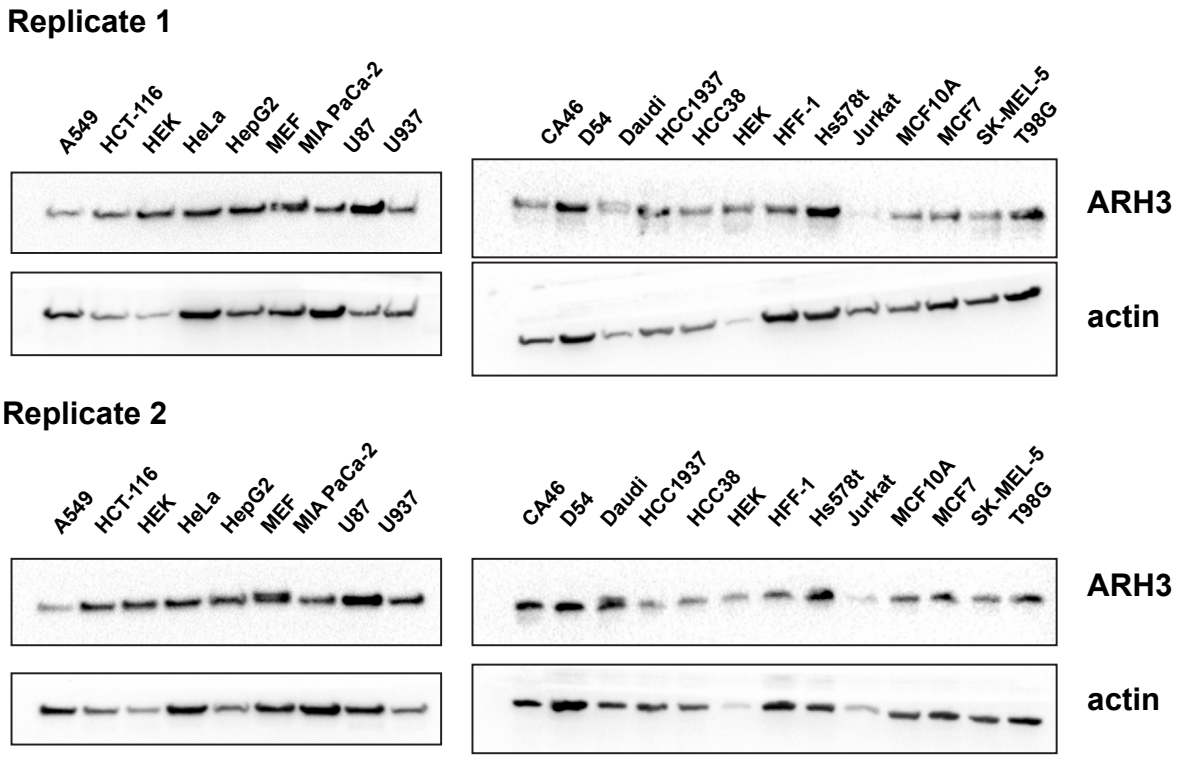

Figure S4: Related to Figure 5. Expanded images of Western blotting to evaluate ARH3 expression. Replicate 1 is same as shown in Figure 5D but without straightening. Anti-ARH3 (1:1000), anti-PARP1 (1:3000), anti-actin (1:3000).

Table S2: Related to Figure 5. Data used to construct Figure 5D.

Cell Line	ARH3 Activity (milli-units/min/µg)	Relative ARH3 expression (ARH3/actin)
U87	290±52	2.3±0.4
HepG2	215±19	3.0±0.9
HEK	192±20	3.3±0.4
HCT-116	173±17	1.54±0.06
Hs578t	170±34	1.5±0.6
HeLa	159±18	1.0±0.2
MIA PaCa-2	157±25	0.49±0.08
MEF	153±38	1.24±0.09
D54	147±34	0.90±0.05
T98G	139±7	0.9±0.2
U937	137±34	1.0±0.3
HFF-1	105±20	0.5±0.1
HCC38	100±19	0.88±0.09
MCF7	92±40	0.8±0.3
SK-MEL-5	87±13	0.7±0.2
HCC1937	76±4	0.9±0.2
A549	67±23	0.38±0.02
Jurkat	36±7	0.3±0.2
Daudi	27±35	1.6±0.7
MCF10A	-5±12	0.8±0.3

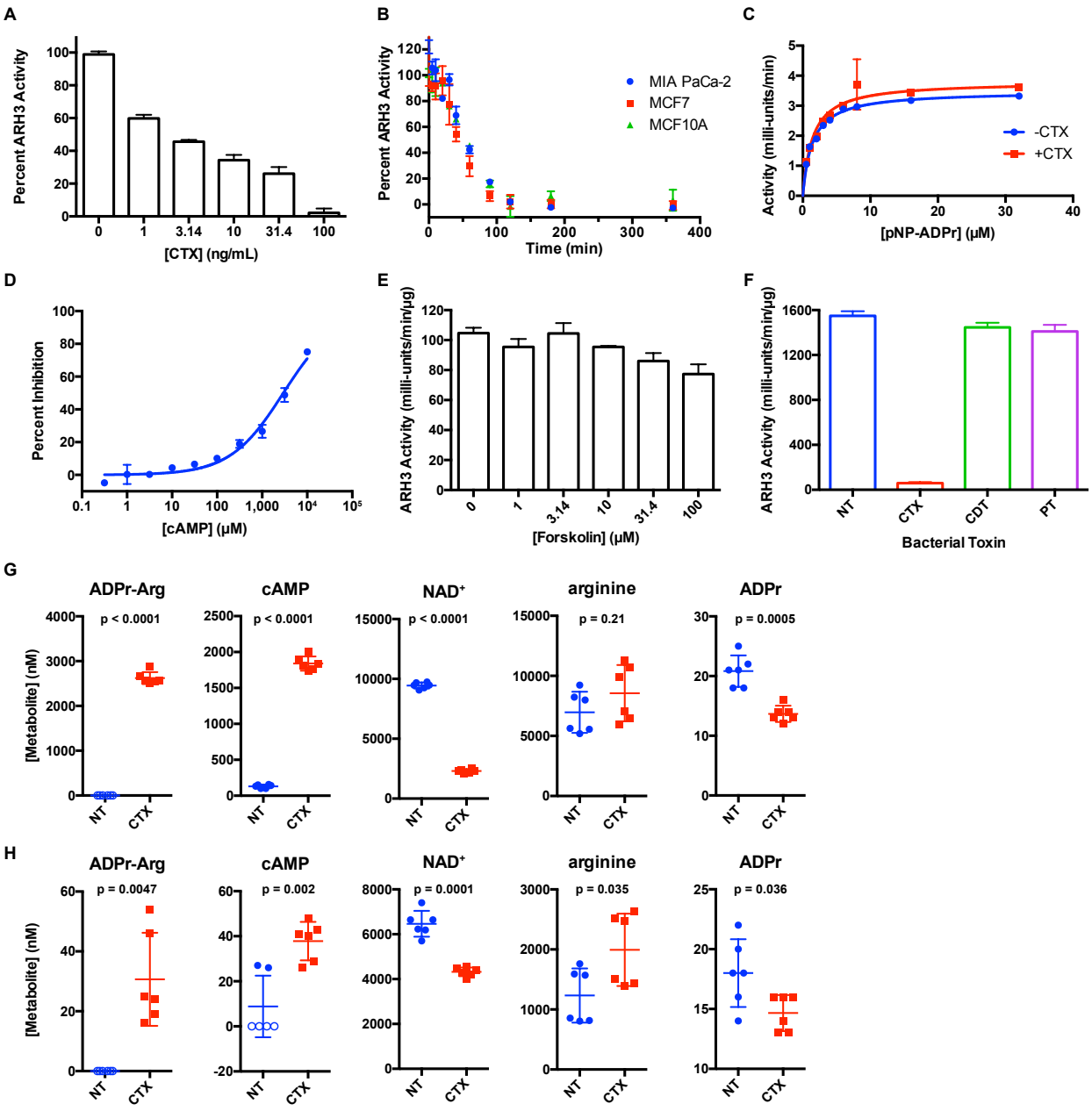

Figure S5: Related to Figure 6. A. MCF10A cells were cultured in the absence of CTX for five passages. Cells were plated 1x10^5 cells/well in 6-well plate. Cells were treated with varied concentration of CTX for 48 h. Remaining ARH3 activity was measured with 200 μM **TFMU-IDPr**. B. Cells were plated 3x105 cells/well in 6-well plate. Cells were treated with 100 ng/mL CTX for the indicated period of time. Remaining ARH3 activity was measured with 200 μM **TFMU-IDPr**. C. In vitro activity of purified ARH3 in the presence or absence of 100 ng/mL CTX. D. Dose-response curve of ARH3 inhibition by cAMP using 200 μM TFMU-IDPr. E. MCF10A cells treated with forskolin for 1 h. F. A549 cells treated with various bacterial toxins for 24 h. Following treatment, ARH3 activity in cell lysate was assessed. CTX, cholera toxin 100 ng/mL; CDT, *C. difficile* toxin 200 ng/mL CDTa 400 ng/mL CDTb; PT, pertussis toxin 100 ng/mL. G. Metabolic profiling of MCF7 cells treated with 100 ng/mL CTX for 6 h. Metabolites (ADPr-Arg, cAMP, ADP-ribose, NAD$^+$, and arginine) in methanolic cell extract were quantified by LC-MS/MS. Samples below the limit of detection are indicated by open points. Error bars represent standard deviation, n = 6. P values are from unpaired t-test with Welch's correction H. Same as G but with U2OS cells.

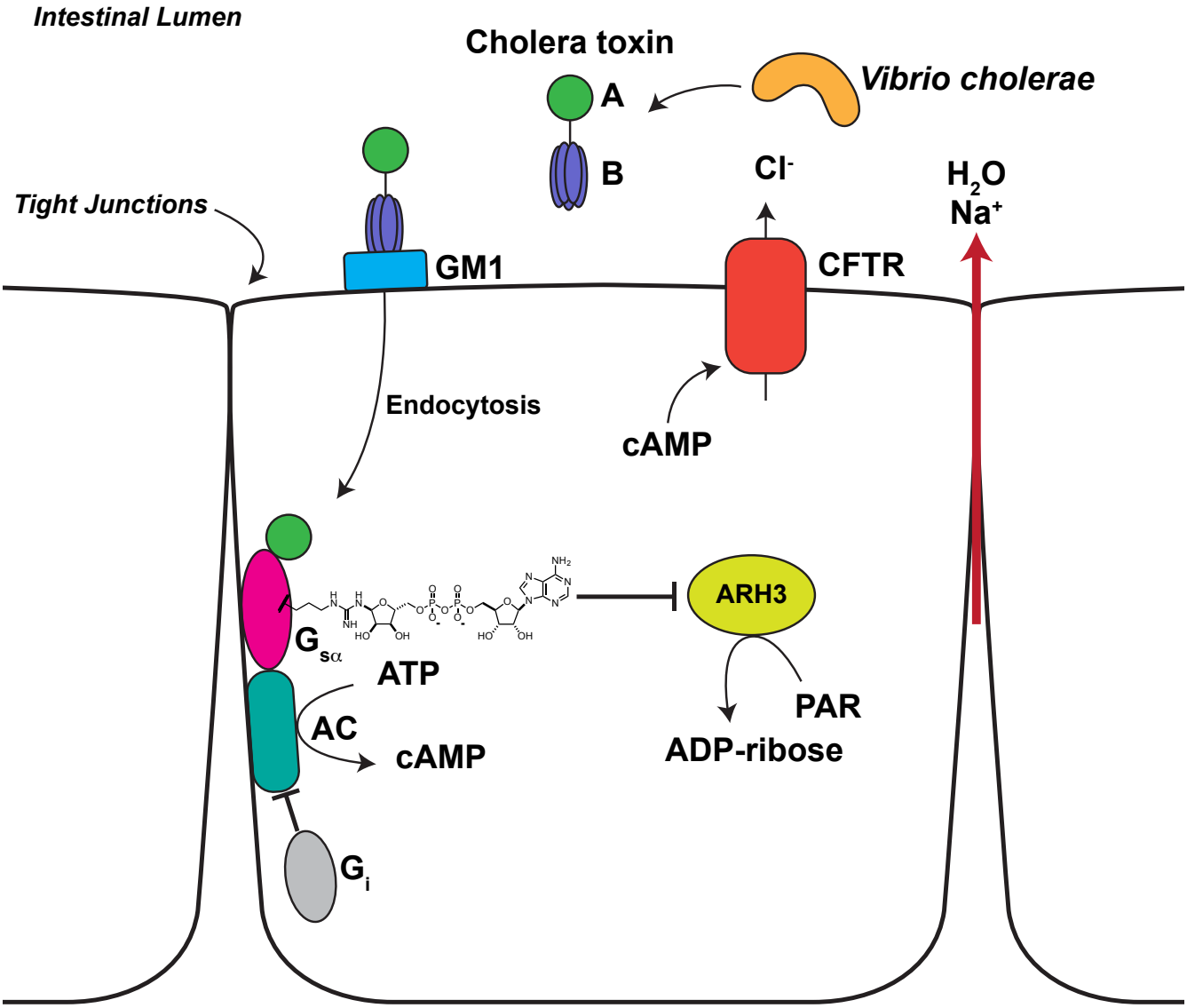

Figure S6: Related to Figure 6. Canonical mechanism of action for cholera toxin and involvement of ARH3. Cholera toxin is secreted as a binary toxin by *Vibrio cholera* within the intestinal lumen. Subunit B binds to GM1 receptor and is endocytosed. Subunit A contains an ADP-ribosyltransferase domain that ADP-ribosylates $G_{s\alpha}$. This PTM causes constitutive activitation of $G_{s\alpha}$, which activates AC leading to cAMP synthesis. Increased cAMP concentrations lead to cystic fibrosis transmembrane conductance regulator (CFTR) activation and efflux of chloride. Tight junctions are weakened leading to sodium and water leakage through the intercellular space, resulting in dehydration and loss of electrolytes (Thiagarajah and Verkman, 2012). Pertussis toxin acts through a similar manner by ADP-ribosylation of G_i which also gives rise to increased cAMP synthesis.

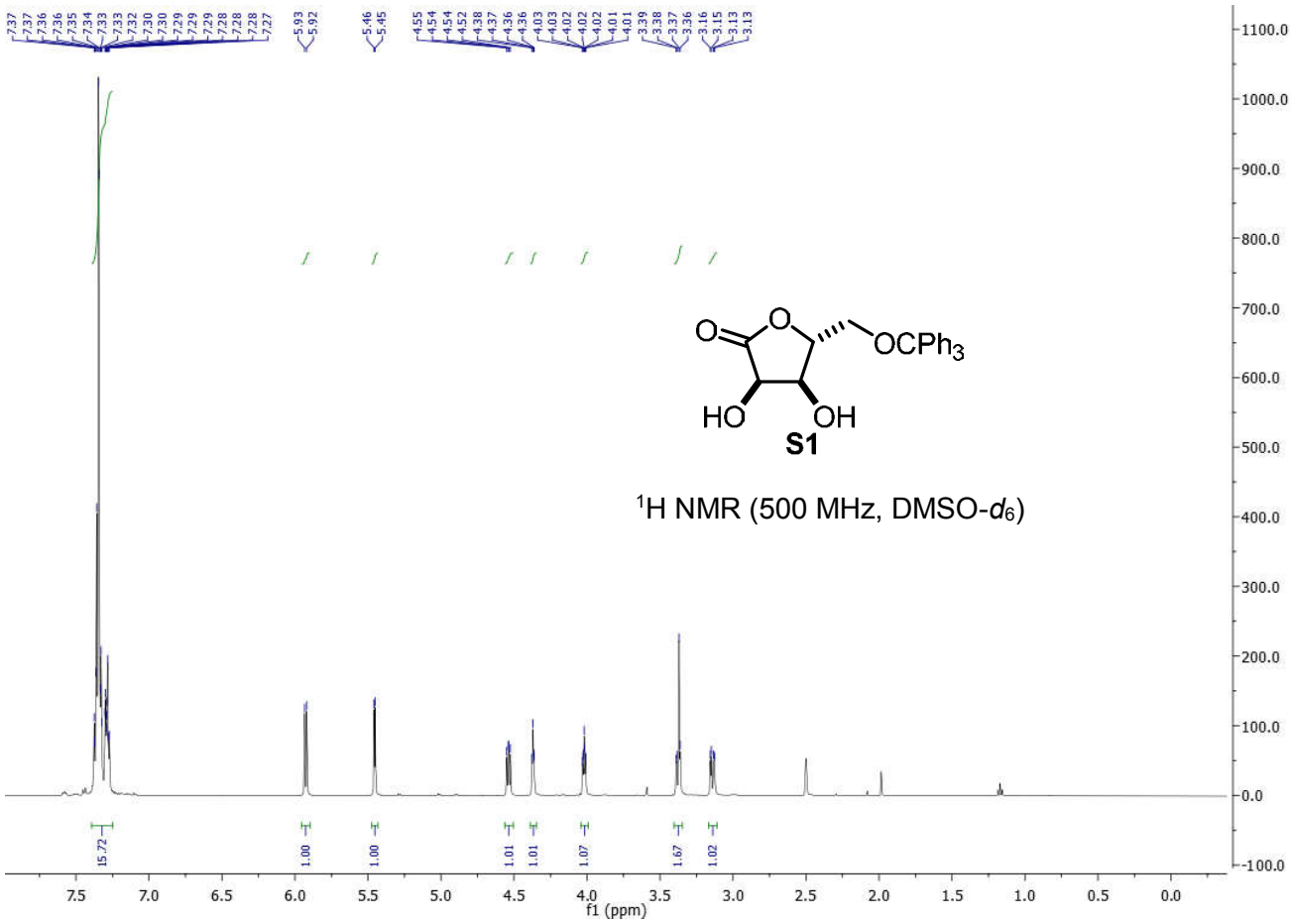

^{1}H NMR (500 MHz, DMSO-d_6)

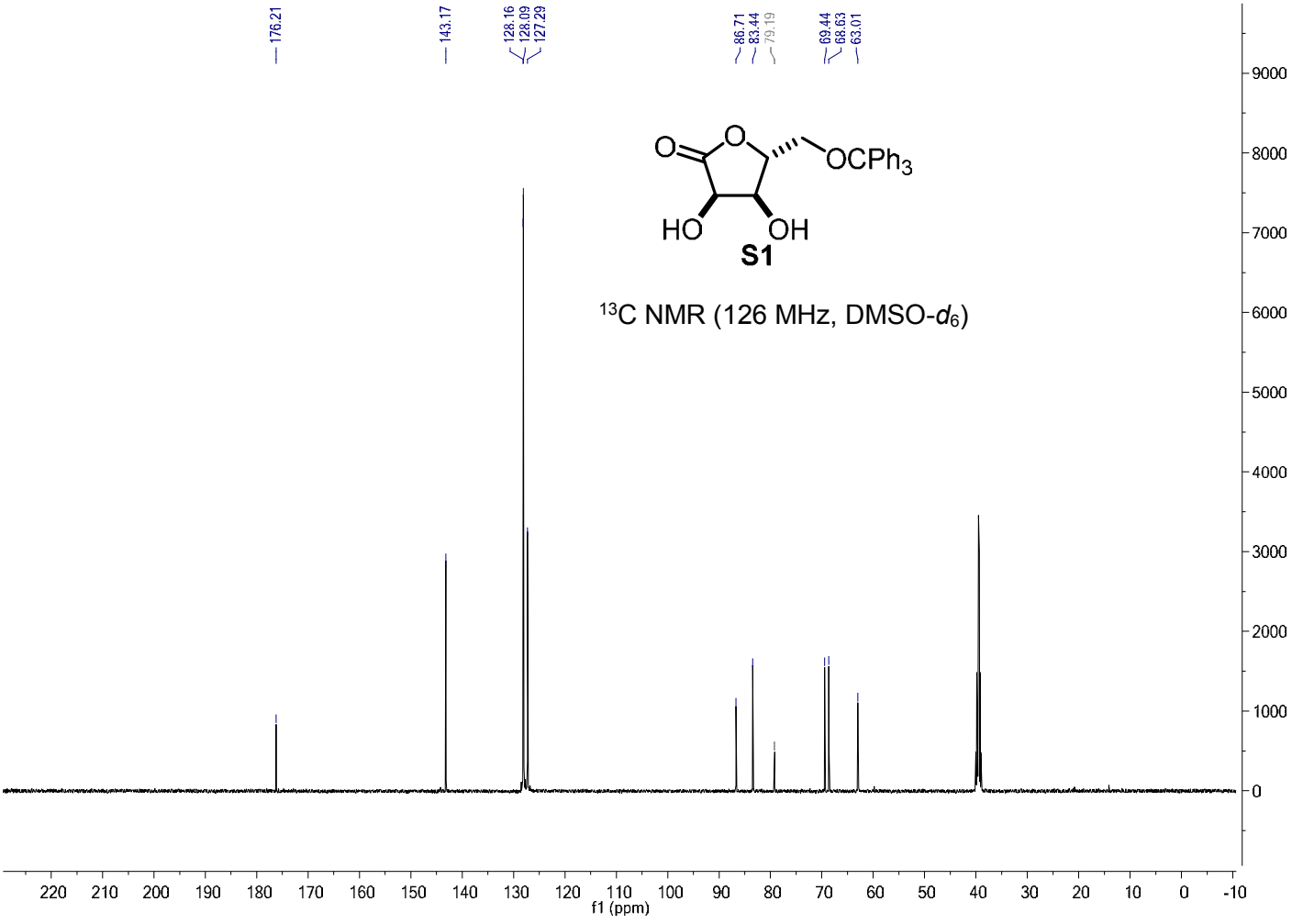

^{13}C NMR (126 MHz, DMSO-d_6)

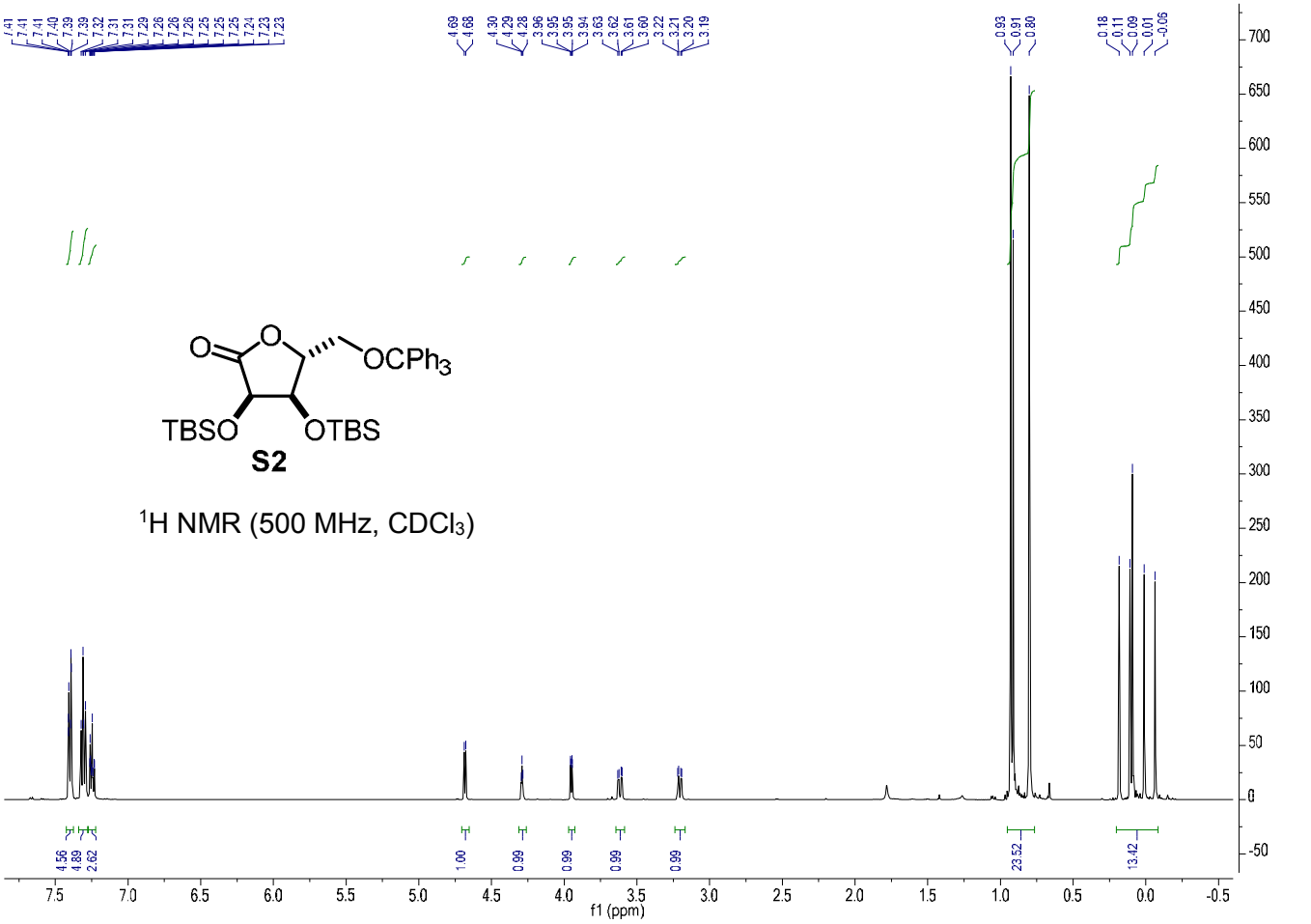

^{1}H NMR (500 MHz, $CDCl_3$)

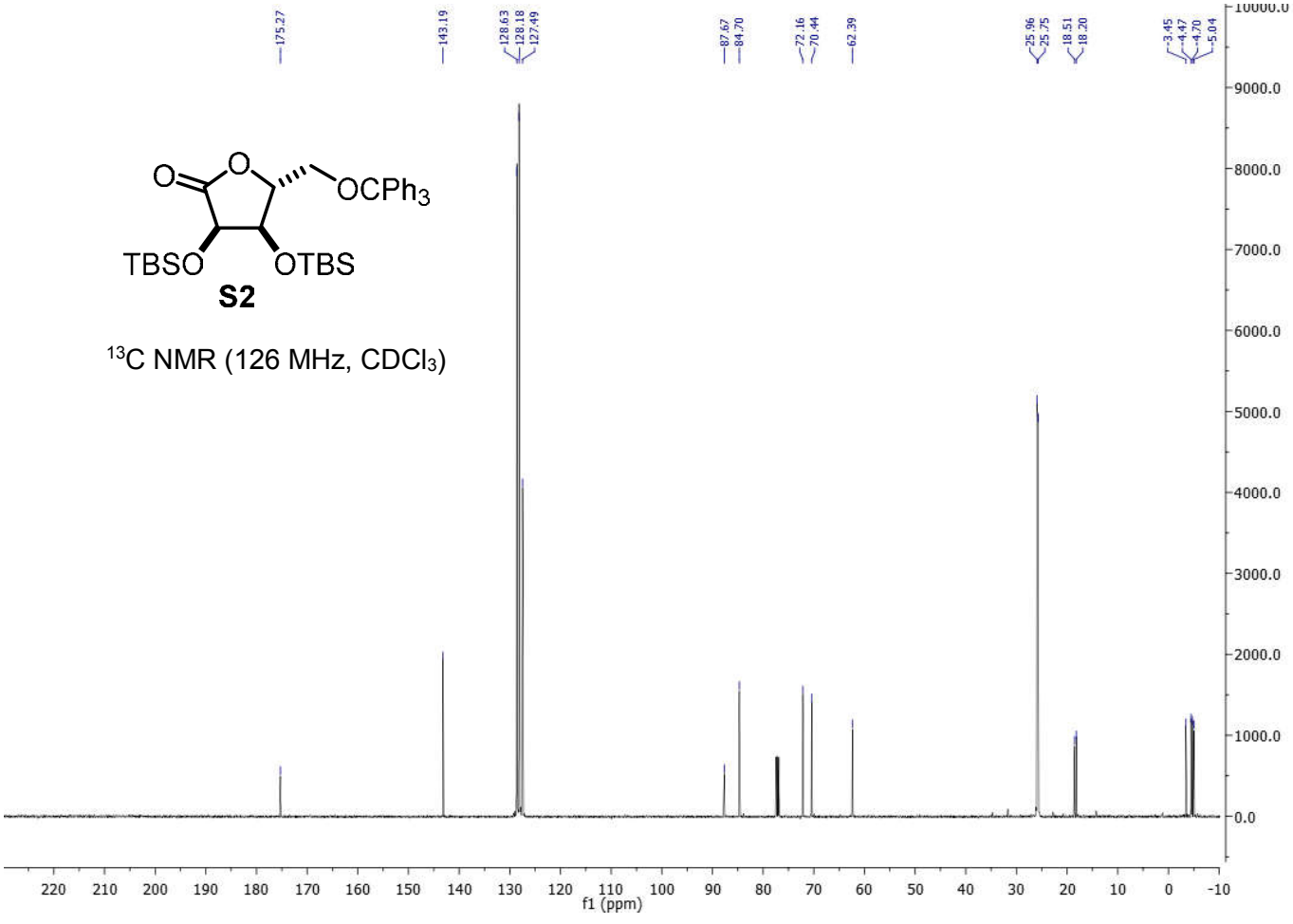

^{13}C NMR (126 MHz, $CDCl_3$)

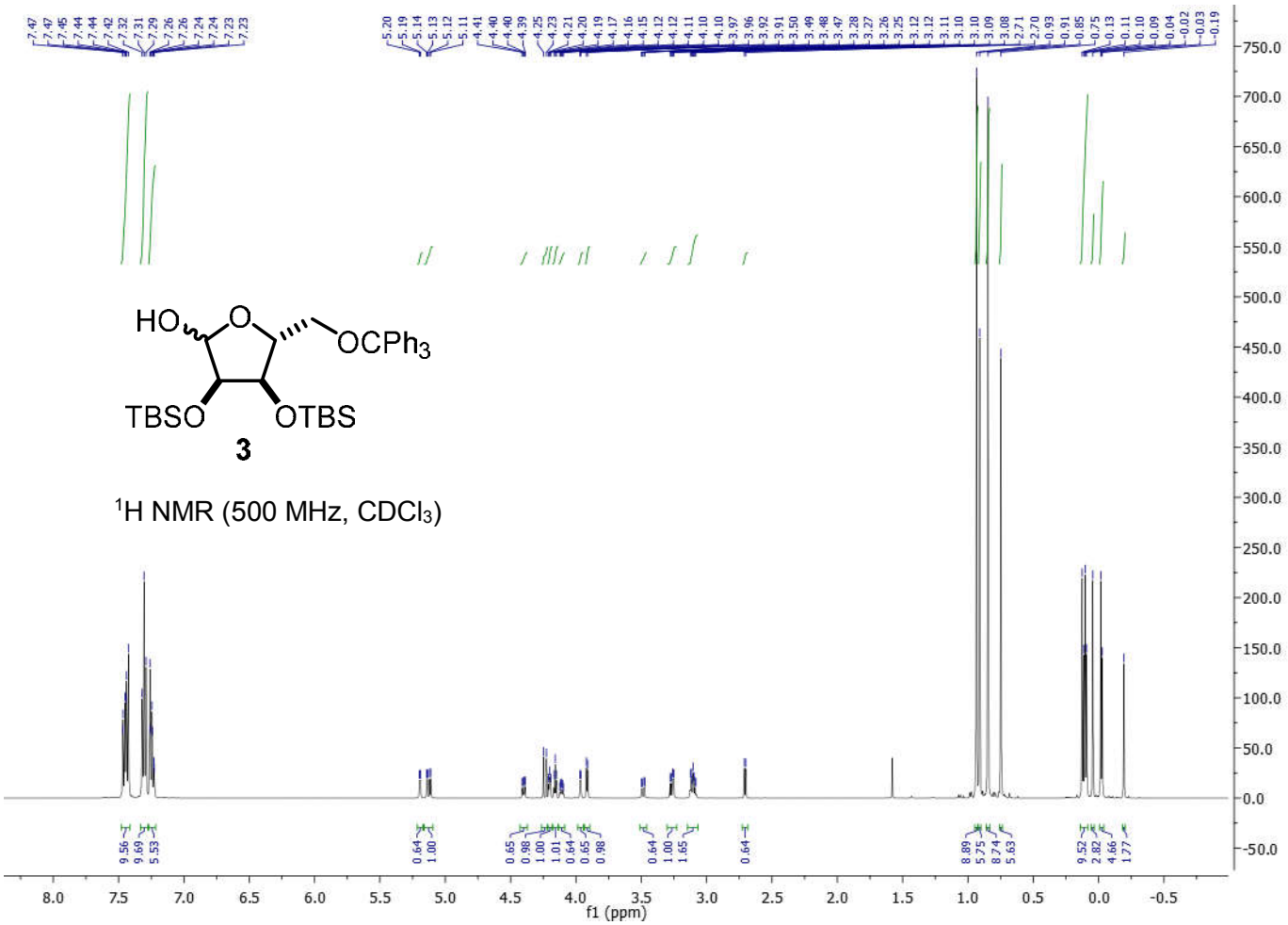

3

^{1}H NMR (500 MHz, $CDCl_3$)

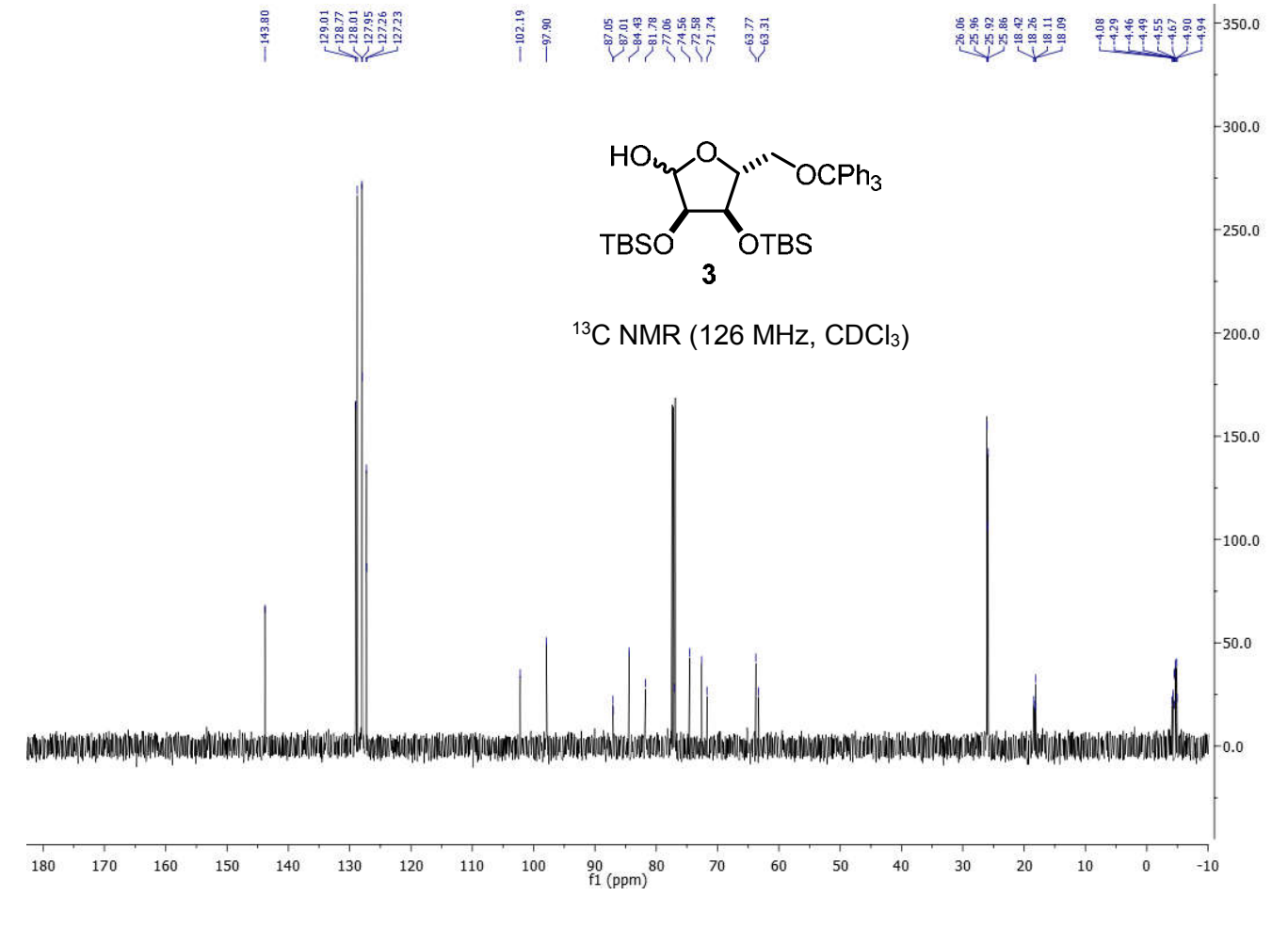

3

^{13}C NMR (126 MHz, $CDCl_3$)

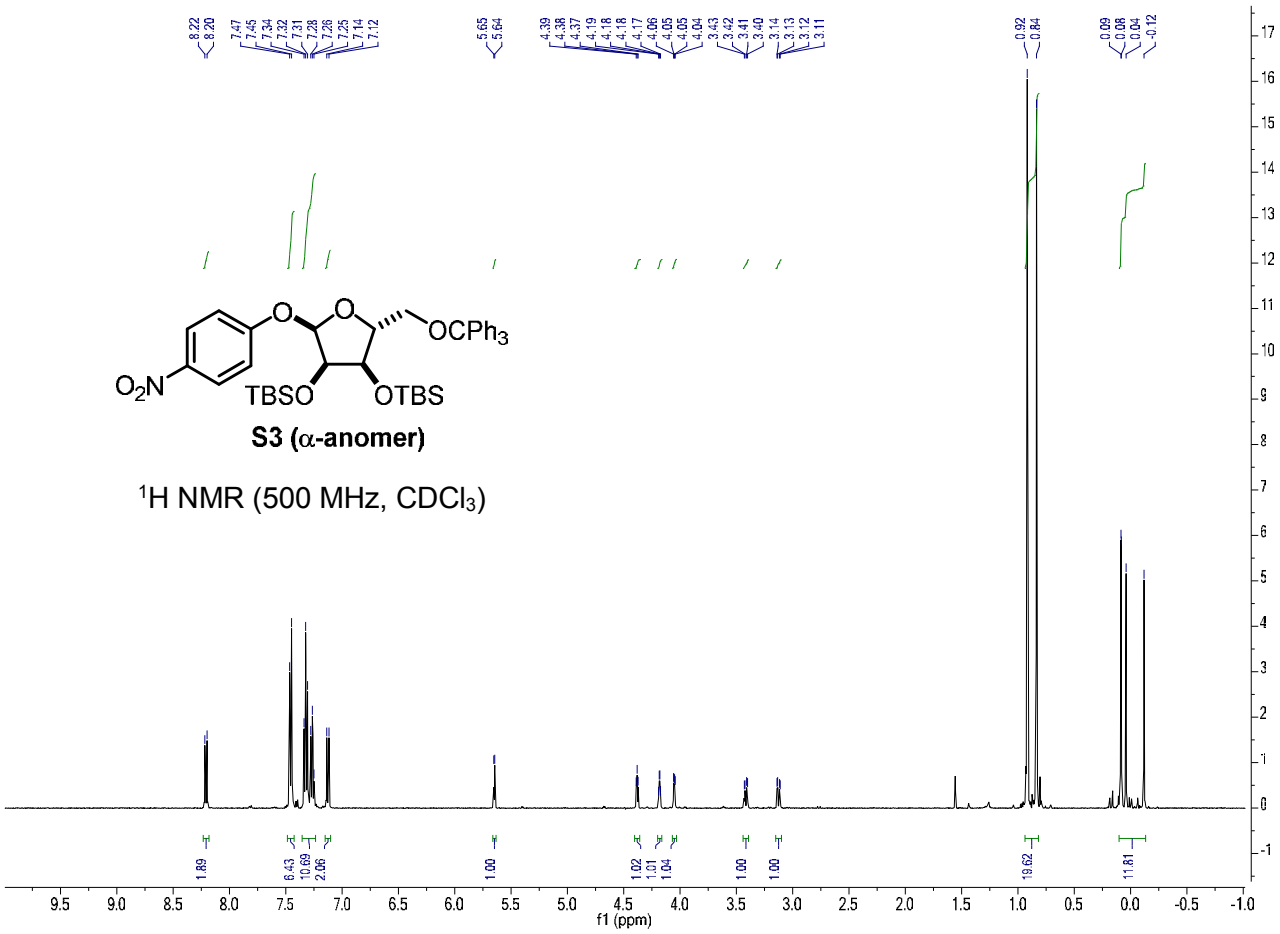

S3 (α-anomer)

^{1}H NMR (500 MHz, $CDCl_3$)

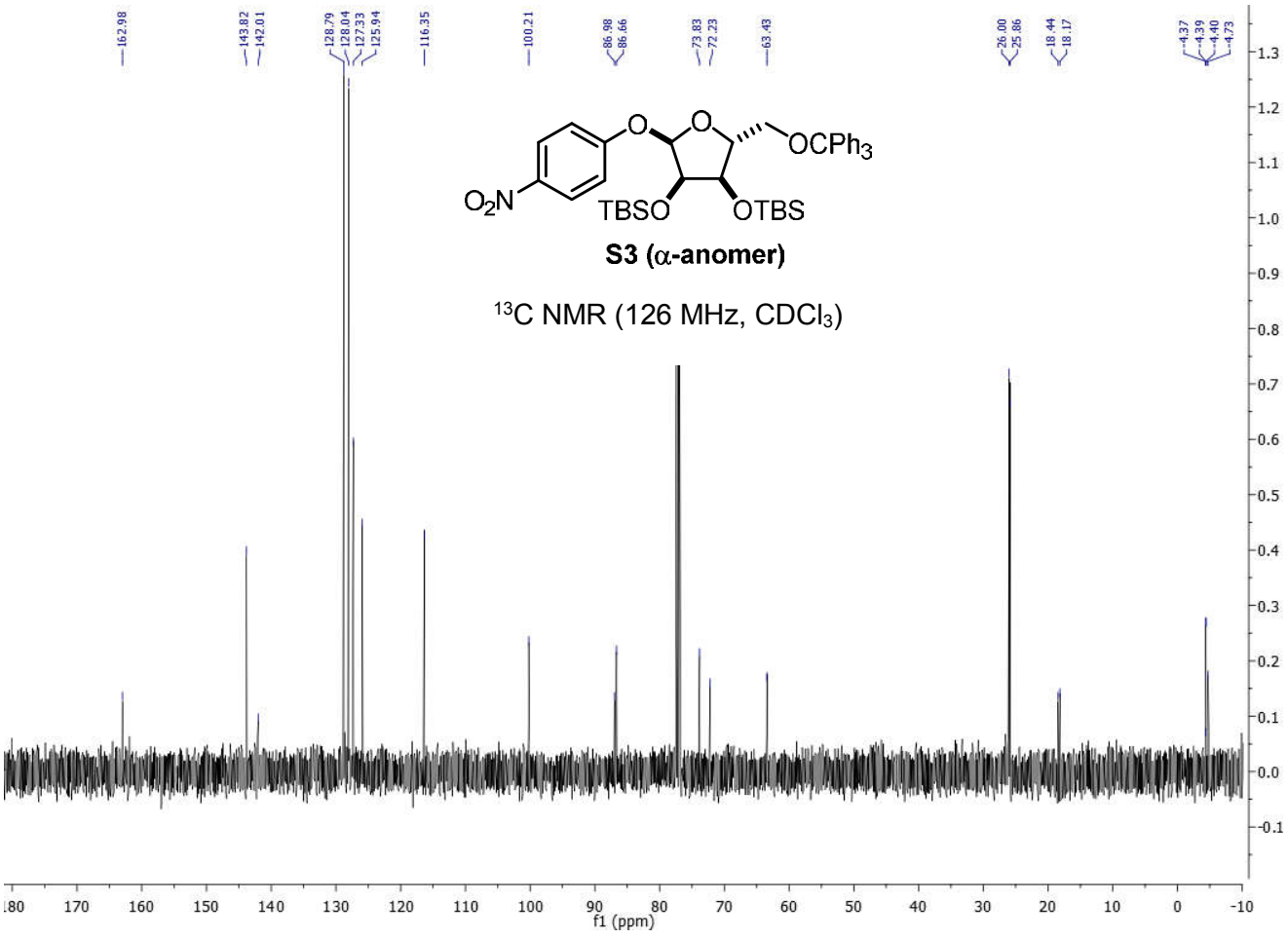

S3 (α-anomer)

^{13}C NMR (126 MHz, $CDCl_3$)

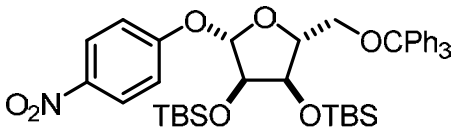

S3 (β-anomer)

^{1}H NMR (500 MHz, $CDCl_3$)

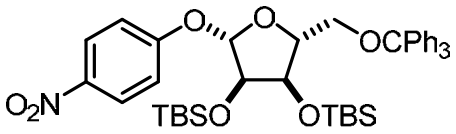

S3 (β-anomer)

^{13}C NMR (126 MHz, $CDCl_3$)

^{1}H DPFGSE NOE (500 MHz, d_6-acetone, mix = 300 ms, d1 = 10 s)

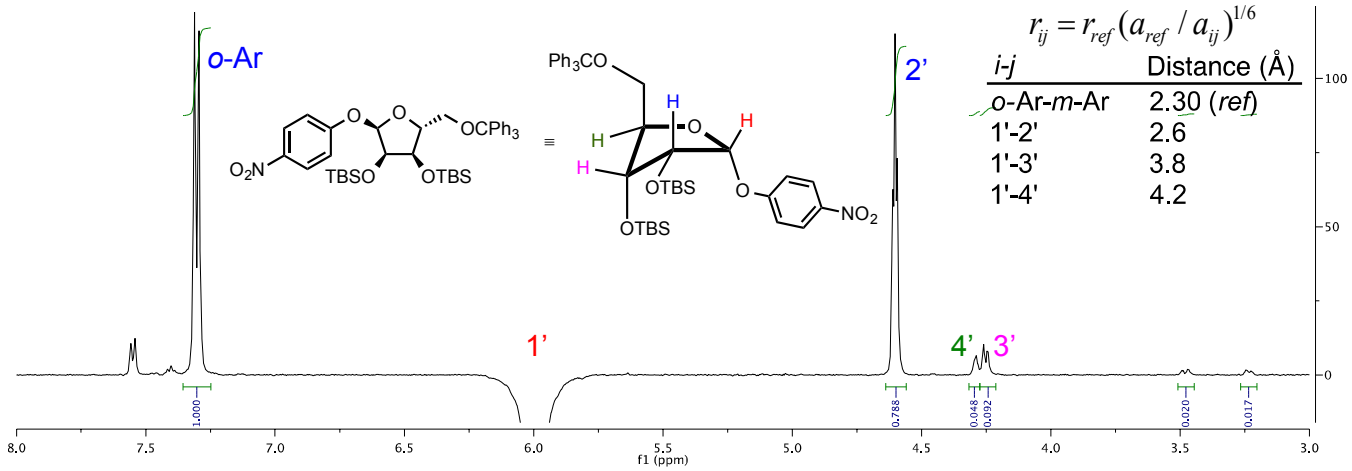

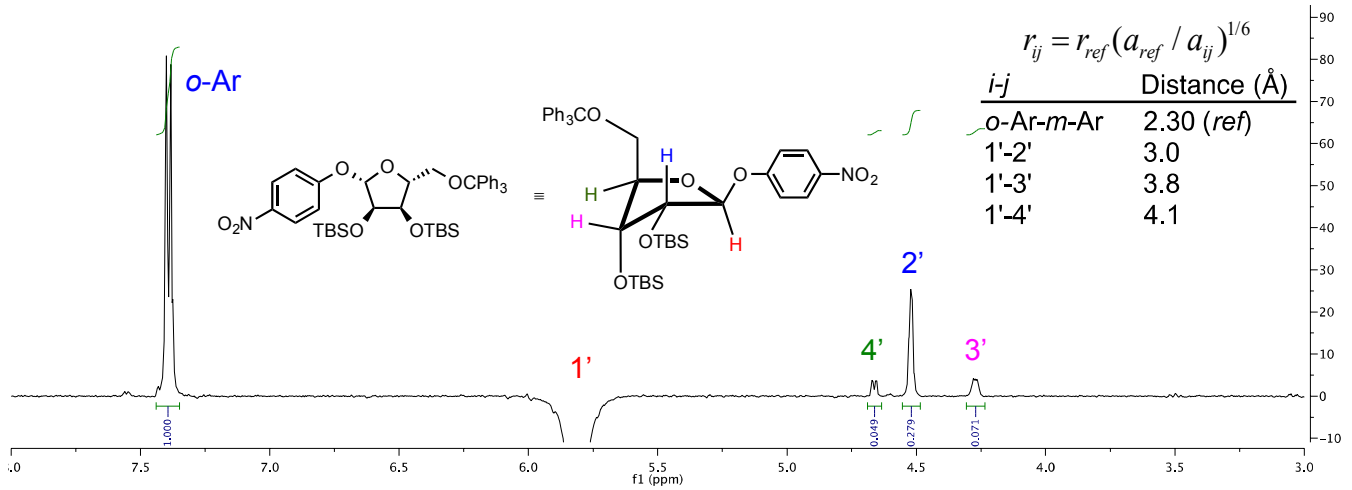

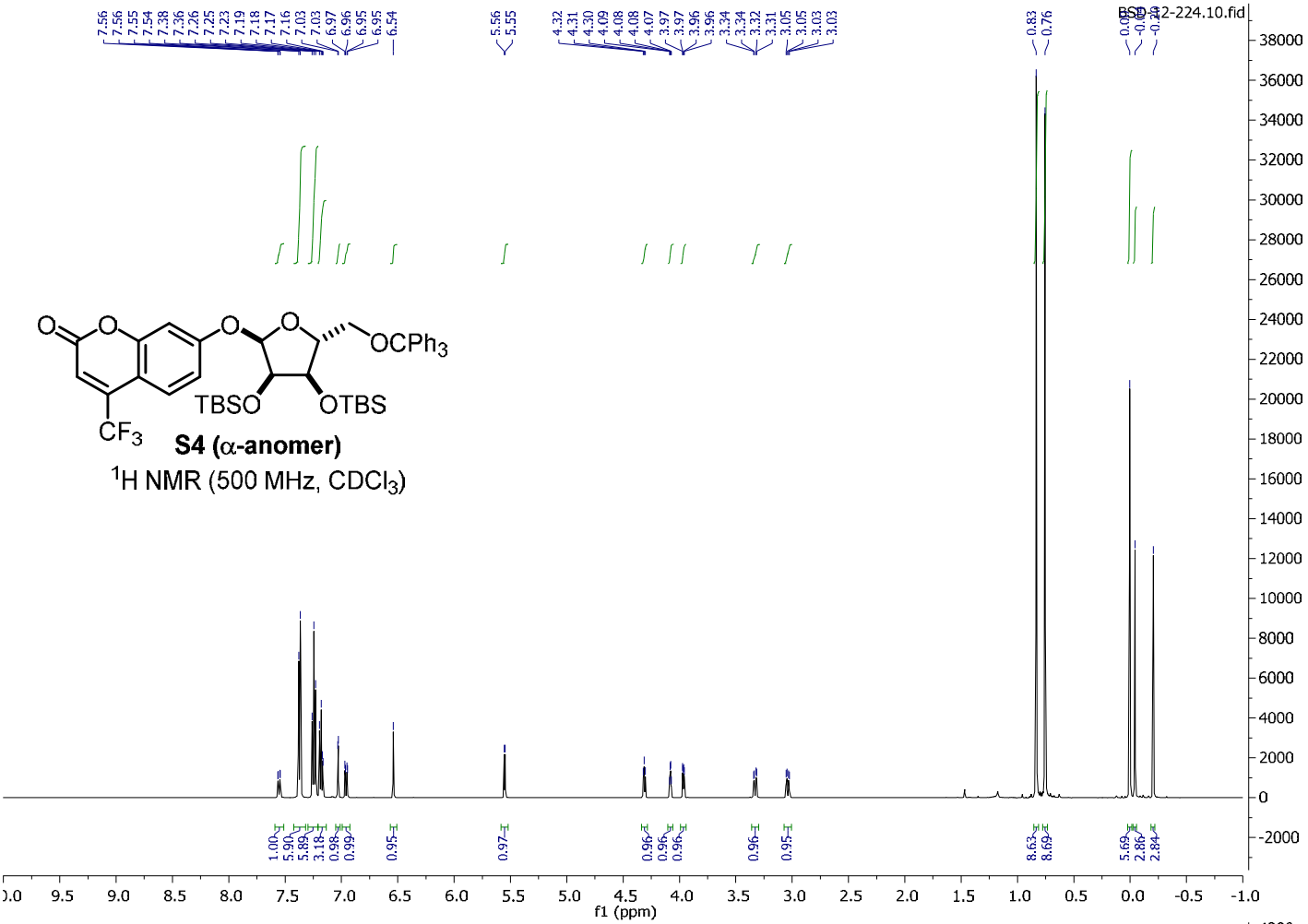

S4 (α-anomer)

^{1}H NMR (500 MHz, $CDCl_3$)

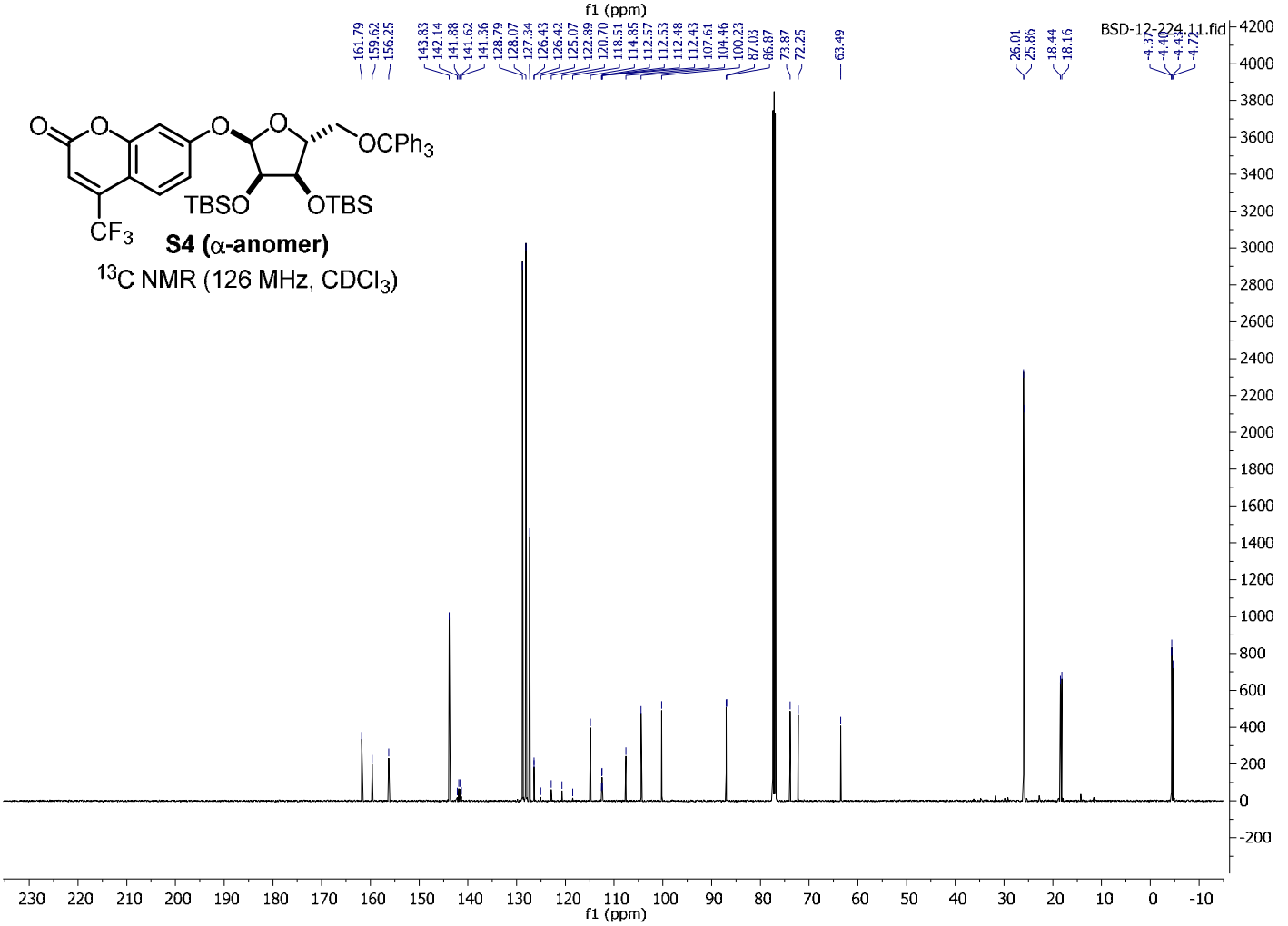

S4 (α-anomer)

^{13}C NMR (126 MHz, $CDCl_3$)

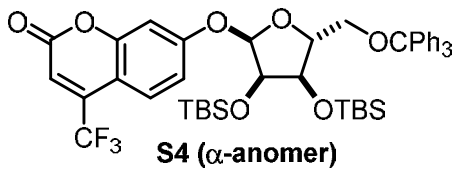

S4 (α-anomer)

^{19}F NMR (471 MHz, $CDCl_3$)

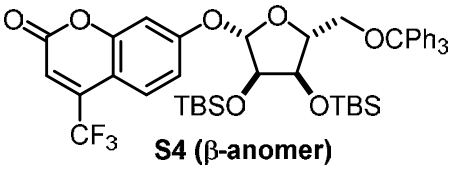

S4 (β-anomer)

^{1}H NMR (500 MHz, $CDCl_3$)

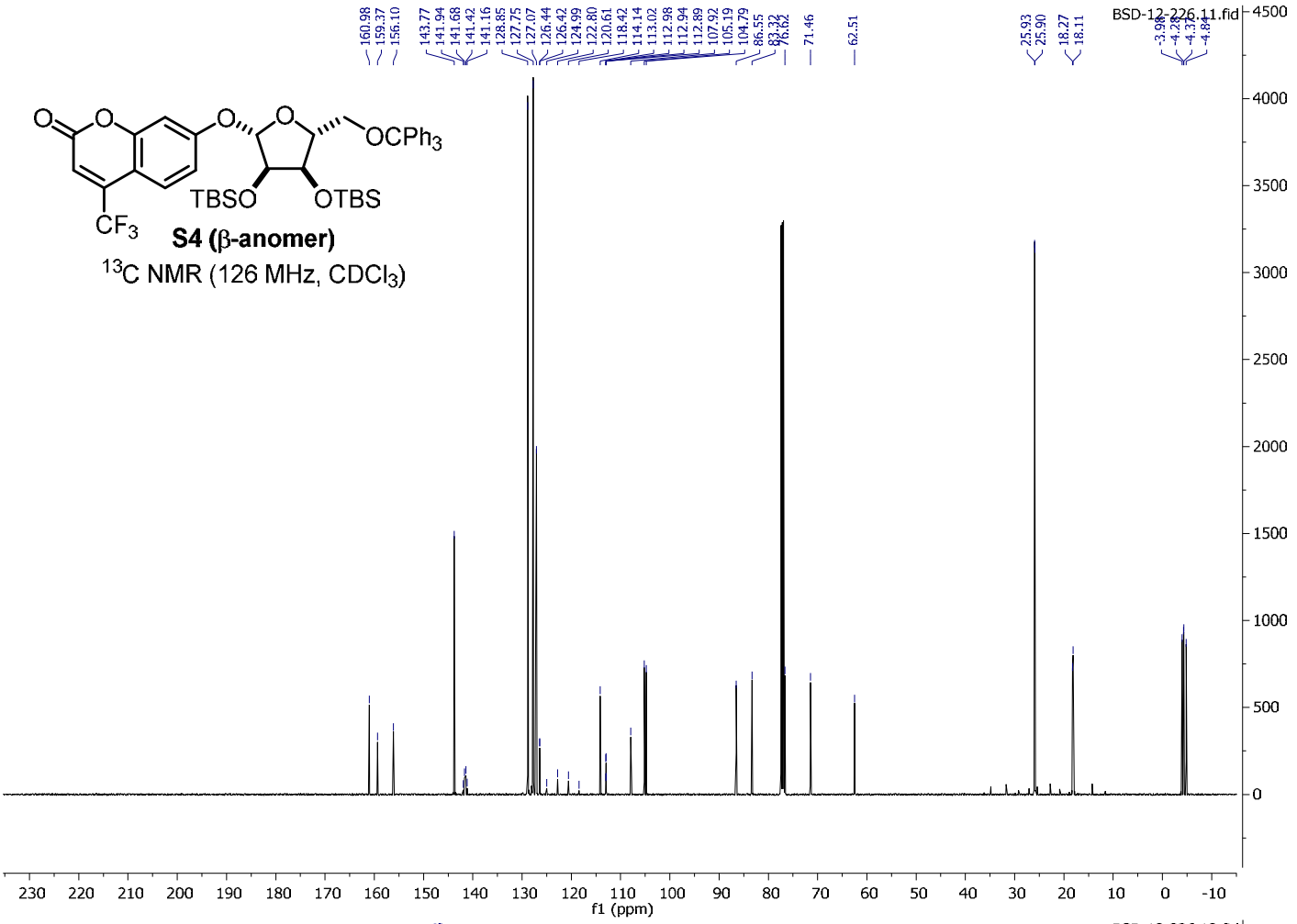
BSD-12-226.11.fid
160.98
159.37
156.10
143.77
141.94
141.68
141.42
141.16
128.85
127.75
127.07
126.44
126.42
124.99
122.80
120.61
118.42
114.14
113.02
112.98
112.94
112.89
107.92
105.19
104.79
86.55
83.32
71.46
62.51
25.93
25.90
18.27
18.11
-3.98
-4.28
-4.37
-4.84
OCPh3
TBSO
OTBS
CF3
S4 (β-anomer)
13C NMR (126 MHz, CDCl3)
f1 (ppm)

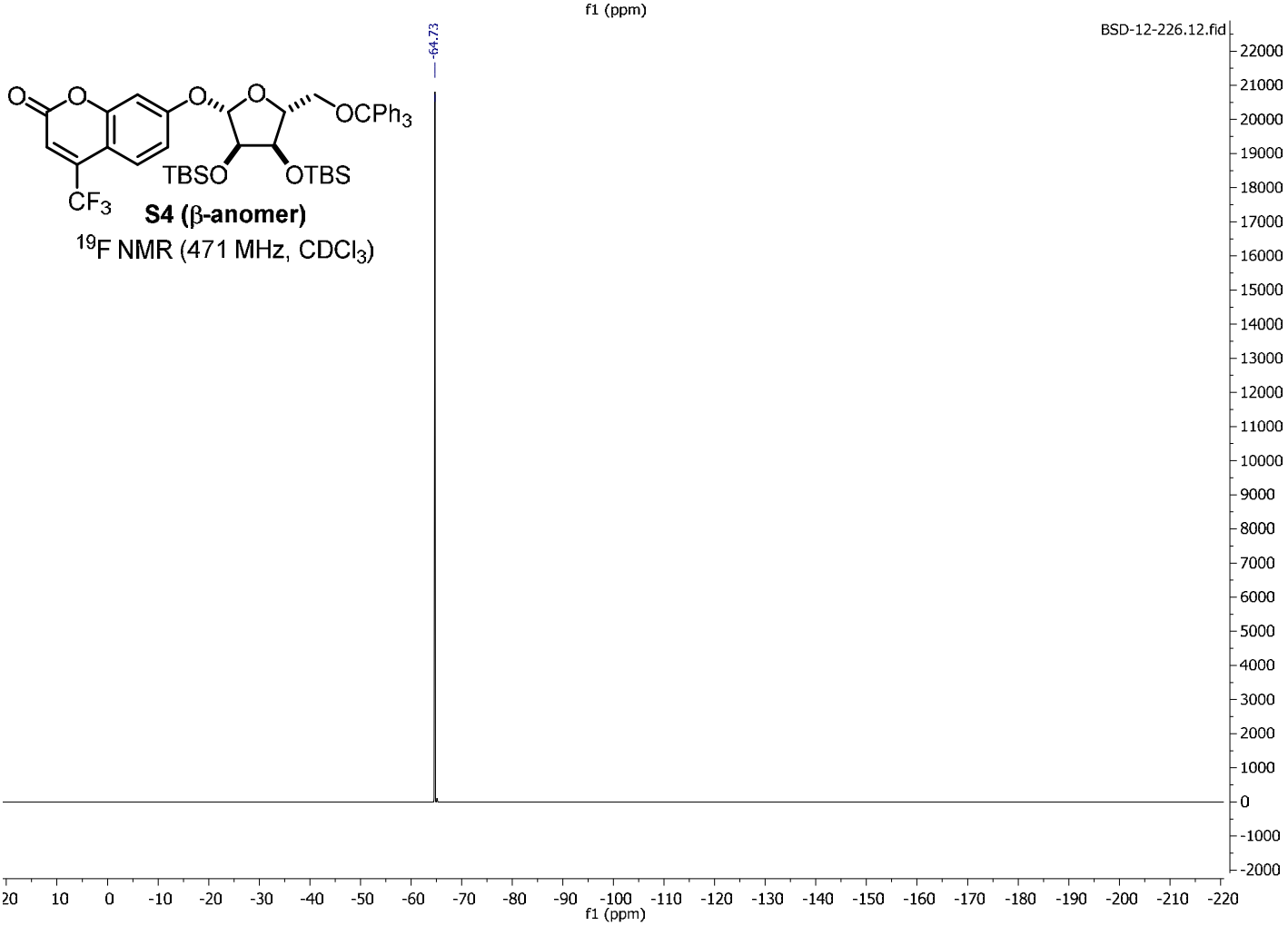
BSD-12-226.12.fid
-64.73
OCPh3
TBSO
OTBS
CF3
S4 (β-anomer)
19F NMR (471 MHz, CDCl3)
f1 (ppm)

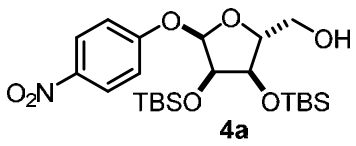

4a

^{1}H NMR (500 MHz, $CDCl_3$)

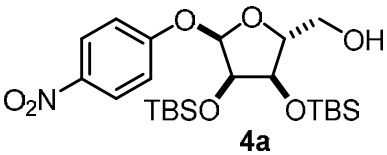

4a

^{13}C NMR (126 MHz, $CDCl_3$)

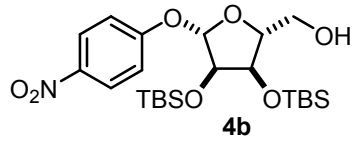

4b

^{1}H NMR (500 MHz, $CDCl_3$)

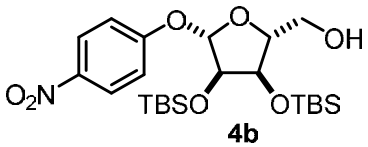

4b

^{13}C NMR (126 MHz, $CDCl_3$)

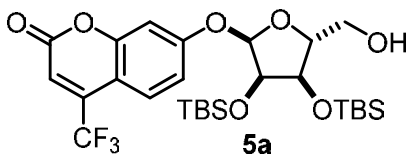

5a

^{1}H NMR (600 MHz, $CDCl_3$)

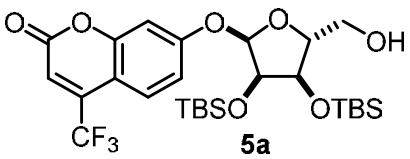

5a

^{13}C NMR (151 MHz, $CDCl_3$)

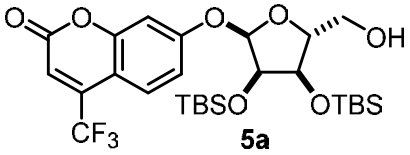

5a

^{19}F NMR (564 MHz, $CDCl_3$)

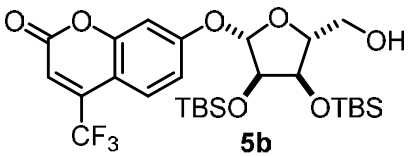

5b

^{1}H NMR (500 MHz, $CDCl_3$)

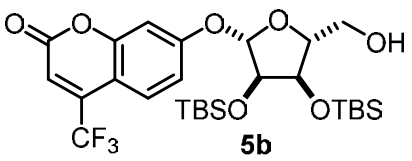

5b

^{13}C NMR (151 MHz, $CDCl_3$)

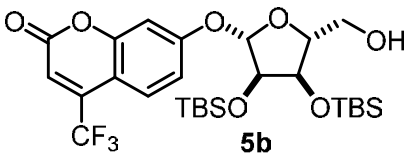

5b

^{19}F NMR (564 MHz, $CDCl_3$)

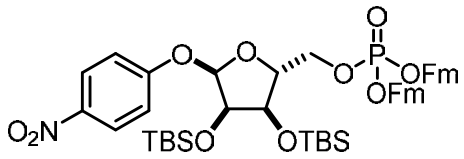

S5

^{1}H NMR (500 MHz, $CDCl_3$)

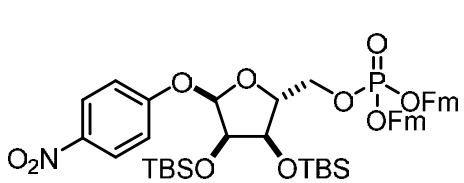

S5

^{31}P NMR (202 MHz, $CDCl_3$)

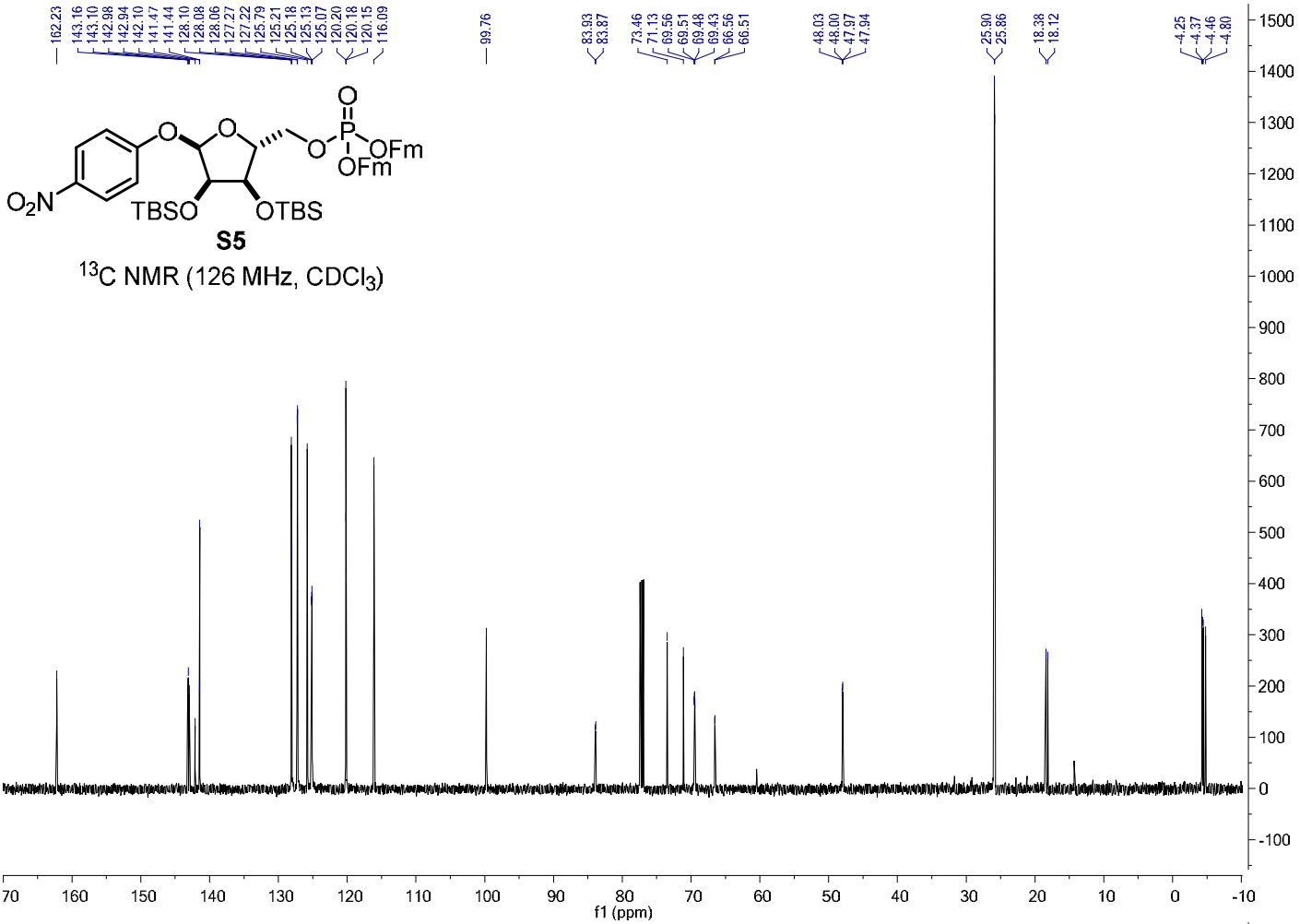
O2N
TBSO
OTBS
O
P
OFm
OFm
S5
13C NMR (126 MHz, CDCl3)
f1 (ppm)

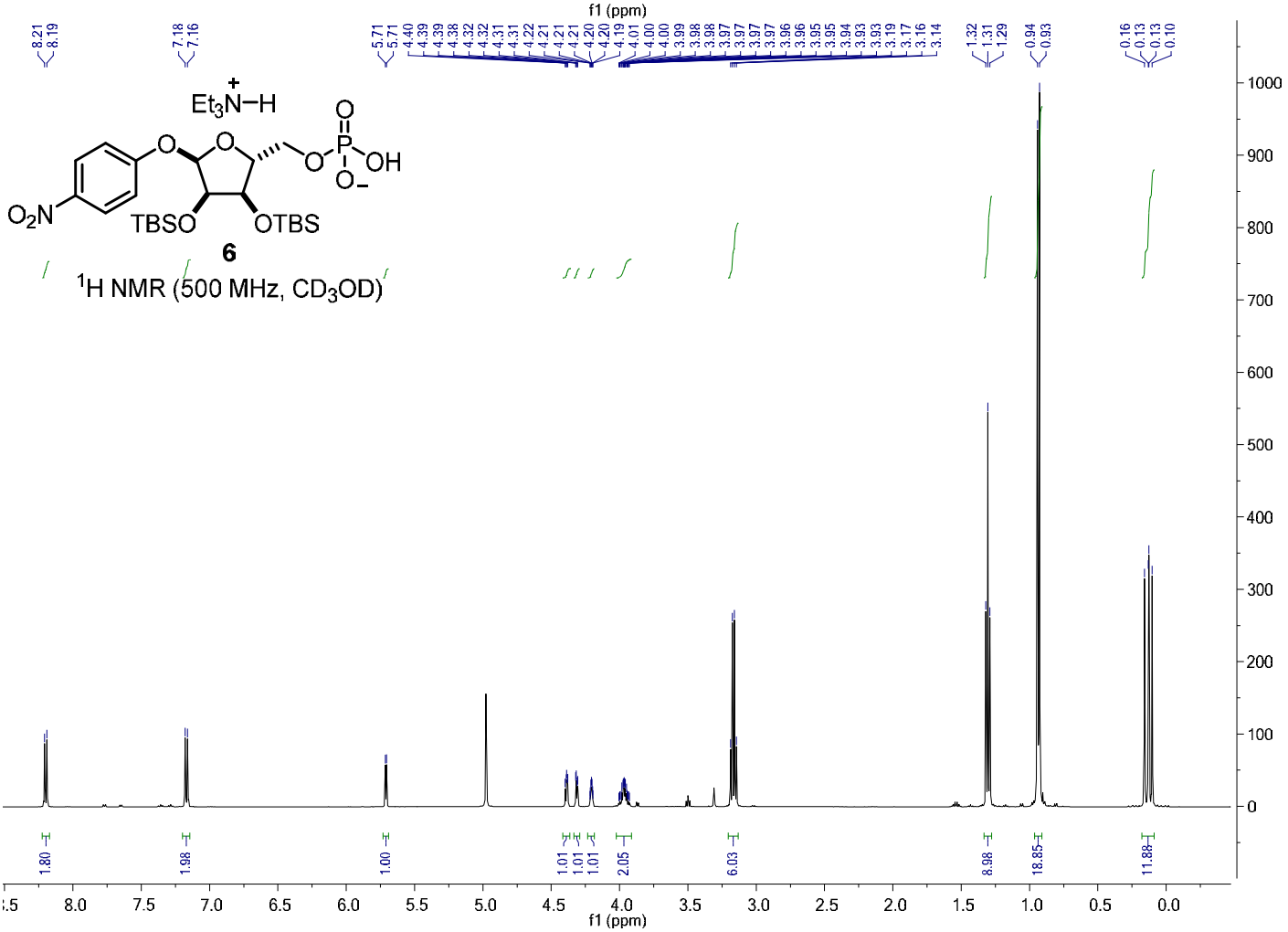
Et3N–H
O2N
TBSO
OTBS
O
P
OH
6
1H NMR (500 MHz, CD3OD)
f1 (ppm)

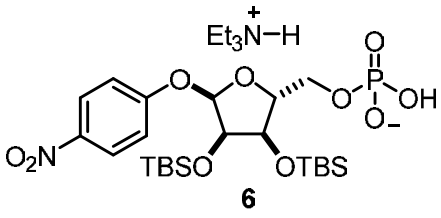

6

^{31}P NMR (202 MHz, CD_3OD)

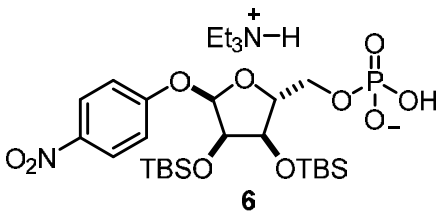

6

^{13}C NMR (126 MHz, CD_3OD)

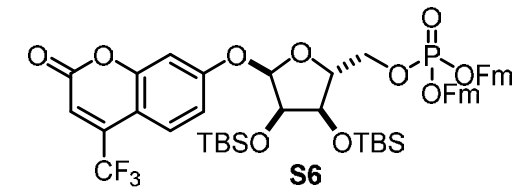

S6

^{1}H NMR (500 MHz, $CDCl_3$)

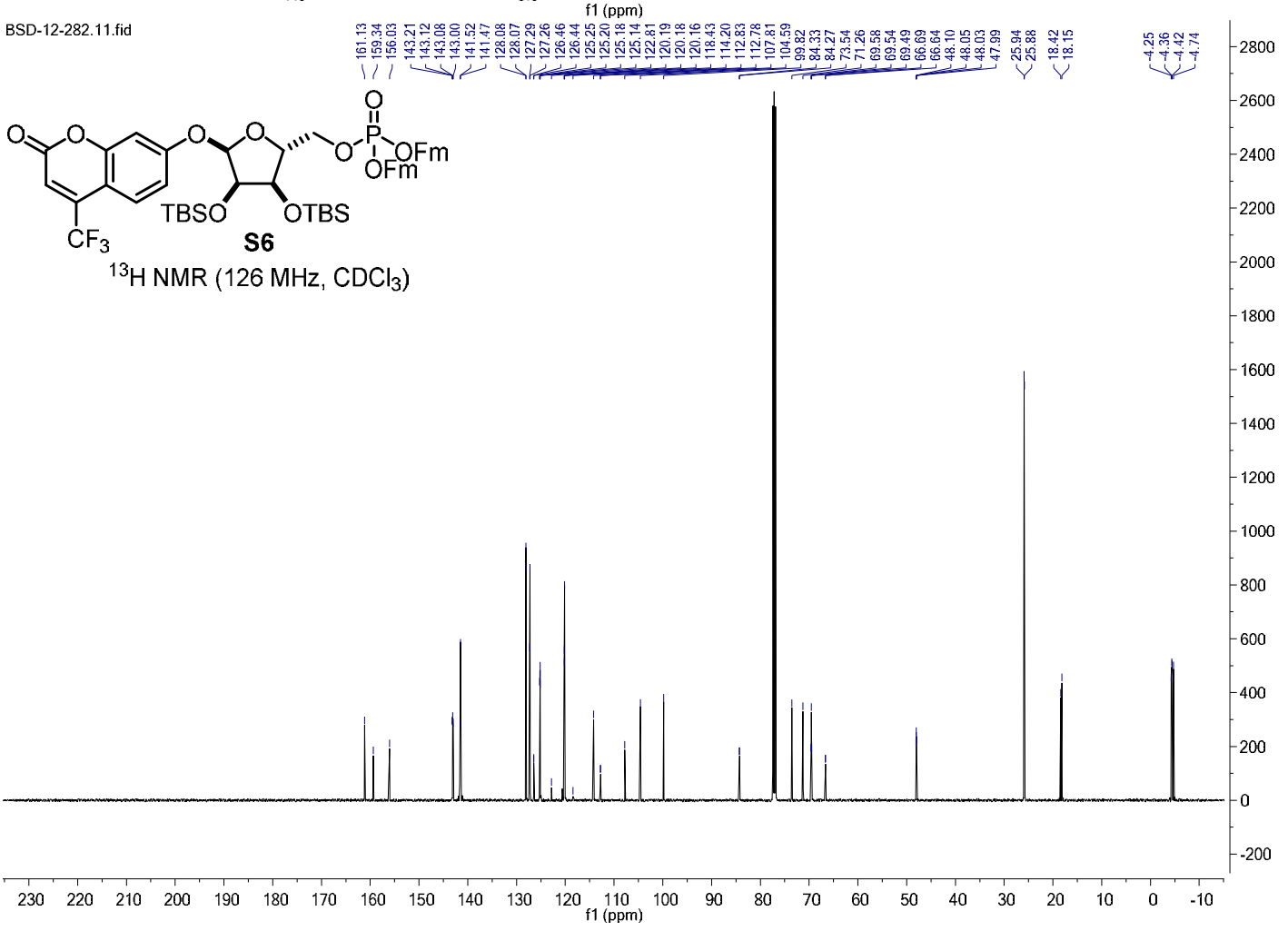

S6

^{13}H NMR (126 MHz, $CDCl_3$)

BSD-12-282.12.fid

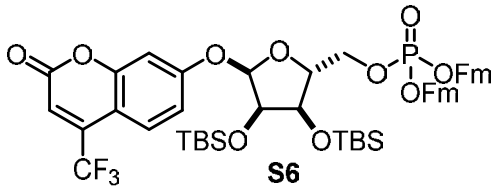

S6

^{19}F NMR (471 MHz, $CDCl_3$)

BSD-12-282.13.fid

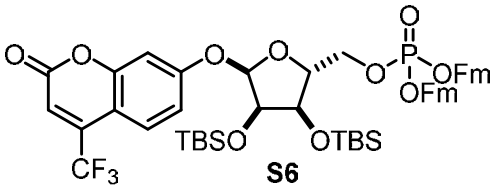

S6

^{31}P NMR (203 MHz, $CDCl_3$)

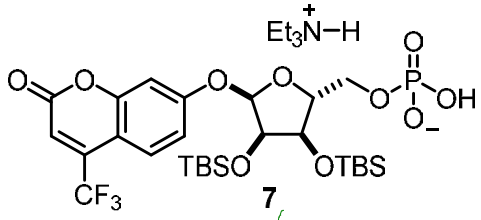

^{1}H NMR (500 MHz, CD_3OD)

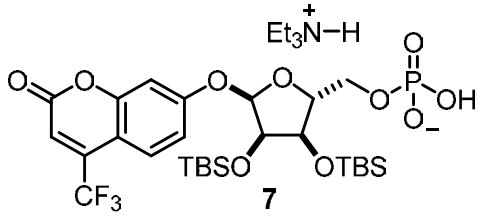

^{13}C NMR (126 MHz, CD_3OD)

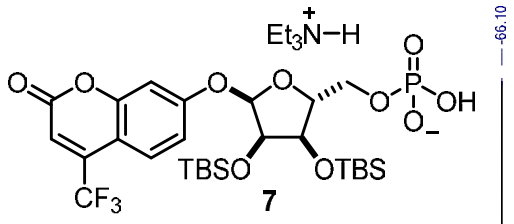

^{19}F NMR (470 MHz, CD_3OD)

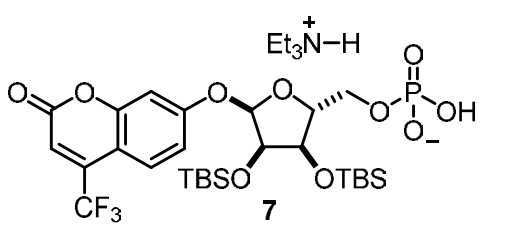

^{31}P NMR (202 MHz, CD_3OD)

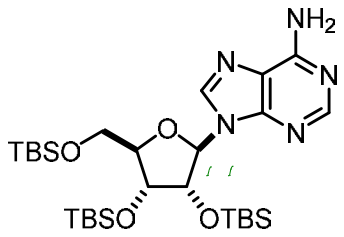

S7

^{1}H NMR (500 MHz, $CDCl_3$)

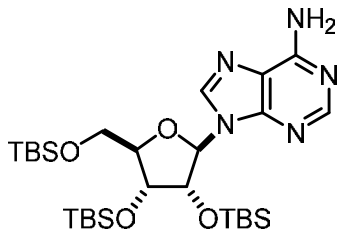

S7

^{13}C NMR (126 MHz, $CDCl_3$)

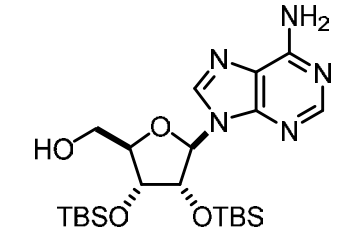

S8

^{1}H NMR (500 MHz, $CDCl_3$)

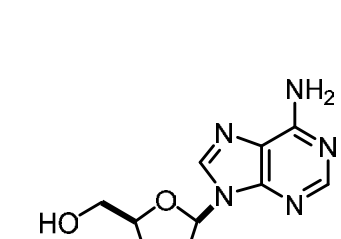

S8

^{13}C NMR (126 MHz, $CDCl_3$)

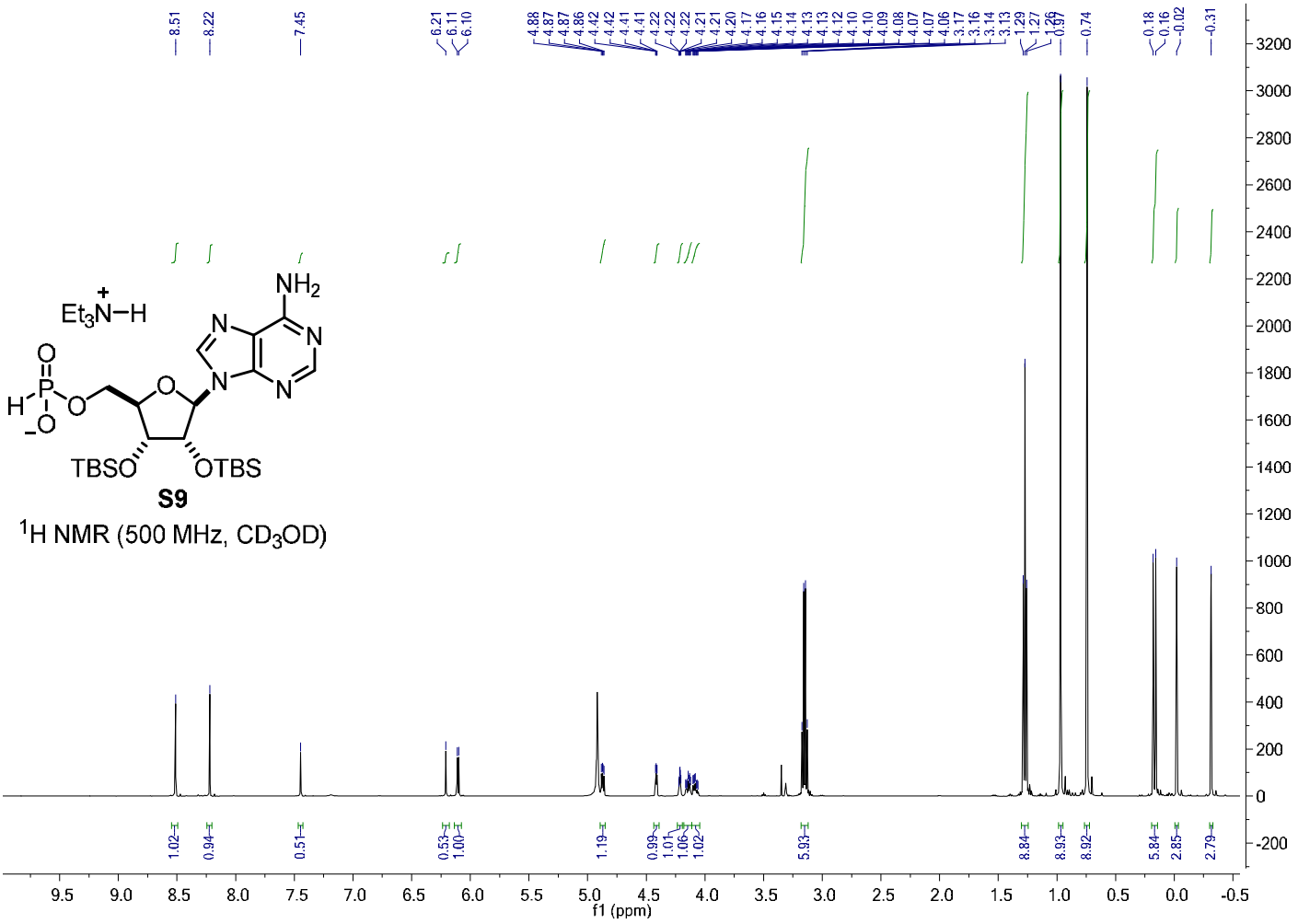
NH2
Et3N–H
TBSO
OTBS
S9
1H NMR (500 MHz, CD3OD)
f1 (ppm)

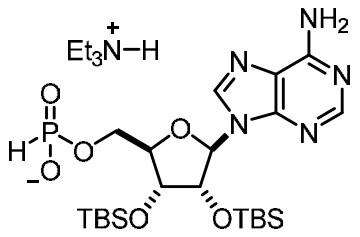

S9

^{13}C NMR (126 MHz, CD_3OD)

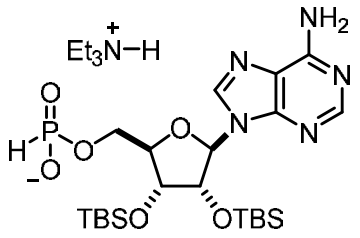

S9

^{31}P NMR (202 MHz, CD_3OD)

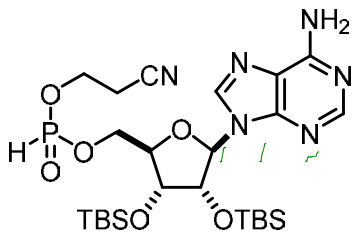

8

^{1}H NMR (500 MHz, $CDCl_3$)

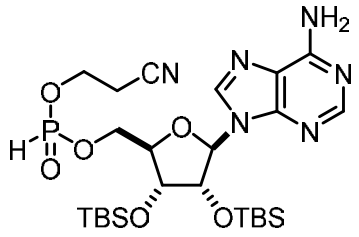

8

^{13}C NMR (126 MHz, $CDCl_3$)

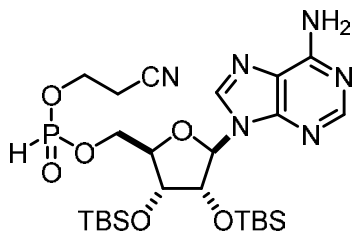

8

^{31}P NMR (202 MHz, $CDCl_3$)

2 DBU−H

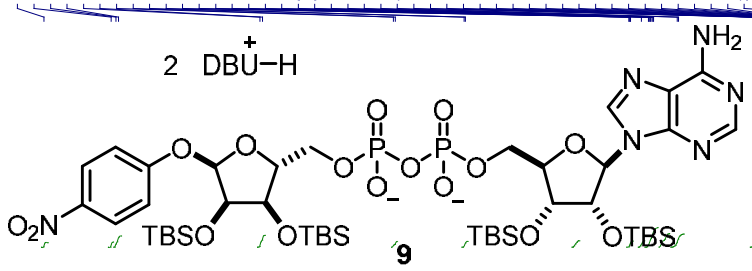

9

^{1}H NMR (500 MHz, CD_3OD)

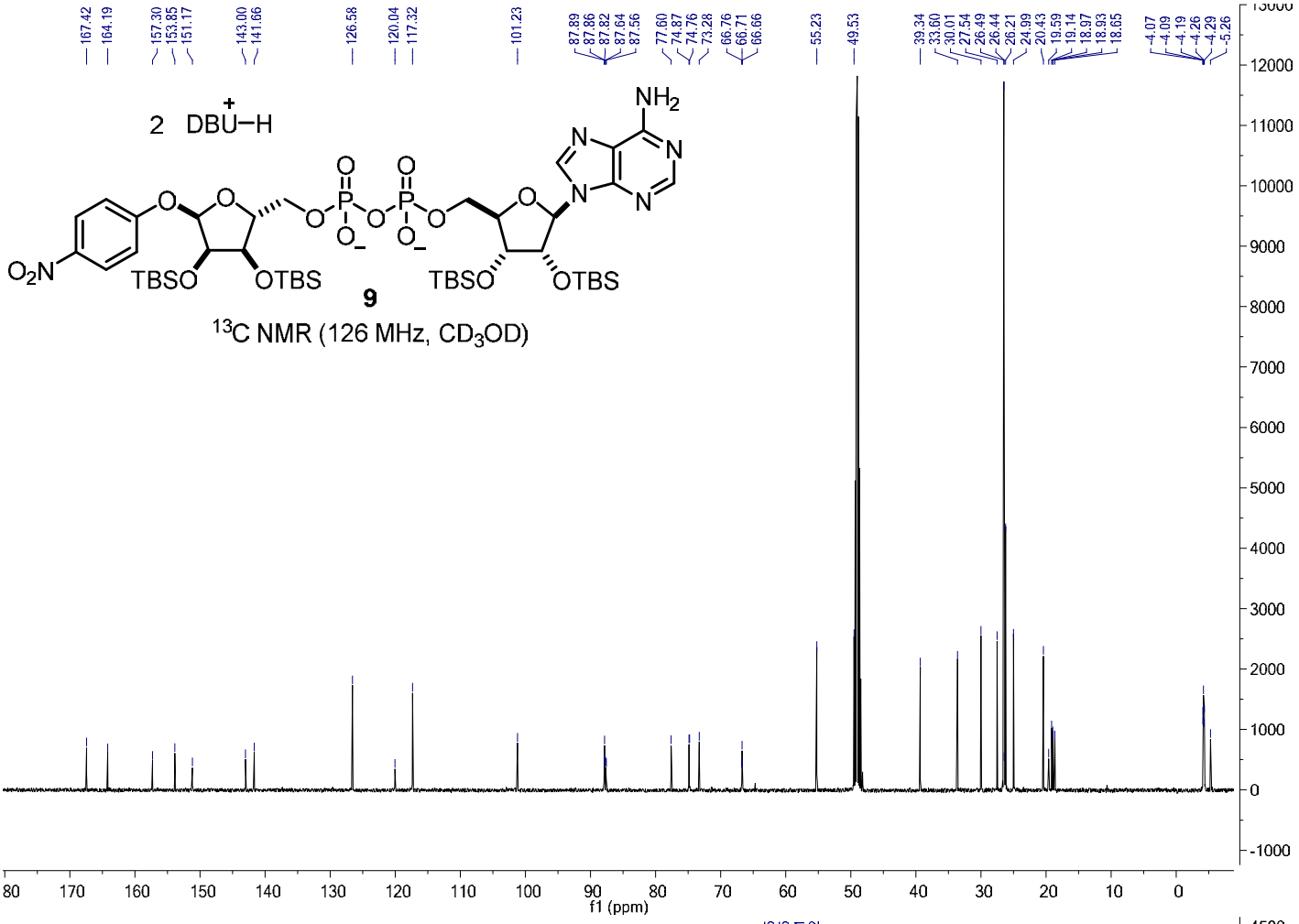
167.42
164.19
157.30
153.85
151.17
143.00
141.66
126.58
120.04
117.32
101.23
87.89
87.86
87.82
87.64
87.56
77.60
74.87
74.76
73.28
66.76
66.71
66.66
55.23
49.53
39.34
33.60
30.01
27.54
26.49
26.44
26.21
24.99
20.43
19.59
19.14
18.97
18.93
18.65
-4.07
-4.09
-4.19
-4.26
-4.29
-5.26
2 DBU−H
NH2
O2N
TBSO
OTBS
TBSO
OTBS
9
13C NMR (126 MHz, CD3OD)
f1 (ppm)

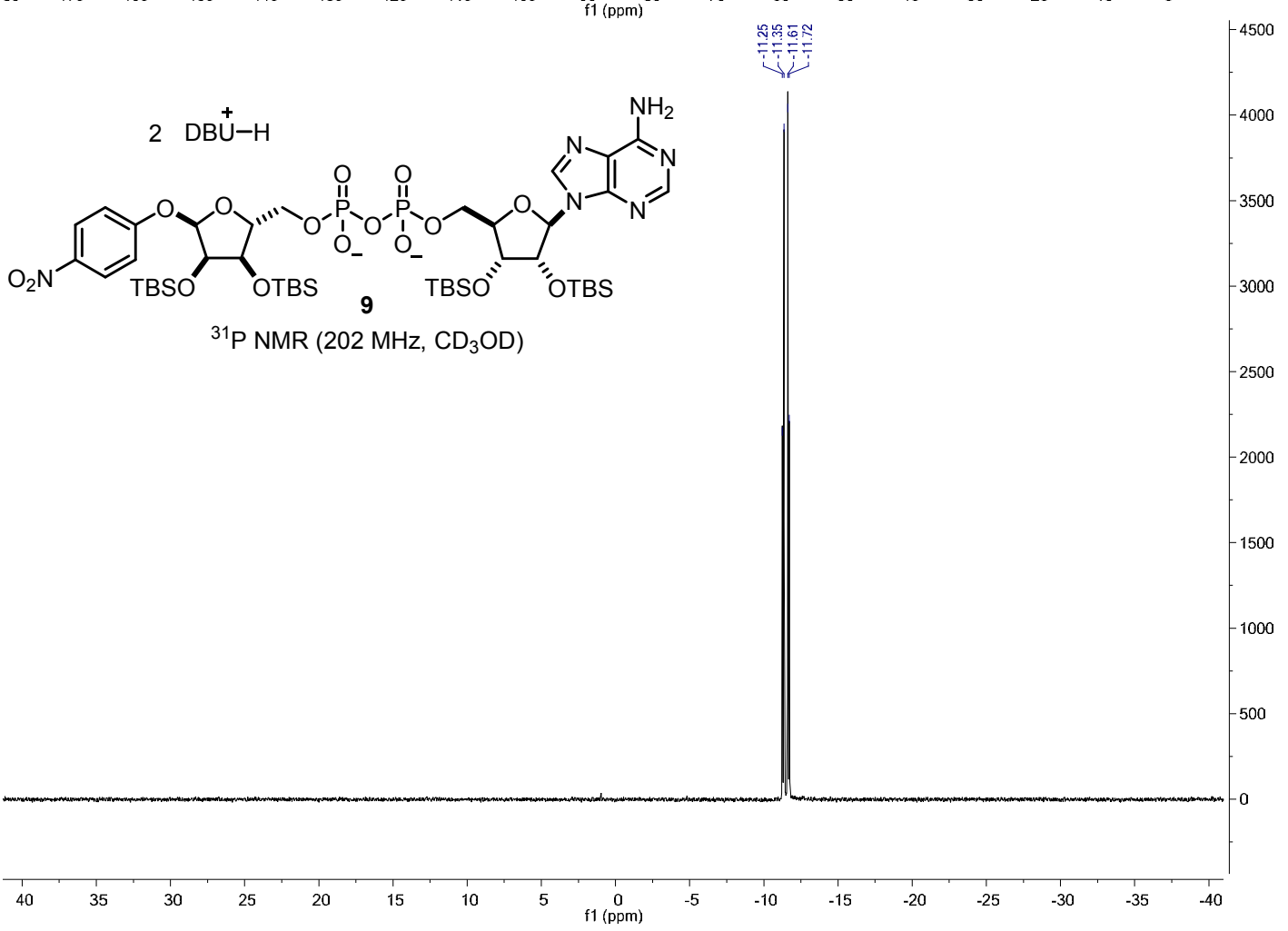
11.25
11.35
11.61
11.72
2 DBU−H
NH2
O2N
TBSO
OTBS
TBSO
OTBS
9
31P NMR (202 MHz, CD3OD)
f1 (ppm)

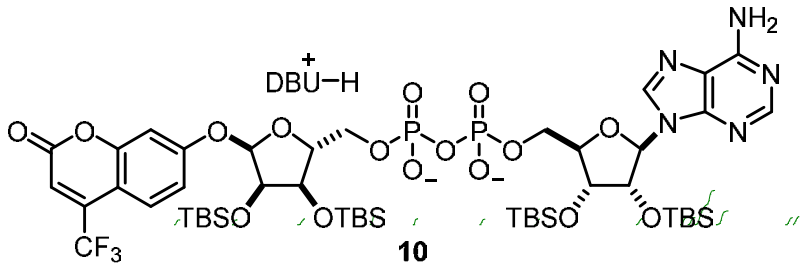

10

^{1}H NMR (500 MHz, CD_3OD)

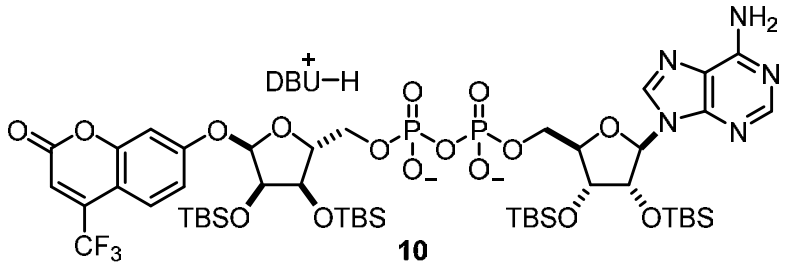

10

^{13}C NMR (126 MHz, CD_3OD)

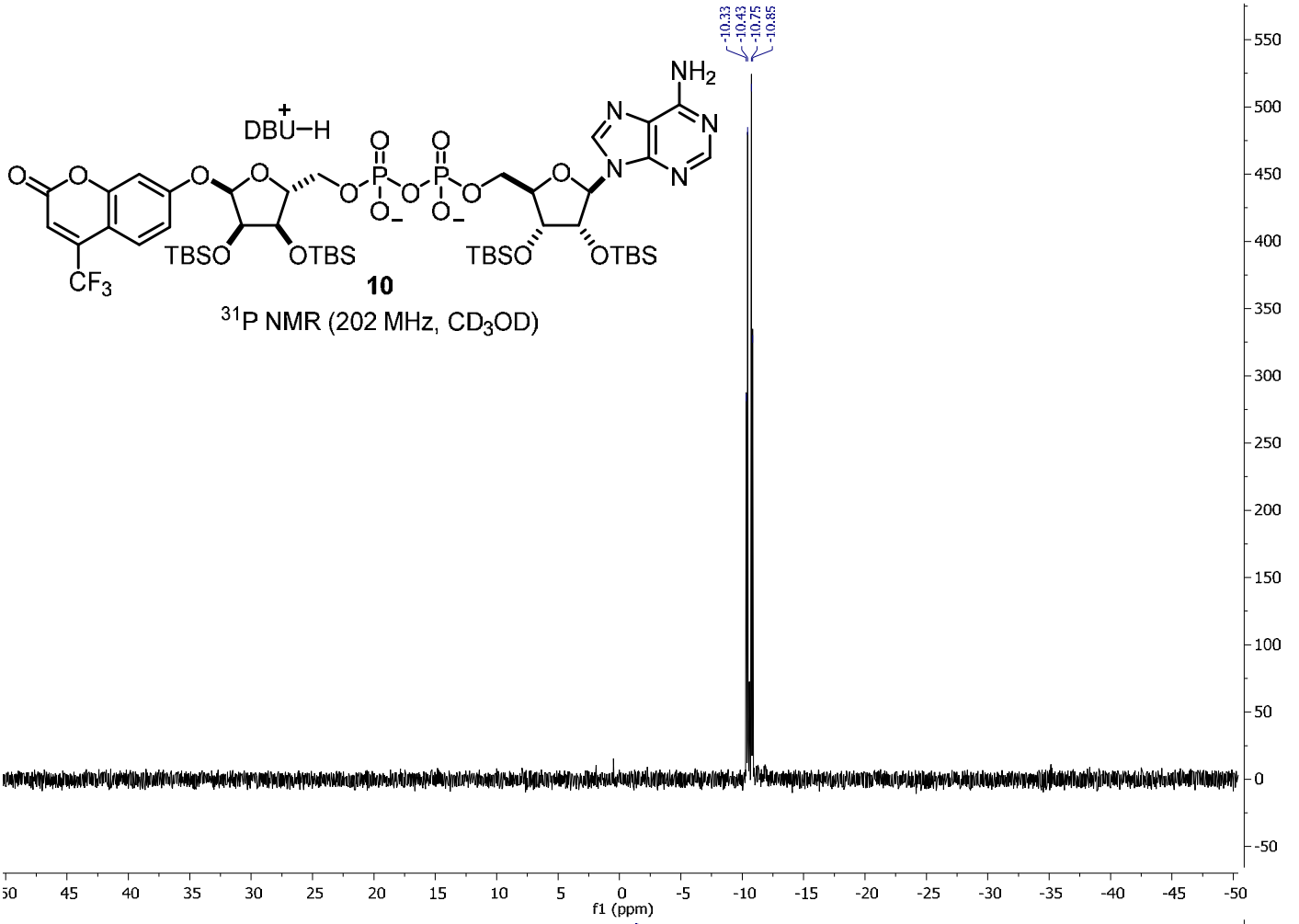

10

^{31}P NMR (202 MHz, CD_3OD)

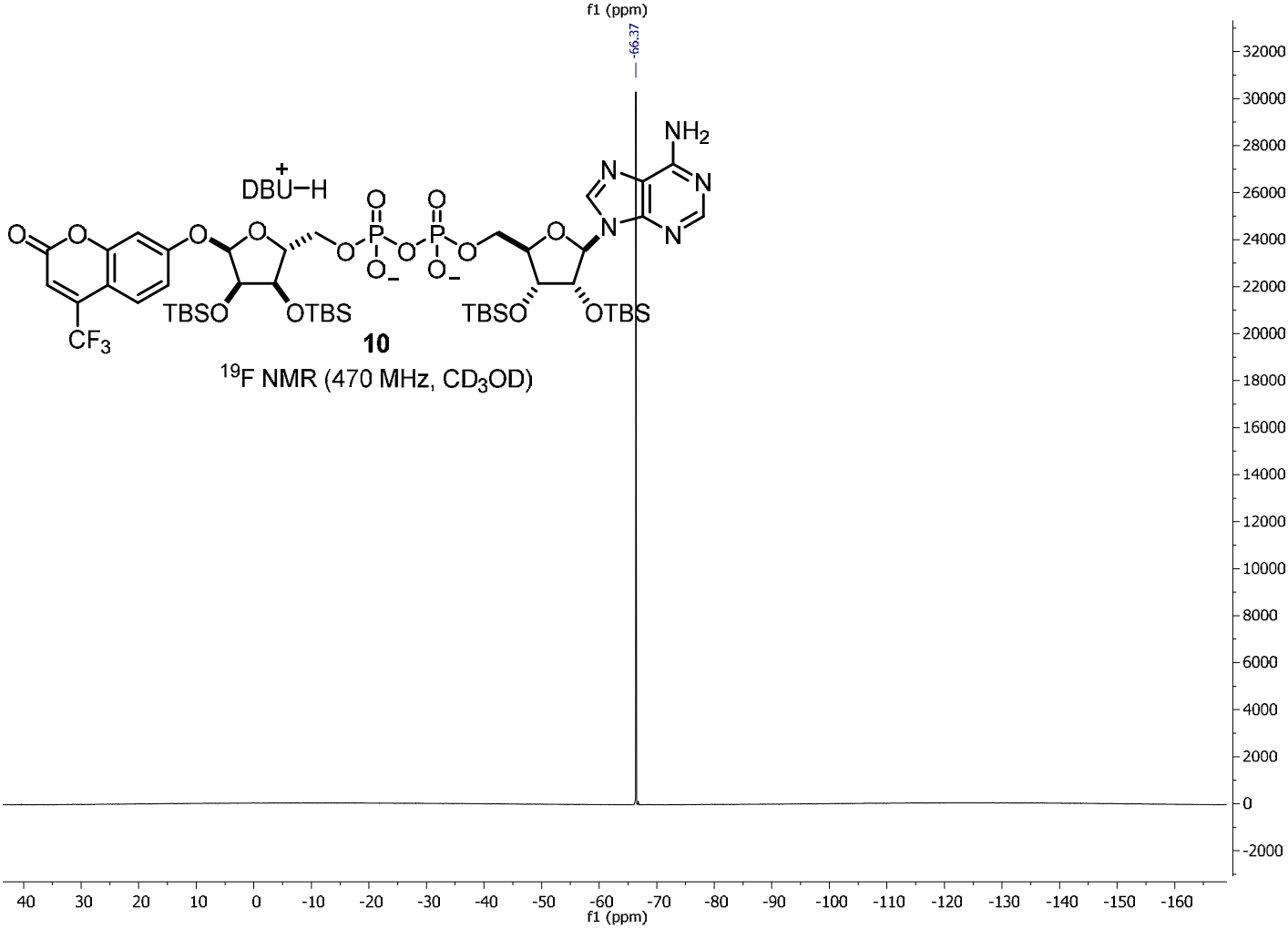

10

^{19}F NMR (470 MHz, CD_3OD)

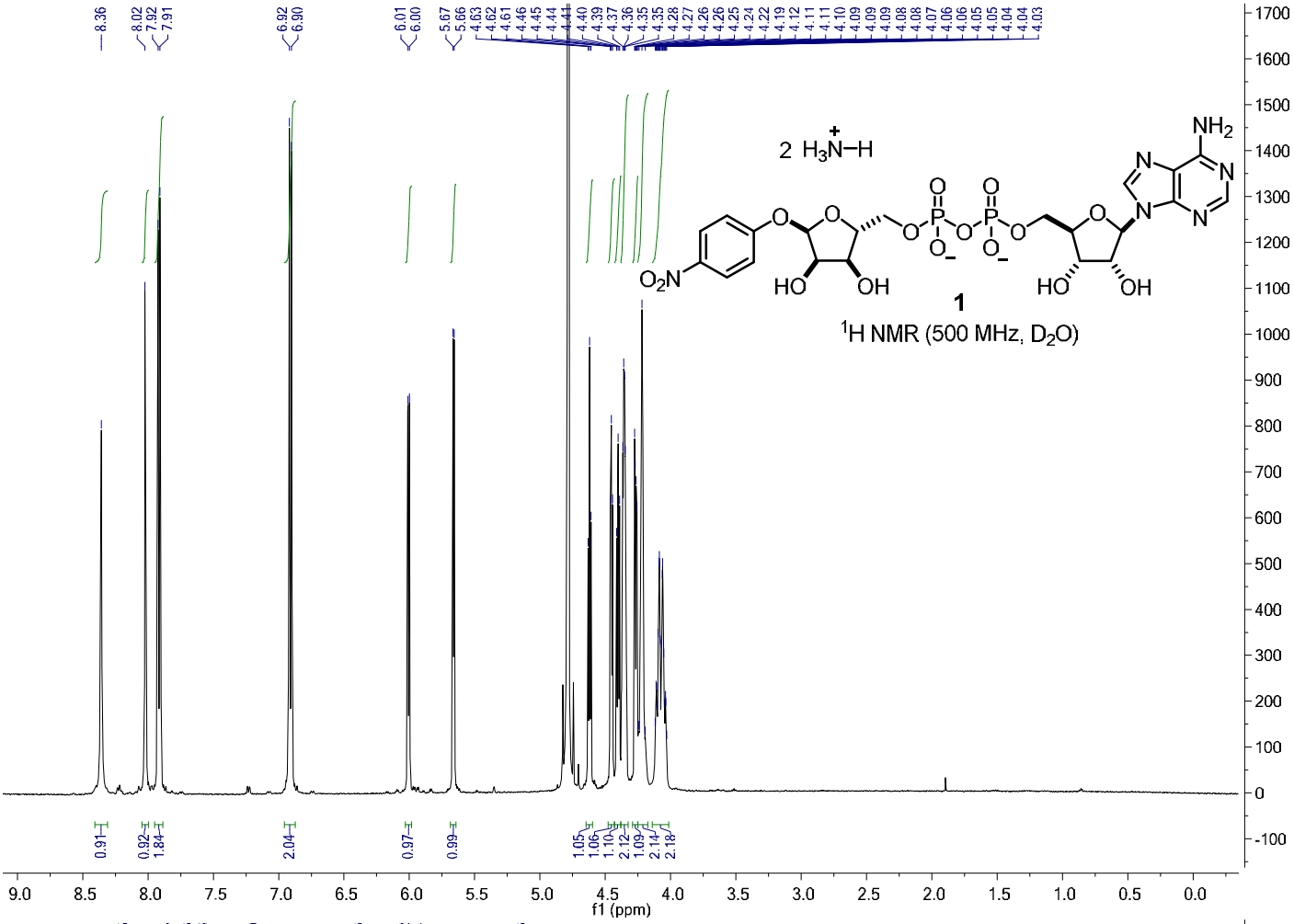
8.36
8.02
7.92
7.91
6.92
6.90
6.01
6.00
5.67
5.66
0.91
0.92
1.84
2.04
0.97
0.99
1.05
1.06
1.10
2.12
1.09
2.14
2.18
2 H3N–H
1
1H NMR (500 MHz, D2O)
f1 (ppm)

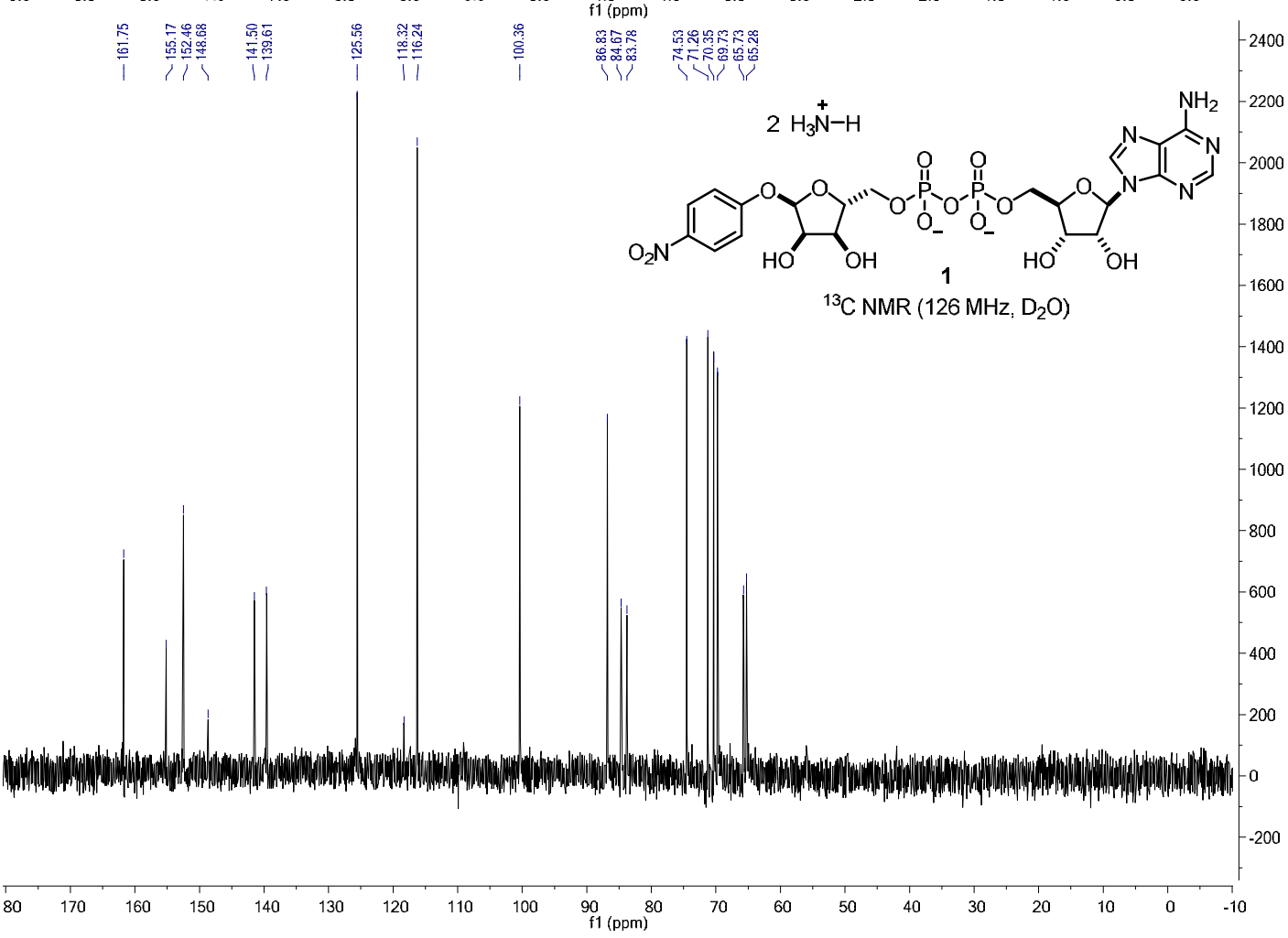
161.75
155.17
152.46
148.68
141.50
139.61
125.56
118.32
116.24
100.36
86.83
84.67
83.78
74.53
71.26
70.35
69.73
65.73
65.28
2 H3N–H
1
13C NMR (126 MHz, D2O)
f1 (ppm)

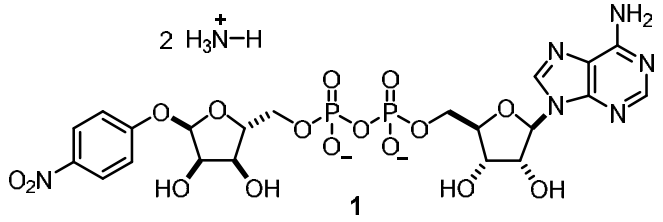

1

^{31}P NMR (202 MHz, D_2O)

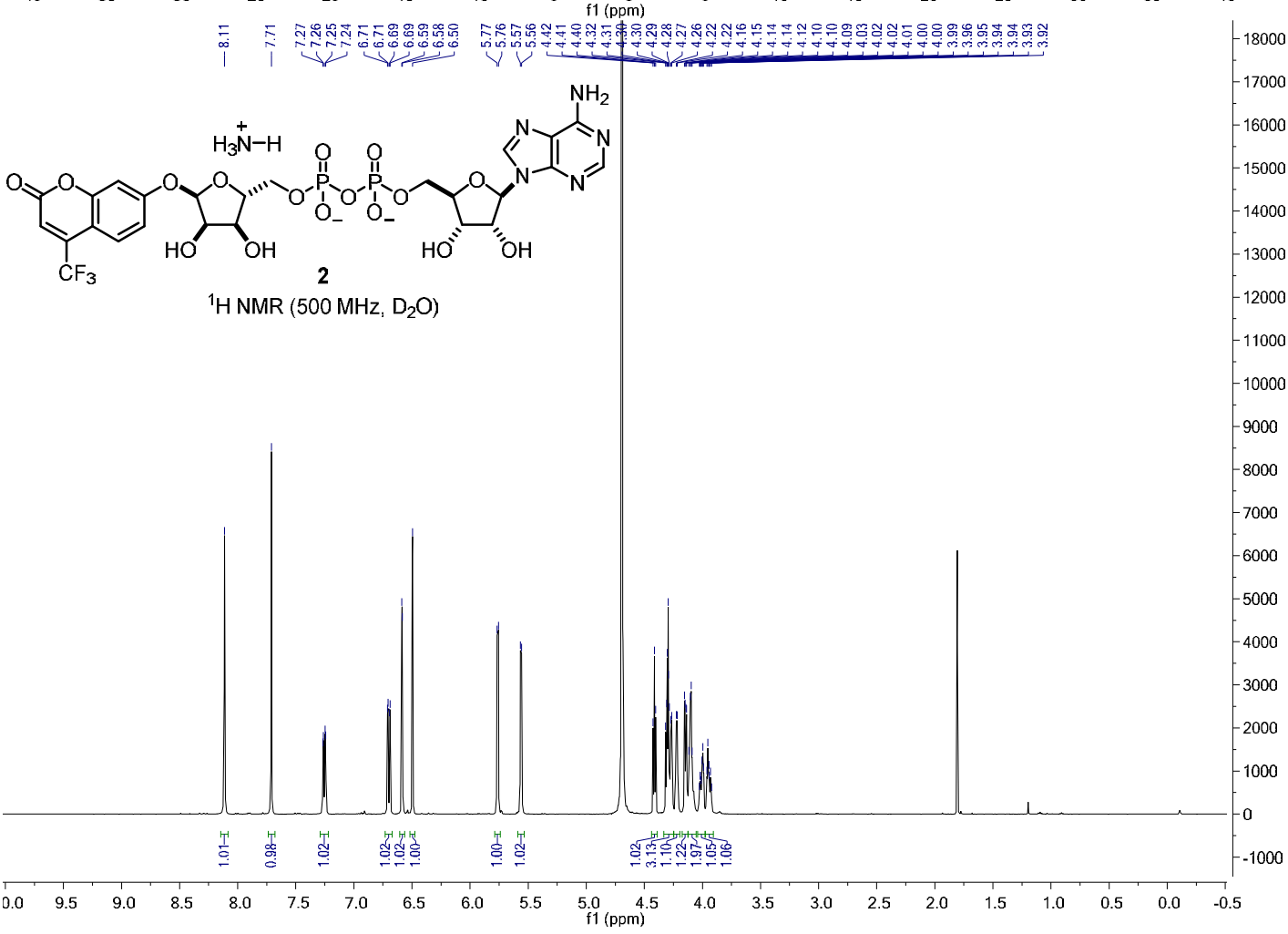

2

^{1}H NMR (500 MHz, D_2O)

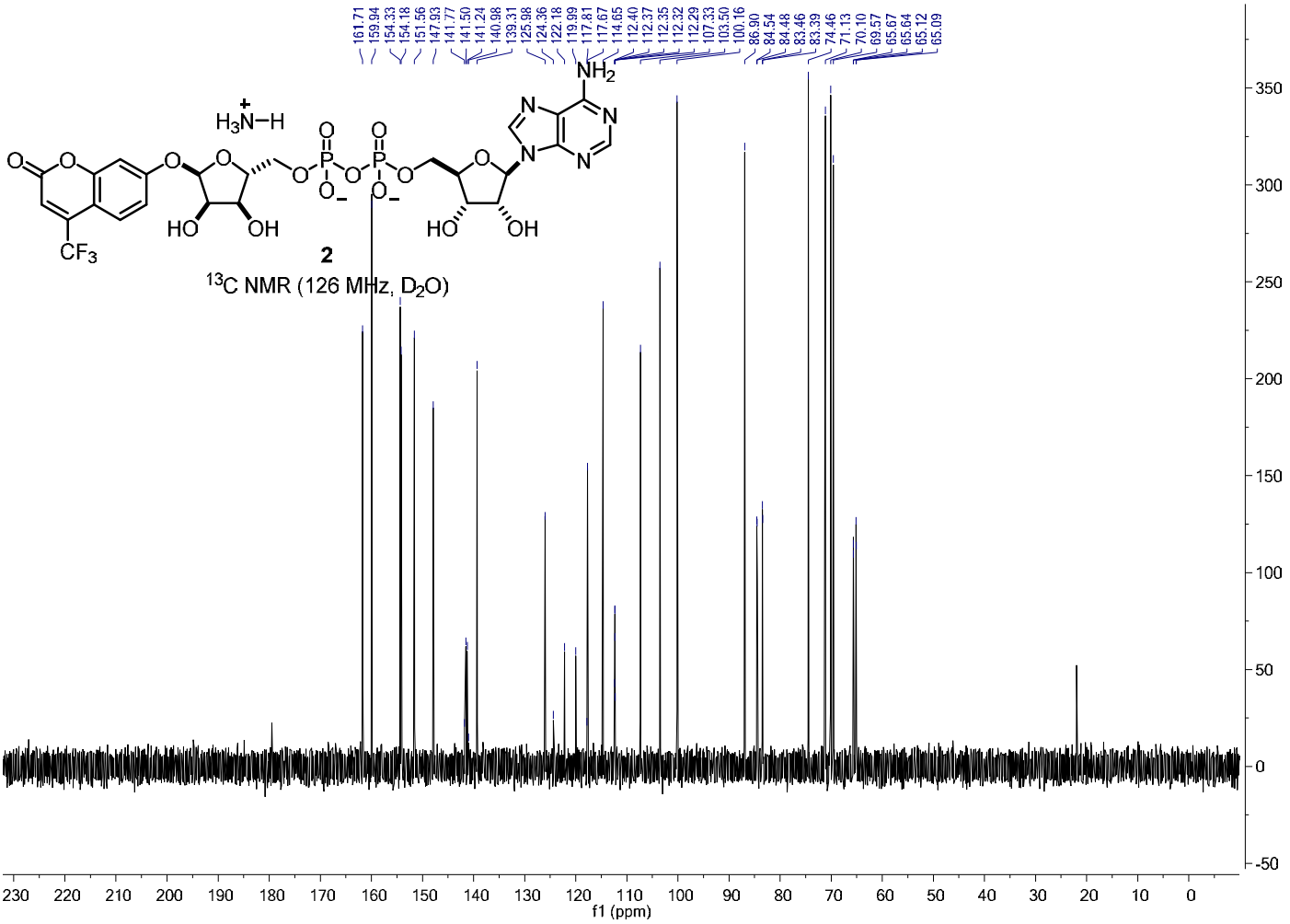
161.71
159.94
154.33
154.18
151.56
147.93
141.77
141.50
141.24
140.98
139.31
125.98
124.36
122.18
119.99
117.81
117.67
114.65
112.40
112.37
112.35
112.32
112.29
107.33
103.50
100.16
86.90
84.54
84.48
83.46
83.39
74.46
71.13
70.10
69.57
65.67
65.64
65.12
65.09
2
13C NMR (126 MHz, D2O)
f1 (ppm)

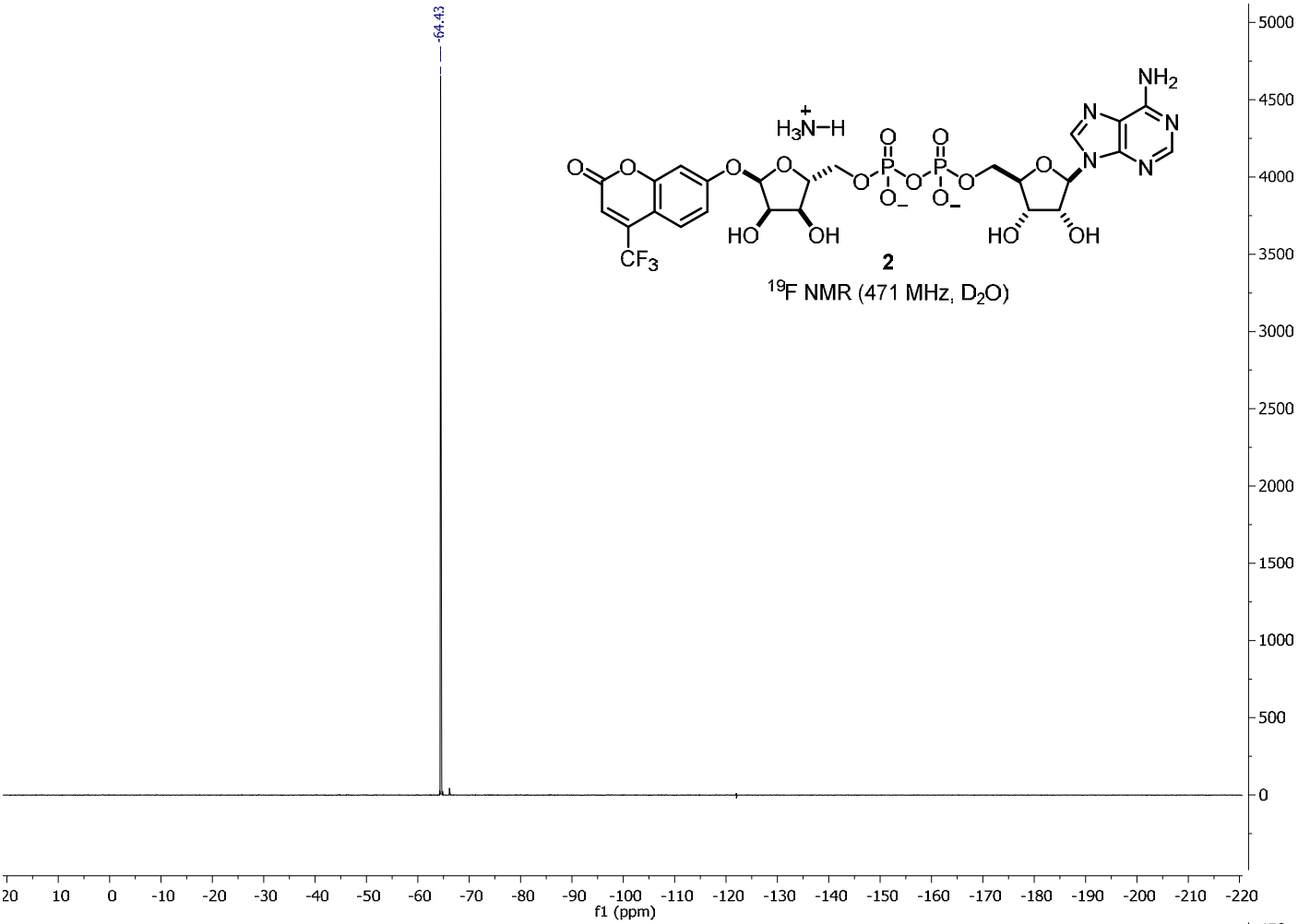

2

^{19}F NMR (471 MHz, D_2O)

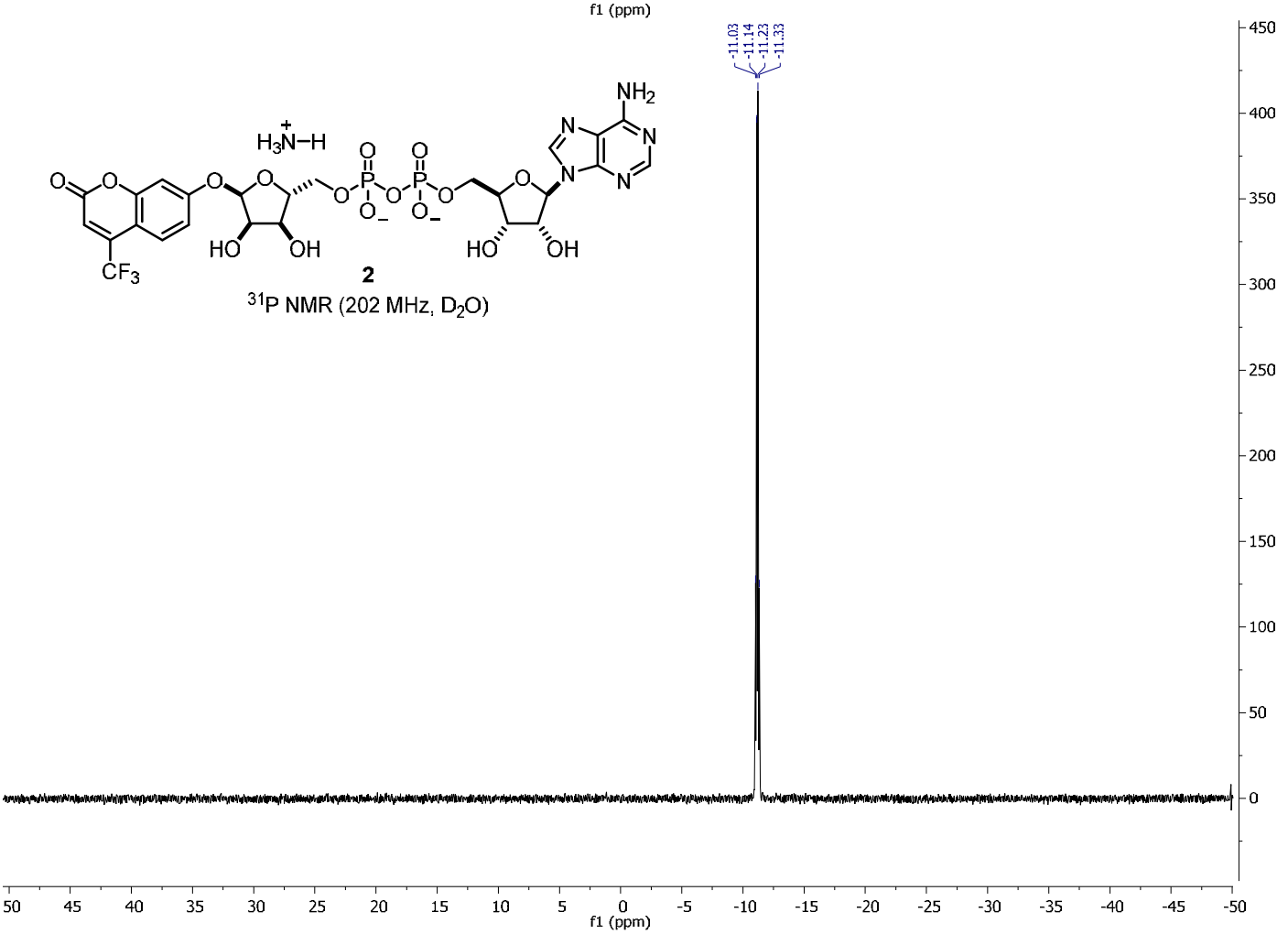

2

^{31}P NMR (202 MHz, D_2O)

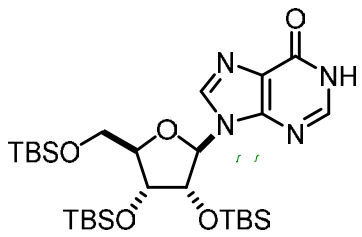

S10

^{1}H NMR (500 MHz, $CDCl_3$)

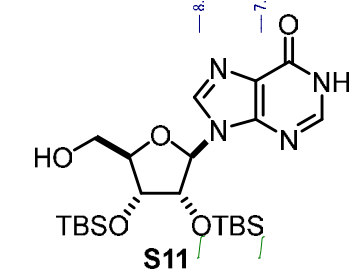

S11

^{1}H NMR (500 MHz, $CDCl_3$)

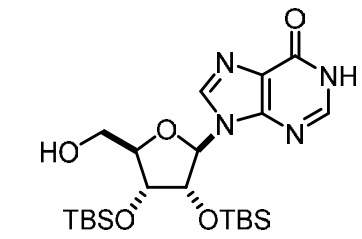

S11

^{13}C NMR (126 MHz, $CDCl_3$)

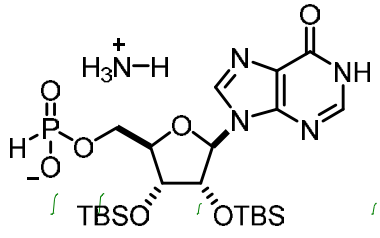

S12

^{1}H NMR (500 MHz, CD_3OD)

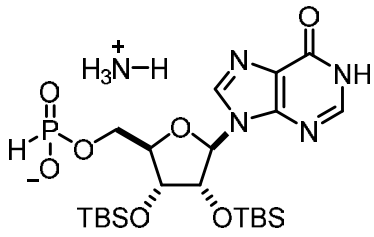

S12

^{13}C NMR (126 MHz, CD_3OD)

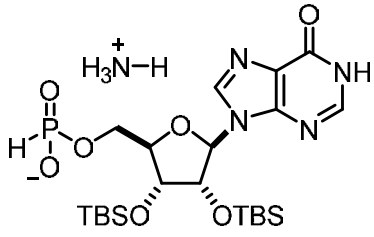

S12

^{31}P NMR (202 MHz, CD_3OD)

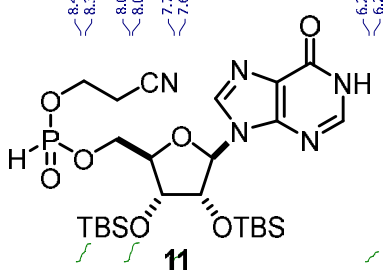

11

^{1}H NMR (500 MHz, $CDCl_3$)

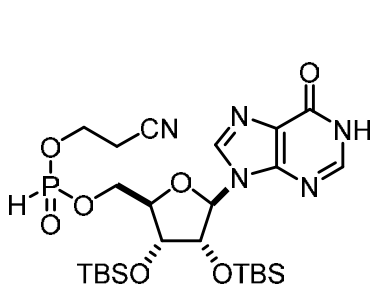

11

^{31}P NMR (202 MHz, $CDCl_3$)

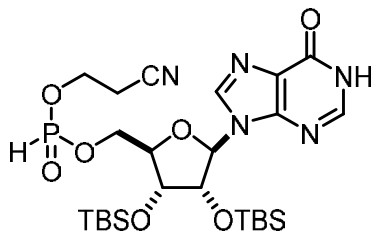

11

^{13}C NMR (126 MHz, $CDCl_3$)

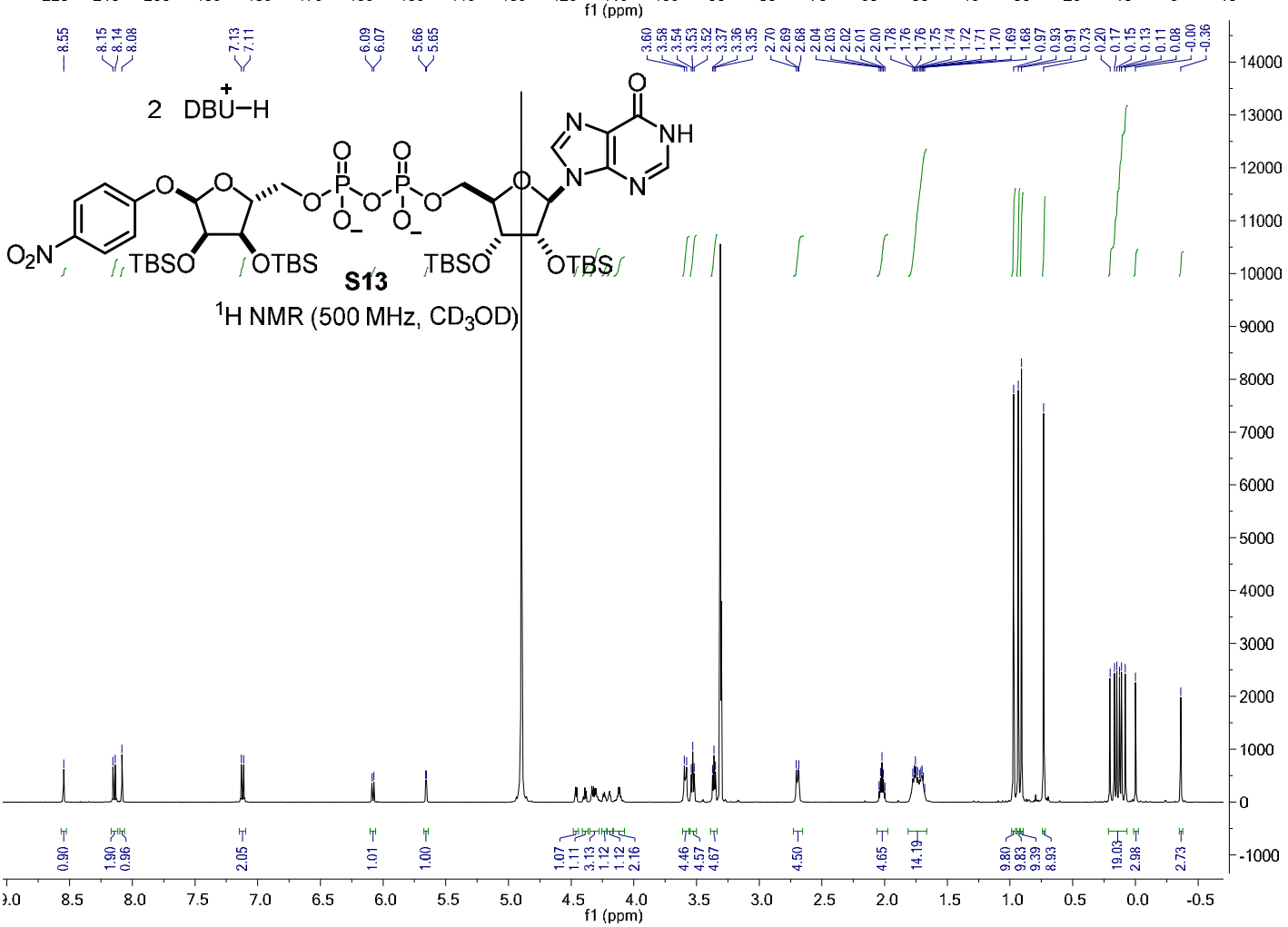

2 DBU^+-H

S13

^1H NMR (500 MHz, CD_3OD)

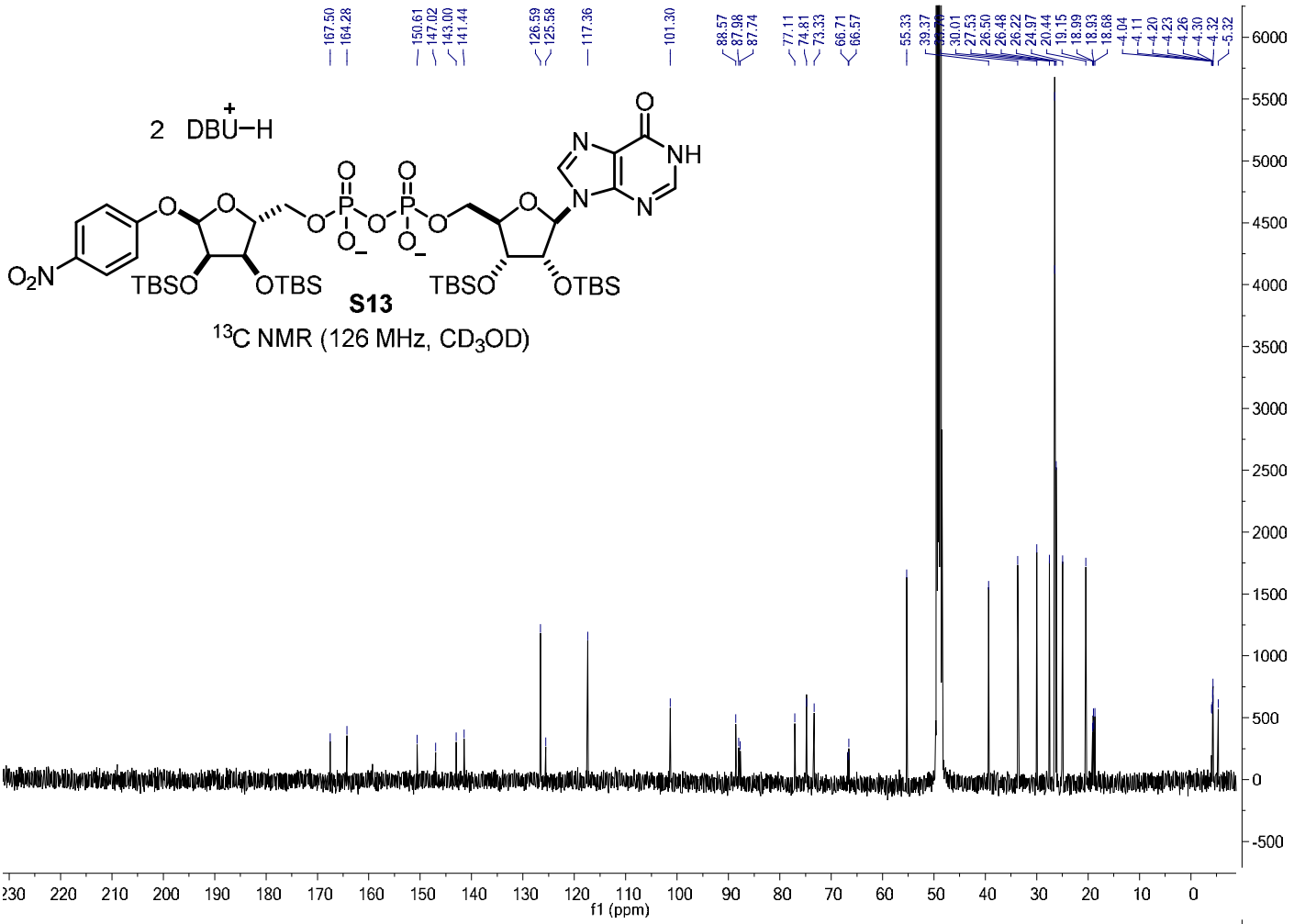

^{13}C NMR (126 MHz, CD_3OD)

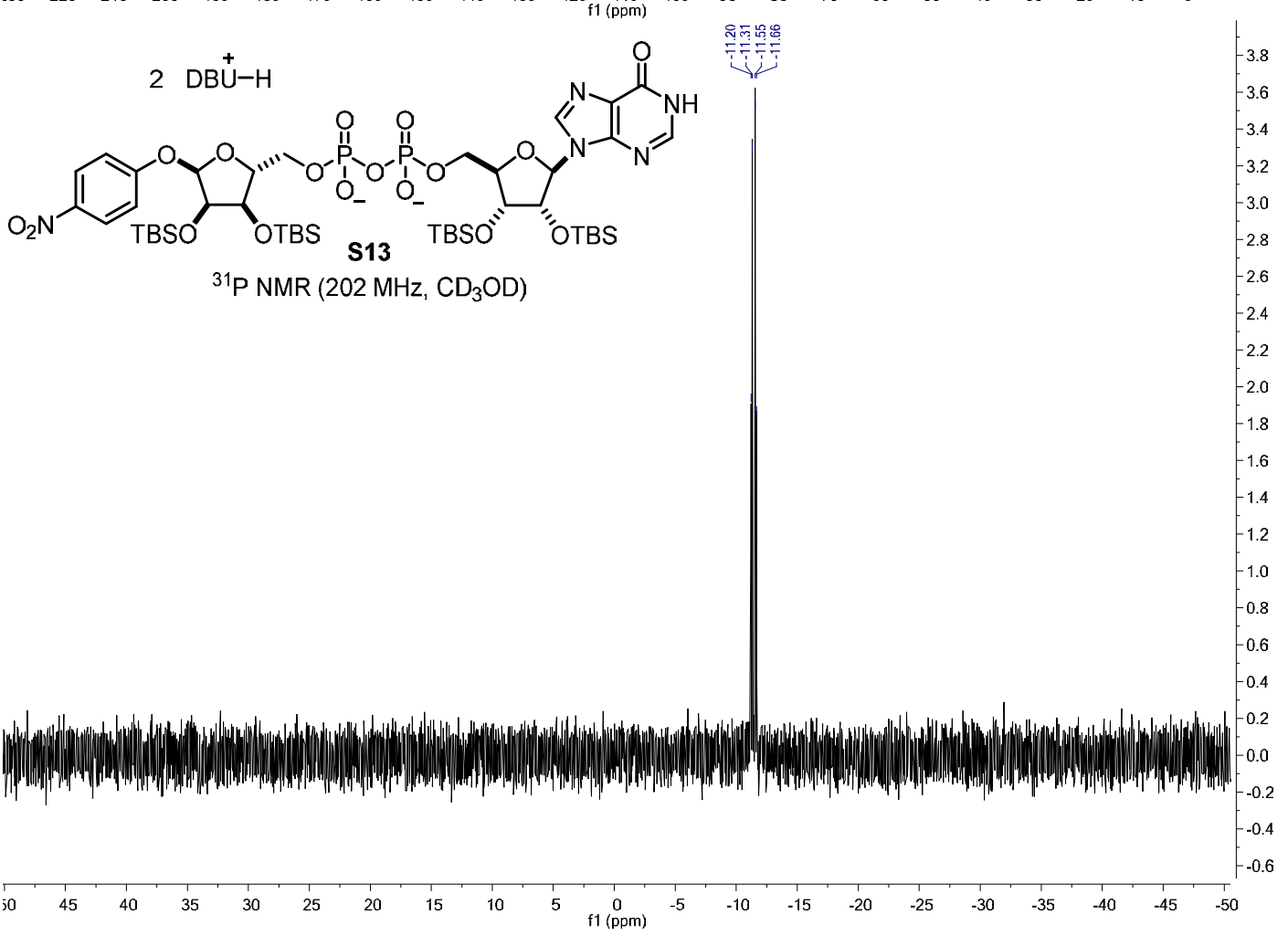

^{31}P NMR (202 MHz, CD_3OD)

BSD-13-44-4.10.fid

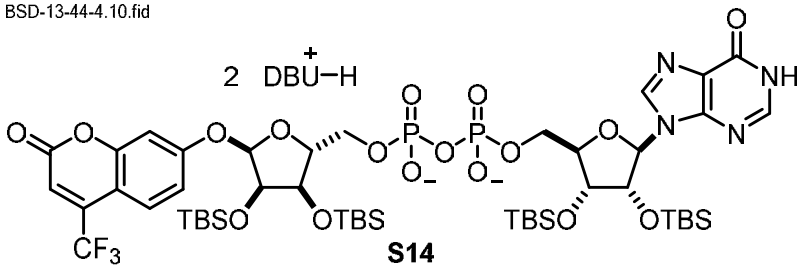

S14

^{1}H NMR (500 MHz, CD_3OD)

BSD-13-44-4.11.fid

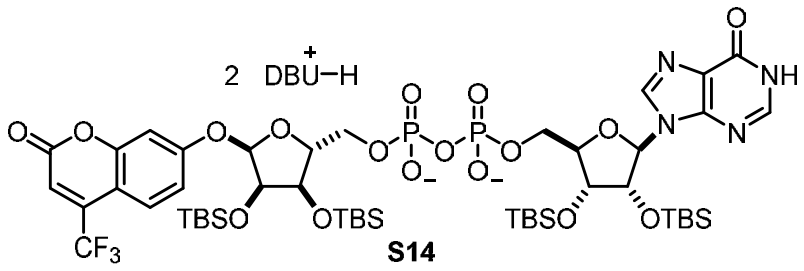

S14

^{13}C NMR (126 MHz, CD_3OD)

BSD-13-44-4.13.fid

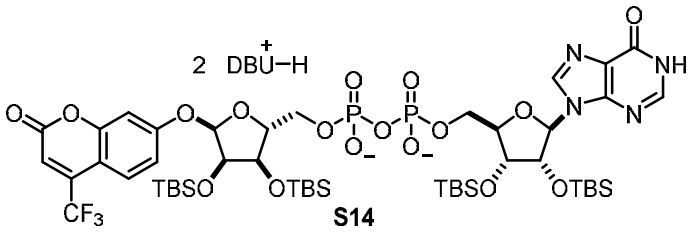

S14

^{31}P NMR (202 MHz, CD_3OD)

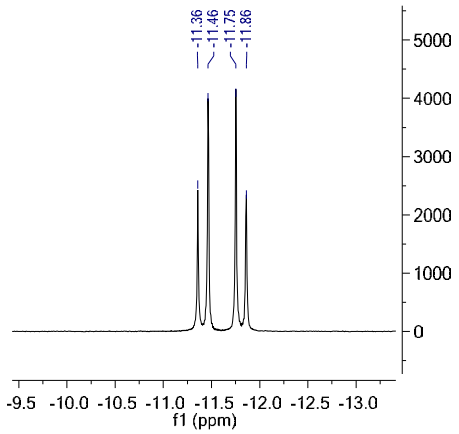

BSD-13-44-4.12.fid

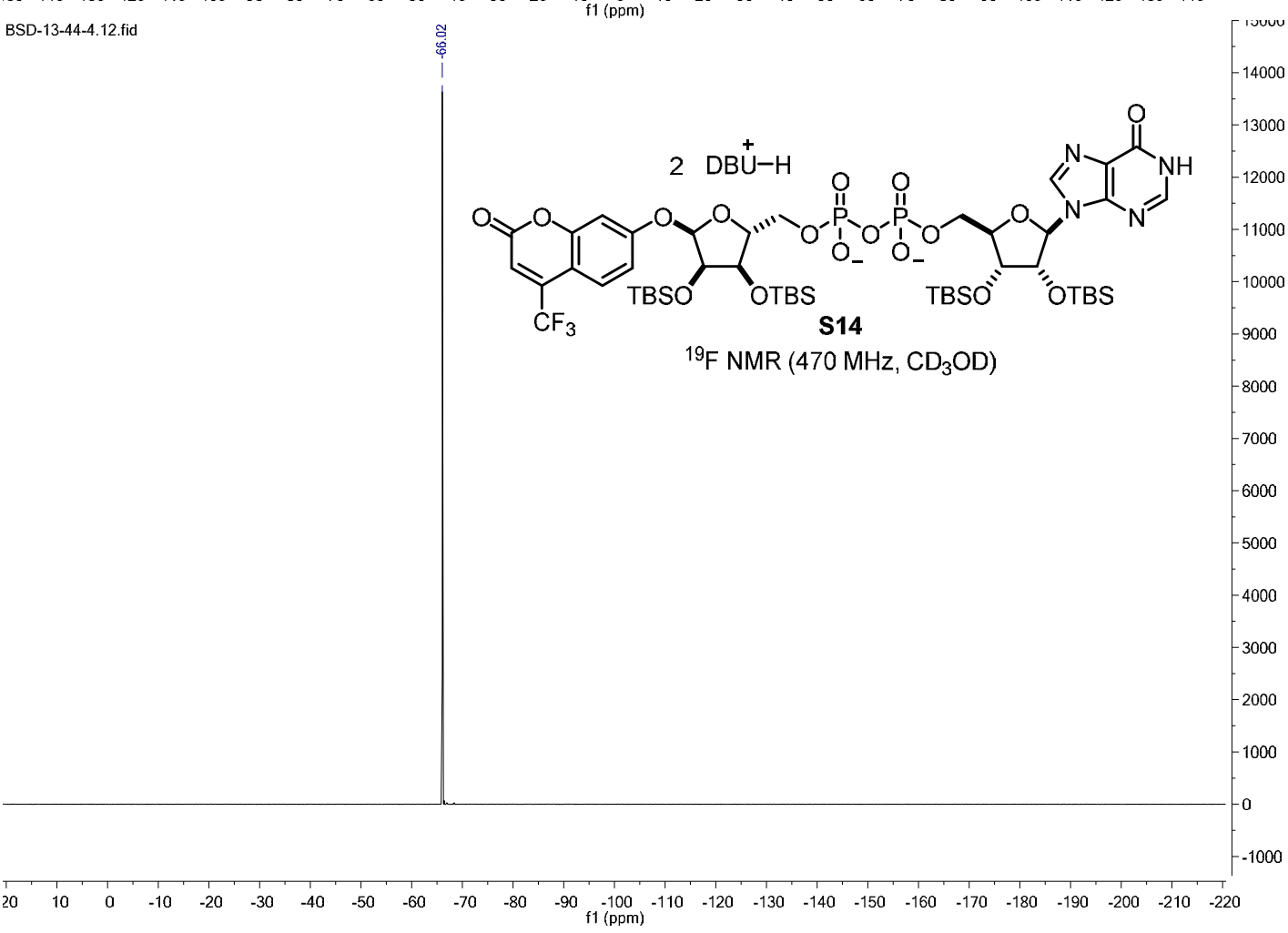

S14

^{19}F NMR (470 MHz, CD_3OD)

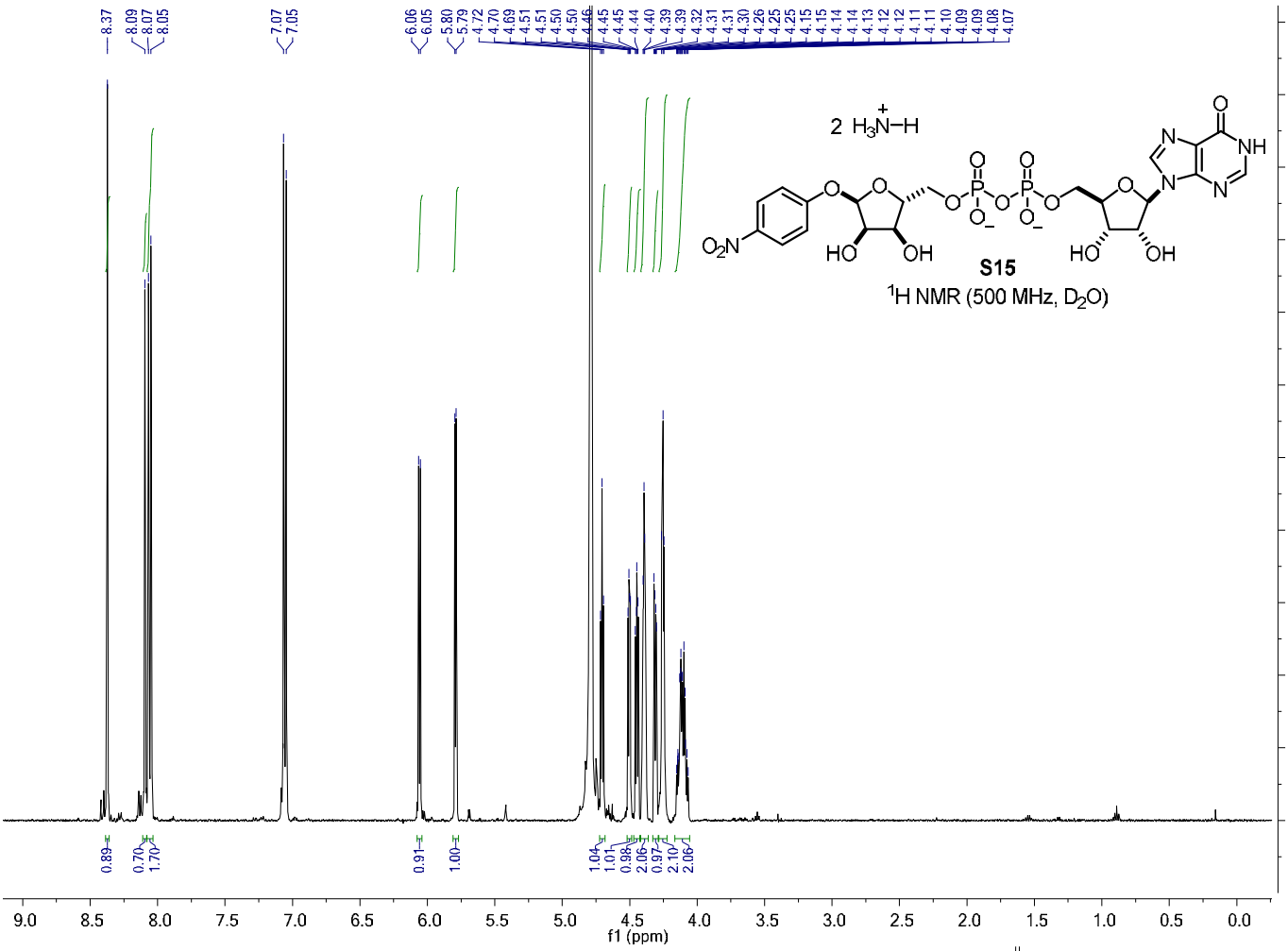
2 H3N+–H
S15
1H NMR (500 MHz, D2O)
f1 (ppm)

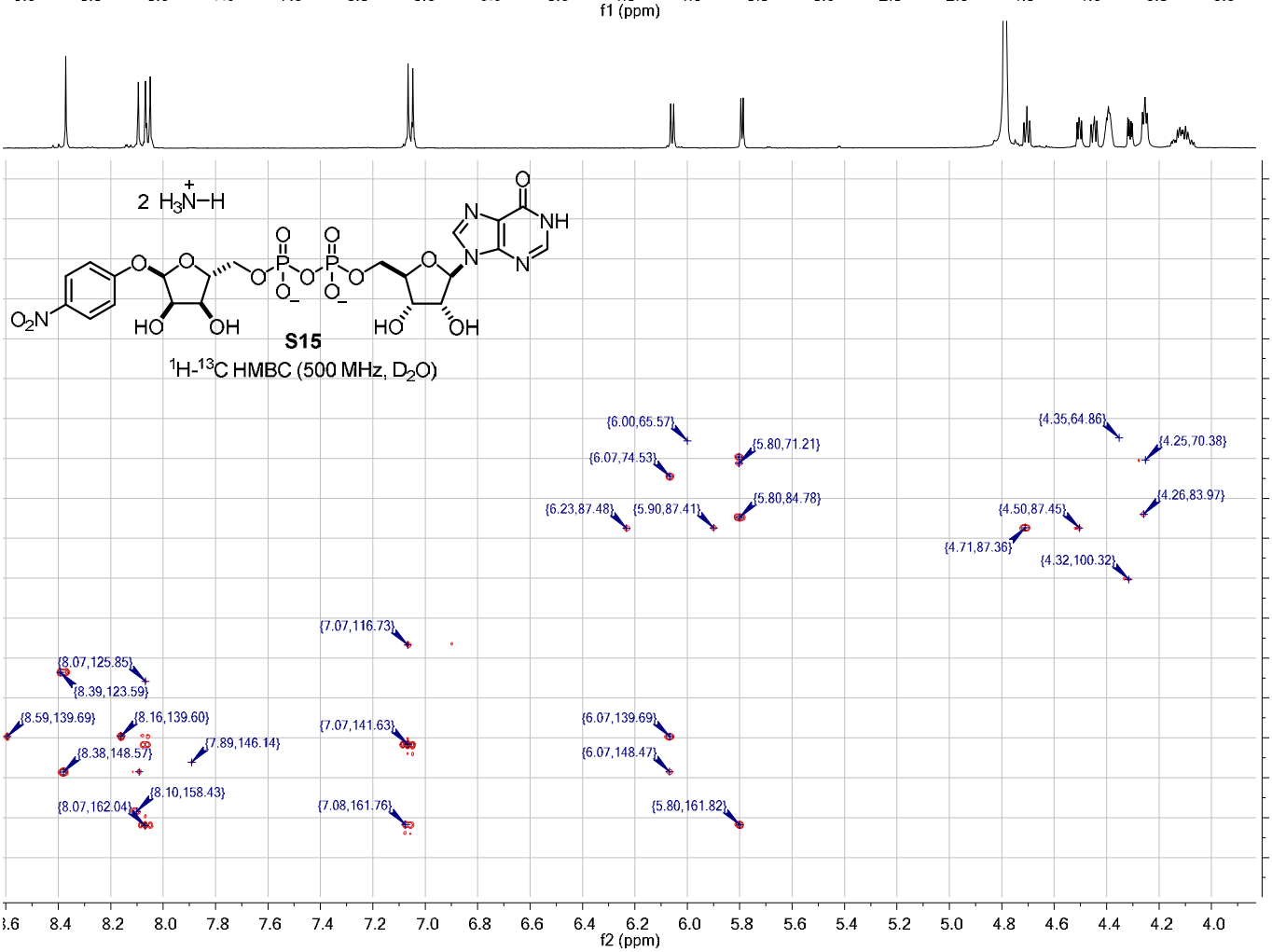
2 H3N+–H
S15
1H-13C HMBC (500 MHz, D2O)
{6.00,65.57}
{5.80,71.21}
{6.07,74.53}
{6.23,87.48}
{5.90,87.41}
{5.80,84.78}
{4.35,64.86}
{4.25,70.38}
{4.26,83.97}
{4.50,87.45}
{4.71,87.36}
{4.32,100.32}
{7.07,116.73}
{8.07,125.85}
{8.39,123.59}
{8.59,139.69}
{8.16,139.60}
{7.89,146.14}
{8.38,148.57}
{8.10,158.43}
{8.07,162.04}
{7.07,141.63}
{7.08,161.76}
{6.07,139.69}
{6.07,148.47}
{5.80,161.82}
f2 (ppm)
f1 (ppm)

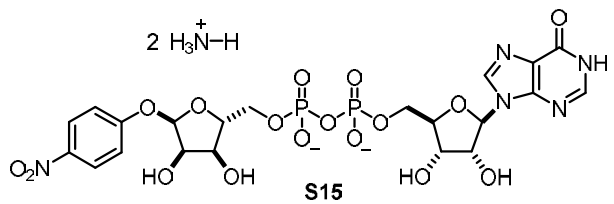

S15

^{31}P NMR (202 MHz, D_2O)

BSD-8-112-3.H
12/4/2015, Bryon Drown, PJH, BSD-8-112-3

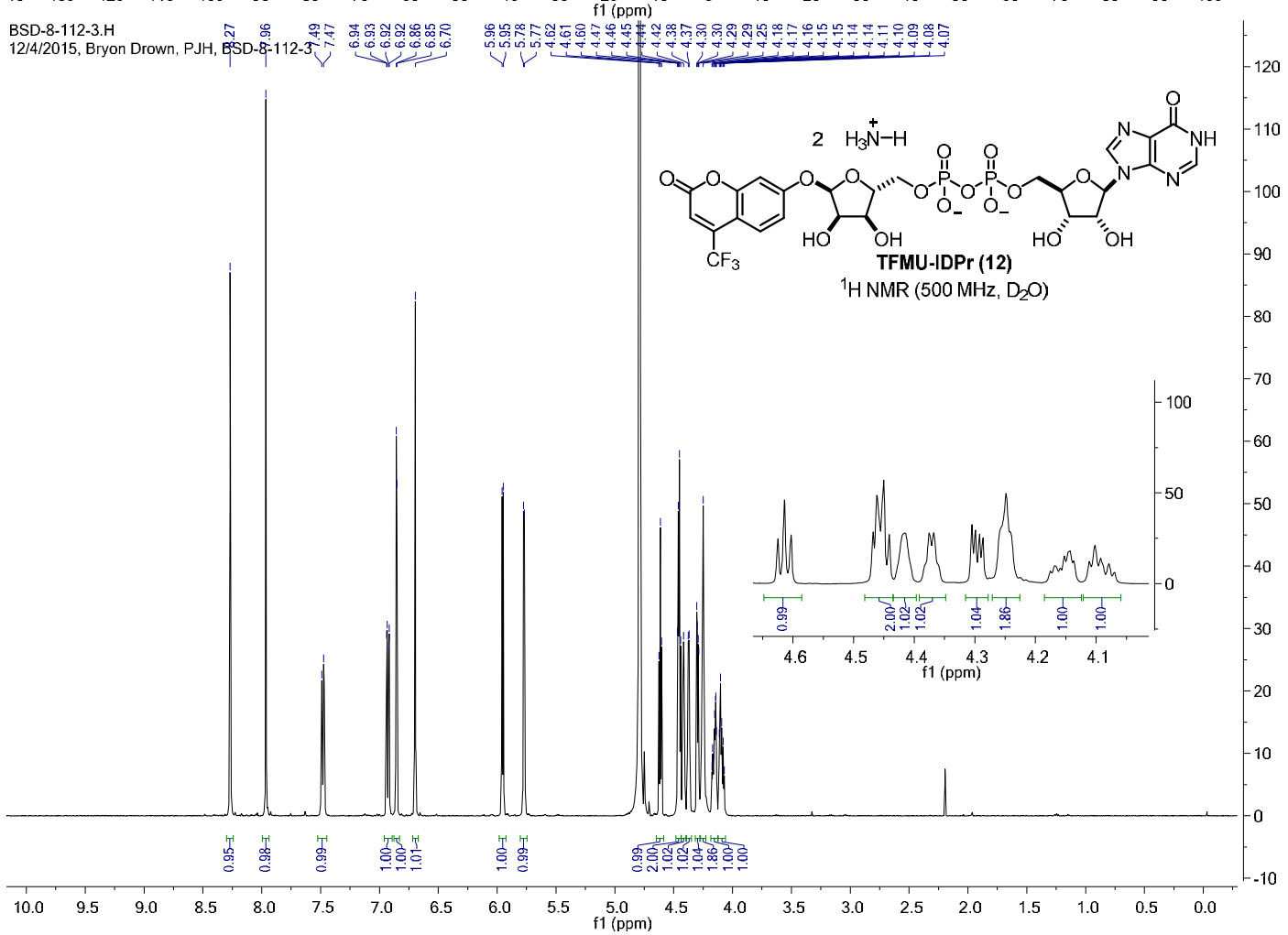

TFMU-IDPr (12)

^{1}H NMR (500 MHz, D_2O)

BSD-8-112-3.C
12/4/2015, Bryon Drown, PJH, BSD-8-112-3

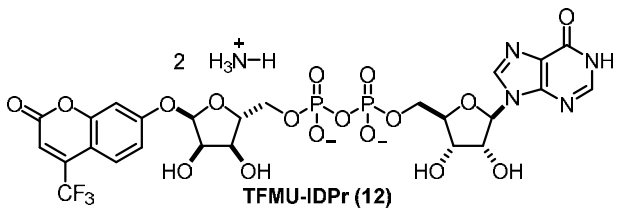

TFMU-IDPr (12)

^{13}C NMR (126 MHz, D_2O)

BSD-8-112-3.P
12/4/2015, Bryon Drown, PJH, BSD-8-112-3

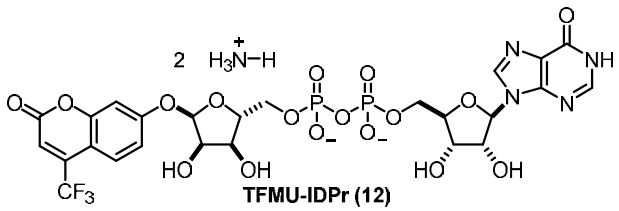

TFMU-IDPr (12)

^{31}P NMR (202 MHz, D_2O)

BSD-8-112-3.F
12/4/2015, Bryon Drown, PJH, BSD-8-112-3

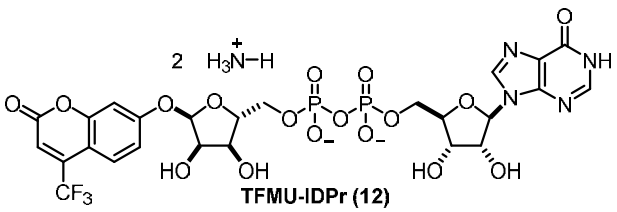

TFMU-IDPr (12)

^{19}F NMR (470 MHz, D_2O)

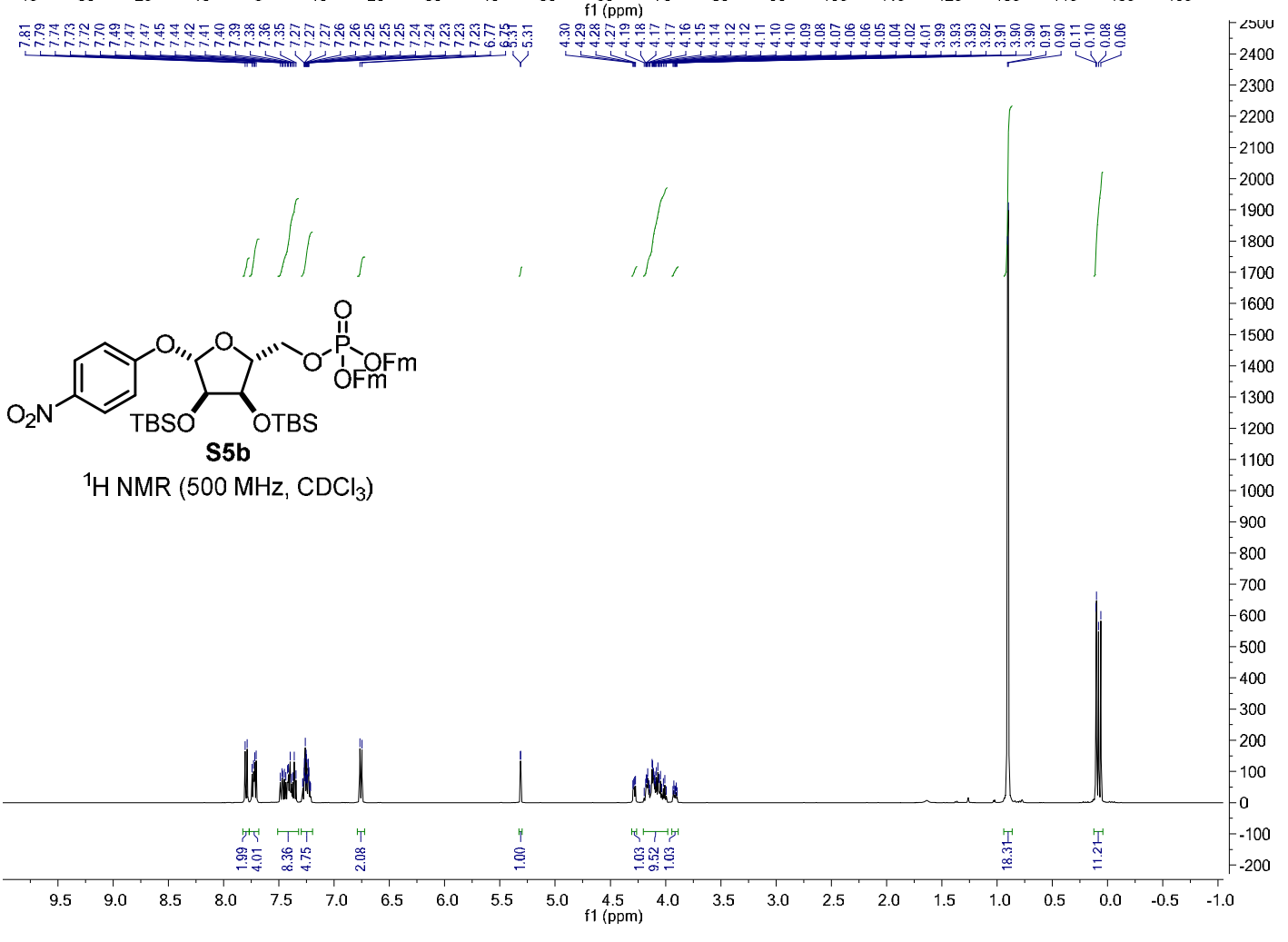

S5b

^{1}H NMR (500 MHz, $CDCl_3$)

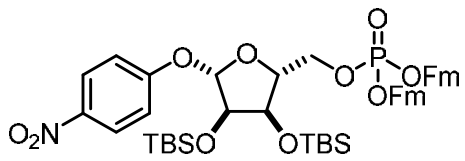

S5b

^{13}C NMR (126 MHz, $CDCl_3$)

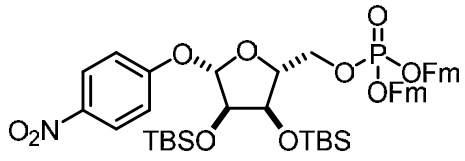

S5b

^{31}P NMR (202 MHz, $CDCl_3$)

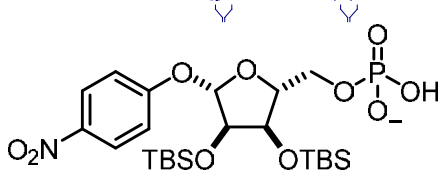

S6b

^{1}H NMR (500 MHz, CD_3OD)

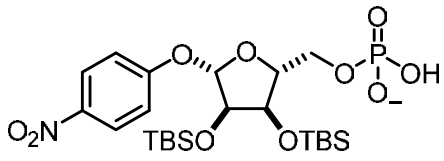

S6b

^{13}C NMR (126 MHz, CD_3OD)

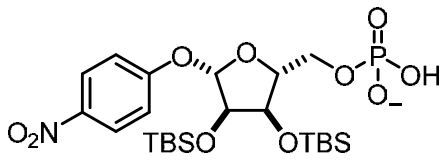

S6b

^{31}P NMR (202 MHz, CD_3OD)

2 DBU^{+}–H

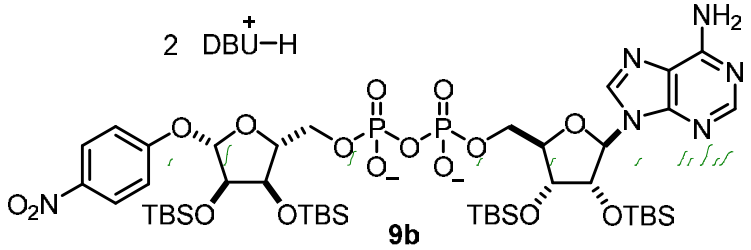

9b

^{1}H NMR (500 MHz, CD_3OD)

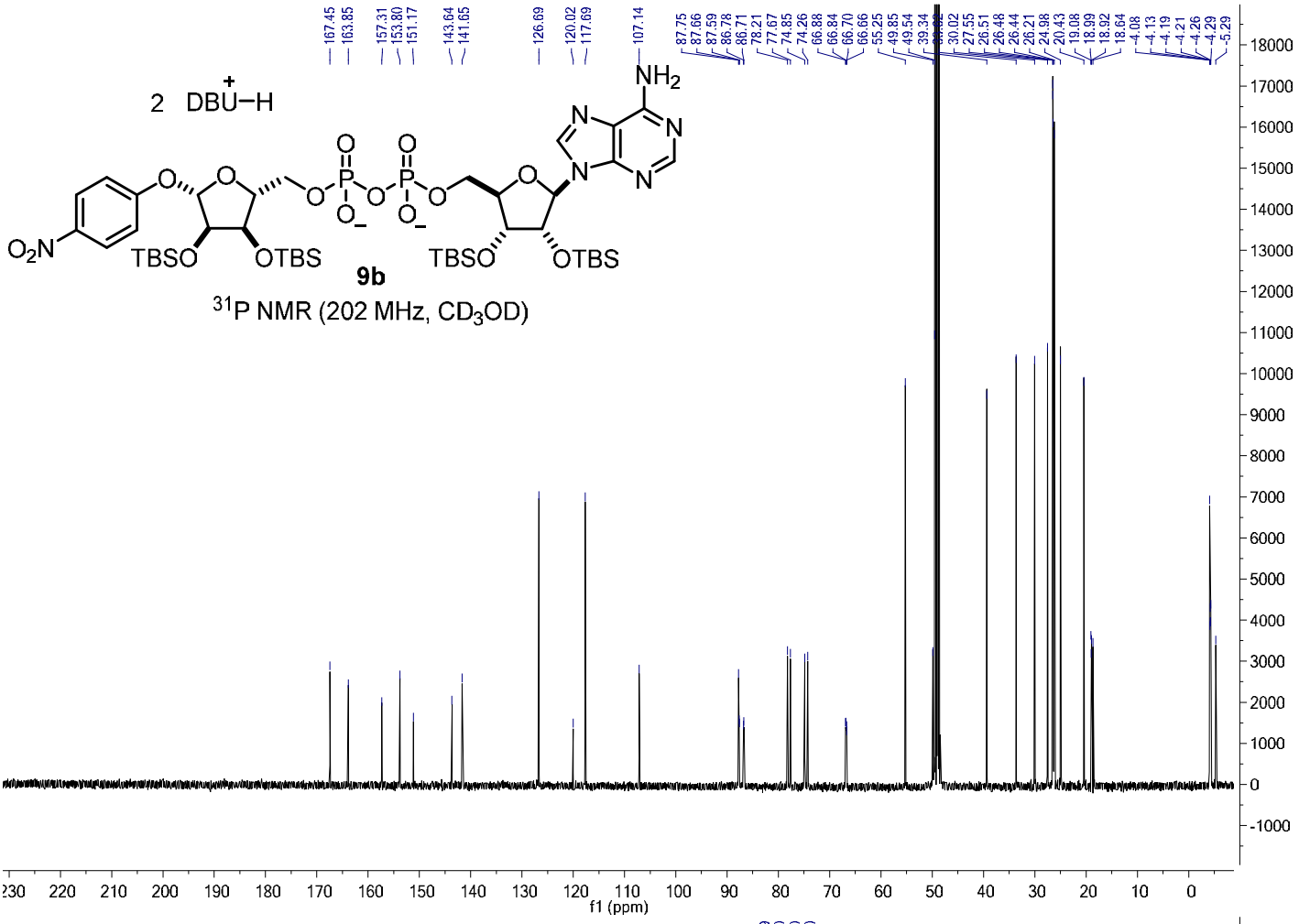
2 DBU−H
NH2
O2N
TBSO
OTBS
TBSO
OTBS
9b
31P NMR (202 MHz, CD3OD)
f1 (ppm)

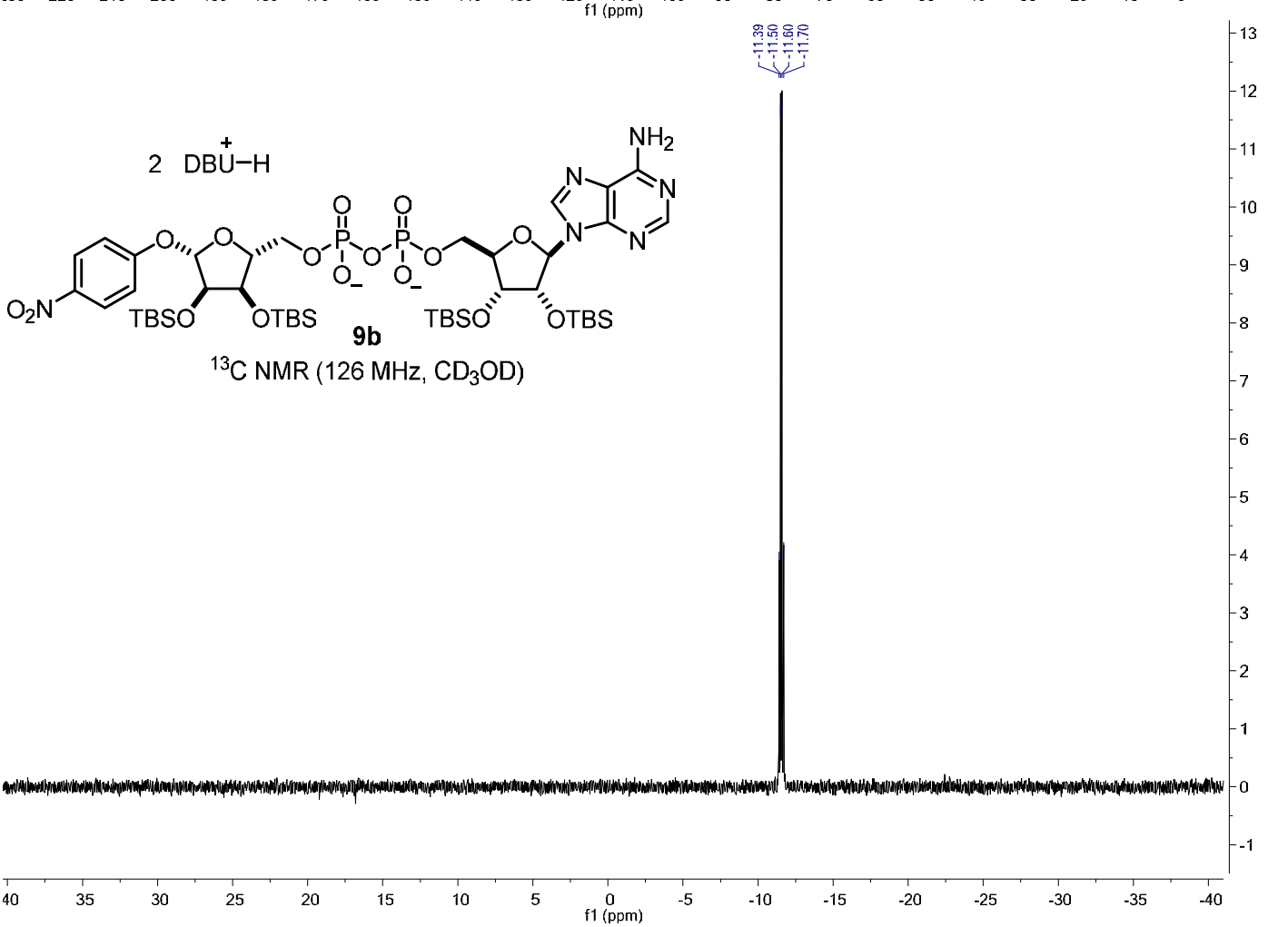
2 DBU−H
NH2
O2N
TBSO
OTBS
TBSO
OTBS
9b
13C NMR (126 MHz, CD3OD)
f1 (ppm)

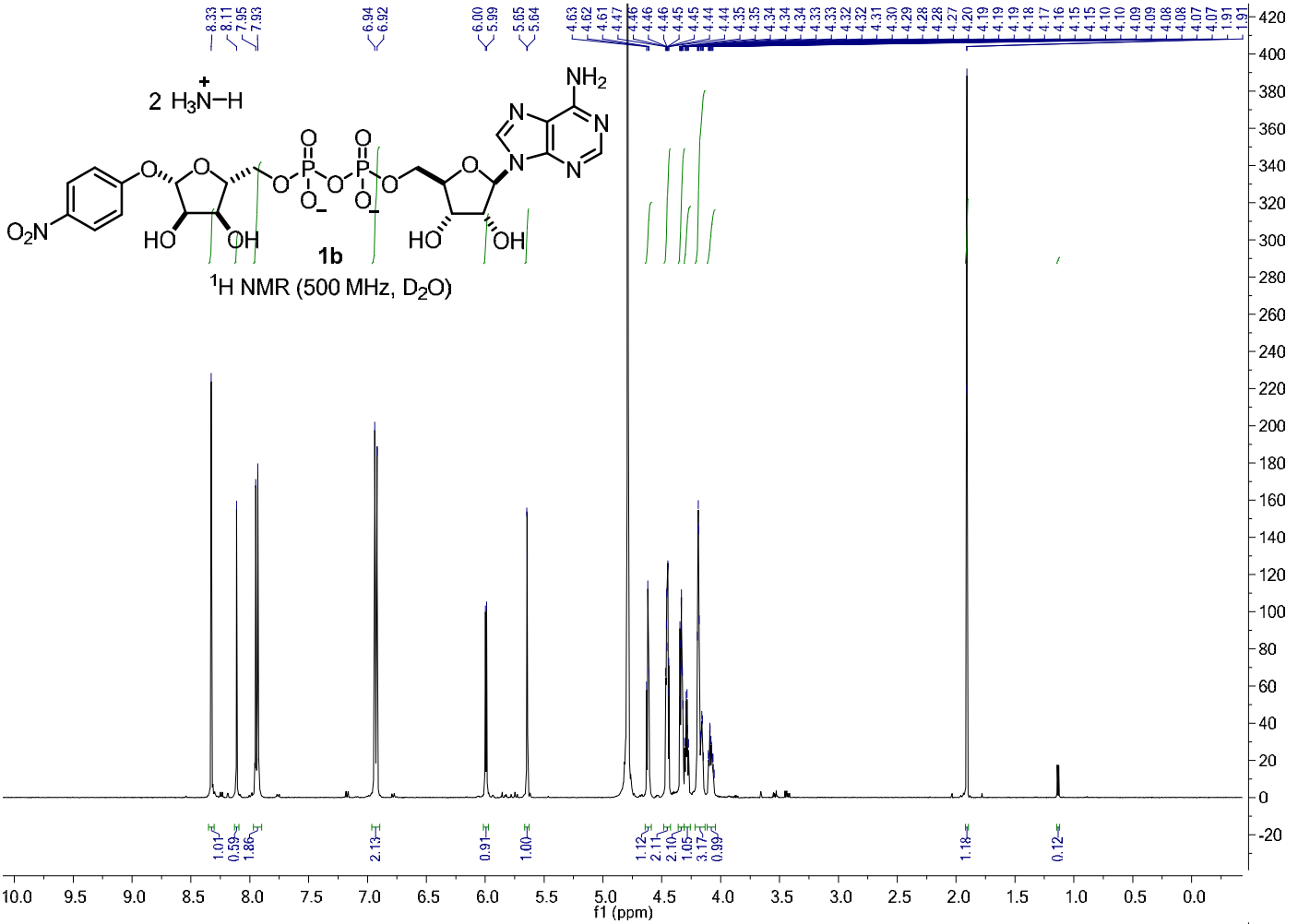
2 H3N–H
NH2
O2N
HO
OH
1b
1H NMR (500 MHz, D2O)
f1 (ppm)

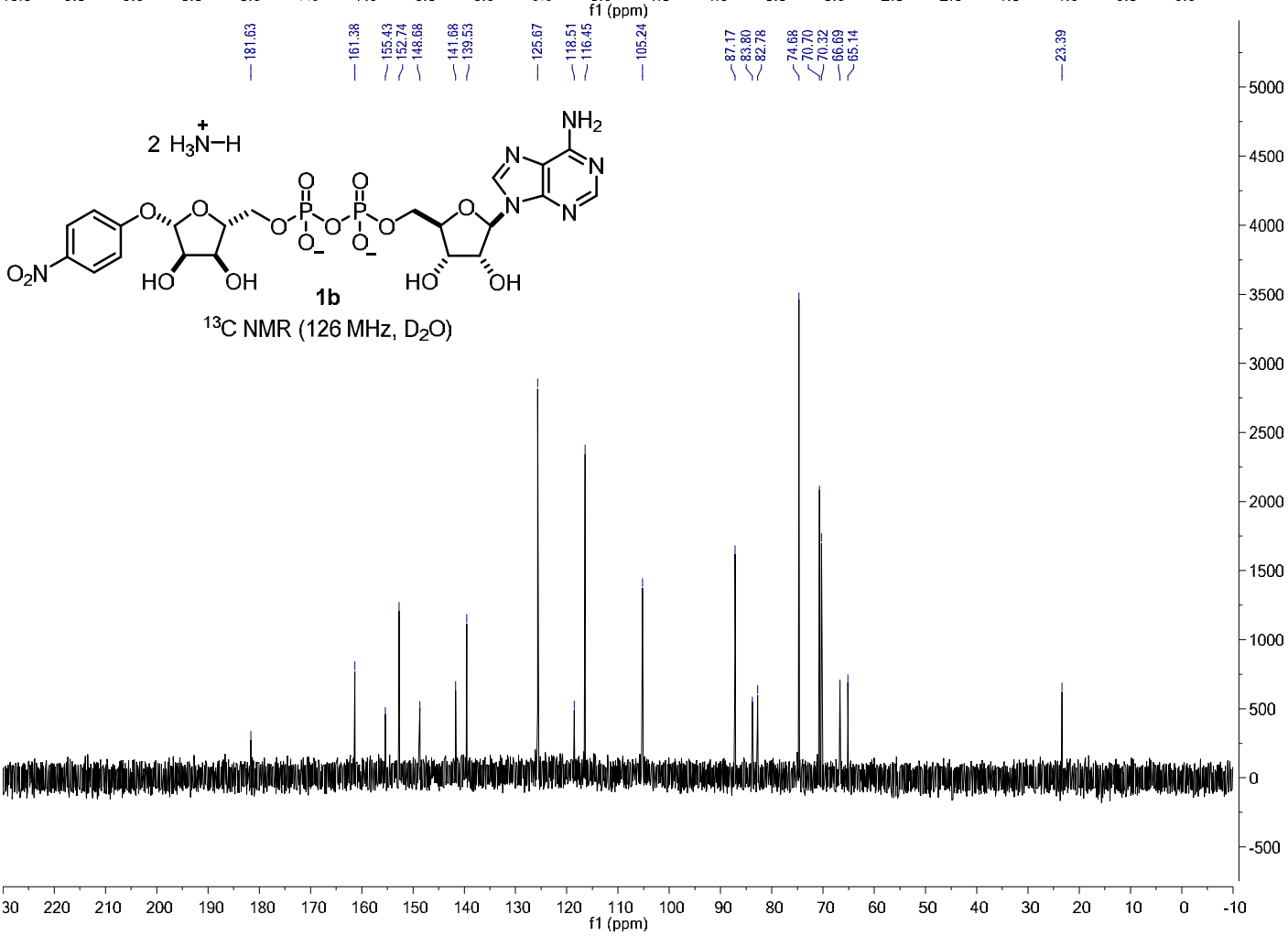
2 H3N–H
NH2
O2N
HO
OH
1b
13C NMR (126 MHz, D2O)
f1 (ppm)

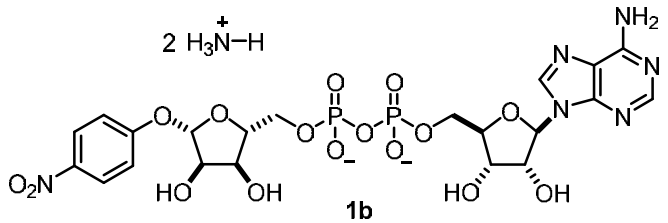

1b

^{31}P NMR (202 MHz, D_2O)

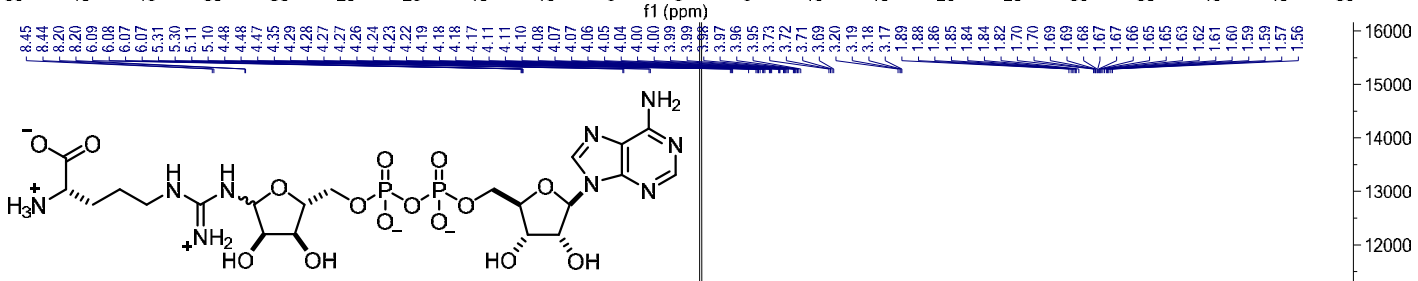

ADP-ribosyl-L-arginine (ADPr-Arg)

^{1}H NMR (500 MHz, D_2O)

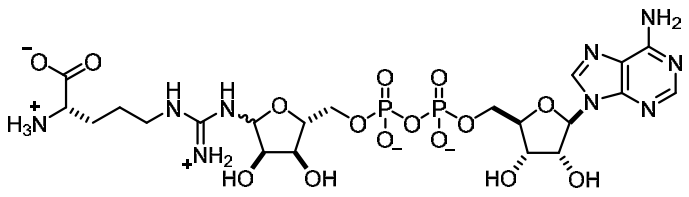

ADP-ribosyl-L-arginine (ADPr-Arg)

^{13}C NMR (126 MHz, D_2O)

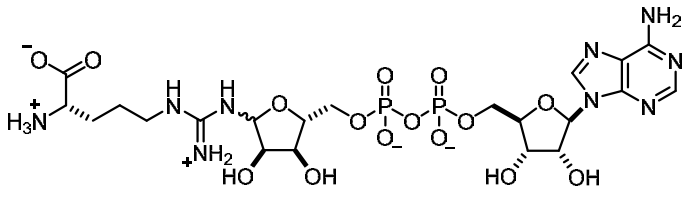

ADP-ribosyl-L-arginine (ADPr-Arg)

^{31}P NMR (203 MHz, D_2O)

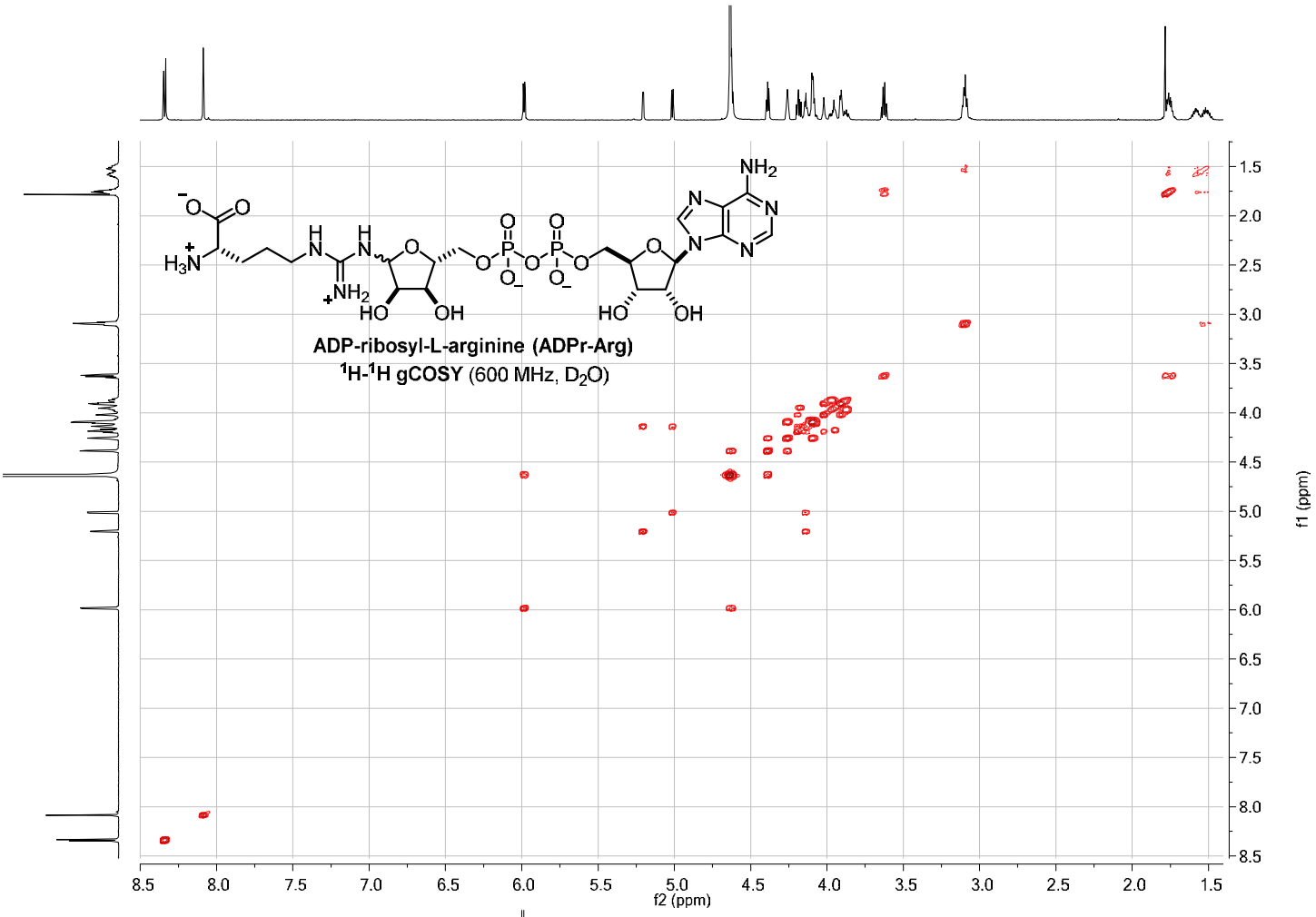
ADP-ribosyl-L-arginine (ADPr-Arg)
^{1}H-^{1}H gCOSY (600 MHz, D_2O)
f2 (ppm)
f1 (ppm)

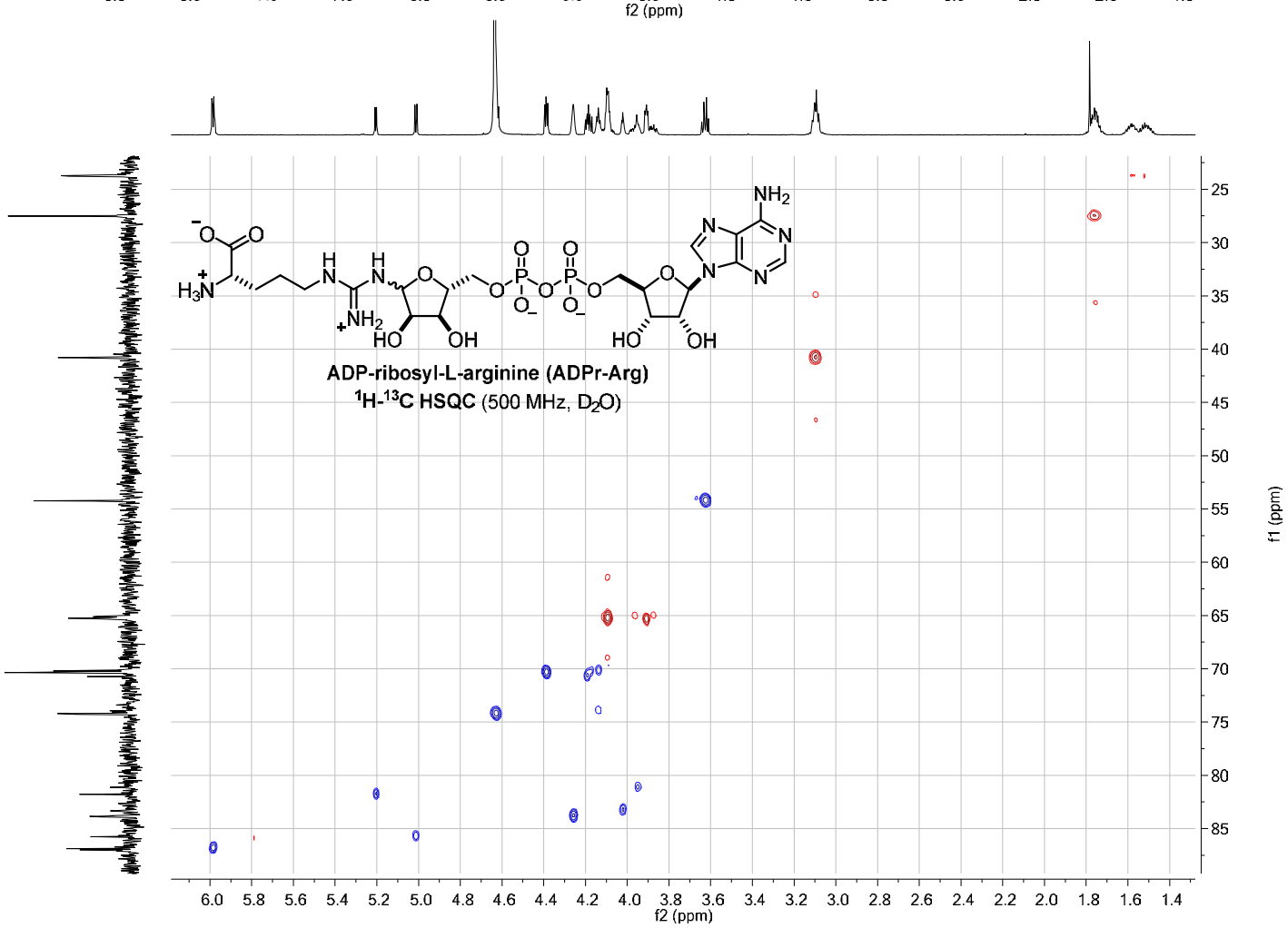
ADP-ribosyl-L-arginine (ADPr-Arg)
^{1}H-^{13}C HSQC (500 MHz, D_2O)
f2 (ppm)
f1 (ppm)

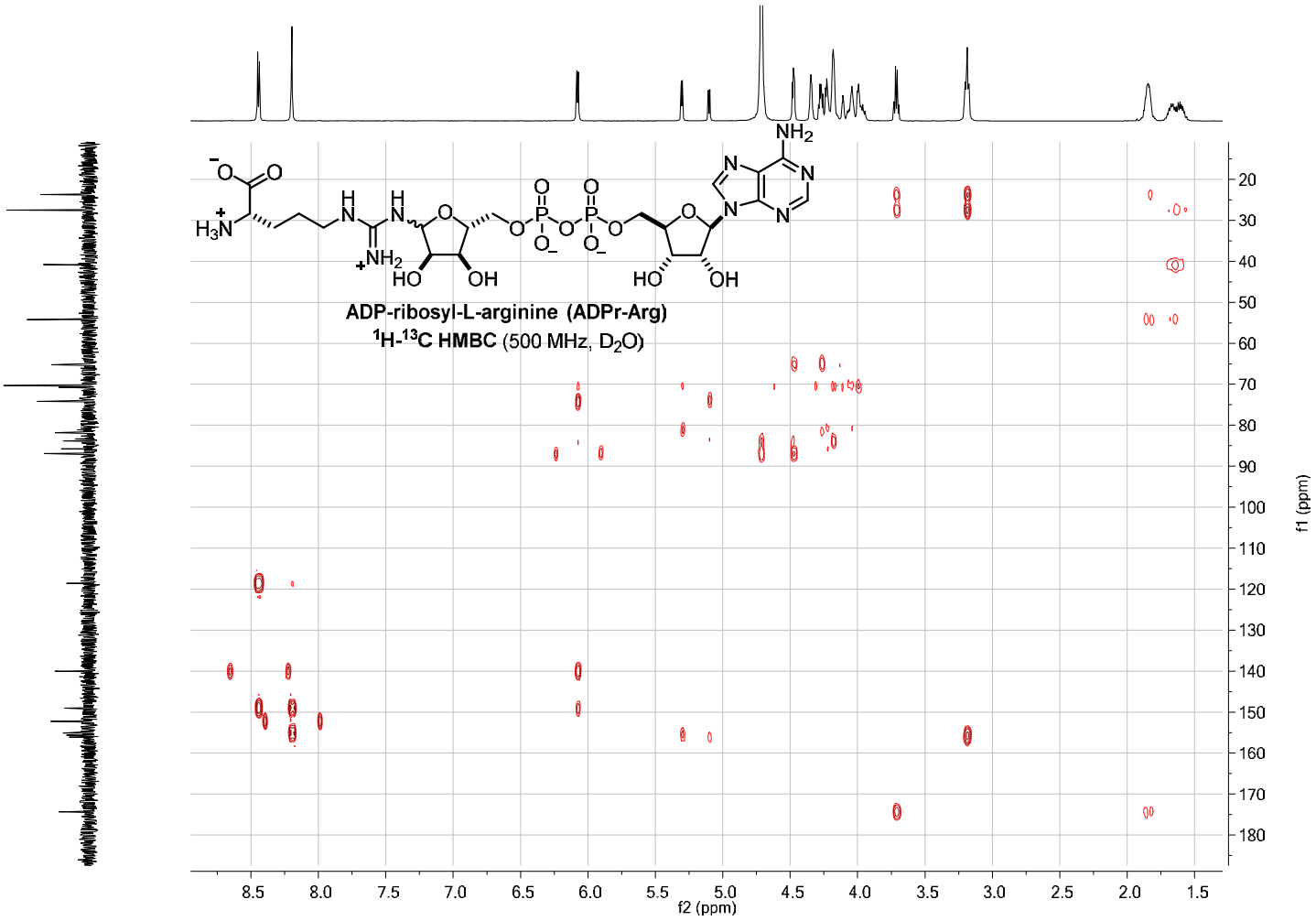
ADP-ribosyl-L-arginine (ADPr-Arg)
^{1}H-^{13}C HMBC (500 MHz, D_2O)
f2 (ppm)
f1 (ppm)